
# REACTION KINETICS IN BIOMASS GASIFICATION (CHEMICAL ENGINEERING).

**Thesis submitted to Cardiff University in Fulfilment of the Requirements for the degree of Doctor of Philosophy in Chemical Engineering.**

**By**

**Hatem Musfer Alkhathami**

**B.Sc. Chemical Eng. & M.Sc. Chemical Eng.**

**School of Engineering-Cardiff University**

**Cardiff, United Kingdom**

**Jan 2022**

# ACKNOWLEDGEMENTS

I would like to express my deep and sincere gratitude to almighty God for giving my energy, time and strength to meet this degree.

The words are not sufficient to express my gratefulness and deepest thanks to my supervisor, Prof. Richard Marsh for his continuous supervision, positive discussions, important ideas through this research work and his various support along my study. Again, I repeat my grate thank for him.

I extend my deepest thanks to Dr. Julian Steer for his expertise and willingness to help and make time for me in spite of inconvenience caused to his busy schedule.

Without the help of the Engineering Workshop, I would not have been able to design and produce a gasifier. In particular, Malcolm Seabourne has always been there to translate my ideas into a workable solution. His technical support has been invaluable to meeting my practical needs.

I am also grateful to my sponsor, Saudi Arabia Government for giving me this great opportunity to pursue my PhD degree with full financial support. As well as the cooperation by the staff of the Saudi cultural bureau - London. I wish I could give individual acknowledgment to all those who have contributed to my work.

Especial thanks go to my father, Musfer, my mother, Salha, my brothers, and my sisters for their support, prayers, and love during my study.

Last but not the least; I would like to thank my beloved wife Shaima for being patient with me during the whole period of study and always pushing me forward to achieve my best, and my children. I would like to express my warm thanks to them all; without their support and encouragement, this thesis would not have been accomplished.

# Abstract

This thesis is concerned with the catalytic fluid-bed gasification of agricultural residue from the Kingdom of Saudi Arabia. The analysis contained herein examined the physical behaviour of this material in a lab-scale gasification reactor and the extrapolation of this behaviour to the potential use of a nation-wide initiative to deploy date crop residues for the generation of renewable energy.

Fluidised bed gasification is an interesting concept for renewable energy due to the availability and sustainability of agricultural waste around the world. Fossil fuels remain a major player in the international energy market which leads to further challenges in deployment of renewable energy, especially across the Middle East, where fossil fuels dominate the energy market.

The desert nature of the Kingdom of Saudi Arabia is a driver for the government to cultivate the desert and to make use of agricultural waste as a source of energy. Due to the abundance of date palms in the Kingdom, the utilization of palm waste (date stone) as biomass has been studied within this thesis.

Using a thermogravimetric analyser (TGA) the pyrolysis kinetics of date stone was studied. A variety of metal bearing catalysts (dolomite, olive, limestone) were tested in the fluidised bed reactor under similar conditions to the TGA using the same percentage of catalyst (10%) to study the activation energy using the Coats Redfern method (results were 44.8, 95.12, 76.19 kJ/mol respectively),. Experiments were conducted for four samples of date stone with dolomite in the following proportions (0%, 5%, 10%, 15%) by using Coats Redfern method and the Activation Energy values were 73.84, 64.94, 44.89, and 50.93kJ/mol respectively.

To study the impact of different ratio of catalyst on gasification performance, gasification experiments were performed on “as received date stone” in a noval lab-scale gasification fluidised bed. The effect of equivalence ratio (0.15-0.35) and bed temperature (450-650°C) on gasification performance was investigated. Based on thermogravimetric measurements using a mass balance model, the activation energy of date stone was found to be 84 kJ/mole.

Using a case study in the Riyadh region of Saudi Arabia, the use of biomass from date palm was investigated. It was demonstrated that this material may provide a feasible sustainable energy supply in Saudi Arabia. The total quantity of potential biomass generated from the residues of date palm in the Riyadh region to produce energy would be 865 x $10^6$ tonnes per year. The overall potential to recover energy from the residues of date palm was forecasted to be 15.63 PJ per year.

# Table of Contents

# List of Figures

# List of Tables

# Nomenclature

| | | |
|---|---|---|
| **NREP** | **National Renewable Energy Program** | |
| **x** | **Conversion** | **dimensionless** |
| **k** | **Rate constant** | **$s^{-1}$** |
| **E** | **Activation Energy** | **kJ/mole** |
| **R** | **Universal gas constant** | **J/mole.K** |
| **A** | **Pre-exponential factor** | **dimensionless** |
| **$m_o$** | **Initial sample mass** | **gram** |
| **m** | **mass of sample at any time, t** | **gram** |
| **mf** | **Final sample mass** | **gram** |
| **f(x)** | **Reaction function** | **dimensionless** |
| **β** | **Heating rate** | **°C/min** |
| **Hs** | **Static bed Height** | **mm, cm** |
| **D** | **Fluidized bed reactor diameter** | **mm, cm** |
| $dp*$ | **Dimensionless particle size** | **dimensionless** |
| $u*$ | **Dimensionless gas velocity** | **dimensionless** |
| **$d_p$** | **Mean particle size of sand** | **µm** |
| **g** | **Acceleration of gravity** | **$m/s^2$** |
| **µ** | **Viscosity of air** | **g/cm.s** |
| **$\rho_g$** | **Density of air** | **$g/cm^3$** |
| **$\rho_s$** | **Density of sand** | **$g/cm^3$** |
| **$u_{mf}$** | **Minimum fluidization velocity** | **m/sec** |

| | | |
|---|---|---|
| **u** | **Superficial velocity** | **m/sec** |
| **$\varepsilon_{mf}$** | **Bed voidage at Umf** | |
| **$\varepsilon_{m}$** | **Bed voidage of the expanded bed** | |
| **TDH** | **Transport Disengaging Height** | **m** |
| **ND** | **Density of orifice** | **No. holes/$cm^2$** |
| **ER** | **Equivalence ratio** | |
| **[AFR]a** | **Actual air fuel ratio** | |
| **[AFR]s** | **Stoichiometry air fuel ratio** | |
| **ṁf** | **Mass rate of fuel** | **g/min, kg/hr** |
| **ṁair** | **Mass rate of air** | **g/min** |
| **HHV** | **Higher heating value of dry gas** | **MJ/$Nm^3$** |
| **Qa** | **Volume flow rate of air** | **Nm3/hr** |
| **Y** | **Gas yield** | **Nm3/kg** |
| **µc** | **Carbon conversion efficiency** | |
| **CGE** | **Cold gas efficiency** | |
| **HHV** | **The gross caloric value of the fuel** | **MJ/kg** |
| **m** | **Mass of char in the reactor** | **g** |
| **Rr** | **Chemical reaction rate** | **g/s** |
| **MAFR** | **Mass air/fuel ratio for stone.** | |
| **NPV** | **net present value** | |
| **ROI** | **return on investment** | |
| **PBP** | **payback period** | |
| **Ca** | **The estimated capital cost of the new power plant in 2020** | |

| | | |
|---|---|---|
| **Cb** | **The estimated capital cost of the new power plant in 2016** | |
| **Ia** | **The chemical engineering plant cost index for 2020** | |
| **Ib** | **The chemical engineering plant cost index for 2016.** | |
| **EP** | **The emissions from electric power production** | |
| **ET** | **Total emissions from combined heat and power production** | |
| **EH** | **The emissions attributable to heat production** | |
| **eH** | **heat production efficiency** | |
| **eP** | **power production efficiency** | |

## Chapter 1

# Introduction

## 1.1 Introduction

The increase in greenhouse gasses, especially carbon dioxide has given rise to the issue of climate change, with a significant contribution from the combustion of fossil fuels. This is an alarming problem as it is likely due to the current rate of population growth and civilisation which boosts the demand for energy supply and hence increasing fuel consumption and subsequently increased emissions.

There are various factors contributing to the greenhouse gasses, however about 70% of the global emissions are due to the direct use of energy sources [1]. Novel scientific evidence had shown that recent climate change phenomena is a direct result of human activities, especially for the past 50 years [2]. Significant amounts of gaseous carbon dioxide are released to the environment daily. In order to mitigate the magnitude of climate change, human interference in the environment must be reduced, and therefore less consumption of fossil fuel is deemed essential.

Fossil fuel is still a major player in the international energy market which drives further challenges in the estimation of the fuel's resources. However, it is commonly agreed that the supply this type of fuel is declining [3]. Therefore, various research was conducted to find more sustainable energy sources to act as a replacement for the declining fossil fuels and the subsequent uncertainly.

Alternative energy sources should be more reliable, sustainable and emit little to no greenhouse gases, and ideally, compliment the phasing-out of existing fossil fuels in order to provide a smooth transition to carbon-free energy. The alternative energy sources include (but not limited to) biomass, wind, geothermal, hydropower, and solar energies. Each of these resources can provide reliable energy while reducing the resultant pollutants relatively to traditional energy sources. The projected fossil fuel usage is shown in Figure (1-1). The figure shows a rise of renewable biomass energy, which is expected to contribute 25% of global direct energy use in 2025 and then increase to a 40% share by 2050 , this includes biomass fuels consisting of different materials, such as methanol, ethanol, hydrogen, and biogas [4].

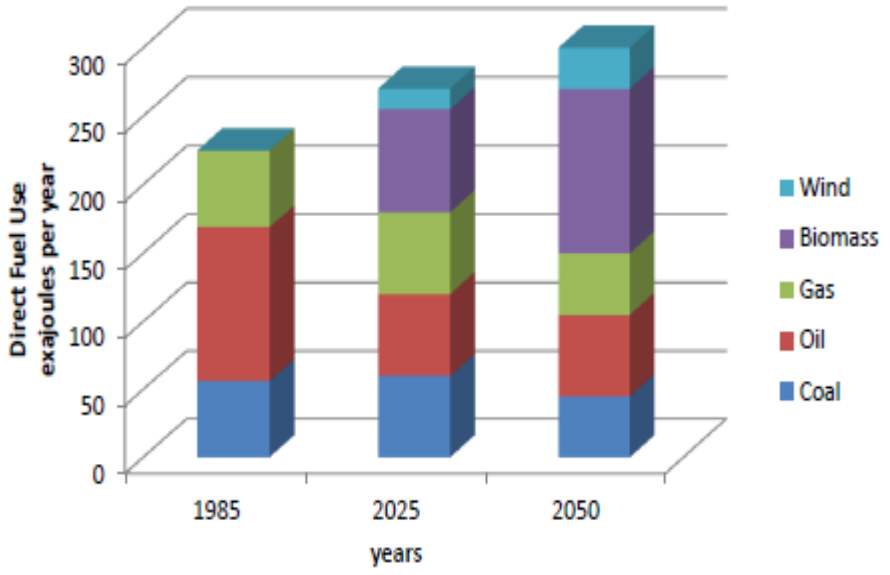


*Figure 1- 1 Direct fuel-use for renewable-intensive global energy scenario [5].*

The future of the climate change management, requires two main approaches, mitigation and adaptation [6]. The first approach; mitigation aims to replace fossil fuels of high carbon with low carbon fuel types that would decrease the emission of greenhouse gasses and therefore reduce the impact on the environment. The second approach is adaptation, which involves a change to the overall process of fuel production and consumption and therefore requires communities to actively change lifestyle and supportive legislation to ensure adaptation. There are various methods to mitigate carbon dioxide, as reported by Sims et al. [7] including the adaptation to renewable energy sources. This thesis can be classified as a mitigation approach, as it aims to further develop and understand the fundamental engineering science of a low carbon energy source.

The World Energy Council provides a manifesto for energy sustainability which includes three key factors [8]. The factors are (1) energy security, (2) energy equity, and (3) environmental sustainability, which when combined forms the 'energy trilemma'. Each trilemma was given a unique definition. Energy security is the ability to reliably provide energy to users and consistently with time. *Energy equity* is the concept of ensuring affordable energy is available to the whole population. *Environmental sustainability* is ensuring that the energy source is sustainable in both efficiency as well as the long-term impact on the environment.

The concepts of the energy trilemma are in direct alignment with the design of a biomass gasifier, to ensure a consistent energy source, in this is case, biomass and a reliable industrial

gasification equipment. To ensure that the produced energy is affordable, the biomass source material cost alongside the manufacturing, construction and operation costs of the gasifier must be carefully considered.

## 1.2 Energy Challenges

As fossil fuel energy sources are declining, and expected to deplete over the next two centuries, demand for energy is increasing proportionally with population increase. The global population is expected to reach 11 billion by the year 2100, that's an increase from the current 7.3 billion, as estimated by the United Nations population division. This will roughly double the world's Gross Domestic Product (GDP) by 2050 according to a DESA estimation conducted in 2015 [9]. This means the demand for energy will massively increase, and the need for reliable and affordable energy is desperately needed to sustain the human civilization.

## 1.3 Energy and Climate Change

Most of the traditional energy sources have a detrimental impact on the environment because of greenhouse gas emissions, namely $CO_2$ and $CH_4$.

The definition of "climate change" is "a change of climate which is attributed directly or indirectly to human activity that alters the composition of the global atmosphere and which is in addition to natural climate variability over comparable time periods[10].

According to National Oceanic and Atmospheric Administration [11] the climate change causes many issue such as:

- A 1 C (1.8 F) rise in the global temperatures from the year 1901 until 2020.
- The sea level rising rate has been accelerated from just 1.7 mm/year to 3.2 mm/year, mostly during the twentieth century.
- Well studied glaciers were found to be shrinking more than 60 feet since 1980.
- Ice covered area of the sea in Arctic was found to be less towards end of the summer season by 40% since 1979.
- A rapid increase on greenhouse emissions contributed even further to climate change. It has increased by 25% since 1958 and by 40% since the commence of the industrial revolution.
- Faster melting time for snow covered areas.

Human activities influence climate change in different forms, e.g. deforestation, energy sources via combustion fossil fuels. An all-time high 9776 million metric tons of carbon dioxide was released to the atmosphere because of the combustion of fossil fuels in 2013 worldwide. This represents a 1.1% increase in emissions year on year as shown on Figure (1 – 2) which is reported by Friedlingstein et al.[12]. This resulted in an excess 410 billion tonnes of carbon dioxide in the atmosphere in 2020.

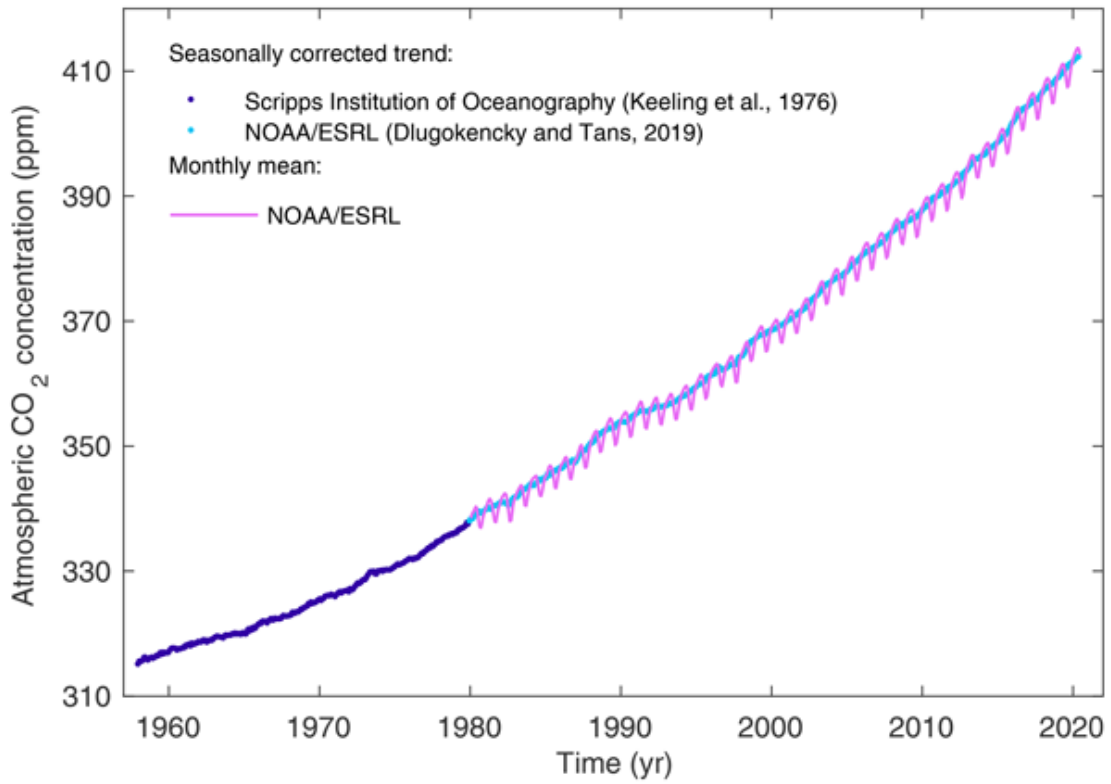


*Figure 1- 2 Annual Global Fossil-Fuel Carbon Emissions* [12].

The increase of carbon dioxide concentration in the atmosphere due to the reasons mentioned above, results in increasing the surface temperature due to the greenhouse effect. This unprecedented increase in the surface temperature significantly impacts the planet, and results on melting of the glaciers and ice caps, consequently increasing sea level. The only way to mitigate this catastrophic scenario is to urgently cut down the carbon dioxide emissions internationally as mentioned by Boden et al.[13].

Therefore, the ultimate challenge is to meet the ever-increasing demand for energy while mitigating negative impacts on the environment, and thus maintain the development of human

civilization in every part of the planet. One of the main answers to this challenge can be represented in the adoption of Biomass Renewable energy.

## 1.4 Biomass as an alternative to fossil fuel

The need to mitigate climate change and ensure energy security is driving the international effort to take advantage of biomass materials as a source for renewable, and sustainable, energy source. Biomass is currently the third largest energy source in the world, after coal and oil [14].

Biomass fits the criteria to being considered a renewable energy source and has minimal impact on the environment when compared to fossil fuel sources. The European Union strategy to keep the temperature rise to below 2 $^{o}$C on the planet includes the uptake of renewable energy sources such as biomass material [15].

Biomass physical properties are measurably different to coal, as it contains higher moisture content, less carbon, lower heating value, more potassium and silica, it also has a lower density value [16]. Due to these physical differences, there are various advantages that arise from using biomass as a fuel, such as:

1. Tackling climate change challenge. Biomass absorbs carbon dioxide from the atmosphere in its production via the photosynthesis process. Therefore, it relatively balances the greenhouse gasses emitted when combusted.
2. It also has a very good potential of being a sustainable energy source for both developed and developing countries. Its international production is estimated to be 146 billon metric tons annually [17].
3. Energy produced via a biomass energy source emits less $SO_X$ and $NO_X$ relative to traditional sources due to the lower sulphur and nitrogen content [18].
4. It has a positive impact on local economies and enables the utilisation of less quality agriculture lands that is not eligible to grow edible crops to grow biomass material.
5. Biomass is not confined to just one source, and therefore there is a diverse range of crops that can be used and therefore it can be easier to establish and maintain [17].

Biomass material is considered renewable as there is the possibility of ensuring a supply chain of the material and consistently substitute the used biomass with fresh sources in a short period of time. Not considering its production and transportation, biomass as an energy source has minimal net carbon emission of its production life cycle if grown efficiently and

sustainability[19]. This has led to plant cultivation being one of the most important factors in closing the carbon cycle. The energy cycle of biomass is shown on Figure (1 – 3) when utilised as an energy source [20].

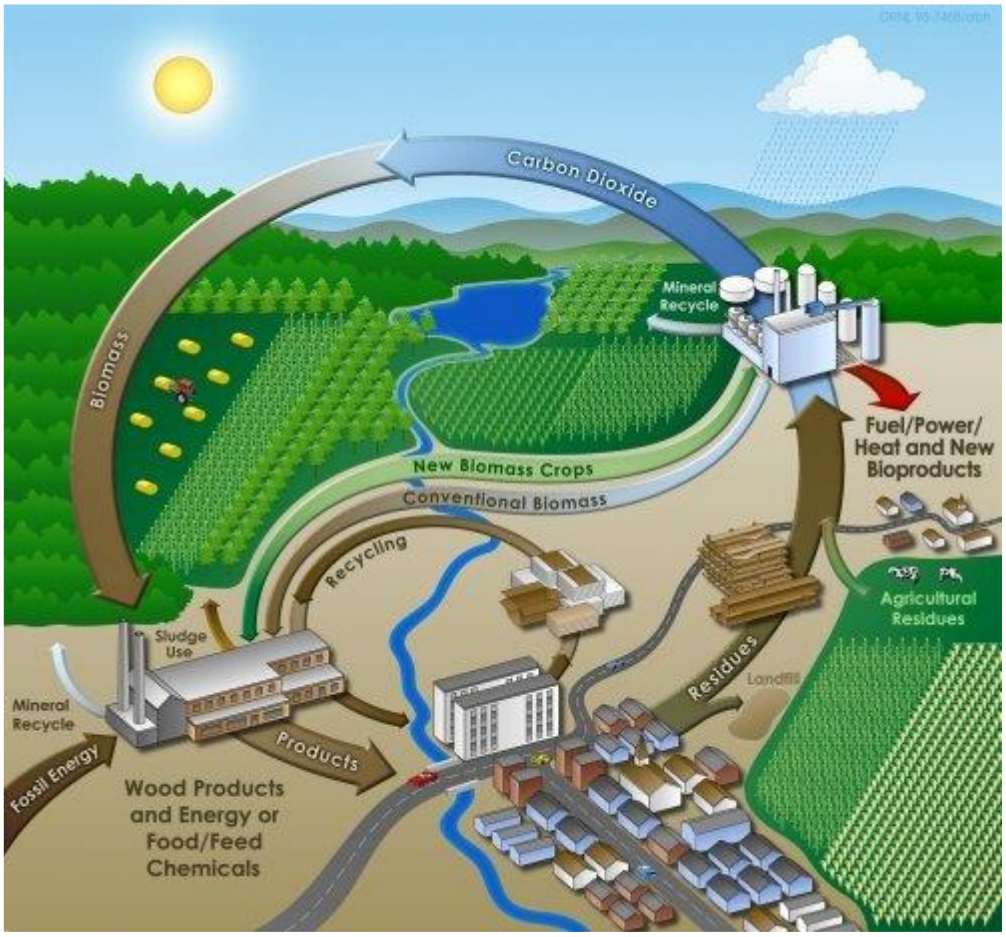


*Figure 1- 3 Biomass Energy Cycle* [20]

The main factors that can result in negative impacts on the environment are production and transportation. This includes agriculture land usage, fertilisers, agricultural machinery used in harvesting the biomass crop and the delivery of the biomass crops to the point of use. Each of these steps or factors results in carbon dioxide and greenhouse gas emissions which can be counterintuitive when using biomass, and therefore they must be considered when evaluating the overall impact on the environment.

Fossil fuel does have an impact on the biomass carbon cycle as shown Figure (1 – 3). The main factors that can cause the impact are as follows:

- The transportation of biomass can contribute to the emission of different harmful gasses to the atmosphere, such as carbon monoxide, volatile organic compounds as well as oxides of nitrogen [21].
- Land usage for agriculture contributes sediment, nutrients and toxic contaminants which can cause water pollution [22].
- Excessive use of chemical fertilisers in agriculture can result in different environmental problems [23].
- Finally, modern agriculture often includes the use of different machinery which also emits harmful gasses.

Each factor contributes to an increase in greenhouse gasses emissions, especially carbon dioxide. Therefore, they must be taking into consideration when assessing the impact of fossil fuel in the biomass cycle.

In order to ensure that the production of biomass as an energy source is sustainable, a cyclical process of release and fixation of the carbon dioxide must be followed during its production and consumption [24].

The idea that biomass-based energy is carbon neutral remains contested in the science and research community. The neutrality of it is highly dependent on the used biomass type and the geographics and timescales considerations.

The strongest arguments in favour for biomass carbon neutrality is because carbon dioxide stored in biomass when harvested, will be classified towards forestry, agriculture and other land-uses emissions of the biomass producing market. Therefore, when biomass is subsequently combusted to be used as energy, the resultant emission would be written off, as they have already been recorded through the plantation phase of the production.

In summary, the resultant $CO_2$ and other possibly harmful gas emissions will not be counted as energy emissions, as the carbon dioxide stored in the biomass has been in-fact absorbed from the atmosphere instead of being produced anew.

On the other hand, the immediate release of greenhouse gasses during the combustion of biomass is considered a carbon debt- which essentially can’t be paid back instantly. This is the counter argument to biomass-based energy sources carbon neutrality. The payback is only feasible through re-growing crops which is a lengthy process and heavily influenced by social and political factors.

The logic behind selecting a short payback period strictly aligns with the current objectives of climate policies which aims to limit greenhouse emission within the next two decades. The objectives' ultimate goal is to avoid a climate tipping point. However, longer payback period can be useful as they allow analysis of the full cycle of the greenhouse gasses, specifically carbon dioxide [25].

Biomass fuels contain lignin, hemi-cellulose, and cellulose components. The latter's molecular weight varies with respect to its structure. While hemi-cellulose doesn't have a defined molecular structure, it tends to have a lower weight than cellulose, which increases its reactivity and reduces its thermal stability [26].

## 1.5 Energy in Kingdom Saudi Arabia

The Kingdom of Saudi Arabia (KSA) is the largest crude oil producer in the world. This fact had a huge impact on the country's socio-economic development over the past century [27]. This change had caused a population boom at around 3.4% growth year on year, as well as the scaling up of living standards. Also, an influx of expatriate workers to the country alongside internal immigration to urban regions from rural areas had increased the urbanisation of the country [28]. All these factors have caused a dramatic increase in energy and electricity demand in the kingdom, as it is expected to grow at about 7% annually in the next decade [29]. Currently, the electricity peak demand stands at 55 GW, and is projected to increase to 120 GW by the year 2032 [30]. This demand is currently only met with fossil fuels as the primary energy source.

KSA is heavily dependent on fossil fuels and crude oils for energy production. More specifically, natural gas and petroleum products [31].

There is a political will to change the current situation in KSA. The Saudi Kingdom's Vision 2030 aims to initially generate 27.3 DW via renewable energy sources by 2024, and increase it to 58.7 GW by 2030 [32].

Due to the unsustainability of the current situation, the KSA government had launched a new initiative to tackle this challenge. The initiative is called the 'King Abdullah City of Atomic and Renewable Energy' or KACARE for short. Its aim is to establish the renewable energy sources through the full dependency on science, research, and industrial participation. KACARE targets that 72 GW of the country's electricity must be generated from various

renewable energy sources by2025, this includes waste-to-water energy (WTE), solar, wind or nuclear energy sources [30].

Additionally, the NREP (National Renewable Energy Program) is a strategic program by the movement that is governed under Vision 2030 and the King Salman Renewable Energy Initiative. It is working to maximise the potential and adaption of renewable energy sources in the country [33].

The program has set out a clear roadmap towards achieving the goal of diversifying energy sources in each region of the country while enrich economic stability and development in the kingdom through the Vision 2030 initiative. the vision aims to establish a renewable energy industry and support the advancement of the research within this promising sector, while fulfilling the country's commitments to reduce carbon dioxide emissions, and maintain a strong and stable economy [33].

## 1.6 Date stones as a renewable energy source

Biomass resources can entail plants and crops by-products, wastes and residues. The date palm is a good example of this waste, as its waste can be used as a by-product and for energy. KSA is the main palm date producer in the middle east alongside various countries in the Arab Gulf region. Therefore, this resource represents a big opportunity for biomass energy utilisation, especially given the renewable energy targets discussed above.

Palm tree cultivation is suitable for KSA's climate conditions. Palm trees are very distinctive as they have long height, no branches, and huge leaves, as shown on Figure (1 - 4).

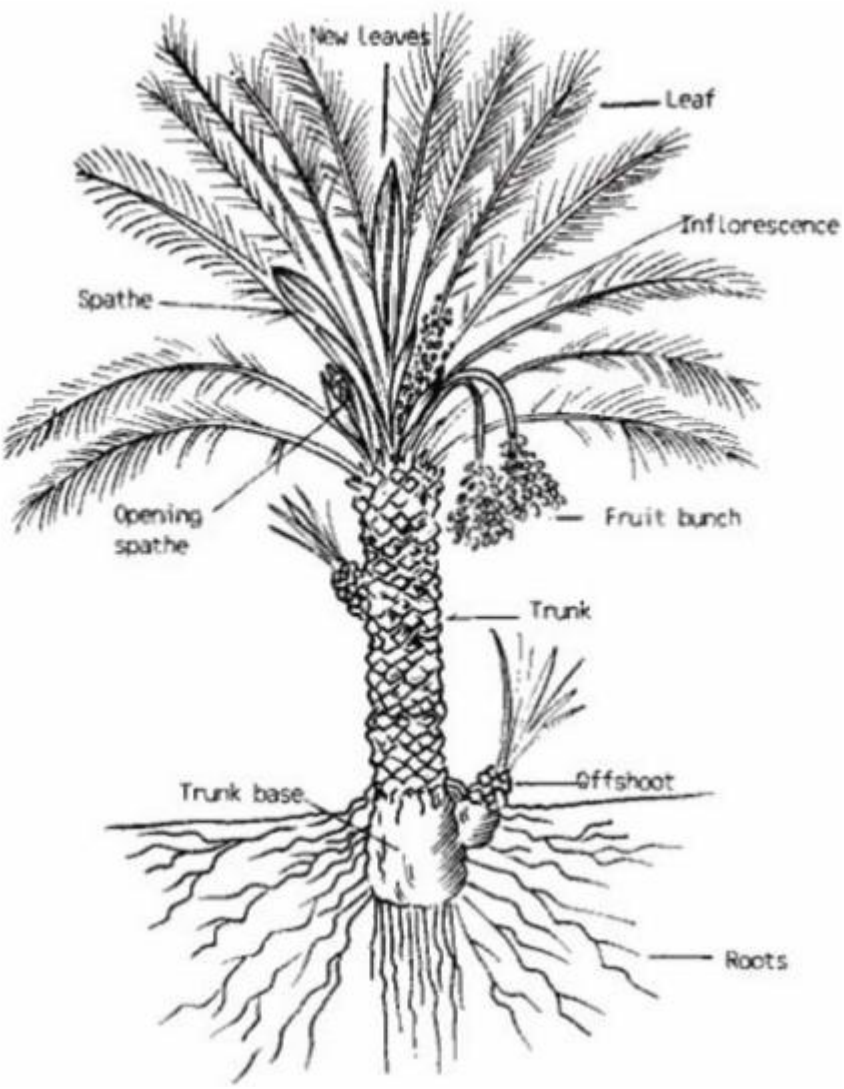


*Figure 1- 4 A date palm tree [34].*

Studies had shown that KSA already contains a large amount of date palm trees. It is estimated to be about 30 million palm trees across the various regions of the country, as shown on Figure (1 – 5) [35]. Date palm trees can sustain a lifetime of up to 100 years or more according to Ali [36].

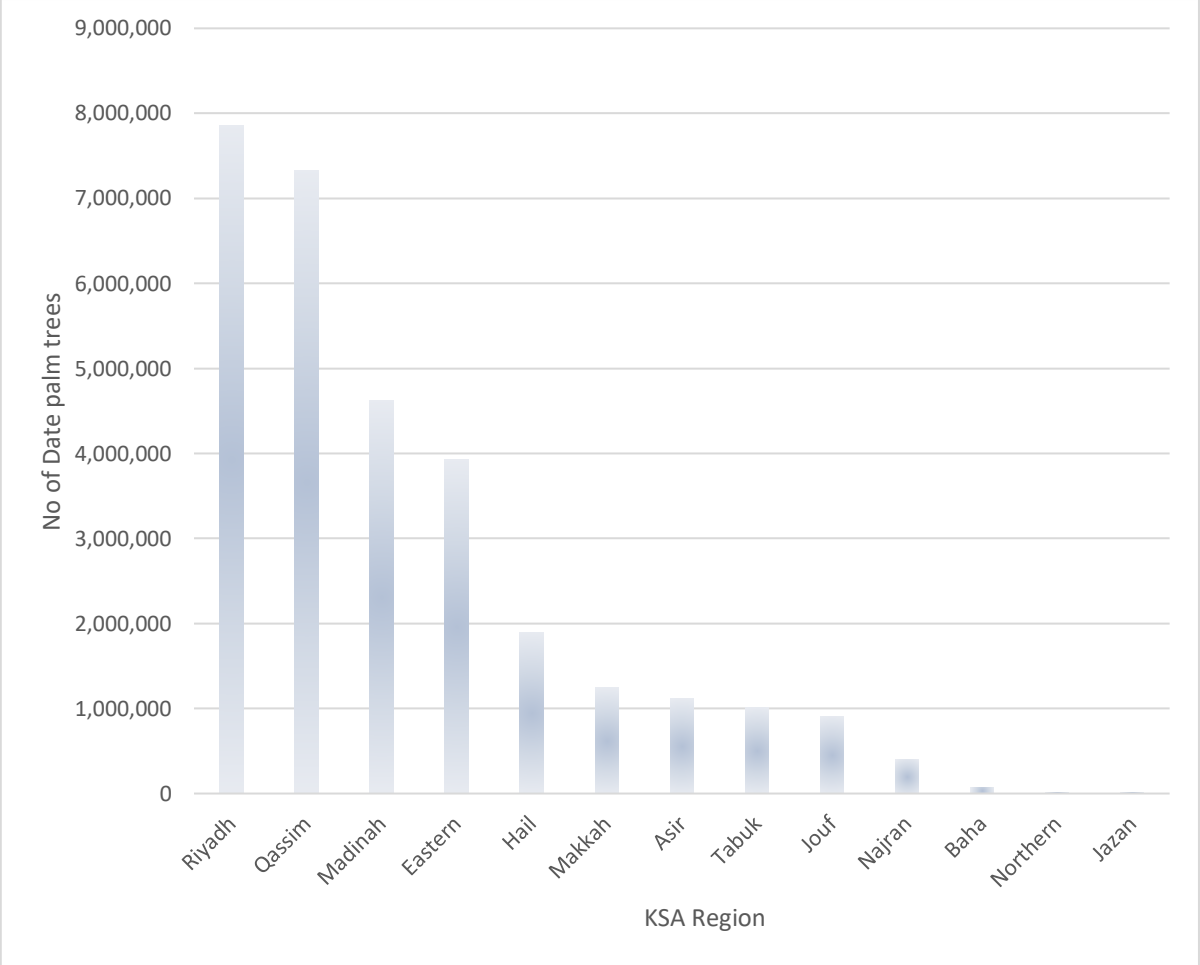


*Figure 1- 5 Production of Saudi date palm trees by states in KSA in 2018* [35].

Date palm trees require specific maintenance to ensure consistent production and must be pruned and cleaned annually. This maintenance process results in about 20 kg of dry leaves and waste every year [37]. The resultant waste includes leaves, rachis, fruit stalk pruning, and date palm residues (trunk) as shown on Figure (1 – 6). All this waste does not have any economic value at present, and therefore is usually destroyed by burning (or sometimes used in cooking in local rural industries). However, this material now has the potential of having a major economic and environmental benefit for the country, and the Saudi economy.


*Figure 1-6: Waste materials of KSA date palm trees*

Previous attempts by the KSA's ministry of agriculture to utilise the palm date trees waste as organic fertilisers has been undertaken. The ministry had erected research centres to achieve this goal, however they cover a relatively small amount of the produced waste nationwide. There is therefore a lack of fundamental understanding of the nature of this material, plus how it might be deployed in emerging technologies such as fluid bed gasification.

It could be argued that KSA's date palm residue can be utilised a main type of biomass solid fuel and subsequently used to produce energy across the country. This study will aim to assess the feasibility of using such residue in the biomass gasification process, and therefore they will be used as the primary feedstock material in the experiments.

The area of the Kingdom is about two million $km^2$, sand covers half of the sedimentary area in Saudi Arabia, and one third of the area of the Arabian Peninsula, and the total area of deserts in the Kingdom is approximately 780,000 $km^2$. The country's land is predominantly drought

without permanent rivers or streams. Although the dry valleys scattered in most parts of the country overflow with water after rainstorms, the actual value of the water is weak, either due to evaporation or due to seepage into the ground [38].

In 2021, Prince Muhammad bin Salman bin Abdulaziz Al Saud, Crown Prince and Deputy Prime Minister, announced that the "Saudi Green Initiative" and the "Green Middle East Initiative", which will be launched soon, will chart the Kingdom and the region's direction in protecting the land and nature and placing it in a roadmap. It has clear and ambitious milestones and will make a strong contribution to achieving global targets.

The Kingdom and the region are facing many environmental challenges, such as desertification, which poses an economic threat to the region (as it is estimated that $ 13 billion drains from sandstorms in the region every year), and air pollution from greenhouse gases is estimated to have reduced the average lifespan of citizens by an average. A year and a half, through the Saudi Green Initiative, we will work to raise vegetation cover, reduce carbon emissions, combat pollution and land degradation, and preserve marine life.

A number of ambitious initiatives will include, most notably the planting of 10 billion trees within the Kingdom of Saudi Arabia in the coming decades, equivalent to rehabilitating about 40 million hectares of degraded land, which means an increase in the area covered by the current trees to 12 times, representing the Kingdom's contribution by more than 4%. In achieving the goals of the global initiative to reduce land degradation and fungal habitats, and 1% of the global target to plant a trillion trees.

The Saudi Green Initiative will also reduce carbon emissions by more than 4% of global contributions, through renewable energy projects that will provide 50% of electricity production in the Kingdom by 2030, and projects in the field of clean hydrocarbon technologies that will wipe out more than 130 million tons. Of carbon emissions, in addition to raising the percentage of waste diversion from landfills to 94%[39] .

In order to promote this initiative, farms need electrical energy to operate it, and thus it becomes costly due to the large geographical area of the Kingdom of Saudi Arabia. While when using biofuels and the feasibility study of that (Chapter Seven), we believe that it can be used for energy production and the success of this project.

## 1.7 Study Objectives

The focus of this thesis is the utilisation of date palm waste as a biomass fuel source, and its feasibility in the gasification process. The discrete research are:

1) To provide data on the fundamental performance of this material via thermogravimetric analysis.
2) Study the effects of the parameters of fluidised bed hydrodynamic on the performance and thermochemical efficiency of a laboratory-scale gasifier.
3) Determine the effectiveness of cost-effective catalysts for the improvement of biomass gasification yield when using date stones as feedstock.
4) Determine the effectiveness of cost-effective catalysts for the improvement of biomass gasification yield, tar cracking, carbon conversion, and product gas composition. when using date stones as feedstock.
5) Evaluate the relationship between the thermogravimetric behaviour of the feedstock (e.g. activation energy) measured at a very small scale, versus the empirical behaviour inside the gasifier at far greater scales. This was achieved using two gravimetric rigs under single batch versus steady state conditions.
6) Evaluate the feasibility of using date palm residues in KSA as a biomass feedstock for the biomass gasification process, with the ultimate goal of supporting the renewable energy goals in the country.

## 1.8 Research Hypothesis

Biomass gasification is still under commercial development, with an aim to understand syngas composition and optimisation. The study herein will analyse different types of fluidised bed reactors, namely bubbling fluidised bed reactors.

The research hypotheses of this study is to prove of catalysts addition on the pyrolysis activation energy, and the performance of the gasification process, when using biomass as the main feed for the process. Different catalysts delivery methods were studied, either individually, or as mixture with sand at different ratios, with respect to the availability and physical properties of the used catalyst.

This study involved experimental investigation, with a focus on the gasification and pyrolysis of biomass. The objectives of the experiments are:

- Utilise a fluidised bed reactor, with built-in load cells used for the dynamic measurement of biomass conversion and characterised by rapid heating rates at high flow rates and uniform temperature distribution inside the bed.
- Study the kinetics of date stone pyrolysis in non-isothermal conditions and at low heating rate using fixed bed thermogravimetric analysis (TGA) using different kinds of catalyst and different ratios.
- Study the effect of operating conditions (e.g. temperature, equivalence ratio, different ratio of catalyst and particle size of biomass) in a bubbling fluidised bed on the produced syngas.
- Study the economic feasibility of using date stone in KSA as a source of energy.

## STRUCTURE OF THE THESIS

### CHAPTER 1

In this chapter, the general overview of energy conservation and climate change is highlighted. Energy resources are discussed, and alternative approaches to reducing sources contributing to climate change are presented. The aims of the current research, hypotheses, and thesis structure are also described.

### CHAPTER 2

The concept of the gasification process and its reactions are described. The influence of gasifier operating conditions on the product gas is presented. The technologies used in the gasification process are explained; these include fixed bed and fluidised bed. Catalysis overview and Steps in heterogeneous catalytic reactions are described.

### CHAPTER 3

The materials and methods to characterise the biomass and silica sand are explained. The method of determining the minimum fluidised bed velocity and terminal velocity is presented. In addition, the methods of Thermogravimetric analysis (TGA) are described in detail.

CHAPTER 4

In this chapter, the details of the experimental rig are described. The procedures that were used during the gasification test are explained. The mass balance model and equations used in gasification performance are presented.

CHAPTER 5

A study of the catalysed pyrolysis of date stone biomass in fixed bed conditions including the kinetic study in a fixed bed TGA, under non-isothermal conditions, are presented in this chapter.

CHAPTER 6

This chapter displays and discusses the experimental results obtained from this study from date stone gasification. In addition, the effect of operating conditions on gasification performance is discussed.

CHAPTER 7

The economic feasibility of using date stone as a source of clean energy in Saudi Arabia is studied by choosing one region as a case study and use gasification to produce energy from the waste of the date palm.

CHAPTER 8

Concludes the findings from this study and recommends further work to be done in the field of pyrolysis and gasification to improve the gas yield and heating value.

## Chapter 2

# Literature Review

## 2.1 The Gasification Process

Gasification is a thermo-chemical process used to convert biomass fuels (date stone in this study) into a fuel gas. For example, 'date stone' is the biomass fuel tested in this study. Subsequently, It can be used to produce chemical products and the generation of both heating and electricity [40].

Biomass gasification is considered amongst the methods to enhance biomass based energy production's efficiency as it allows biomass utilization across a variety of feedstocks [41]. It has become more important as a mean of converting low energy-density such as biomass feeds or into a transportable high value gas for heat and power generation, chemicals and fuels [42].

The Biomass gasification process consists of three stages. The first stage is 'upstream processing' which ensures the biomass's size reduction to a suitable a particle size and drying it to an appropriate moisture level. The second stage involves the actual gasification process which will be explored in further details in this chapter. The final stage is the downstream process and the clean-up of the gas product [43].

The most important stage is the gasification step which is considered to be the heart of the entire process. It utilises a thermal-chemical reaction to convert the biomass into combustible gas in a controlled environment, while using different gasifying agents such Oxygen, Carbon Dioxide or in the presence of air. Therefore, the gasification process is undertaken in a gasifier, in which the biomass undergoes a sequence of physical and chemical transformations as well as combustion through oxidation.

Generally, gasification is split into four steps: drying (endothermic reaction), pyrolysis (endothermic reaction), oxidation (exothermic reaction), and reduction (endothermic reaction) [44]. They are shown in Figures (2-1) and (2-2) and explained further as following:

- **Drying:** In this stage, biomass's moisture is evaporated by drying. The evaporated material contributes to chemical reactions at later stage. According to Hamad et al. between 10-15% of moisture is reduced by drying [45].

- **Pyrolysis:** as mentioned above, this is an endothermic reaction, and it is considered to be the first step in the gasification process. Unlike combustion, pyrolysis occurs in the

absence of oxygen, except for when it is done through a partial combustion, as a way to supply the required energy in these processes [46].

Biomass is heated to remove the volatile components which forms about 70% to 86% of a dried biomass [47]. The pyrolysis yield is dependent on various factors; namely the type of the biomass used, moisture content, particle size, reaction temperature, reaction time, heating rate, carrier gas type and the flow rate of carrier gas, catalyst, and reactor type [48].

At 300 °C and higher, biomass pyrolysis takes place in the same site where the moisture was eliminated from the drying process (the first step), it also produces with $H_2$, CO, $CO_2$, $CH_4$, and tar (devolatilization) which are needed for full pyrolysis [49].

According to Guedes et al.[50], pyrolysis is split into three forms which arise from the operating conditions. The forms are slow, fast and flash pyrolysis.

Generally, about 70% to 86% of the biomass is converted to volatile materials in the form of gases and liquids, and its residual is named char, which consists of carbon and ash [51].

- **Gasification**: This follows the pyrolysis step and utilises the pyrolysis gases, pyrolysis tars, and char residues. The latter is partially oxidised using the pre-existing gasifying agent at high temperatures roughly between 600 °C to 1500 °C, yielding mainly hydrogen ($H_2$), carbon monoxide (CO), carbon dioxide ($CO_2$), methane ($CH_4$) and traces of ethane and propane. Furthermore, tar and char are the outcomes of the incomplete reaction of biomass [52].

- **Combustion**: gasification contains a chain of exothermic and endothermic reactions. Thermal energy which is required for the endothermic reaction is gained from combustion of biomass, gases or char rely on the design of the reactor to maintain thermal efficiency [41].

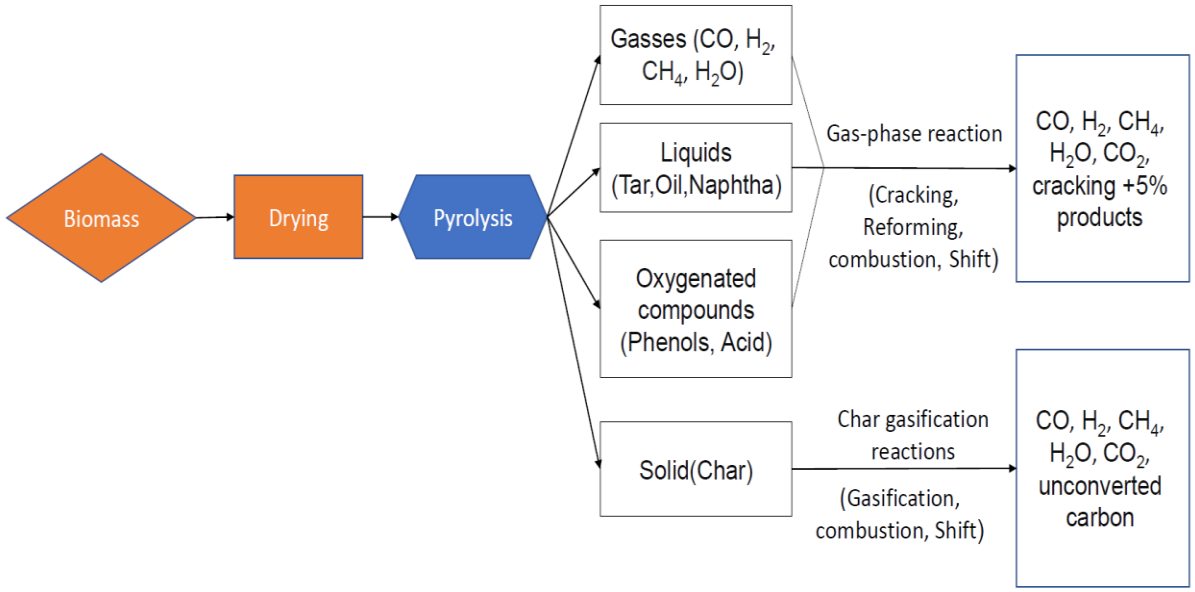


*Figure 2- 1 Schematic steps of biomass gasification [53].*

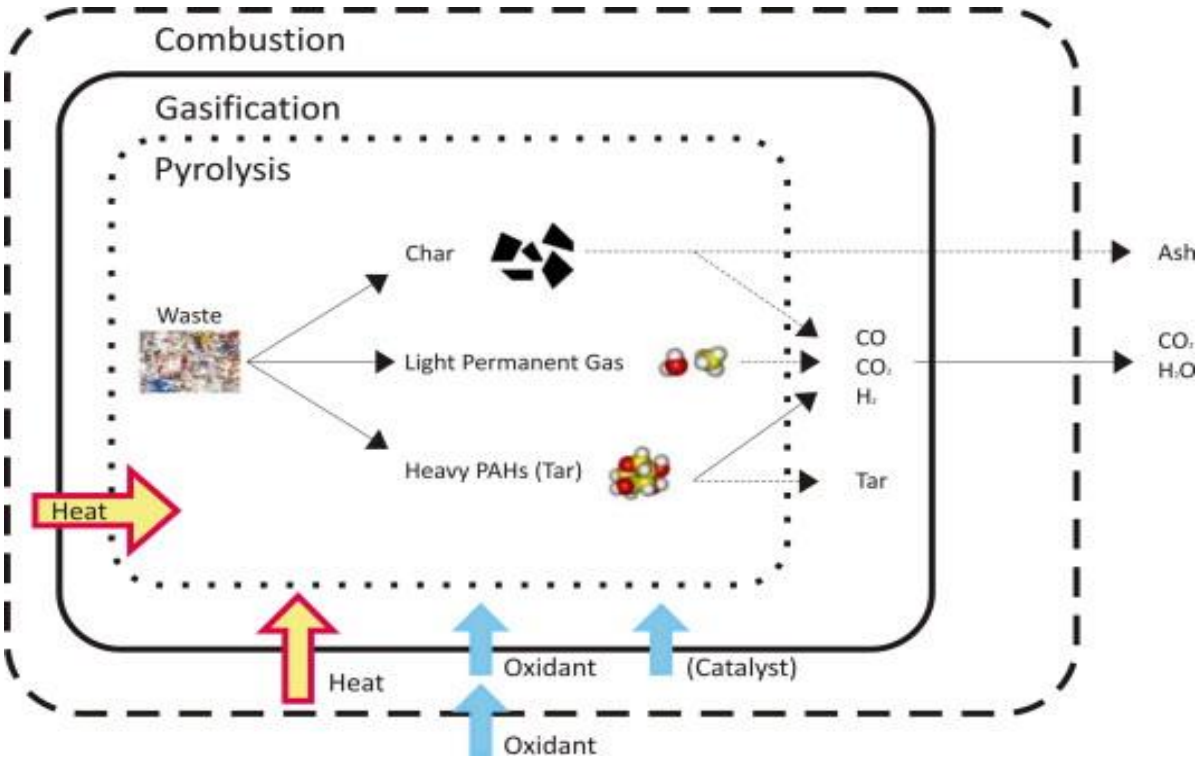


*Figure 2- 2 Schematic representation thermochemical process [54].*

Several thermal processes occur in the gasification step. Moreover, various exothermic and endothermic reactions occur between carbon, carbon dioxide, steam, and hydrogen in the gasifier, if the appropriate operation conditions are met.

As a result of the reversible nature of the gasification reactions, the direction, and conversion of the reactions, a thorough understanding of the reaction kinetics and thermodynamics is needed to maintain the overall efficiency at an acceptable rate. The efficiency and quality of the produced gas relies on several parameters, mainly on thermodynamic equilibrium coefficient of the gasification reactions. The main chemical reactions taking place in the gasifier are described in the next section.

## 2.2 Biomass Gasification Reactions

As mentioned above, the biomass undergoes a sequence of endothermic and exothermic reactions. The contrast of both reaction types creates an environment suitable a complete gasification process at an adequate efficiency. Below is the description of each reaction, while a breakdown of the reactions is showing in Table (2.1). Table 2.1: A breakdown of the biomass gasification reactions occurring in the gasifier.

| Equation | Equation Name | Produced energy kj/mol) | Reaction No |
|---|---|---|---|
| Pyrolysis biomass → char + tar + gases* | | | R1 |
| Tar → $CO_2$ + CO + $H_2$ + $CH_4$ + light H/V | | +131 kJ/mol | R2 |
| C + $H_2O$ → CO + $H_2$ | Water - gas | +131 kJ/mol | R3 |
| C + $CO_2$ → 2CO | Boudouard | +172 | R4 |
| C+ 0.5$O_2$ → CO | Oxidisation Reaction | -111 | R5 |
| C + $O_2$ → $CO_2$ | | -394 | R6 |
| CO + $H_2O$ ↔ CO2 + $H_2$ | Water-gas shift | -47.98 | R7 |
| $CH_4$ + $CO_2$ ↔ 2CO + 2$H_2$ | Dry reforming | +247 | R8 |
| C + 2$H_2$ → $CH_4$ | Methanation reaction | -75 | R9 |
| $C_nH_{m(tar)}$ + n$CO_2$ → (m/2)$H_2$ + 2nCO | | | R10 |
| S + O2 ➔ SO2 | Sulphur oxide | −297 | R11 |

*Table 2- 1 Main reactions in heterogeneous and homogeneous phase during the solid biomass gasification process*

*The produced gasses in (R1) are inclusive of: $H_2$, CO, $CO_2$, $CH_4$, $C_nH_m$.

The chemical reactions of gasification can proceed to different extents depending on the gasification conditions of temperature, pressure, and the feedstock type. The most significant gasification reactions are Water-gas reaction (it is considered a principal gasification reaction, Due to its products CO and $H_2$ gases), Boudouard reaction (the reaction of carbonaceous raw materials with carbon dioxide to produce carbon monoxide [55]), water gas shift reaction (an important reaction in the industry which hydrogen is produced from water or steam while carbon monoxide is converted into carbon dioxide [56]), Methanation reaction (a chemical reaction that converts carbon monoxide to methane [57]).

### 2.2.1 Water-gas reaction (R7)

This a heterogeneous reaction that occurs between carbon and steam at a high temperature. The reaction produces carbon monoxide and hydrogen as follows:

$$C + H_2O \rightarrow H_2 + CO$$

It is worth mentioning that this reaction is an endothermic one, therefore it needs continuous heating to maintain the produced gasses.

### 2.2.2 Boudouard reaction (R13)

It is a heterogeneous reaction between carbon dioxide and carbon molecules at high temperatures, typically higher than 700°C at atmospheric pressure:

$$C + CO_2 \rightarrow 2CO$$

Furthermore, the product of this reaction increases when increasing the temperature above 700 °C [58].

### 2.2.3 Water-gas shift reaction (R8)

This is a homogeneous reaction between carbon monoxide and water in vapour state ($CO+H_2O \leftrightarrow CO_2+H_2$). This reaction is exothermic and used to increase the hydrogen content and consume carbon monoxide in the product gas.

### 2.2.4 Methanation reaction (R12)

In this reaction, methane is produced from hydrogen and carbon or carbon dioxide. This reaction is categorized as exothermic. However, the best condition for this reaction is high

pressure and low temperature. methane is used in combustion processes due to its higher heating value comparing to carbon monoxide or hydrogen [42].

### 2.2.5 Steam methane reforming reaction (R9)

This reaction is a homogeneous (gas-gas), highly endothermic reversible reaction.

The diagram on Figure (2-3) shows the above reaction sequence in the gasifier

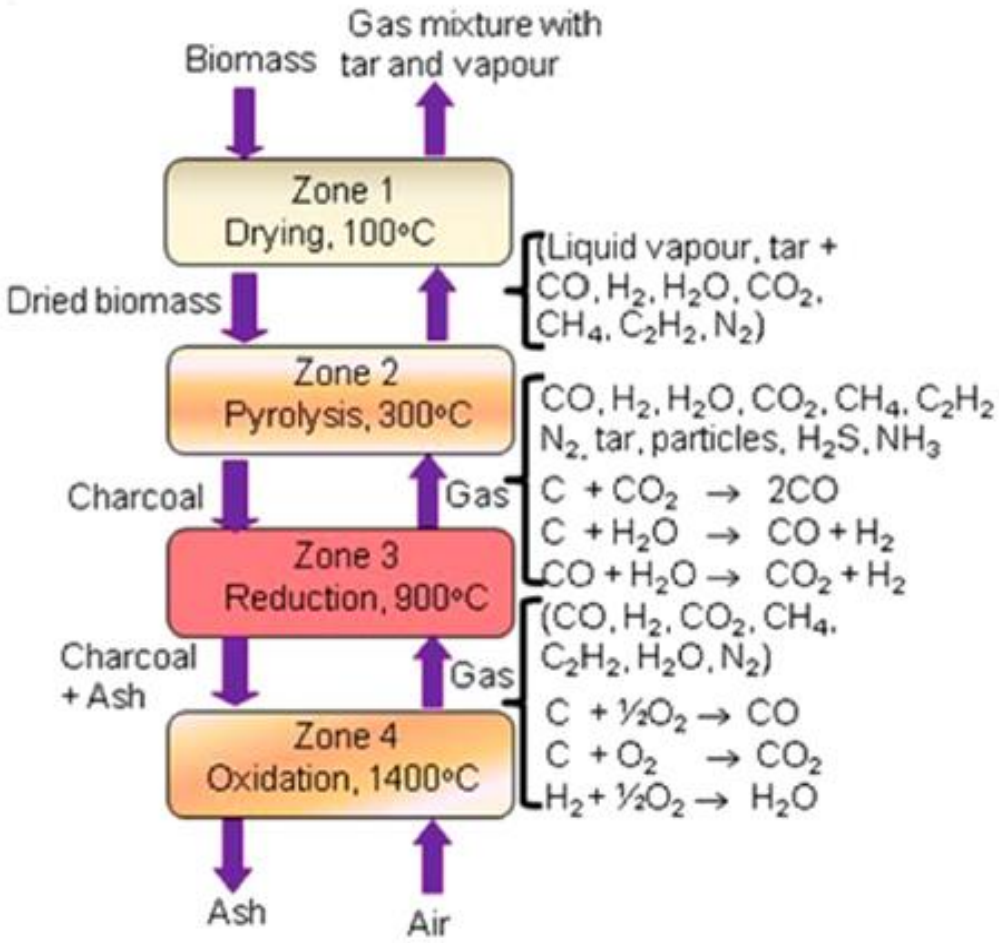


*Figure 2- 1 a diagram of where these reactions occur in a updraft gasifier [12]*

## 2.3 Biomass gasification products

Gasification and combustion are defined as the chemical processes which converts carbon-based materials (e.g. biomass) into either chemical feedstock or gaseous fuels. The produced material would consist of both product gasses and bio-syngas, as shown in Figure (2-3).

The product of biomass gasification exhibits differences in terms of heating value. Unlike combustion, the energy stored in the chemical bonds is not rapidly released. The process's products are described below.

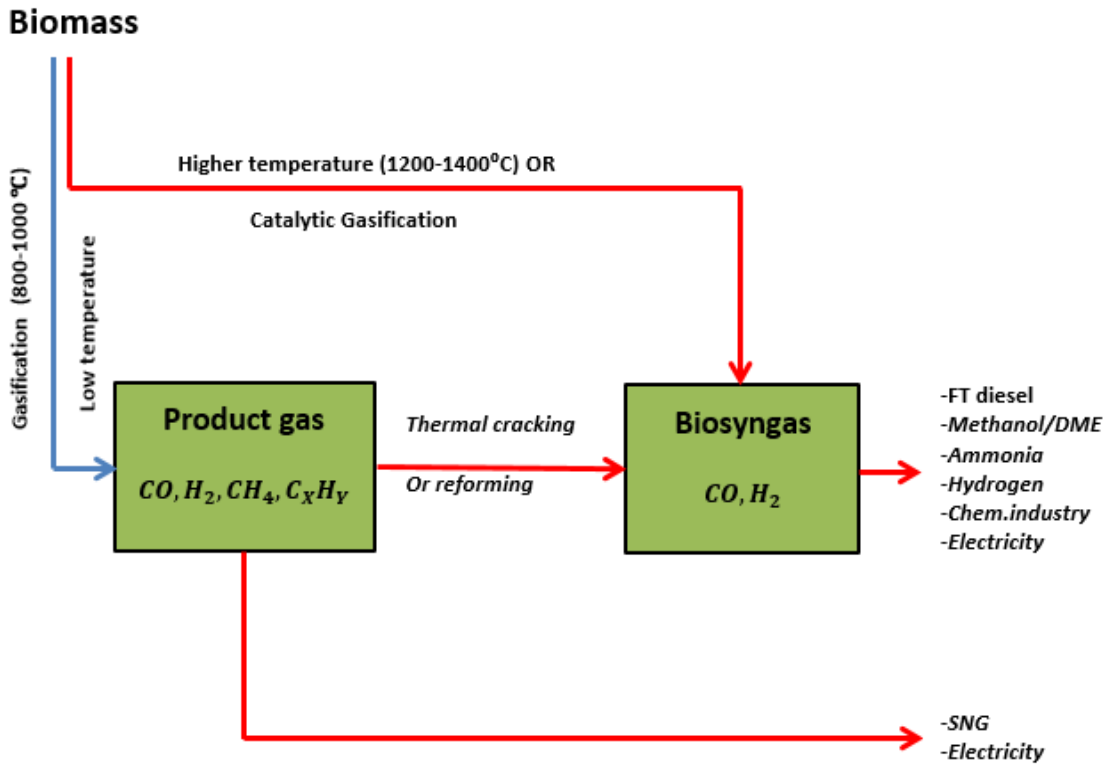


*Figure 2- 3 The main difference and their typical applications between 'product gas' and 'bio-syngas'.*

- **Product gas**: this is produced when the temperature in the gasification processes is less than 1000 °C. It contains CO, $H_2$, $CH_4$, $C_xH_y$ aliphatic hydrocarbons, benzene, toluene, and tars (beside $CO_2$ and $H_2O$).

$H_2$ and CO in the syngas contains approximately 50% of the energy, while the rest is contained in $CH_4$ and higher (aromatic) hydrocarbons [59]. Product gas used mainly in home heating and electricity generation [60].

- **Bio-syngas**: There are two different ways that biomass gasification can yield bio-syngas:

  (1) It can be produced via the biomass gasification process without a catalyst present and at high temperature; usually higher than 1200 °C).

  (2) Alternatively, catalytic gasification can be used to produce the bio-syngas instead.

## 2.4 Key factors affecting the gasification process.

Many factors affect the product gas's quality such as composition, gasification performance, and its energy content [61]. These all are dependent on the process's operational conditions, gasifier configuration, and raw material origin [61]. It is important to know which parameters affect the quality of the product gas.

### 2.4.1 Operating conditions

During biomass gasification, the operation conditions play a significant role in the whole process [62]. These conditions affect parameters such as tar formation, carbon conversion, tar reduction, and product gas composition [62]. The most important operating conditions are the bed temperature, ER, gasification agent, feeder location, static bed height, and particle size. The conditions will be discussed in more detail in the following sections.

#### 2.4.1.1 Bed Temperature

Bed temperature is considered among the most important operation parameters. Mainly as it affects both the product gas composition and the resultant heating value [63].

Increasing the bed temperature in the gasifier increases the resultant heating value, the combustible gas content, hydrogen content and gas yield, it has also been shown that increasing temperature reduces the tar content dramatically [64].

Jin Woo Kook et al. [64] reported that tar content can be reduced by several methods, either by increasing the temperature or changing the feeding position. It was observed that increasing the temperature inside the gasifier from 720 °C to 825 °C increases the gas yield from 2.1 $m^3$/kg to 2.7 $m^3$/kg, as the carbon conversion of biomass increases [65]. Furthermore, Maria Cortazar et al. [66] reported that higher temperatures have a positive effect on carbon conversion, gas

yield, and tar removal, and hence the overall increased efficiency of the process. They studied the effects of increasing the temperature from 800 °C - 900 °C and found that the concentration of tar fell from 49.2 $gNm^{-3}$ to 6,7 $gNm^{-3}$.

Moreover, the hydrogen yield rose by 7.28 wt% at 900 °C. From the material mass balance, the amount of CO and $H_2$ increased with increased temperature, due to promotion of endothermic water-gas and Boudouard reactions in the gasifier. $CO_2$ decreases with the higher temperature, while the concentration of $CH_4$ remains relatively stable [67].

Ebubekir et al. [68] investigated the gasification of pine cone particles and wood pellets [68]. Their experiments have shown that the percentage of produced $H_2$ and CO in the yield grows by increasing reactor temperature.

Behashti et al. [69] used Aspen Plus simulators and dedicated FORTRAN subroutines to investigate the bed temperatures further in the range of (600-800°C). They developed a process simulation for gasification of biomass in a bubbling fluidized bed for hydrogen and syngas production, the results showed that the high temperature is more suitable for production useful syngas($H_2$ and CO) [69].

In summary, various research have proven that the bed temperature is directly proportional to the yielded [63][22][23][24][25][26][27]. Therefore, it is vital to ensure that the temperatures are high enough to obtain optimum efficiency.

2.4.1.2 Equivalence Ratio (ER)

The stoichiometric ratio is defined as the minimum ratio of gasifying agent to fuel/biomass which is exactly enough to burn the fuel completely. The difference between combustion and gasification is combustion uses the minimum stoichiometric ratio of gasifying agent to fuel whereas gasification uses gasifying agent fuel ratio lower than the stoichiometric ratio. On the other hand, the ratio between the gasifying agent-fuel ratio of the gasification process and the gasifying agent-fuel ratio for complete combustion is defined as the equivalence ratio [70].

$$\boldsymbol{ER} = \frac{\left(\frac{air}{biomass}\right)actual}{\left(\frac{air}{biomass}\right)\mathbf{stoichiometric}}$$

Pyrolysis, gasification, and combustion represent the various thermochemical zones. The zones can be seen shown when plotting ER against temperature, as shown in Figure (2-4) [71]. According to Ghassemi, [72] the amount of $H_2$ is inversely proportional to the ER due to the presence of $O_2$ in the system, leading to hydrogen oxidation. The ratio of CO in the product increases with increasing ER, however it declines above an ER value of [72], which subsequently lowers the heating value predicted in the product gas [73]. Notably, the production of $CO_2$ is high in cases of higher ER values, due to the formation of a strong oxidation reaction.

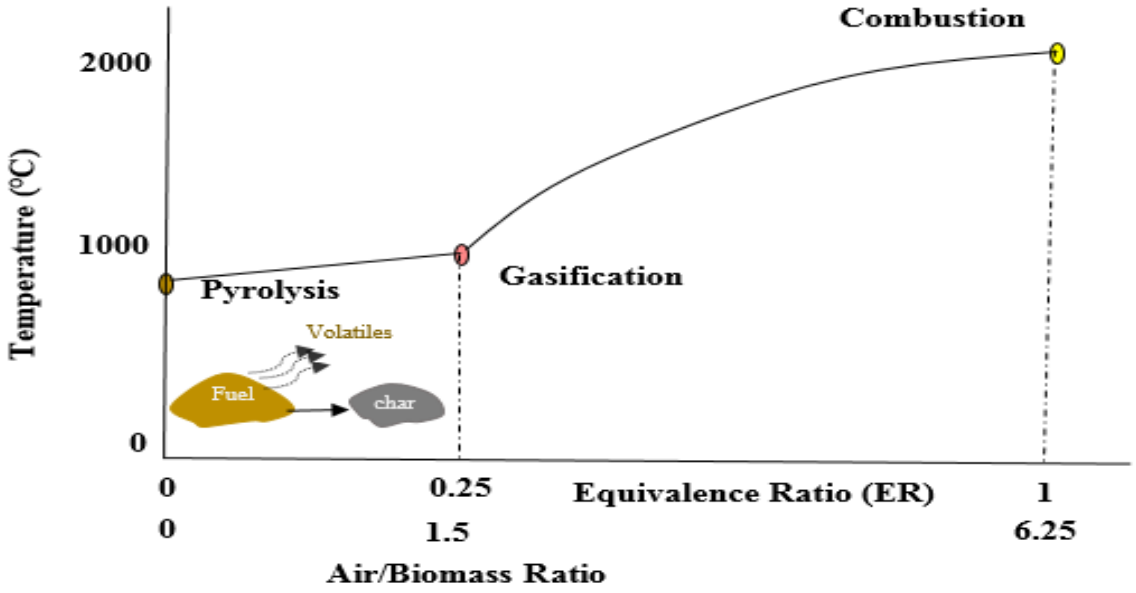


*Figure 2- 4 Equivalence Ratio and Air/ fuel diagram.*

This process at high ER values yields the energy needed to satisfy the endothermic reactions needed for an effective biomass gasification process [71][29]. Hence, the temperature in the gasification zone is low, when the ER is low which is unfavourable for further gas producing reactions so the H2 yield drops. However, the oxidation reactions are strong at a large ER value, which produces more CO2 gas, but less H2 gas. Therefore, the ER can improve product quality to a certain extent.

Pratik et al. examine the effect of ER on the producer used waste wood in biomass gasification to produce hydrogen energy, and found when increasing ER, the concentrations of $H_2$ and CO are also increased, however, $CO_2$ show opposite trends compare to $H_2$ and CO concentrations. moreover, the result shows that the increase of ER will increase the production rate of producer gas [74].

In gasification, the energy required to sustain the endothermic reactions is obtained by limited combustion of the biomass. The equivalence ratio determines the fraction of biomass that is gasified and the fraction that is combusted. The optimum ER should supply sufficient air for partial oxidation of biomass and self-sustain the process without significantly affecting the product gas yield ($H_2$ and CO)[75].

#### 2.4.1.3 Gasification Agent

In the gasification process, numerous gasifying agents are used and have been studied in literature. They often consist of oxygen, air, carbon dioxide, hydrogen in appropriate ratios [76]. The ratio of the gasification agents help categorising the gasification product according to its lower heating value (LHV) which relies on the type of gasifying agent employed as explained in Table (2-2) [77].

*Table 2- 2 Classifications of producer gas according to lower heating value.*

| LHV level | LHV ($MJ/Nm^3$) | Gasifying agent |
|---|---|---|
| Low | Low 4-6 | Using air and air/ stem |
| Medium | High 10-15 | Using $O_2$/ steam |
| High | High 15-20 | Using $H_2$ |

Shayan et al. [78] carried out biomass gasification experiments using wood and paper as a feedstock with four different gasification agents; air, oxygen-enriched air, oxygen, and steam. The results indicate that higher values of hydrogen ares produced when using steam, followed by oxygen, oxygen-enriched air, and air as the gasification agents [78].

According to Mustafa et al. [79] the best gasifying agent is Oxygen but it is more costly. Additionally, the gasification process turns to combustion in the case of a high concentration of oxygen, which leads to the production of “flue gas” instead of “fuel gas”. Various researchers reported that the most optimum gasifying agent from an economical aspect is steam, as it leads to more Hydrogen yield [80]. Pinto et al. [81] studied the effect of the different gasifying agents (Mixtures of air, oxygen, steam, and $CO_2$ with different compositions of two or more components) with a feedstock of waste products (rice husk, straw and plastics). The

results showed that the optimum technical option was a mixture of oxygen and steam, as it was not diluted in nitrogen causing a 42% increase in the heating value [82].

#### 2.4.1.4 Location of Feed.

The distribution of product gas is affected by the location of biomass feeding, according to Sikarwar et al. [83]. Generally speaking, there are two locations of feeding; updraft which allows the fuel to enter from the top of the gasifier and the gasification agent from the bottom [83]. The second is downdraft which both the fuel and gasifying agent enter from the top [83].

There are a few differences in each feeding location set up. In downdraft gasifier feeding, the product from pyrolysis passes through a perforated bed which supplies effective mixing of the product gases [84]. The amount of tar in downdraft is reduced due to cracking through the bed, which increases the yield of $H_2$ and CO [84]. Nevertheless, the downdraft feeding position requires low moisture content; ideally less than 25wt%, in the exhaust dust and ash should be present, this is very attractive due to low tar formation in the product, ease of operation and fabrication [85]. The benefit of using the updraft is its simplicity and high energy efficiency due to active internal heat exchange [86]. Hanif et al. [87] reported the efficiency of the process of updraft could be high as a result of low temperate of the product leaving the gasifier.

In summary, the feeding position in the gasifier has a significant impact on the gasification process. It can be concluded that the use of an updraft gasifier is more applicable to the research conducted herein due to the significant amount of previous research, and the proven nature of such rigs in laboratory research.

#### 2.4.1.5 Bed height

The height of the gasifier consists of both the bed and the adjacent freeboard Figure (2-5)[88]. The bed height is an important design parameter, due to the gasification reactions being slower than combustion reactions. A deep bubbling-bed gasifier tends to be used instead of a bubbling-bed in the combustor [46] due to the greater residence time required.

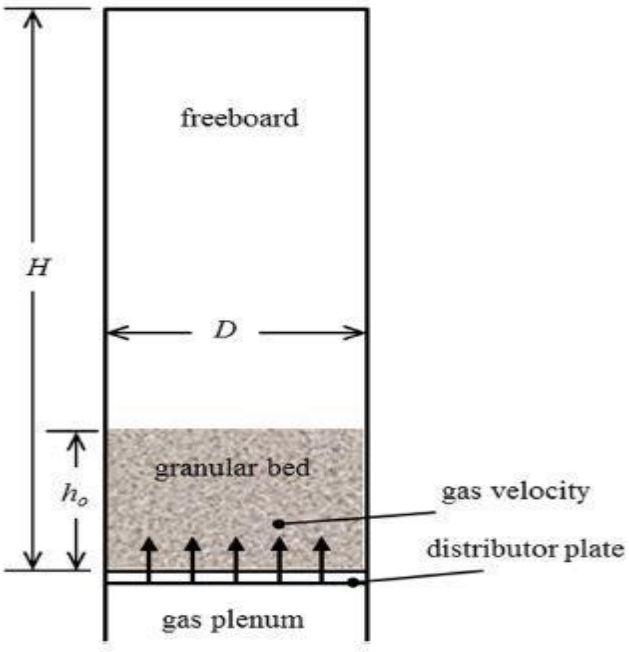


*Figure 2- 5 Schematic of fluidised bed column*

The bed height depends on several technical aspects such as a higher bed results in higher pressure losses, a taller reactor, and issues relating to fluidization dynamics [88]. In the fluidized bed gasifier, the effect of bed height increases the pressure drop which leads to larger gas bubbles and reduced heat transfer [89]. Yupeng Et al. [90] investigated the pressure drop of Geldart's group B particles and minimum fluidization velocity with different column diameters and bed heights. They reported that at decreasing bed diameters and increasing bed height the wall effect was increased, resulting in a rise in minimum fluidization velocity and pressure. Other research investigated the minimum fluidization velocity increase with increasing bed height [91]. Higher bed height permits longer gas retention time which is considered an advantage. However, when the depth is greater than the diameter, it causes slugging. The advantage of long retention times is that it allows further heat transfer, resulting in an increase in the conversion of tar and char to product gas. Even so, short retention time yields smaller quantity releases of volatile matter which can damage the integrity of the process.

The overall height of the bed in the gasifier plays a major role in the process, and therefore it is important to use an appropriate height to achieve optimum results [88][90][46].

2.4.1.6 Biomass particle size

In gasification process, the energy efficiency (The effectiveness of the gasification process was evaluated in terms of higher heating value of dry gas (HHV), carbon conversion (CC) and cold gas efficiency (CGE) ( as described in Section 4.5) is increased by reducing the particle size, however it also increases the cost of the processes [92]. According to Warnecke, [93] to reduce the particle size for a 5-10 MWe gasification plant, about 10% of the produced energy is required.

Smaller particles results in higher surface area, which improves mass and heat transfer through them [94]. Additionally, the efficiency of gasification reactions, namely the Boudouard reaction, water gas reaction and carbon conversion, are improved as a result of effective heat transfer.

When decreasing the particles sizes, both the hydrogen and carbon monoxide content increase, also it reduces the $CO_2$ content, tar and char [94]. Li et al. [95] used different particle sizes in the range of 0.15 to 5 mm. It was found that small particles produced extra $H_2$ and $CO_2$ and lower $CH_4$, CO when compared to using larger particles.

Low amount of LHV was gained by utilizing large particles sizes [95]. Inayat et al. [96] investigated a downdraft gasifier of wood chips/coconut shells with particles sizes of 5-10, 10-25 and 25-50 mm. The outcomes show a higher gas yield of $H_2$, CO, and $CH_4$, as well as HHV using the 5-10 mm particle size [96].

Similarly, Jia et al. [97] performed the same test but under diverse operation conditions, bed-to-surface heat transfer of three kinds of biomass (Douglas fir, pine, and switchgrass) in a fluidized bed. It also proved that small particles of biomass lead to faster heat transfer and smooth fluidization [97]. Jand et al. [98]found through a study of the influence of particles size in fluidized bed gasification that the quantity of the CO and carbon content in the product was decreased, whilst char and $CO_2$ increased, as a result of the large particles is tended to char combustion, which speeds the freeing of $CO_2$.

Using a research-scale fluidized bed, Fremaux et al. [99] studied hydrogen-rich gas production via steam gasification of biomass with three particles sizes; 0.5-1, 1-2.5 and 5 mm of wood residue at 900 °C. They observed that $H_2$ yield improved using small particles due to the heat transfer resistance decreased with the smaller size of biomass [99]. Other studies examined the

effect of different particle sizes of fruit residue on ranges of higher than or equal to 0.2mm and lower than 2mm on producer gas, carbon conversion and high heating value in a fluidized bed at 800 $^{o}$C. Results indicated that the $H_2$ and CO compositions, producer gas yield, heating value and carbon conversion increased when particle size decreased [100].

Various research and experiments have shown that using smaller particles in the gasification process yields more efficiency (HHV, CC and CGE) [92][48][49][50][55]. The main reason is that crushing the particles to smaller sizes, ideally between 1 – 5 mm in diameter was to offer much higher surface area allowing more efficient mass and heat transfer processes [92][48][49][50][55].

### 2.4.2 Gasifier Configuration

In gasification processes, reactor design is critical for composition, efficiency, and heating value of the product gas, also for the formation of tar. According to Siedlecki et al. [101] there are three types of gasifier used in biomass gasification. The first type is fixed-bed gasifiers, which are split into three further types based on the feeding position; updraft, downdraft and cross-draft gasifiers. The second type is the Entrained flow gasifier, while the third type is the spout fluidised bed gasifier. The latter consists of different set ups based on the bed type, namely, bubbling or circulating fluidised bed. The beds types are discussed further below.

#### 2.4.2.1 Fixed Bed Gasifiers

The fixed bed gasifiers is considered to be the simplest and oldest technology in this field [102]. These have been used and studied, mostly for small scale production, due to simplicity of construction and relatively simple operation, whilst yielding high thermal efficiency and lower pre-treatment of the biomass feedstock [103].

From the reactor technology aspect, the fixed bed has a large temperature distribution across its design [104]. This results in a longer time for heating up, ease of scale-up, low specific capacity, hot spots and ash fusion. It is complicated to maintain consistent operation temperatures while keeping sufficient gas mixture in the bed. As a result, the gas yield is unpredictable. As mentioned, the types of the fixed bed gasifiers are the updraft, downdraft and cross draft ones due to the place where the gasifying agent enters the gasifier [105]. The types are discussed in more details below:

- **Updraft gasifier**: The feedstock and gasification agent (air or oxygen) shift in the cross direction [106]. The raw material (i.e. biomass) feeds from the upper point in the gasifier while the Gasifying agent enters from the distributor located in the downside of the gasifiers.

  Updraft is considered to be the simplest gasifier and has a low-cost process [106]. In this method as illustrated in Figure (2-6), the combustion (Oxidation) takes place at the bottom, which is the highest temperature in the reactor. Further, on the top of the gasifier, the drying and pyrolysis processes occur [106]. It is important to ensure the removal of moisture from the feedstock by using hot product gases, which exit from the top of the gasifier.

  The advantage of updraft gasifier is its ability to operate with different raw materials [105].According to Wang et al. [107] one of the main drawbacks of the updraft gasifiers is its high tar in syngas, low syngas yield and extended start-up time.

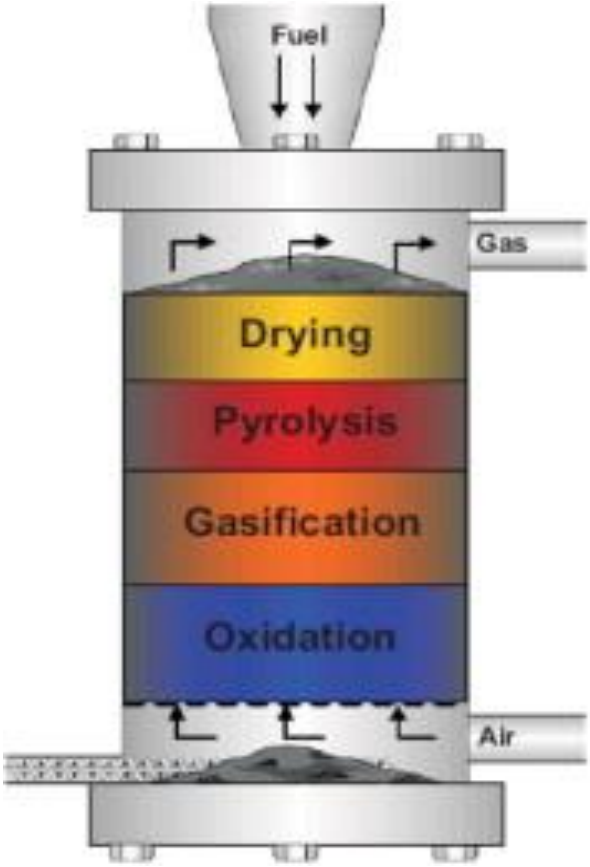


*Figure 2- 6 Fixed-bed updraft gasifier*[266]

***Downdraft fixed bed gasifier**:*

The biomass (fuel) and gas enters in the same direction and the product gas flows out from the bottom as shown in Figure (2-7) [108]. The amount of tar in the product in the updraft gasifiers is the main problem in this gasifier, this can be overcome by inserting the gasifying agent above or at the oxidation zone in the gasifier [108].

According to Sayigh, [109] the products from both the down, especially CO, $H_2$, $CH_4$ and $CO_2$ are comparatively clean and without or less quantity of tars. which allowed to use in the application in heat and power generation using gas turbines[109]. The product gas tends to need cleaning as it runs the risk of having contaminates such as ash and fine particles [110]. According to Chandolias et al. [111] the downdraft process is less thermally efficiency when compared with updraft as a result of the product from devolatilization do not go through the highest temperature zone of the gasifier.

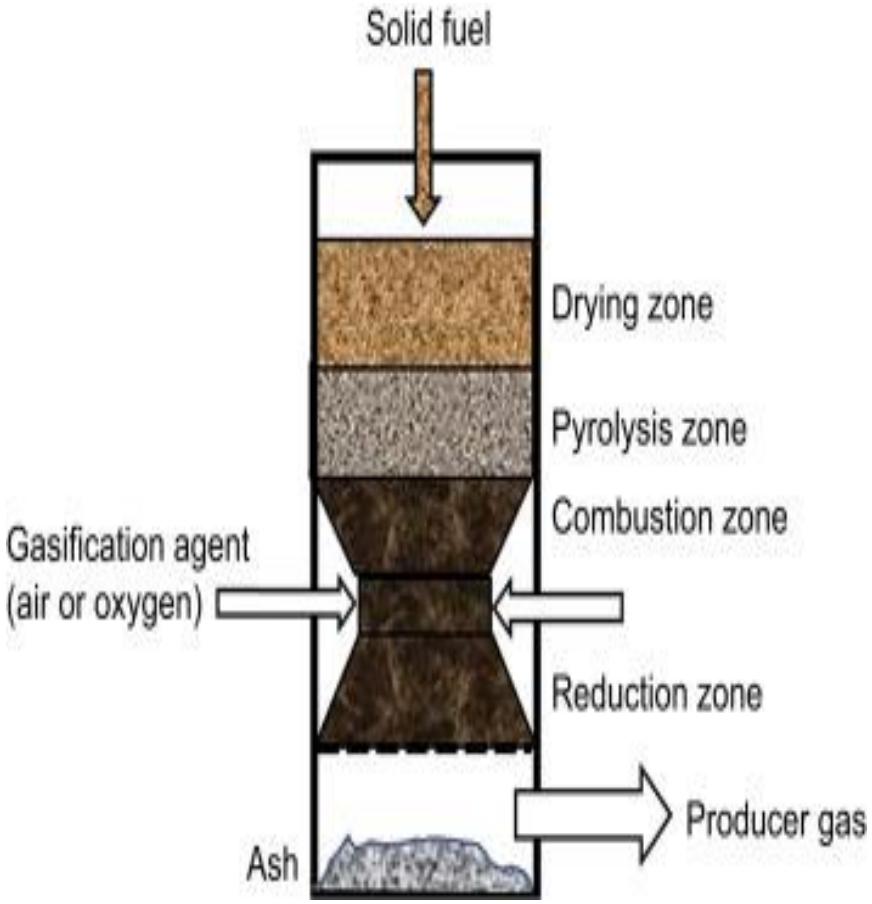


*Figure 2- 7 Sketch of the downdraft fixed-bed gasifier*[267].

**Cross draft gasifier**:

The feed (biomass) is fed from the top of the gasifier and the gasifying agent from the side as shown in Figure (2-6). The idea of cross draft is the fuel shifting down the different zones in the gasifier (drying, pyrolysis) and finally gasified whilst the air exits from the other side of the gasifier [112].

The product gas exits almost at the same level of its entrance [112]. The advantage of the cross draft gasifier is its short start-up time relative to both the updraft and downdraft gasifiers, however, it is only applicable for low volatile content (e.g. charcoal) [113] [114].

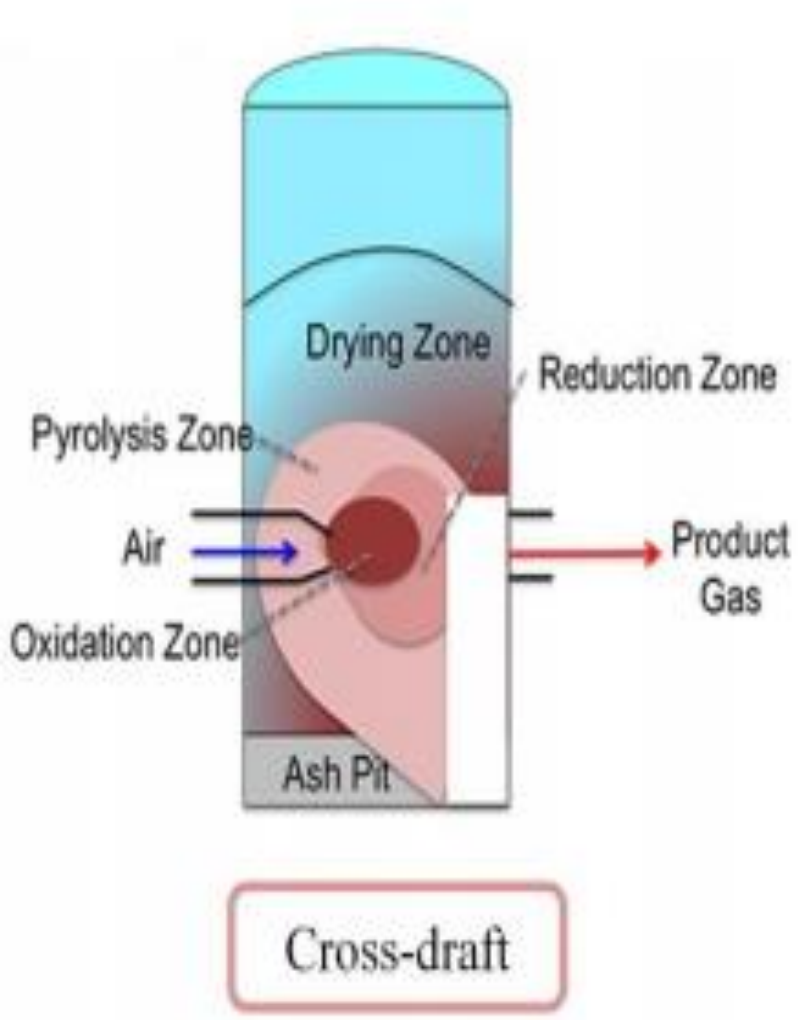


*Figure 2- 8 Sketch of the Cross-draft gasifier* [268].

2.4.2.2 Fluidised Bed Gasifiers

Fluidised bed gasifiers employ combustion of a solid fuel in static material bed such as sand, which will be tested in this study, is the bed is fluidised by the upward gas flow [115]. The hydrodynamics in a fluidised bed gasifier causes strong mixing for new particles with old ones and promotes even temperature distribution throughout the bed [116]. Fluidised bed gasifiers are used in large scale applications for biomass thermochemical conversion as a result of their capability for high heat and mass transfer rates, [117]. Fluidisation is used in different applications like pyrolysis, gasification, and combustion of various feedstocks such as biomass [118].

The reason for using this type of gasifier is their fuel flexibility resulting from good mixing of feedstock and oxidant to ensure efficient heat and mass transfer, and their ability to deal with small particles [119]. other author finds the advantages of using fluidised bed are feeding flexibility, scalability, good mixing capacities, high heat and mass transfer rates, and high reaction rates and conversions [120]. Moreover, fluidised bed gasifiers are used to convert biomass, particularly agricultural residues, into energy because they possess many advantages. These include: high gas-solid interaction; a high degree of random movement; good mass and heat transfer characteristics; effective temperature distribution; increased volumetric capacity and heat storage [121].

The efficiency of heat exchange in a fluidised bed reactor and temperature control is better when compared to fixed beds [122]. Belgiorno et al. [123] stated that the fluidised bed performance is about five-times that of fixed bed gasifiers. Due to high mixing rates in a fluidised bed gasifier, there are no different reaction zones, on the contrary to fixed bed gasifiers. Moreover, the fluidised beds are understood to give effective thermal conversion of various kinds of biomass fuel because of enhanced mass and heat transfer for the reactants [124]. As mentioned above, the fluidised bed gasifier is classified as follows:

- **Spout fluidised bed gasifier**

The spout fluidised bed structure is shown in figure (2-7). Historically, this configuration has been used in the chemical and petrochemical industry [124]. More recently, they have been extended to different thermochemical processes such as gasification, combustion, and pyrolysis [124][125].

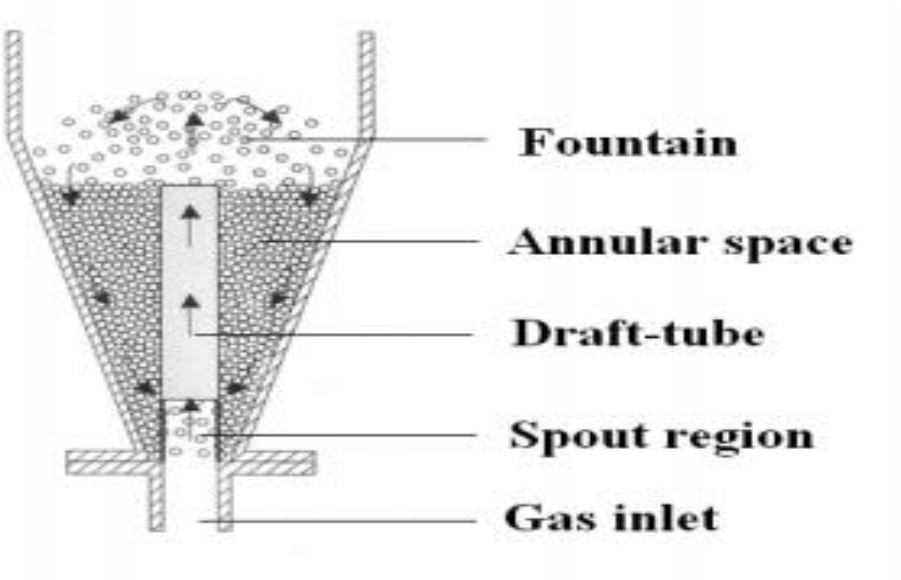


*Figure 2- 9 Spout Fluidised Bed Reactor* [269].

A typical spout bed includes a conical vessel with an orifice in the base of the conical section. In the spout bed, there are two regions, the spout, and the annulus. The spout is centric of the conical vessel where the particles in a low-density phase are suspended as a result of high fluid velocity which enters from the office [126].

After reaching the highest level of the reactor (above the bed), the particles fall onto the annulus, which is made of high particle density, resulting in a slow downward motion. Thus a systematic cyclic pattern of particles is founded, with contact between the fluid (biomass) and particles, and with very effective hydrodynamics [127][128].

The main difference between the spout fluidised bed and the fluidised bed is the dynamic behaviour of the solid particles in each reactor [129]. In the spouted bed, a consistent motion is established with effective connection between the gas and the solids involved. The benefit of using a spout bed is its ability to handle high ash content ensuring appropriate amounts to gasify different fuels types [130].

Moreover, it has the capability to accommodate various fluidisation velocities without risking severe slugging, which minimizes the capacity of the gasification system. Furthermore, raising the fluidization rate leads to accelerate the fluid-solid contact in the annular regions and reduces the particles agglomerating and sticking to the wall of the vessel [131].

Spouted beds have a minimum spouting velocity, similar to the fluidised bed reactors. Nevertheless, spouted bed space is limited due to maximum spouted bed height [132], while no maximum height can be established in a spouted fluidised bed because it relies on the diameters of gas inlet and particle. Even so, the spout bed height is increased when the contactor angle increases and the particle size decreases [133] [134].

- **Bubbling fluidised bed gasifier.**

The bubbling fluidized-bed (BFB) is shown in Figure (2-8), the gasifying agent enters from the bottom of the gasifier and the product is exited from the top whilst the fuel is inserted to the bed [135].

Historically, in 1921, Fritz Winkler has developed the BFB gasifier and it has been used commercially for coal gasification [46]. According to Basu BFB are deemed the popular technologies for biomass [46].

As illustrated in Figure (2-10) BFB contains screw feeders, a fluidised bed with a freeboard column unit, air blower, gas plenum (gas box), the distributor plate and cyclone. In a BFB gasifier the particles are kept in a state of suspension by enough velocity of gasification agent through a bed. The raw material (biomass) enters into the hotbed to be mixed and heated up to the bed temperature [136].

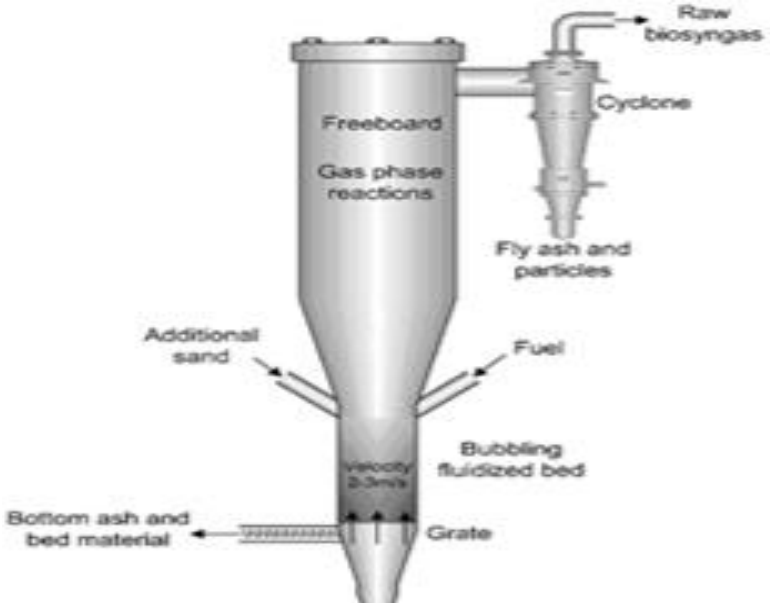


*Figure 2- 10 Spout Fluidised Bed Reactor* [126].

The advantages of BFBs when utilised to convert biomass into energy are: (1) a high degree of random, (2) high gas-solid interaction, (3) good mass, heat transfer, and (4) effective temperature distribution; increased volumetric capacity and heat storage [137].

Moreover, a catalytic agent can be added in the BFB and operated at partial load. The bubbling fluidised beds are adequate and economic for continuous biomass gasification, BFB gasifiers can be utilised with different biomass and particle sizes including pulverized feedstocks [138]. Additionally, the gas product from BFBs has low tar content and low unconverted carbon [138].

On the other hand, the BFBs are sensitive to ash content which is another important issue especially in bubbling fluidized bed gasifiers, which affects the practical operation of the gasifier. It does not affect the producer gas composition directly. Chemically, ash content is an inorganic solid material, which is mainly composed of metal oxides and some of their salts. Ash content can be measured by proximate analysis for biomass [139] and[128]. The issues and negative effects of the ash content lies in the following: 1) a high amount of ash will reduce the heating value of the solid fuel. 2) When the ash contains a high amount of alkali oxides and salts, which are promoted in the existence of chlorine and especially with high silica content in bed material forming eutectic materials (sticky compounds) of low melting points about 770oC for alkali-silicates ($K_2O$-$SiO_2$), whereas it is lower for $K_2O$-CaO-$SiO_2$. These materials lead to agglomeration phenomena especially in high temperature bubbling fluidized bed gasifiers causing a bed material defluidisation and therefore gasifier shutdown [139].

Unlike the spout-fluid bed. The risk of agglomeration increases when biomass has a relatively higher content of ash and the temperature inside the gasifier is higher than 950 °C[139]. The higher temperature rises the bed de-fluidization and reduces the efficiency of the gasifier, so the highest temperature is restricted by the fusion point of the bed material. The gasification reactions do not reach their chemical equilibrium as a result of low temperature and short gas residence times, except when using a catalyst [139]. According to Alberto et al. the operation range in BFB is among the minimum fluidisation velocity and the velocity on which the bed particle would be dragged by the passing gas, being usually 1.2 m/sec [140].

The yields of gaseous fuel in BFBs with using air as the gasifying agent have comparatively high heating values, and minimum to no heat added to the gasifier, which considers as a promising technique [141].

- **Circulating fluidised bed**

Due to the limitation of BFB gasifiers in handling a high level of solid material mixing, a low solid conversion rate is observed [142]. The extension of a recirculating loop improves the conversion by returning unreacted particles to the reaction zone through a cyclone, thus leading to improved solid residence time [143].

According to Yang, circulating fluidised bed (CFB) Figure (2-9) has been used for the gas-solid process since the 1970s [144]. CFB has a wide application in the industry, mainly for biomass and coal gasification [145]. Sikarwar et al. [146] reported that CFBs can deal with high quantity of biomass in high pressure ranges. The high velocity of the stream with recirculation leads to rising mixing which also increases the heat and mass transfer inside the gasifier. This improves the quality of the product gas due to the near optimum environment formed in the gasification [147].

According to Basu.[46] the fluidization velocity in a CFB is much higher than the types mentioned above, as it goes up to 3.5–5.5 m/s; for context the velocity in a bubbling bed reactor is 0.5–1.0 m/s.

The carbon conversion in the CFB is greater than BFB due to the rising speed of the recirculation and improved mixing of material [148]. On the other hand, the high gas velocity in the CBFs increases the corrosion rates when compared with BFB [149]. In addition, a CFB involves higher cost, increased height of the reactor, catalyst agglomeration, and complication in design, construction and operation [150].

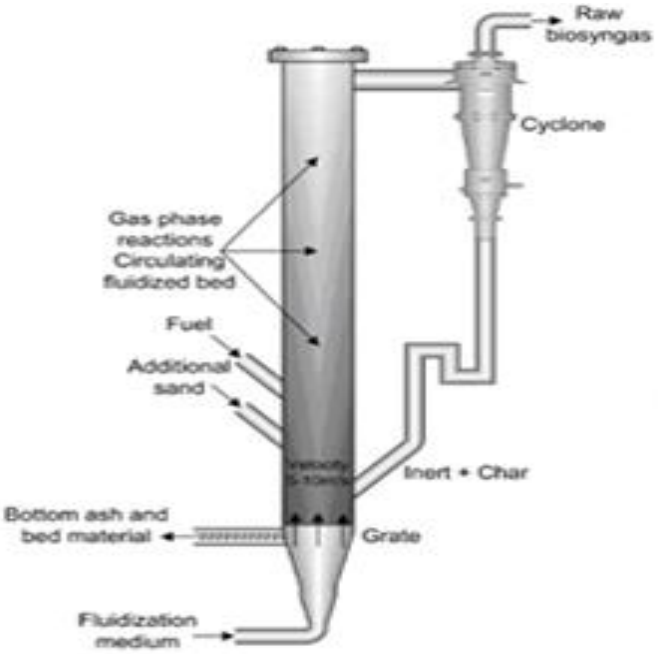


*Figure 2- 11 Bubble Fluidised Bed Gasifier* [270].

# 2.5 Catalytic Processing of Gasification Product Gas

## 2.5.1 Catalysis overview

Catalysis can be defined as the study of catalytic reactions, essentially the description of any material that may accelerate or increase the efficiency of a chemical reaction without impacting it equilibrium and thermodynamics [151]. Catalysis plays an important role in manufacturing, environmental protection and sustainable development [152]. Different types of catalyst are used in the commercial sector, including heterogeneous catalysts (solid), and homogeneous catalysts ( liquid) [153].

Historically, a catalyst was used in the industry since 1746 by J. Roebuck [154], and since in different industrial processes such as the purification of crude oil and biomass gasification [154]. Heterogeneous catalysts are widely utilised in gasification processes due to their capability to resist higher temperatures. The aim of using a catalyst in gasification processes is to enhance the quality of the product gas in terms of heating value, enhancing the desired gas ratio and reduce impurities. According to Shahbaz et al. [111] for commercial biomass gasification processes, the perfect catalyst for tar reduction, higher product yield and active life of the catalyst are still in under investigation and ongoing research.

Mineral based and synthesized catalysts are the main types of catalysts which can used biomass gasification, as shown in Figure (2-10) [155].

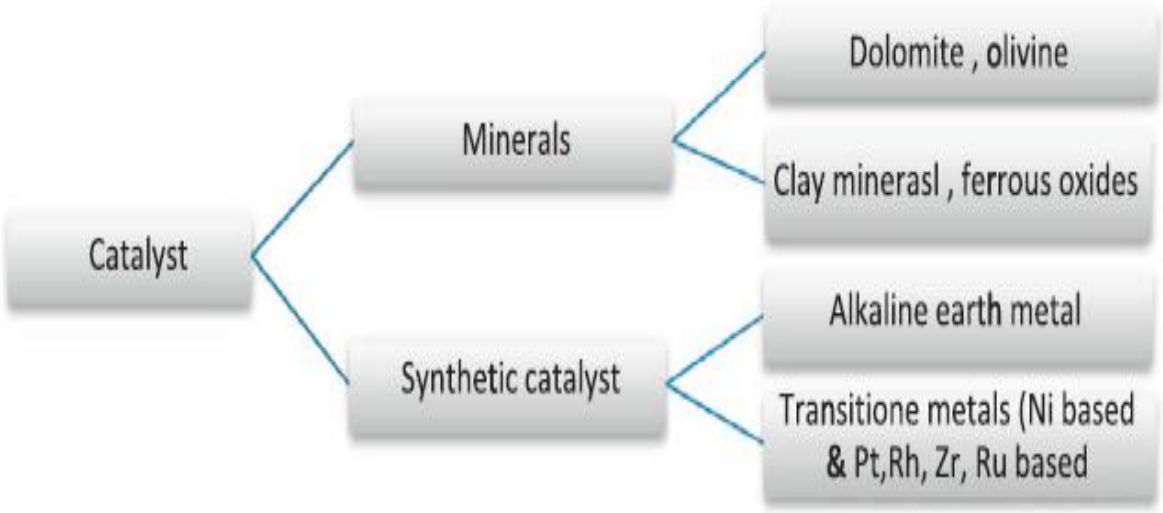


Figure 2-10 Types of catalyst used in steam biomass gasification. *[155]*.

Fluidized bed reactors remain the most suitable technology for integrating catalysts into the gasifier. Catalysts implementation as bed additives in fluidized bed reactors is a frequently considered option to achieve in-situ catalytic tar reforming.[156]

In-bed use of dolomite is not a new process. Corella et al. [157] already did it at small pilot plant scale, and in Scandinavia it is often used in the VTT pilot plant [158] and in the Car- bona plant at Va¨rna¨mo, Sweden. Narva´ez et al. [159] have also described the improvement of the quality of the raw gas when dolomite is fed to an air-blown gasifier mixed with the biomass. So, there are at least four institutions in the world who have found this in-bed use of dolomite in biomass gasifiers of fluidized bed type useful [160].

The catalyst can be used in two ways, primary and downstream catalyst. Primary catalyst reduces tar formation and enhances the tar reforming into desired product[155].

Dolomite is an ore of magnesium and calcium with the formula MgCO3.CaCO3. it has an extra advantage of being used as a primary or downstream catalyst and bed guard material.[155]

According to Dayton [161] dolomites are considered to be the most widely non-metallic catalysts used in biomass gasification processes. Therefore, Tian et al. [162] compared the catalytic properties between calcined dolomite and olivine during biomass gasification for tar reduction and syngas production during biomass gasification. This resulted in more clarification in the available catalysts for a more effective biomass gasification process, which is discussed in the following section.

### 2.5.2 Steps in heterogeneous catalytic reactions

Catalytic reactions that utilise heterogeneous catalysts involve separate steps, each step is either chemical or physical in nature. The chemical reactions take place when the reactants are in contact with the active sites. The transport of reactants to the active sites is promoted by physical processes namely: diffusion, adsorption and desorption. Typical steps for heterogeneous catalysts are [163]:

i. Diffusion of the feed materials to the surface of the catalyst.

ii. Diffusion of the feed materials into the support pores.

iii. Adsorption of the reactants on the inner surface of the pores.

iv. Chemical reaction on the catalyst surface.

v. Desorption of the products from the catalyst surface.

vi. Diffusion of the products out of the pores.

vii. Diffusion of the products from the catalyst surface.

Using a catalyst depends on the adsorption of the reactants and desorption of the products. The rate of adsorption increases with increasing the reactor's temperature. Therefore, the catalytic reactor's temperature needs to be carefully controlled to protect the reproducibility of the experiment.

### 2.5.3 Factors affecting catalyst performance.

Most heterogeneous catalysts lose activity during the catalysis process. The common causes of loss of catalytic activity are fouling, poisoning, sintering, attrition and loss due to vaporisation of active sites. Fouling and poisoning cause similar effects on catalyst performance; fouling refers to a physical coverage of active sites by either trace materials in the feed or the feed materials themselves. These foreign materials can undergo chemical adsorption (chemisorption) forming a strong adsorptive bond with the catalyst surface, thus covering the active sites, this is also known as catalyst poisoning. In biomass gasification, catalyst poisoning is caused by the deposition of carbon (coking). Carbon deposits on catalysts originates from hydrocarbons contained in the producer gas and the by-products formed during the catalytic reaction. Coking of catalysts depends on the oxygen storage capacity (OSC), which is the ability of the catalyst to absorb and release oxygen at elevated temperatures[164].

Increasing OSC in a catalyst can reduce the coking problems through oxidation processes. A deactivated catalyst can be regenerated by controlled combustion of the carbon layer.

Another potential setback is sintering. This is a result of a change of crystallite size of the active sites due to the fusion of particles at higher temperatures. Atoms of any material become mobile and coalesce when heated above the Tamman temperature, which is defined as half of the material melting point, in Kelvin)[165][166].

Increased sintering results in the loss of active surface area, thus, decreasing the catalyst activity. Therefore, the use of catalyst supports with high thermal stability is recommended.

Attrition is defined as the breakup of the catalyst into fine sizes as a result of particle to particle or particle to wall collisions in the fluid-bed reactors. The generated fines may transport along with the gas stream or cause blockages. Although supported catalysts in fixed beds are stationary, high abrasion resistance is required to avoid loss of active sites due to attrition.

Another factor that affects the performance of a catalyst is the loss due to evaporation of active sites[163]. This loss is mainly caused by higher operating temperatures of a catalytic reactor. One might be tempted to go for lower temperatures, but lower temperatures can lead to formation of toxic compounds. For instance, at temperatures below 150 $^{o}$C, nickel catalysts deactivate by forming nickel tetracarbonyl in the methanation of synthesis gas. This implies that, apart from losing the required chemical reaction, poor control of the process temperature may yield unwanted products.

## 2.6 Summary

Operating conditions control the gasification reactions. The literature identified that in high-temperature gasification, endothermic reactions the secondary cracking and reforming of heavy hydrocarbons are favoured and hence this enhances the overall process efficiency.

Reducing biomass particle size improves the product gas due to positively influencing the heat and mass exchange within the reactor. ER has several effects on the process, for example lower ER values result in a lower reactor temperature and therefore pyrolysis conditions are met in the biomass reactions. Combustion occurs at higher ER, leading to the low heating value of acquired product gas. The gas heating value are usually improved by using top feeding of biomass, however the amount of tar increased.

A fixed bed and fluidised bed are described. From this literature, a bubble fluidised bed reactor considers as the most suitable technology to gasify the biomass. The range of LHV was between 3.7 and 8.4 $MJ/Nm^3$, which is suitable for internal combustion engines.

Finally, catalysts are vital for the biomass gasification process, and it is important to select the appropriate configuration taking into consideration possible setbacks discussed above and will be explored further in this study.

**Chapter 3**

# Materials and methods of characterisation

# Chapter 3:

# Materials and methods of characterisation

## 3.1 Introduction

Both the biomass fuel and sand bed materials are characterised in this chapter, in terms of their preparation before subsequent experimentation in the gasification and TGA experiment. One of the most important parameters in the bubbling fluidised bed gasifiers is the particle hydrodynamic parameter, therefore it is essential to understand its characterisation procedure, especially in terms of minimum fluidised bed velocity. This property is used in providing the data needed to calculate the performance of the gasification process.

## 3.2 Biomass characterisation

In order to understand the characteristics of the biomass used, it is vital to individually analyse material in an 'as-received' state, which means the materials should be analysed as soon as they have been received without any further alteration or property change due to storage conditions.

In addition to understanding the characterization, it is also important to assess the gasifier's optimum operating conditions e.g. air-fuel ratio, feedstock mass and amount and the process temperature. Each condition is dependent on the physical and chemical properties of the feedstock used.

### 3.2.1 Proximate analysis

A fuel's properties can be assessed using its proximate analysis, which encompasses the moisture content, fixed carbon, ash and volatile matter. Proximate analysis refers to the behaviour of the fuel when it is burnt or gasified. The proximate analysis of the fuels used in this thesis are outlined in Table (3-1).

#### 3.2.1.1 Moisture content measurement

Table (1-3) shows that the gasification process is likely to be inhibited by the solid fuels' high moisture content, as it lowers the process's temperature through its evaporation as well as the fact that the char's chemical reaction with steam is endothermic.

ISO DIS 18134 (14774-3) is the main reference used in determining the biomass (date stones) moisture content. To ensure accuracy, the analysis was performed three times whilst monitoring variations in the obtained readings.

The containers (dished and lids) were dried completely in a 105 ℃ oven. They were then left in a desiccator to cool down to room temperature. Once cooled, they were weighed to the nearest 0.1 mg. A gram of the sample (weighed to the nearest 0.1 mg) was then evenly spread over each of the dishes.

The dishes and samples were put back into the oven and heated to 105 ℃ for 2 hours. After heating they were immediately put back into the desiccator. Note that the lids were also put in the oven with the dishes, but not covering them, this is to mitigate the biomass from absorbing the moisture as dried biomass is very hygroscopic. Once this is completed, the dishes (including the samples) are re-weighted and using the difference in weights before drying up the sample and after the moisture content ($M_{ad}$) can be calculated as shown in equation (3-1).

$$M_{ad} = \left(\frac{m_2 - m_3}{m_2 - m_1}\right) x\ 100 \qquad \textit{Equation 3- 1}$$

Where:

Mass of the empty dish and lid: $m_1$

Mass of the pre-heated dish and lid (including the sample): $m_2$.

Mass of the post-heated dish and list (including the sample): $m_3$.

3.2.1.2 Ash content measurement

The ash content is defined as the remainder of the inorganic material mass after complete oxidation of a fuel, under specified conditions according to BS EN 14775:2009. It is expressed as the mass ratio of the ash in the fuel to its total mass, usually presented as a percentage. The test was repeated three times in order to ensure accuracy.

Three empty porcelain dishes were put in the oven at a temperature of 550 ℃ (±10 ℃) which is the standard biomass ash method, it is a lower temperature so that volatile metals contained in biomass ash (sodium and potassium) are not lost. 900 is the method used to determine the quantity of volatiles [167].

for at least one hour to ensure full volatilisation of surface contamination. After removal of the dishes, they were left to cold down, for 10 minutes in a desiccator until they reached ambient temperature and weighed.

A gram of the sample biomass was then spread over each of the dishes and then placed into an oven at room temperature. The oven was then heated for a period of 30 minutes until it reached 250 ℃ and held at 250 ℃ for 30 minutes - at a heating rate of 7.5 ℃ per minute. The temperature was maintained for an hour to ensure that all the fuel's volatile content was removed prior to ignition.

The oven's heating rate was then increased to 10 ℃/min, until it reached 550 ℃, causing ignition to the fuel, and then maintained for a minimum of 120 minutes to ensure complete combustion.

Once the combustion was complete the dishes were then removed from the oven and left to cool down for about 10 minutes on a heat resistant surface and then transferred to a desiccator (in order to prevent moisture absorption from the room's atmosphere). Upon completion, the dish's mass was recorded again, and like the moisture content method, the ash content (Ad) can be calculated using the difference in masses as shown in Equation (3-2).

$$A_d = \left(\frac{m_3 - m_1}{m_2 - m_1}\right) x\ 100 \qquad \textit{Equation 3- 2}$$

Where:

m1 is the mass of the empty dish.

m2 is the mass of the dish and the test sample.

m3 is the mass of the dish and ash.

3.2.1.3 Volatile matter content measurement

BS EN ISO 15148:2009 protocols were used in determining the volatile matter content. Similar to the above, the readings were taken three times for each test sample to ensure accuracy. In order to ensure clear readings, fused silica crucibles are used with each of the three samples and placed into an oven at 900 ℃ for exactly 7 minutes in a purpose-made rack. It should be

noted that the lids were also added in this stage to mitigate absorption of any volatilises from the atmosphere to the fuel samples tested.

The samples were then removed from the oven, left to cool on a heat resistant surface and then moved to a desiccator.

The purpose-made rack that was used within the oven to hold the crucibles allows each individual crucible to be heated for the same exact amount time as the rack allows insertion and removal of all the units simultaneously. The weights were then measured again, and the crucibles were loaded with the sample fuels and re-inserted into the oven. Upon removal (and letting them cool down to room temperature), the content of volatile matter ($V_d$) was estimated using the weight differences, similar to equations (3-1) and (3-2) and as shown in equation (3-3).

$$V_d = \left(\frac{m_2 - m_3}{m_2 - m_1}\right) x\ 100 \quad \textit{Equation 3- 3}$$

Where the parameters ($m_3$, $m_2$ and $m_1$) are the same as in the moisture content calculation in Equation (3-1) and (3-2).

3.2.1.4 Fixed carbon content calculation

The fixed carbon content (FC%) is not measured directly. It is defined the remainder mass of the fuel after removing all moisture, volatile matter and ash content from the biomass, and therefore can be calculated by subtracting the values as shown in Equation (3-4).

$$FC\% = 100 - M_{ad} - V_d - A_d \quad \textit{Equation 3- 4}$$

Where,

Moisture content of the sample biomass: $M_{ad}$

Volatile matter content of the sample biomass: $V_d$

Ash content of the sample biomass: $A_d$

*Table 3- 1 Proximate analysis and high heating value of date stone.*

| Date stone (wt. %, wet basis) | |
|---|---|
| Fixed carbon | 6.73 |
| Volatile matter | 82.27 |
| Ash | 1.45 |
| Moisture | 9.55 |
| HHV($MJkg^{-1}$) | 18.965 |

### 3.2.2 Heating value

The heating value is also known as the calorific value. It is defined as the amount of released heat by a unit mass of a fuel substance during complete combustion and is measured as in joules per kilogram of fuel.

Heating value can be described in two ways:

1. The High Heating Value (HHV), also known as the gross heating value. This includes the heat of condensation from the water produced in the combustion reaction.
2. Low Heating Value (LHV) also known as lower calorific value. This does not include the heat of condensation of the water from combustion.

HHV can be measured in a laboratory setting and can be obtained during the combustion process, with the condition that the energy from the condensation of water to be included in the process.

A bomb calorimeter was used in this study in order to measure the calorific value of the fuel substance. The working principle of the bomb calorimeter is based mainly on the heat of combustion generated by a sample of solid fuel that is burned in an oxygen-rich atmosphere in a closed pressure vessel called (the bomb) under controlled conditions. This vessel is

surrounded by a cover of water that absorbs the energy released by the combustion of the sample and the resulting change in temperature is observed inside the absorbing medium. Thus, the heat of combustion is calculated. The test is carried out according to BS EN 14918.

The apparatus was a 6100, manufactured by the Parr Instrument Company. The device is shown on Figure (3 – 1). The method used is described below.

The combustion of the bio-fuel sample was measured under controlled conditions in an oxygen-rich environment and a closed pressure vessel, also known as a bomb vessel. The released heat from the sample's combustion flows from the bomb via a stainless-steel wall and flows to a water-jacket fitted around the vessel. This causes the temperature of the jacket to rise, which is then recorded and used to calculate the heat of combustion. This test follows BS EN 14918 [168].

Prior to the testing process, the bomb calorimeter calibration process was performed via three separate benzoic acid pellets. A gram of the sample biomass was sealed within the bomb and pressurised in (40 atm) of oxygen [169].

The bomb vessel is a cylindrical reactor submerged in 2,000 ml of distilled water prior to igniting the fuel via an electrical charge. The released energy due to the combustion was recorded and marked as the sample's HHV value via the machine's software. This process is repeated three times in order to ensure the repeatability between each of the samples. Each sample was measured twice (via a duplicate) and the mean value is shown herein.


*Figure 3- 1 Parr 6100 Bomb Calorimeter*

Both HHV and LHV differs that the latter is not inclusive of the water vapour's latent heat. LHV is calculated using Equation (3 - 5) [170].

$$LHV = HHV - h_g * (\frac{9*H}{100} + \frac{M}{100}) \quad \textit{Equation 3- 5}$$

Where,

High heating value is HHV

Low heating value: LHV

Hydrogen percentage: H

Moisture percentage: M

$h_g$ is the latent heat of steam constant and equates to 2.260 MJ/kg.

The High Heating Value (HHV), also known as the gross heating value. This includes the heat of condensation from the water produced in the combustion reaction. While the Low Heating Value (LHV) also known as lower calorific value. This does not include the heat of condensation of the water from combustion.

The main difference between HHV and LHV is that the LHV does not include the latent heat contained in the water vapour.

### 3.2.3 Ultimate analysis

An elemental composition of the samples was found via the 'Ultimate analysis' method., This method measures the carbon, hydrogen, nitrogen, sulphur and oxygen, in the sample by mass**.** Each of the components are measured within a specific fuel in its complete combustion. They are then used to determine an appropriate equivalence ratio value for either the combustion or the gasification process.

A CHNSO-IR LECO spectrometric analyser device was used to measure the biomass's ultimate analysis in this study. The as received date stone biomass materials' ultimate analysis results are given on Tables (3 – 2). These measurements were undertaken at a UKAS certified laboratory at Minton Treherne and Davies Ltd.

Testing is based on BS / ISO range for coal and coke, this sample is not a solid fuel but the methodology used is based on the methods as they are applicable and to hand for a fuel material:

Moisture in the sample is based on BS ISO 11722, drying at 105-110 °C under nitrogen purge to reduce potential oxidation effects, loss in mass is water.

Ash is based on ISO 1171 but modified to combust at 500 °C for a biomass material. (Coal would be 815 °C, biomass is typically burnt at lower temperatures, and it does all burn off)

Carbon and Hydrogen based on BS1016 part 6 – high temp combustion at 1350degC and gravimetric determination of combustion oxides, CO2 for carbon and H2O for hydrogen, corrected for moisture in sample mass at the time of testing, the hydrogen reported does not derive from the moisture present.

Sulfur also based on BS1016 section 106.4.2 / ISO 351 – high-temperature combustion at 1350 °C with oxidation of SO2 from combustion via H2O2 to sulphuric acid and titre finish, corrected for chlorine present.

Nitrogen would have been via LECO analyser, combustion, and IR detection of NOX in the exhaust gases, these tend to be standard now in fuel labs.

Oxygen by difference as per BS1016 part 6.

*Table 3- 2 Ultimate analysis of date stone.*

| Ultimate analysis (wt.%, dry basis) | |
|---|---|
| Date stone | |
| C | 45.5 |
| H | 6.0 |
| N | 0.94 |
| S | 0.07 |
| O | 38.52 |
| ASH | 0.97 |

### 3.2.4 Biomass size reduction

The date palm stones were imported from the Kingdom of Saudi Arabia. Their dimensions ranged between 20 to 25 mm in length and had a thickness of 6 to 8 mm. This is a relatively large size, which increases the difficulty to fluidise the bed and to control the feeding rate, therefore size reduction was deemed necessary. The reduction was achieved via a Retsch model BB20 crushing machine, shown in Figure (3 – 2b) which is suitable for medium-hard, and tough material. The crushing process results in a post-process particle size of 2 to 4 mm.

The selected batches of date stone particle sizes for this study were in the ranges of 300 to 500 µm, 500 to 710 µm, 710 to 1180 µm and 1180 to 1140 µm. In this case size was reduced by utilising a Lab-tech-Essa LM1 ring-mill device, shown in Figure (3 – 2a), and the obtained sizes were achieved by sieving, following to BS 1377-9 1990.


*Figure 3- 2 Biomass grinding machine a) Labtech-Essa; b) Retsch.*

## 3.3 Sand bulk density

Bulk density took into consideration both the particle volume as well the voids between the particles. Bulk density was estimated as the particle batch's mass divided by the total volume of the batch. This measurement was made following the BS 1337-9:1990 protocol.

The device used to calculate bulk density consisted of two main parts (1) the pouting cylinder, which is a long cylinder fitted with a cone at its base and (2) a calibrating container (flanged dish). The device is shown n Figure (3 -3).

The bulk density of a bed material was measured using the following steps:

- The volume ($m_3$) was measured as well as the weight (kg) ($m_1$) of the calibrating cylinder (before use).
- Weigh the bed material to fill the conical portion of the long cylinder ($m_2$).
- Filled the long cylinder completely with sand, fitted the long cylinder of the flanged calibrating container and then opened the valve to allow the sand to run freely and completely fill the calibrating cylinder as well as the cone space ($m_3$).

The mass ($m_4$) of the sand within the calibrating contain can be calculated via:

$$m4 = m3 - m2 - m1 \quad \textit{Equation 3- 6}$$

Subsequently, the bulk density was calculated by dividing the mass calculated above (m4) by the corresponding volume.

$$\textit{Bulk Density} = \frac{m4}{Volume} \quad \textit{Equation 3- 7}$$

It is worth noting that in order to prevent any human interaction in the process, a weighing (formed by a hump of material that forms within the cone) is used to create a flat sample in the calibration container. For example, sweeping the sand manually (i.e. by hand or a piece of paper) can alter the bulk density within the container.

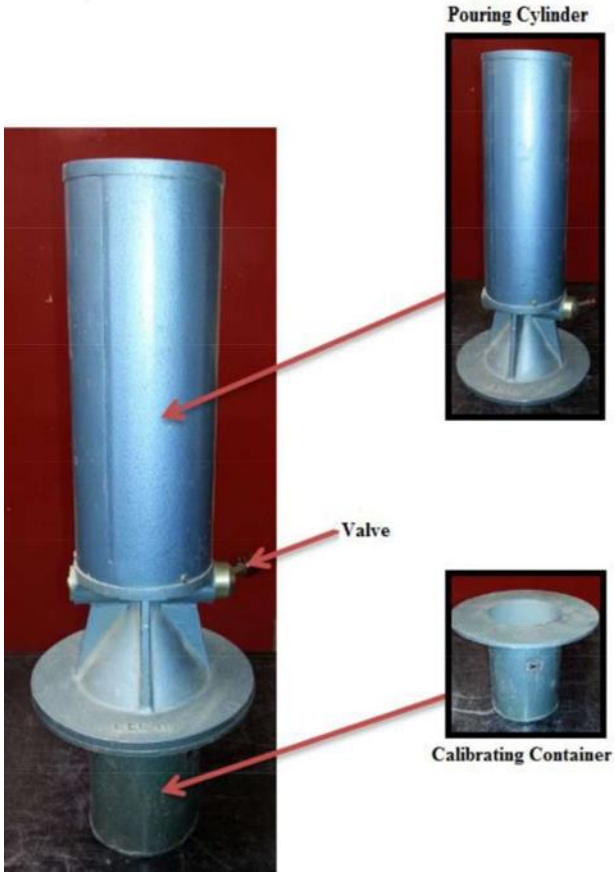


*Figure 3- 3 Sand bulk density apparatus; pouring cylinder and calibrating container.*

## 3.4 Fluidization regime

The minimum fluidisation velocity ($U_{mf}$) is a major parameter in determining the design and operation of any fluidised bed reactor.

Not only does it represent the drag force, which is a necessity in achieving solid suspension within the gas phase of the reactor, but also it plays as a major indicator for the intensity of the fluidization regime growth, especially at elevated velocity levels [171]. Additionally, $U_{mf}$ represents the fluidisation onset. As such this is a key parameter in reactor design.

There are two main methods for finding the appropriate value for $U_{mf}$, the first method is an empirical one while the second method is an experimental one via pressure drop measurements; both methods will be discussed briefly in this section.

The empirical method predicts the $U_{mf}$ value using previously published correlations [5].This depends on the physical and design parameters of the reactor itself as well as the bed material used [172].

This poses a threat for accuracy, as the formula is usually adapted to specific reactor designs, for example it may contain different diffuser plates, or a reactor diameter, and therefore it is not advised to apply the formula universally on any design. However, such methods have been shown to be effective in yielding an approximate value for optimisation and forecasting [5][7].

The experimental method to measure $U_{mf}$ is achieved via measuring the pressure drop across the bed. This is directly proportional to the air flowrate (U). Therefore, the value of U is less than $U_{mf}$, however it equates to $U_{mf}$ when reaching a critical condition, this is when the pressure drop is at its maximum. The particles then re-arrange on increasing the gas velocity slightly, resulting in the voids between the particles ($\varepsilon$) to change from the corresponding voidage of the expanded (fixed) bed ($\varepsilon_m$) to the bed voidage ($\varepsilon_{mf}$), while a pressure drop is observed as seen on Figure (3 – 4).

The pressure drop becomes consistent from this point onwards in this case, while the bed state transforms from being a 'fixed bed' to a 'fluidised bed'. The pressure drop can then be calculated as the bed weight divided by the cross-sectional are of the bed, as shown in Equation [144].

$$\boldsymbol{\Delta P = \frac{W}{A}} \qquad \textit{Equation 3- 8}$$

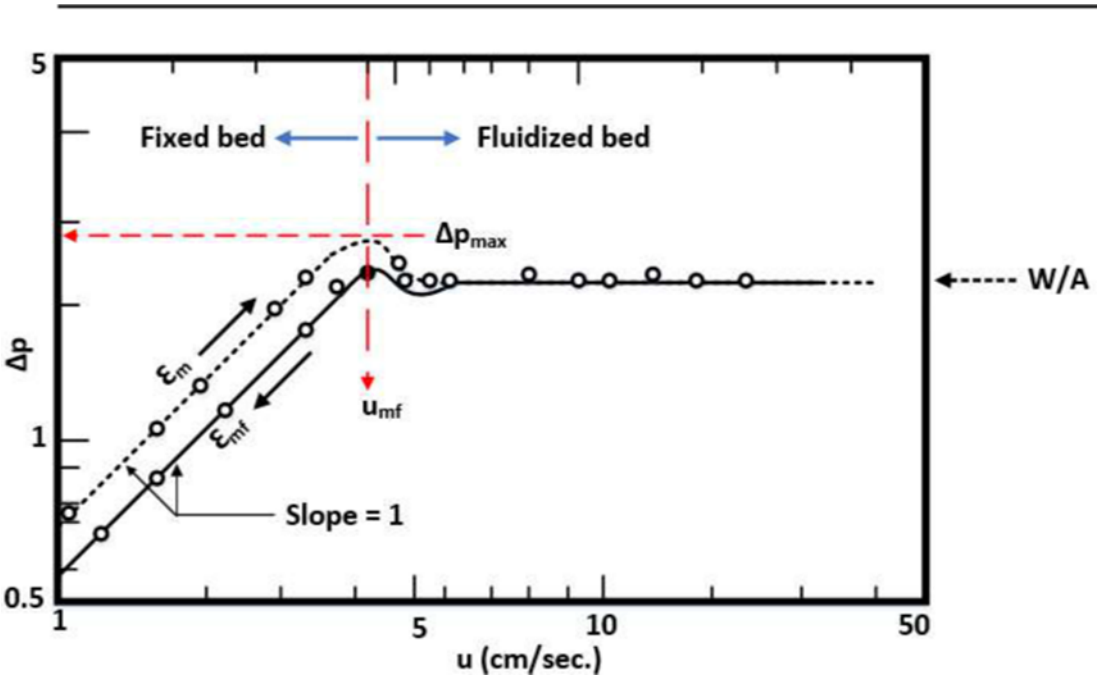


*Figure 3- 4 Pressure Drop Across a Fluidised Bed as Function of Fluid Velocity.*

The performance of a fluidised bed gasifier relies on the fluid dynamic models used within it at both medium and elevated temperatures. Increasing the superficial velocity to the minimum fluidisation velocity ($U/U_{mf}$) has an influence on both the attrition and elutriation rates [173].

The fluidisation medium' s physical properties can be altered by changing the temperature, as subsequently this impacts the fluid density and hence the hydrodynamic phenomena within the bed which is manifested by changes in the minimum fluidisation velocity.

When a fluid flows upward through a packed bed of solid particles, at a specific velocity the drag force of the fluid holds the particles medium, and a continuous motion of solids particles is formed producing a loosened suspension bed. This bed is called a fluidised bed. It behaves like a fluid, which can flow through pipes and valves. These phenomena can be used in wide applications to obtain high mixing and agitation of the fluid-solid particles, which produces an excellent contact between the solids and the solids itself, the fluid and the column wall.

Research by Pattipati [174] showed that small particles (roughly below 2 mm) see an increase in the $U_{mf}$ value when temperature increases, and this relationship is directly proportional to particle size for larger particles (roughly higher than 2 mm). Therefore, for practicality reasons

it is best to investigate the $U_{mf}$ values at elevated temperatures to ensure applicability to real gasification processes at elevated temperatures.

Generally, as described above, the bed material properties significantly impact the hydrodynamics of fluidisation. Therefore, the material is classified to four groups based on bed behaviour when fluidised by a gas, accordingly to Geldart (1973). The groups are shown on Table (3 – 3); group (B) is the most appropriate regime to ensure the bubbling of fluidised bed gasification, based on the Gedlart's classification approach.

*Table 3- 3 The fluidised bed material classification by Geldart (1973).*

| | |
|---|---|
| **Group (A)** | **The bubbles form and appear at velocities larger than the minimum fluidisation velocity (dense phase expansion before the beginning of bubbling).** |
| **Group (B)** | **Gas bubbles appear at the minimum fluidisation velocity. Sometimes these are called sand like or bubbly particles.** |
| **Group (C)** | **Fine and cohesive particles and difficult to fluidise.** |
| **Group (D)** | **Coarse particles. Sometimes known as a spoutable group.** |

According to Geldart's classification, there are four solid particle materials, which are classified according to its fluidization properties based on particle density and mean particle size (Geldart 1973) (Daizo and Levenspiel 1991), (Cocco et al. 2014):

1. Type A particles:

Are describe as aeratable particles. Density is less than about 1400kg/m3 and means diameter between 30 and 100 μm. In this type, the bubbles form and appear at a velocity larger than the minimum fluidisation velocity, i.e. Umb > Umf. Fluid Cracking Catalysts FCC particles are one material of this type of particle.

2. Type B particles:

Sometimes these are called sand-like or bubbly particles. Density is in the range between 1400-4000 kg/m3 and having a mean diameter in the range 40 to 500-600μm. In this type, the bubbles appear and form at the fluidisation point at once, Umb = Umf. Due to their easy fluidisation,

they have a wide range of use in industrial applications. Glass beads and coarse silica sand materials are examples of this type of particle.

3. Type C Particles:

These are very fine and cohesive particles. Their mean diameter is less than 30 μm. Due to their high inter-particle force, these very fine solids are difficult to fluidize (Harriott 2003). Materials of this type of particle are starch, talc, fly ash, and flour.

4. Type D particles:

Sometimes they called a spoutable group. This type has very large solid particles greater than 1000 μm and spouted beds may be formed. Some roasting metal ores, wheat, and coffee beans are classified in this type of particle.

### 3.4.1 Experimental measurement of minimum fluidization velocity.

Sand is among the most popular bed materials, as it is mechanically very sound, low-cost and simple to procure. Its good performance is evidenced by numerous industrial usage, especially in the circulating fluidised bed field as well as in the implementation of bubbling fluidised bed combustion [175].

The increase in temperature leads to a decrease in the density of the gas (as the density of the gas is inversely proportional to the temperature) as well as increases the viscosity( as it is known that the amount of viscosity increases with the increase in temperature) therefore these changes can modify the size of the fluid forces that are exerted on the particles and thus Reduce the minimum fluidised velocity [176].

Moreover, it was showed that small particles (roughly below 2 mm) see an increase in the Umf value when temperature increases, and this relationship is directly proportional to particle size for larger particles (roughly higher than 2 mm). Therefore, for practicality reasons it is best to investigate the Umf values at elevated temperatures to ensure applicability to real gasification processes at elevated temperatures.

In this study, a prepared charge with a size fraction range between 500 μm to 600 μm silica-sand was added at the top of the fluidised bed column. This is illustrated on Figure (3-6), while

a detailed description of the fluidised bed column and the design of the diffuser unit is given in the next chapter (Chapter (4)).

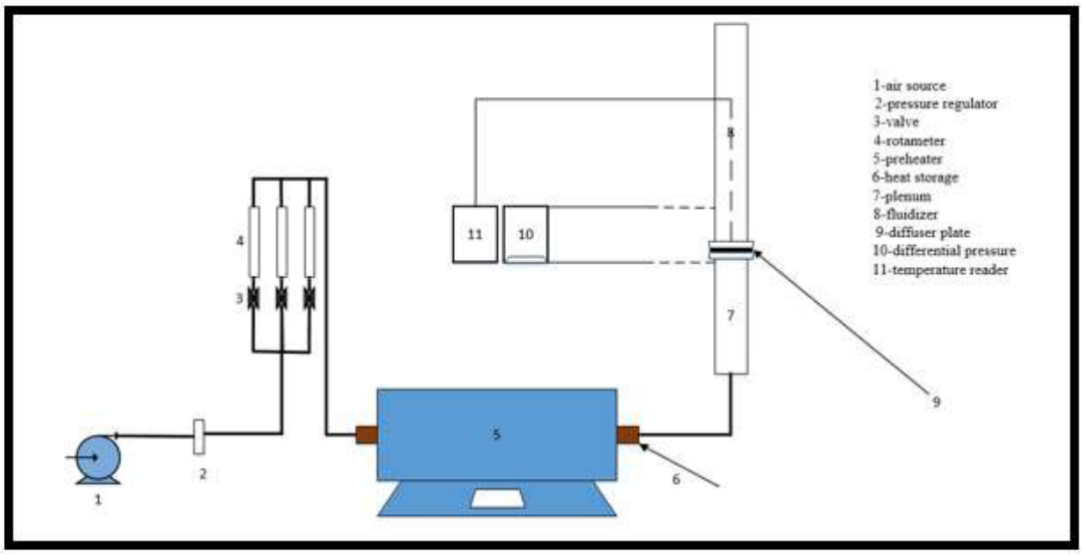


*Figure 3- 5 Bubble fluidised bed.*

This sand size was chosen for several reasons, including:

- Bubbles appear and form at the liquefaction point once, $U_{mb} = U_{mf}$.
- It is widely used in industrial applications due to its ease of liquefaction.
- Density ranges from 1400-4000 kg/m$^3$ with an average diameter in the range 40 to 500-600 μm.

The dimensions of the reactor studied herein were set such that the height of the static bed (Hs) and the overall reactor's diameter (D) were examined at a ratio of 0.5 and 1 for $H_s$ and D. The reactor apparatus was operated until it reached thermal equilibrium, whilst the temperatures were set accordingly. The airflow was increased until bed fluidisation onset had begun, then the velocity of the gas was reduced gradually until the cessation of the bed fluidisation.

The measurement of the pressure drop was undertaken using manometers to measure the differential pressure across the distributor plate, via drilling two measuring points in the plenum and freeboard units.

Once all the data above (change in the superficial velocity and the pressure drop) was measured and recorded, results were plotted graphically to understand the behaviour and extrapolate the

critical value of $U_{mf}$. The graphs are shown on Figures (3 – 7a) and (3 – 7b), using $H_s$ ratio of 0.5D and D, respectively. It is worth noting that the minimum fluidisation velocity is usually measured alongside a decreasing fluidisation velocity to mitigate the reliance on incipient loading [17][25].

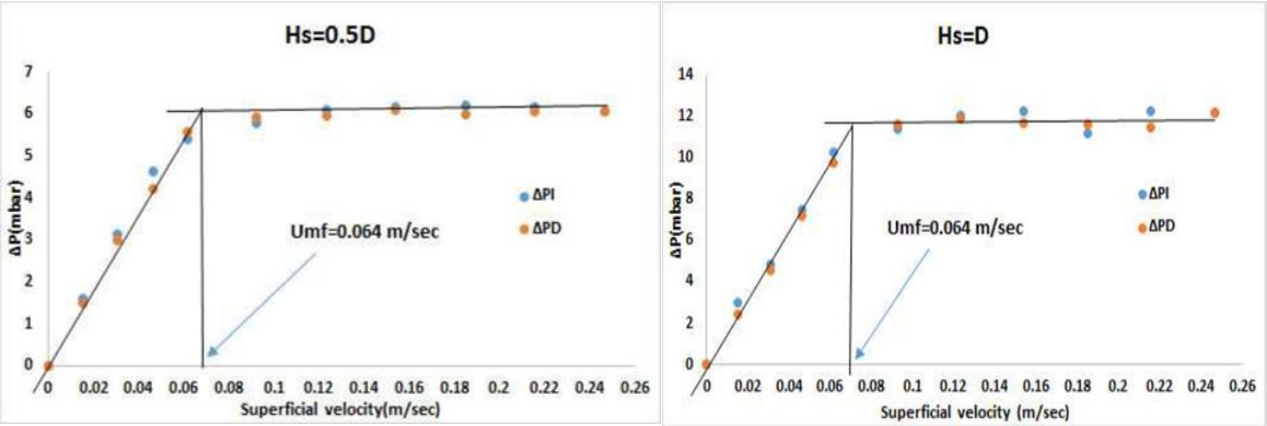


*Figure 3- 6 The plot of pressure drop against gas velocity at T=300°C at different diameters for silica sand of range (500 – 600 µm) (a) Hs=0.5D (b) Hs = D.*

The minimum fluidisation velocity ($U_{mf}$) is the intersection point between the horizontal and diagonal lines on the above graphs. At 300 °C, it was found to be 0.064 m/second at both Hs = 0.5D and $H_s$ = D. This shows that the height of the static bed does not have a significant impact on the $U_{mf}$ value over the conditions studied, however it causes a measurable increase of the pressure drop within the bed [177].

Particles with a superficial gas velocity higher than the terminal velocity are found in the carried-over cyclone products of the reactors, according to Choi et al [178]. Therefore, a further goal of this study was to ensure a lower superficial velocity, maintaining it below the particle terminal velocity to avoid bed material loss due to potential elutriation during the experiments. The terminal velocity can be calculated using the formulae that were put together by Kunni and Levenspiel; Equations (3-9) and (3-10), while the latter is specifically for spherical particles [179].

$$d_p^* = d_p * \left[\frac{\rho_g * (\rho_s - \rho_g) * g}{\mu^2}\right]^{1/3} \quad \textit{Equation 3- 9}$$

$$u^* = \left[\frac{18}{d_p^{*2}} + \frac{0.591}{d_p^{*0.5}}\right]^{-1}$$ *Equation 3- 10*

Where,

dp* is a dimensionless particle size.

u* is a dimensionless gas velocity.

Combining the equations result on Equation (3-11):

$$u_t = u^* * \left[\frac{\mu*(\rho_s - \rho_g)*g}{\rho_g^2}\right]^{\frac{1}{3}}$$ *Equation 3- 11*

Where,

$d_p$ is the mean particle size (m)

g is gravity in $m/s^2$

μ is the gas viscosity in $kg/m^s$

$\rho_s$ is the solid particles density ($kg/m^3$)

$u_t$ is the terminal velocity (m/s)

The bulk density of the silica sand as a bed material was 2,650 $kg/m^3$ in the experiment. It was sieved in BS sieves to ensure that the particle sizes were in the range between 500 μm to 600 μm, while the mean particle size was calculated using Equation (3 -12).

$$d_p = \frac{1}{\sum_{i=1}^{n}(\frac{x_i}{d_i})}$$ *Equation 3- 12*

Where,

The volume fraction of a $d_i$ average diameter particles is $x_i$.

A Malvern Mastersizer 3000 was used to obtain the required measurement, the device is shown on Figure (3 – 7). It uses a laser diffraction size analyser to determine the sand distribution within the bed, the distribution pattern of the tested material herein in shown in the graph on Figure (3 – 8). In this technique, a laser beam passes through a dispersed particulate sample and the angular variation in intensity of the scattered light is measured as shown on Figure (3-7). The light is scattered at small angles, relative to the laser beam, by large particles. Whereas it is scattered at large angles by small particles. By using the Mie theory of light scattering, this angular scattering data is then analysed to calculate the size of the particles. This size is then reported as a volume equivalent sphere diameter. The pattern shows a relatively narrow particle

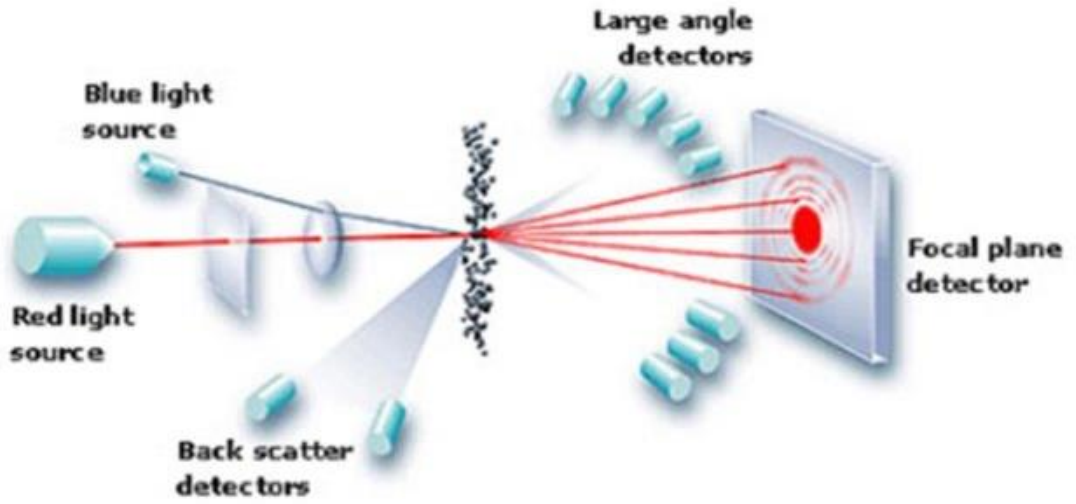


*Figure 3-7: Principle of a laser diffraction*

size distribution, which reduces the chances for the smaller particles sizes from slipping into the void spaces between the larger sizes. The mean particle size measured was 540 μm.

It measures particles from 10nm up to 3.5mm. The principle of the measuring of the particle size distribution in Mastersizer-3000 depends mainly on the laser diffraction technique. In this technique, a laser beam passes through a dispersed particulate sample and the angular variation in intensity of the scattered light is measured. The light is scattered at small angles, relative to the laser beam, by large particles. Whereas it is scattered at large angles by small particles. By using the Mie theory of light scattering, this angular scattering data is then analysed to calculate the size of the particles. This size is then reported as a volume equivalent sphere diameter. The pattern shows a relatively narrow particle size distribution, which reduces the chances for the

smaller particles sizes from slipping into the void spaces between the larger sizes. The mean particle size measured was 540 µm.

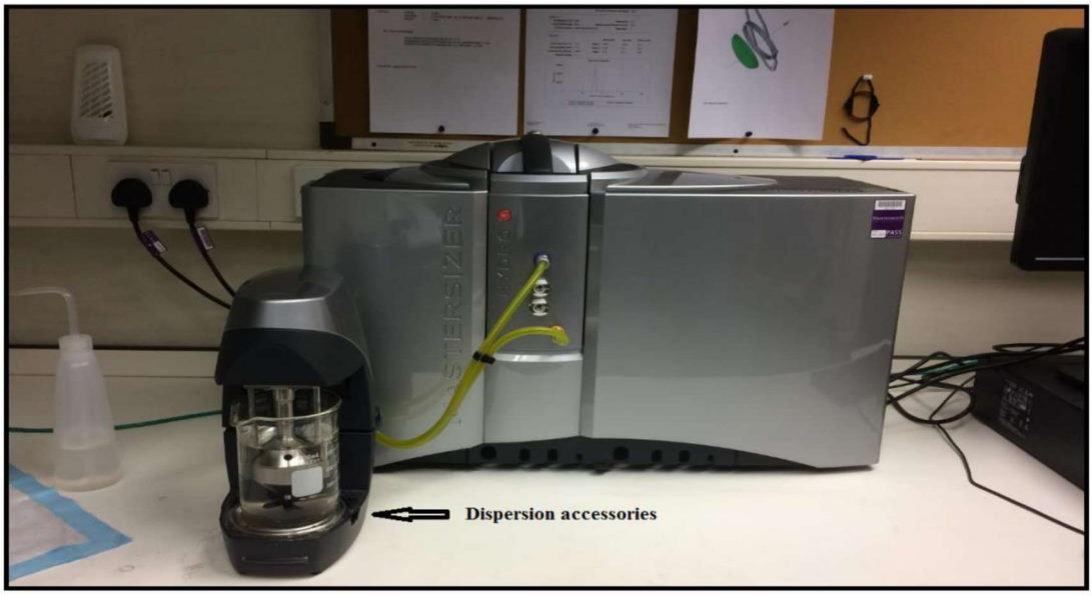


*Figure 3- 7 Malvern Mastersizer 3000.*

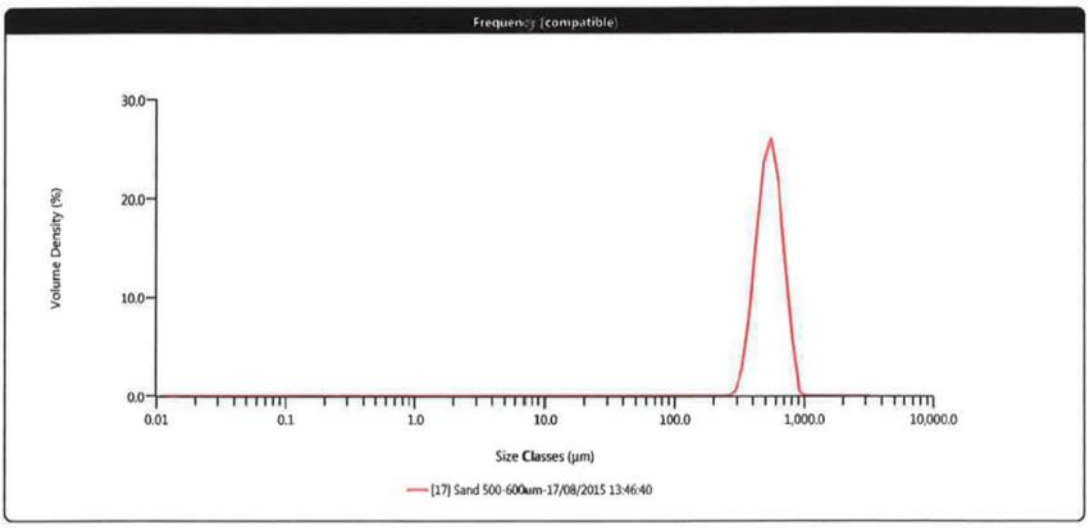


*Figure 3- 8 Particle size distribution of sand (500-600µm).*

The following constant values were used in the above calculations:

- Air density ($\rho_g$) = 1.2 * 10-3 g/cm$^3$
- Viscosity (µ) = 1.8 * 10-4 g/cm.s

- Sand diameter ($d_p$) = 540 µm
- Sand bulkd density ($\rho_s$) = 2.65 g/cm$^3$

The terminal velocity ($U_t$) was calculated using equations (4.7 – 4.9) and was found to be 0.89 m/second higher than the upward gas flow superficial velocity.

Note that palm stone density was found to be 560 kg/m$^3$ [180].

As mentioned in Section (4.1.2), the biomass was fed from above the reactor via a pipe that reaches all the way down into the bed itself. A closed top hopper was attached in order to reduce any biomass stream from flowing from the reactor. This is a further prevention of sample elutriation which is important in ensuring the measurement accuracy of the reactor's mass changes.

## 3.5 Thermogravimetric analysis (TGA).

The Thermal decomposition of a range of date stone biomass particle sizes conditions was investigated under inert conditions. The investigation was done using a thermogravimetric analyser (TGA) device.

The material's mass is monitored with respect to time and temperature to conclude a thermogravimetric analysis (TGA). The technique works best when a sample material is exposed to a controlled environment.

TGA is often used to study the thermal behaviour in various process, such as gasification, combustion and pyrolysis. It determines the mass loss characteristics of the biomass in a range of heating rates between 0 to 60 ℃ per minute and provides accurate results in temperatures up to 1300 ℃ in in an atmosphere environment. TGA can be used in investigating the degradation mechanism and reaction kinetics of biomass in a thermochemical conversion process. The analysis provides data that can be used to plot a thermogravimetric (TG) curve, which illustrates the dynamic mass decay against temperature and/or time. Differentiating the data results in differential thermogravimetric data (DTG) which can be used to indicate the biomass conversion rate during the thermal process.

The date stone pyrolysis analysis was done in a Mettler Toledo TGA device, which is shown on Figure (3 – 9). The analysis was undertaken as follows, 10 mg of the biomass sample was

loaded into an alumina crucible, which was tapped to a clear and rough surface in order to make sure that the biomass sample was distributed appropriately.

Once the sample was distributed accordingly, the crucible was placed carefully into the TGA carousel using tweezers. Having automatically loaded the sample into the furnace, a 20 ℃/min heating programme was then activated in an inert atmosphere. The inert atmosphere was arranged using a nitrogen flow with a rate of 50 ml/minute, the flow carries away both the condensable and gaseous products out of the environment which reduces potential secondary vapour phase interactions.

After preparing the volume to be tested from the date stone, one gram is taken and the percentage to be added from the catalyst materials is added to it and mixed well, then 10 mg of this mixture is taken for testing in the TGA device.

During the temperature programme, the corresponding mass losses are carefully recorded. Once the programme completes, all the recorded and imported data are then analysed using bespoke TGA software.

In this study, the date stone sample tested under the pyrolysis conditions are of particle sizes of:  300 to 500 µm, 500 to 710 µm, 710 to 1180 µm and 1180 to 1400 µm.

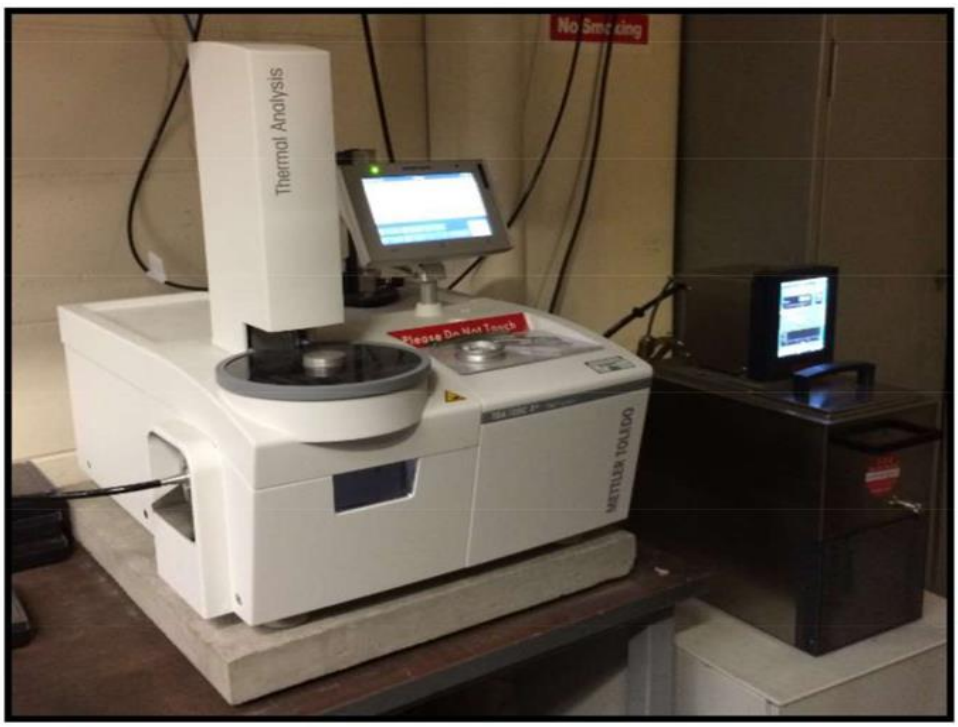


*Figure 3- 9 TGA-DTA system.*

## 3.6 Summary

This chapter has discussed the methods and materials used in characterising the properties and Thermogravimetric characteristics of the bed material (sand) and biomass.

Date stones were studied as examples of as-received solid biofuels; they were characterised as per the appropriate standardised methods.

A Malvenr Mastersizer 3000 analyser device was used to measure the sand's mean particle size, while its bulk density was measured accordingly. Oversized particles were crushed using grinding machines to ensure biomass size reduction as necessary.

Ultimate and proximate analysis was utilised to characterise the biomass fuels used in the experiments. This is important as it is needed to determine the appropriate height to particle diameter ratios in the bed material. Furthermore, Thermogravimetric analysis (TGA) was used to plot and investigate the material's mass decay with respect to both time and temperature; this gives a clear explanation for the thermal behaviour of different particle sizes of the date stone under pyrolysis conditions.

Finally, the minimum fluidised bed velocity ($U_{mf}$) has been measured experimentally via the pressure drop within the bed, this was favoured against empirical methods to ensure relevance to the condition's studies herein.

# Chapter 4

## Gasifier equipment, and experimental procedure

Chapter 4

Gasifier equipment, and experimental procedure

# 4.1 Gasifier methodology

## 4.1.1 Introduction

This chapter discuss various subjects within the gasifier's methodology. Namely, the gasification procedure, its operation condition. Additionally, a rig setup experiment will be assessed alongside the method's performance equations, and gas analysis. The work involves using a Small Pilot Fluidised Bed Reactor (FBR) is used in this study shown in Figure (4-1), which was designed and built in Cardiff University – School of Engineering.

*Figure 4- 1 Fluidised Bed Gasifier*

A flow-chart schematic representing the Fluidised Bed Gasifier operation is shown in Figure (4-1). The main sections in the reactor are marked in Figure (4-2) as following:

1. The bio-mass feeding system.
2. Gasifier containing perforated distributing plate and an air box.
3. Air delivery system.
4. Heating system.
5. Cleaning system; specifically design to clean the downstream gas.
6. Gas analyser.

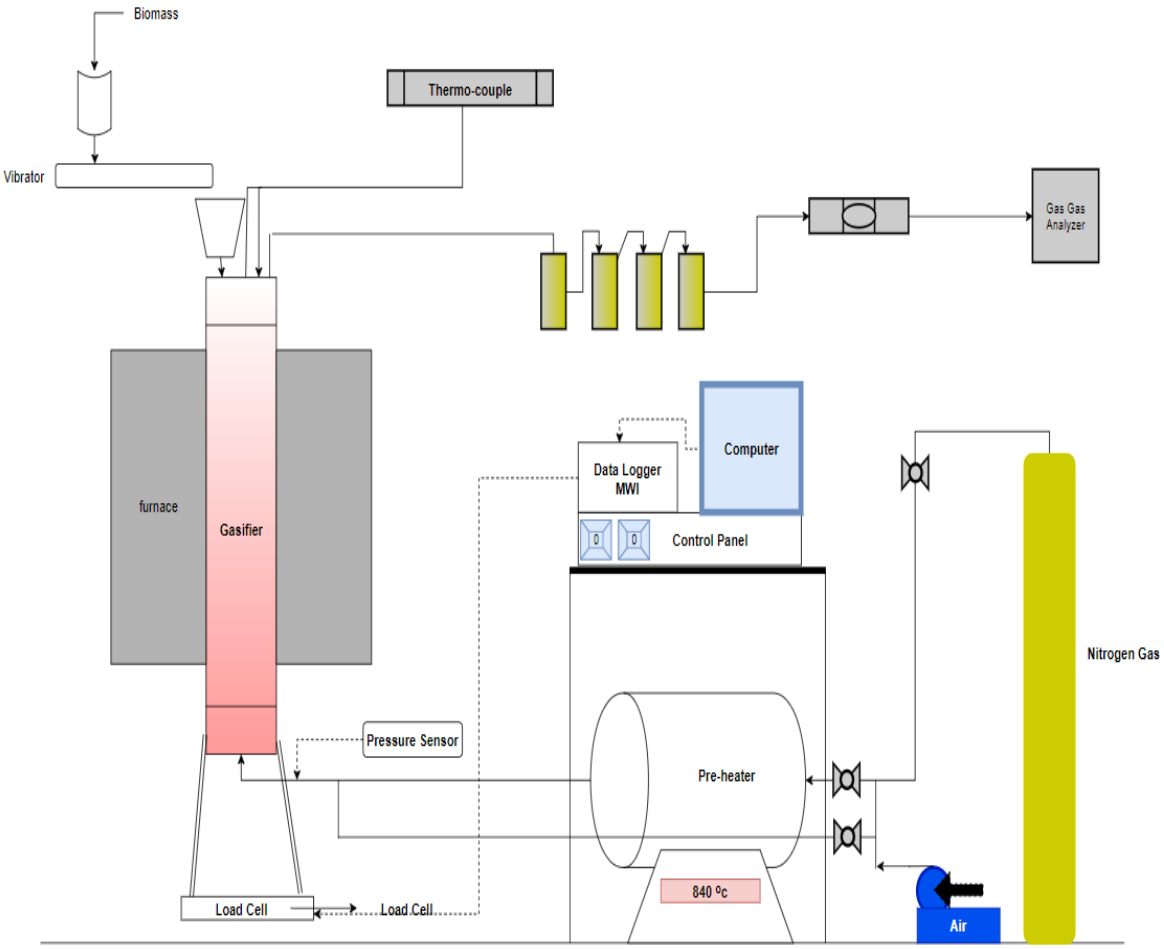


*Figure 4- 2 Fluidised Bed Gasifier (flow-chart schematic).*

Each of the components will be discussed in more details in the following section.

## 4.1.2 Biomass screw feeder design

The screw feeder (model DDSR20) was fabricated by 'Brabender Technology' and supplied by 'Genesis Process Solution Limited (UK). The maximum mass flow rate allowed through this design is 24 kg/hr, the model main components are shown in Figure (4-3).

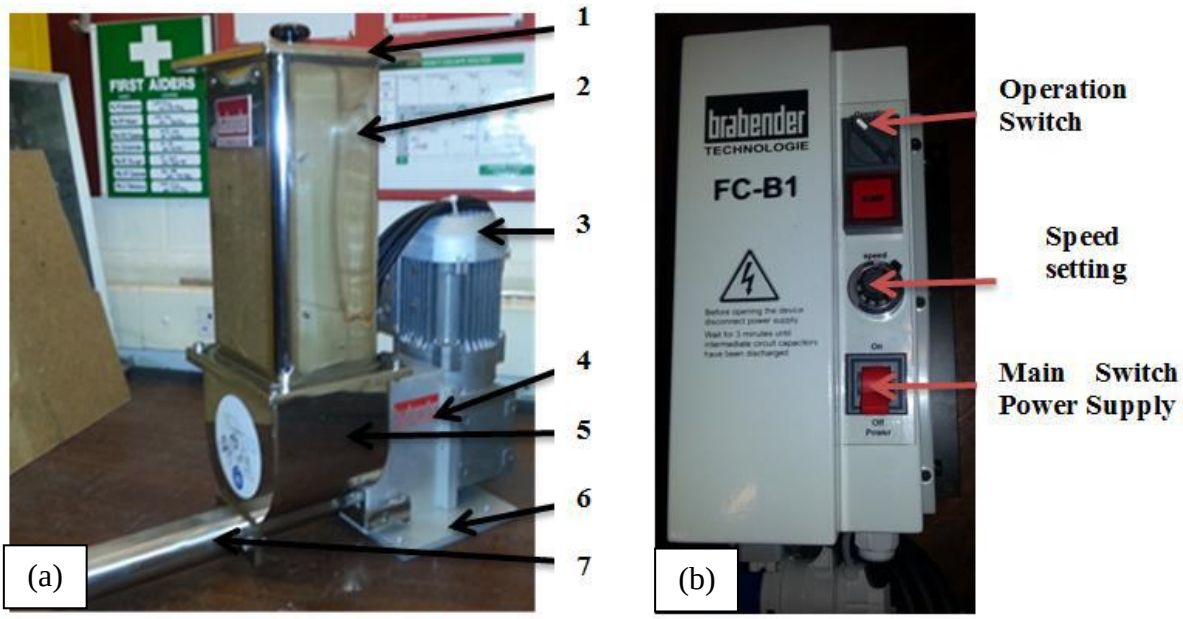


*Figure 4- 3 DDSR –20 biomass screw feeder: (a) Complete screw feeder unit, consists of: 1-Hopper lid 2- Hopper 3- Drive motor 4- Spur gear unit 5- Agitator trough 6- Screw feeder base 7- Twin-screw arm, (b) Power supply and drive controller unit.*

This design consists of two main components. The first being the auger screw feeder used to feed the biomass into the gasifier; shown in Figure (4-3a). The second unit is the controller and power supply unit, shown in Figure (4-3b).

Solid biomass is conveyed via pouring it into the device's hopper (Figure 4 - 3a 2). The fed material is then driven via an electric motor (Figure 4 - 3a 3) into the twin screw of the screw feeder (Figure 4-3a-6). The feed trough is supplied with the downward fed biomass, and enhanced by using a trough agitator (Figure 4-3a 5). The agitator is driven through the motor via a spur gear unit (Figure 4-3a4) and above the twin-screw feeder.

The provided drive control system unit (FC-B1) comprises of:

(1) The primary power supply through a switch control; shown in (Figure 4-3b 1).
(2) The screw feeder's speed, which can be set between a percentile-based range via a potentiometer regulator; shown in (Figure 4-3b 2).

(3) Switching the operation on/off, shown in (Figure 4-3b-3). Noting that this option is slightly different that the power supply control, as it starts the feeder gradually.

A main expectation of the feeder is to be able to obtain a calibration curve specifying the mass flow rate of the biomass. The model above (DDSR-20) is used to control the mass flow through the feeder system, which is essential in evaluating the gasification process's real time equivalence ratio.

Before starting the experiment, the sample is dried to get rid of moisture to prevent any chance of blockage through the feeding tube.

To block any reverse current stream of flow coming from the reactor, the biomass was dropped into a closed hopper as explained in Figure (4-4). After that, the biomass is moved through a 1-inch diameter pipe from the hopper to the reaction zone. As a result of no direct connection between the feeder and the hot bed material, the feed systems are usually less troublesome.

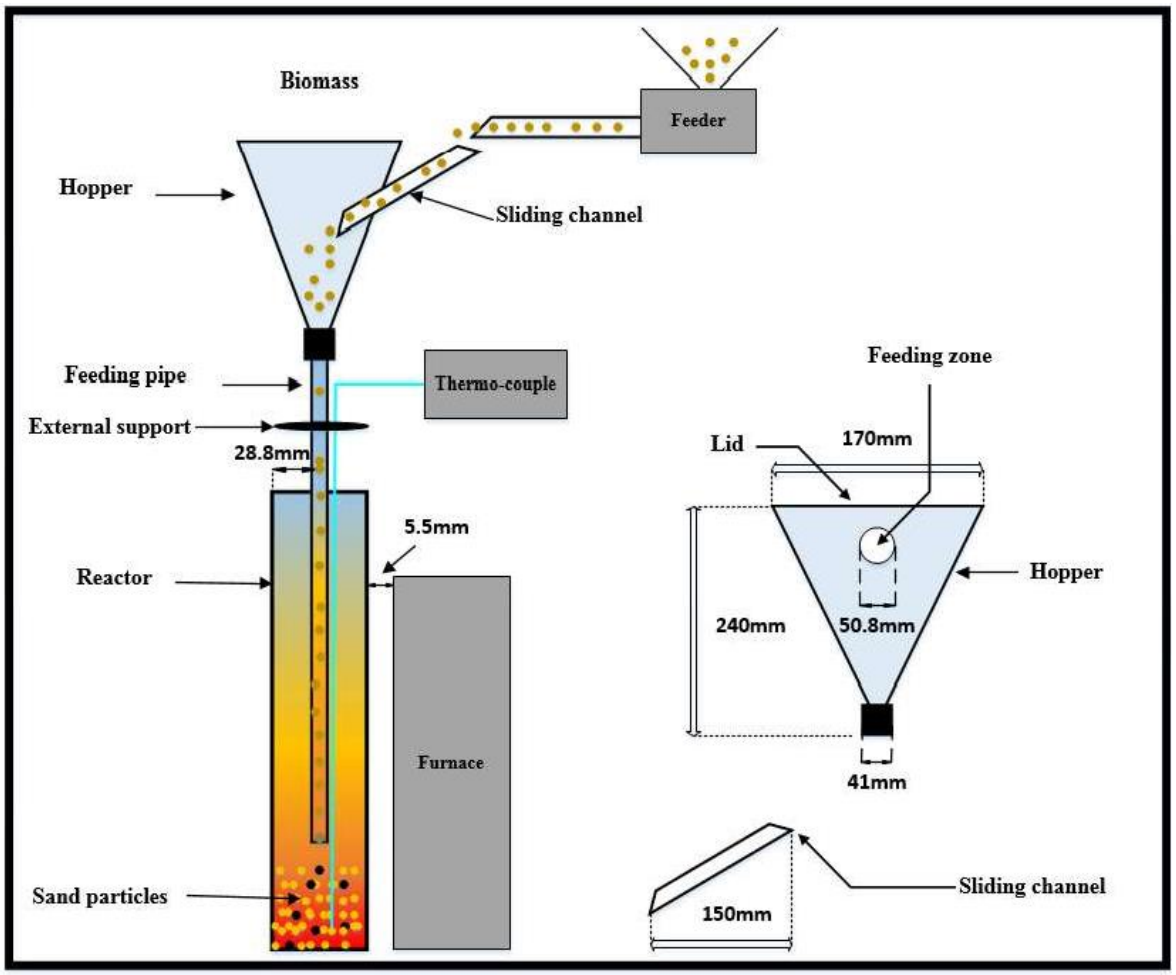


*Figure 4- 4 Schematic diagram design of hopper and the accompanying feeding system unit.*

### 4.1.3 Gasifier

The gasifier is at the heart of the gasification process, as it hosts the gas solid reaction between both the gasification agent and the biomass material. As a reactor it needs to be carefully built to host several reactions whilst maintaining the appropriate conditions. It consists of a fluidised bed reactor, freeboard, plenum, a diffuser plate, an air delivery system, a heating system as well as safety and measurement units. Each component will be discussed in further details in the next sections.

#### 4.1.3.1 Fluidised bed reactor and freeboard.

A 316L stainless-steel cylindrical tube is used to house the fluidised bed, measuring 83 mm in inner diameter (D) and 1,250 mm in height ($H_s$). Typically, the height of the used static bed in the gasification tests is $H_s = 0.5D$, with the remainder of the height is the freeboard, which is defined as the space between the upper surface of the bed material and the end of the tube.
It's worth noting that the freeboard height should be equal or more than the transport disengaging height (TDH), which is a vital factor in the fluidised bed column. The TDH factor can be calculated in meters as following [144]:

$$TDH = 0.85 * U^{1.2} * (7.33 – 1.2 * \log(U)$$

As U represents the superficial velocity (m/s).

#### 4.1.3.2 Plenum or air box

The lowest section of the gasifier is known as the plenum or an air box, specifically beneath the perforated diffuser plate. The primary function of the air box is the distribution of the entering air which results in maintaining a steady air flow rate through each perforation.
It is logical to build the plenum using the same material as the reactor's pipe. The used stainless-steel pipe dimensions are 82 mm in internal diameter, and 89 mm in outside diameter, and a height of 500 mm. The plenum also contains a flat plate which contains a 1-inch diameter hole in its center, which fits a pipe of the same diameter. The used pipe is made of stainless steel and has a total distance from its end side to the plenum's top level of 100 mm. Moreover, a tube with a bigger diameter with a length of 50 mm is used as a flange and welded into the it

in order to hold the diffuser plat in the gasifier, the plenum also known as the air box is shown in Figure (4-5).

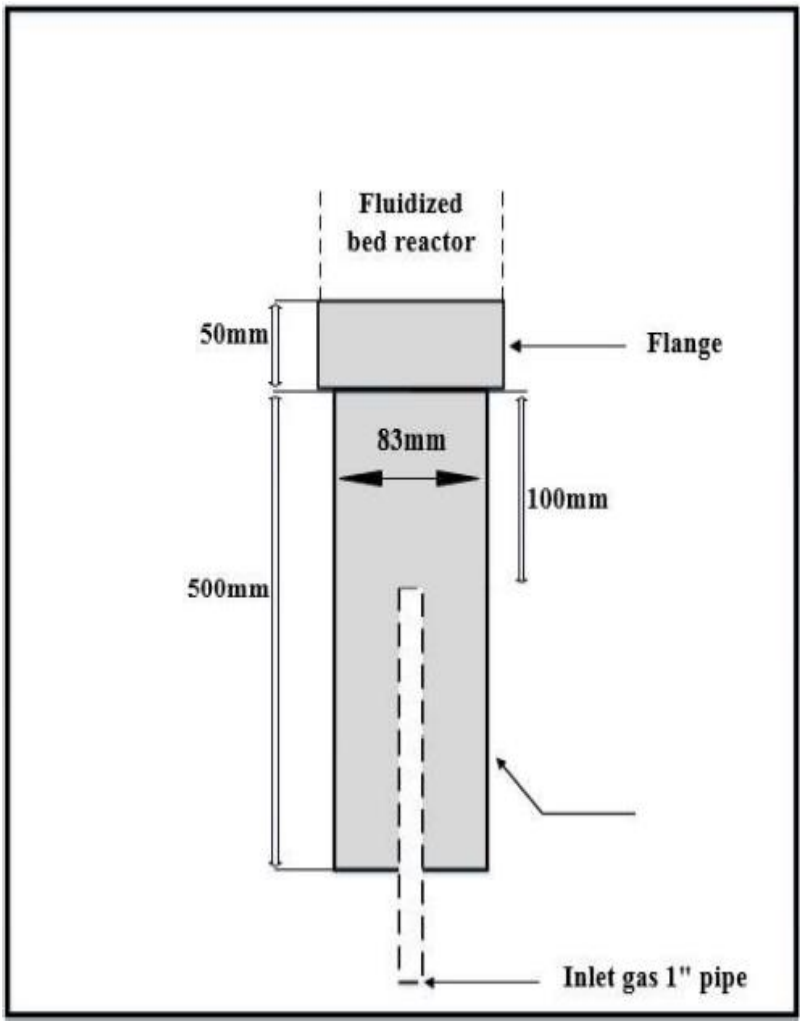


*Figure 4- 5 The plenum or air box schematic*

Surrounding the plenum area with an appropriate heater can result in preheating the entering air before reaching the fluidised bed. This design consideration has not been discussed in details in the literature, Yang has set appropriate configurations which is being applied in the experiment here [144], however it is important to consider testing different plenum set ups to understand the impact on the gasifier.

4.1.3.3 Diffuser Plate

The used perforated diffuser plate is 5 mm thick and made from stainless stee. It contains 151 holes that are uniformly drilled across the plate, each hole has a diameter of 1 mm and follows

a triangular pattern. The used plate is shown in Figure (4-6) below.

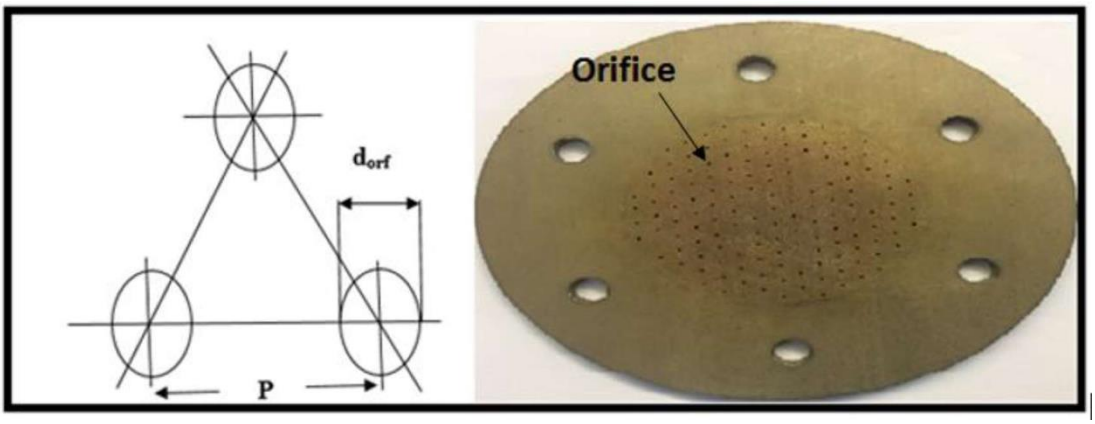


*Figure 4- 6 The used diffuser plate with the triangle patterned hole shown.*

As discussed earlier, the perforated plate is used to ensure enough retention of the fluidization material in the reactor bed and thus ensuring a homogeneous air distribution accordingly. One of the main reasons of using the plate is its ability to reduce any segregation tendency, alternatively a porous plate could have been used however this would have resulted in less efficient mixing [181].

It is possible to estimate the orifices' density (ND) using the number of holes/orifices, as well as orifice pitch ($P_{pitch}$), which can be calculated as following:

$$ND = \frac{Number\ of\ Holes}{Area\ (cm^2)}$$

The calculated ND is inversely proportional to the orifice as follows:

$$P_{pitch} = \frac{1}{\sqrt{ND * \sin 60^o}}$$

### 4.1.4 The air delivery system

An air compressor with a pressure of 7 bar is used to supply the required air. This is controlled via an upstream rotameter valve.

Three Platon rotameters are used to measure the air flow rate with the aim of reaching these rates: 12 l/min, 50 l/min and 150 l/min at room conditions, the manufacturer calibration manual

confirmed an error margin of ±1.25% of the standard reading. Therefore, it was important to use multiple rotameters to ensure an accurate air flow rate in the hydrodynamic measurements.

### 4.1.5 Heating system.

A vertical split tube furnace (produced by LTF) is used to supply the required heating energy inside the gasifier. More specifically, a furnace of model (PSC 12/100/900) was used due to its feature of providing uniform and consistent temperature zones across three different levels. Its maximum temperature is 1,200 $^{o}$C.

The electric furnace is set up to sit around the gasifier reactor by relying on the split tube for support, it is meant to provide the needed heat with minimal impact on the load cell's mass reading for each biomass load. Therefore, the gasification changes in the mass can be measured with less error margins or external factors impacting the readings. The used heating system is shown in Figure (4-7).

.

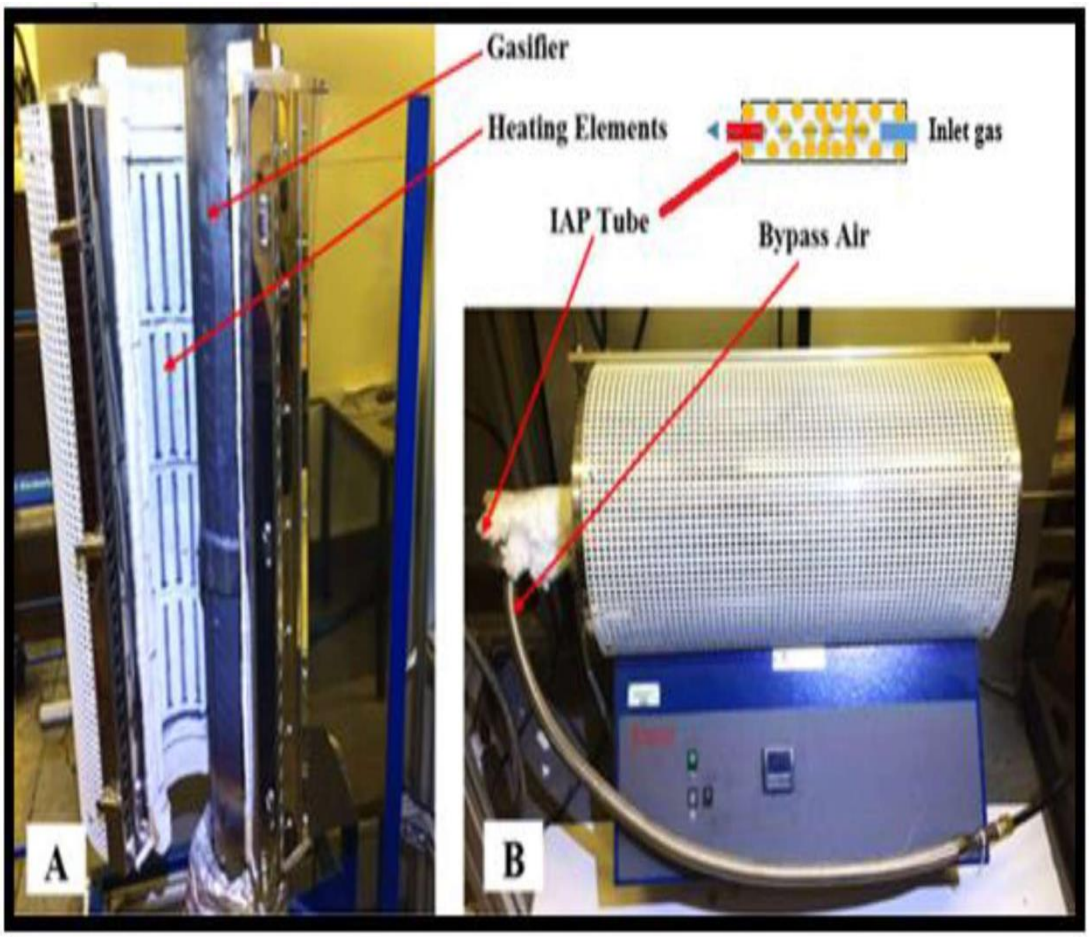


*Figure 4- 7 The used heating system which consists of: (a) Electric split furnace, (b) Pre-heating tubular furnace.*

There is no physical contact between the gasifier outlet pipe Figure (4-4), the analyzing computer system, the feeding system and the thermocouples. Therefore, external physical contact is limited. The main external physical contact is the flexible stainless-steel gas supply entering the gasifier through the feeding the system which is attached to the plenum's base.

In order to improve the overall heat transfer, the fluidizing air is passed through a 670 mm long tube with a diameter of 50 mm that is filled with impervious alumina porcelain (IAP) beads. Additionally, an LTF electrical horizontal tube furnace is wrapped around the tube to ensure appropriate heating levels. The preheating system is shown in Figure (4-7b).

In summary, it is important to maintain a consistent, homogeneous and evenly distributed heating energy for the materials entering the gasifier to ensure good operation, this has been carefully considered in the setup of this experiment.

### 4.1.6 Measurement apparatus:

#### 4.1.6.1 Mass Measurement:

A load-cell produced by Coventry Scale Company was specifically designed for this experiment shown in Figure (4-8a). One of the main reasons of selecting this scale is its enhanced sensitivity, as its tolerance is set as 0.5 gm (+/-) and could weigh any object up to 25 kilograms, the computer/indicator set is shown in Figure (4-8b).


*Figure 4- 8 (a): A load-cell based bespoke scale. (b) A multi-function weight indicator (model ID: DFW06XP).*

The unit allows connection to a computer in order to store the data, in this instance a model DFW06XP multi-function weight indicator was used to facilitate that connection.

Mass measurements and recorded is tracking agglomeration within the gasifier during the test. A sudden increase in its mass would indicate its occurrence, suggesting a reduction in the bed's fluidization, and that mass has been accumulating in the furnace.

#### 4.1.6.2 Pressure Measurement:

A measurement of the pressure drops between two separate points of the set up was needed. In order to pressure transducers are used for the pressure drop measurement inside the reactor and to assess agglomeration risk. Another consideration is for safety, in which the appropriate pressure gauges are needed to ensure appropriate pressure levels across the reactor. Thus, a gauge was fitted at the plenum's inlet.

Another benefit of the real-time mass measurements and recorded is tracking agglomeration within the gasifier during the test. A sudden increase in its mass would indicate its occurrence, suggesting a reduction in the bed's fluidization, and that mass has been accumulating in the furnace.

#### 4.1.6.3 Temperature Measurement:

Type (k) thermo-couples are used to monitor the reactor's temperature. Two thermo-couples are fitted in the reactor, which are marked in Figure (4-2) of this chapter. One thermocouple is installed 30 mm above the distributed plate in the bed zone, while the second is fitted within the freeboard.

The temperature readings were regularly recorded via a data collection hardware produced by Omega, which then relays the readings into the computer system. In order to manage the reading efficiently, a DAQ central data logging software was used in the host computer. Microsoft excel was used to analyse the data once all the data points are transferred to the computer.

### 4.1.7 The Downstream cleaning system

The product gas is cleaned via a downstream cleaning section which contains a tar capture unit. The unit is made of four dreschel bottles (model MF 29/3/250) filled with 99.8% isopropanol,

shown in Figure (4-9).

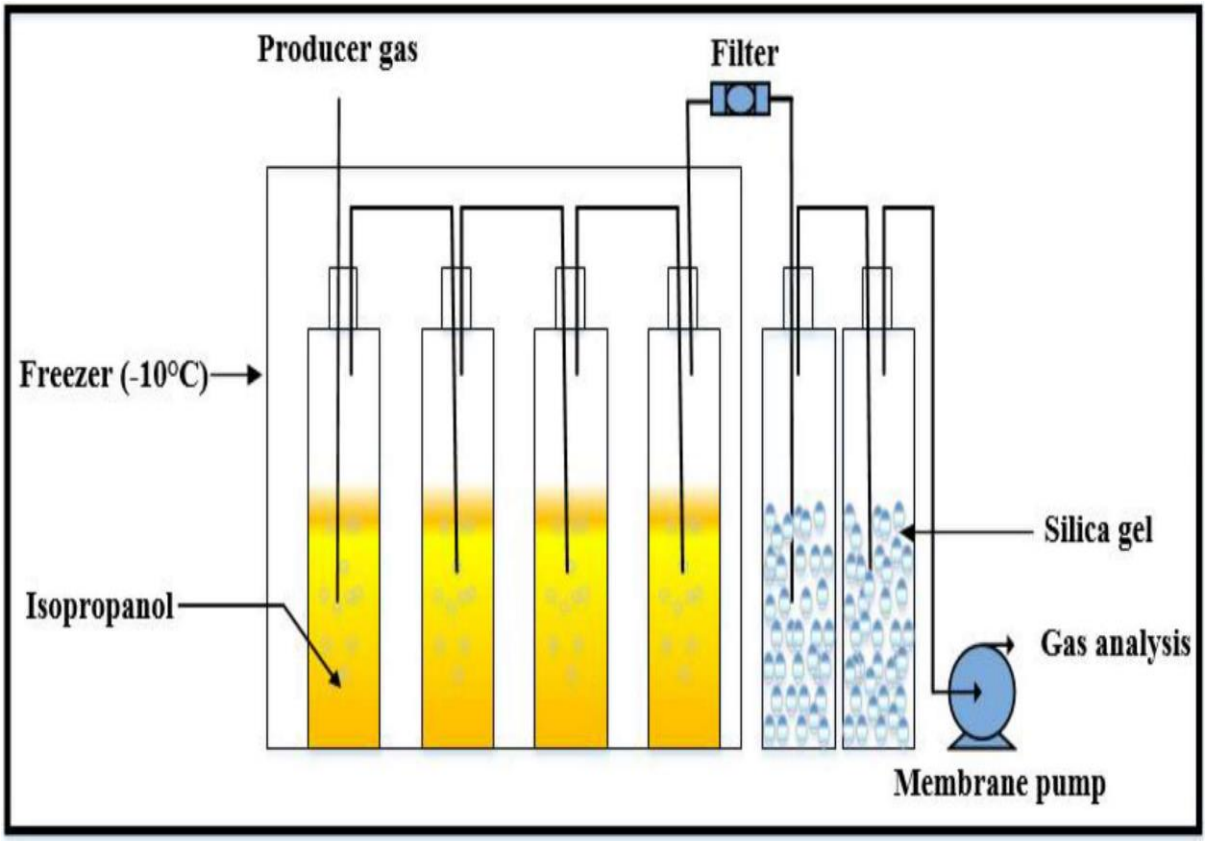


*Figure 4- 9 The downstream gas cleaning system.*

The used filter is a fiber filter trap, which is followed by two more bottles filled by silica gel. At this stage the filtration process is completed. However, using a membrane pump, the filtered gas is then pumped to a gas analyser to measure its efficiency, the pump also compensates for the pressure drop during the tar capture unit and the subsequent filtration bottles and therefore maintains the product gas flow.

### 4.1.8 Gas analyser

As mentioned above, the produced gas should be analysed to ensure its quality. An Emerson XStream analyser was used in this experiment (model number: XEA04303555317), shown in Figure (4-10).


*Figure 4- 10 Xstream Gas Analyser that was used in the experiment, with both the inlet and outlet pipes*

The gas analyser needs a consistent flow rate in order to operate effectively, as the maximum allowed flow rate is 1 l/min, and therefore the flow-rate of the gas existing the gasifier and filtration units were monitored carefully to ensure smooth operation.

The chosen gas analyser can measure  up five different gasses with any combinations as it uses an ultraviolet analysis (UV), non-dispersive infra-red analysis and an electrochemical and paramagnetic oxygen analysis ($eO_2$ and $pO_2$). It is worth noting that the analyser does not provide the actual mass of each individual gas, but instead it provides a volume percentage of each gas's flow against time.

Gas analysis $H_2$. Thermal conductivity is the property of a material that indicates its ability to conduct heat. Thermal conductivity measurement primarily is used for measuring concentrations of hydrogen ($H_2$) and helium (He). These gases are characterized by a specific thermal con ductility, differing clearly from that of other gases. [182].

In this instance, the gas analyser detected the presence of carbon monoxide, carbon dioxide, methane, hydrogen and oxygen.

## 4.2 Reactor and operational safety

Using any type of reactors imposes different risks on both the equipment and personnel. Some of the hazards expected with the gasifier discussed in this study are:

- Combustible gases toxicity, namely hydrogen and carbon monoxide.
- Skin burns due to involvement of incredibly high temperatures.
- Carcinogenic substances; namely tar.
- Explosive hazard from the heavily pressurized nitrogen and air gases.
- High voltage from the power supply; electrocution hazard.

Various safety measures have been taken with the aim of controlling the above hazards. The location of the gasifier was selected to ensure complete isolation within the combustion lab, while a powerful extraction system was used to remove the produced combustible gases. It is located above the gasifier.

Also, fixed gas detectors have been used to ensure appropriate alarm systems. One of the fixed detectors was placed on the left-hand side of the gasifier, and the second (mobile) detector was attached to the person performing the experiment at all times.

Finally, a remote-control system was used to enable switching the system on/off without the need to be near the reactor, this is in case of fire or other hazards that may be prominent upon entering the area.

## 4.3 Gasification procedure

Having prepared the equipment and tools needed to experiment the gasification process, there were more steps and procedures needed before starting the actual operation. In the following section, a step by step of procedures the operation started is described.

- **Step (1**): Each of the Dreschel bottles which have a capacity of 250 ml, was filled with four sets of 100 ml isopropanol, within the tar capture unit.
- **Step (2):** The gas analyser was zero calibrated with nitrogen used as a baseline. For the full calibration of the analyser, a composition of carbon monoxide (conc 15%), carbon dioxide (conc 15%), hydrogen (conc 15%) and methane (conc 5%) was used.

- **Step (3):** An amount of silica sand is added to the bed material within the gasifier. The silica sand's density is 2,650 kg/$m^3$, and its particle size range between 500 to 600 µm. The needed amount is determined based on the $H_s$/D ratio that was discussed earlier in (section 3.4.1).
- **Step (4):** The computer system as well as the data logger, multi-function weight indicator tool was switched on.

- **Step (5):** The split furnace, air blower and the pre-heater were all activated. Using the data logger equipment, the temperature rise was closely monitored, while superficial velocity was kept constant at 40 l/minute (double $U_{mf}$).
- **Step (6):** The final needed step before starting the experiment. It is the gravimetric calibration of the feeder. It is done for each mass flow rate and done via weighting the biomass for 5 minutes against the ER value.

Having completed all the above steps, the biomass is fed directly after drying at room temperature from about 80 mm above the distributor, via a stainless-steel tube. The biomass passes via the hopper section (the lid must be opened). The biomass flow rate varies with the selected ER value of the distributor while maintaining the remaining parameters at constant values.

The ER value for each fuel sample is not identical for each biomass as they exhibit different stoichiometries, and the temperature of the reactor is controlled by the furnace controller. Finally, the above procedure was repeated three times to ensure consistently similar repeatability, and then the hopper was filled with the biomass in order to begin the gasification testing. In the following section, a test run will be discussed alongside settings and reaction considerations within the test.

### 4.3.1 Experimental test run.

Having completed the pre-test procedure steps, the gasifier is started and driven to the required temperature, steady-state conditions should be achieved. At this stage, the lab extraction system is switched on, mainly to ensure that the product gas is fed into the gas analyser, where the suction pump is activated. A consistent flow of the entering biomass is achieved via the feeder equipment, at a certain ER into the gasifier. At this point, the split furnace is switched off to avoid overheating.

In order to maintain the biomass passing through the gasifier's reactor, its direction is controlled via closing and opening the relevant valves. More specifically, valve (a) was closed while opening valve (b) (both marked in Figure (4-1) of this chapter); the latter valve allows ambient air to quench the generated heat within the reactor.
As the gasifier is now activated, the load cell has begun recording the incoming data of the dynamic mass within and logged via the computer. Also, the gas analyser starts recording the product gas data in real-time. The analyser records the volume concentration of each gas produced from the reaction (and filtered thereafter) in terms of concentration percentiles.
Five hours cool down periods were spent in between test runs. This is to allow the gasifier to reach room temperature after shutting it down.

As a preparation for the subsequent test run, the gas analyser with purged with $N_2$ and re-calibrated using the same method mentioned earlier in this section. Finally, the tar capture unit and the stainless-steel pipes should be cleaned of the captured tar in order to prevent blockage to the filtration system, and as a fail-safe the PVC pipes which is used to move the gas from the filtration section to the gas analyser is replaced with fresh pipes.

## 4.4 Feed rate settings.

As discussed previously ER plays a prominent role in the gasification process, as it determines the amount of silica needed, as well as the main operation conditions of the reactor. The air to fuel ratio is discussed thoroughly in the literature, please refer to Chapter (2) of this study for more details. ER is defined as the ratio between the actual air per unit mass of the biofuels entering the gasifier to its stoichiometric air. This relationship is shown in the following equation (4-1):

$$ER = \frac{(air/biomass)_a}{(air/biomass)_b} \qquad Equation\ 4-1$$

where, a: actual and b: stoichiometric

It's worth noting that the stoichiometric air flow rate can be determined from the ultimate analysis of the complete combustion of carbon, hydrogen and sulfur (C, $H_2$ and S), while

nitrogen ($N_2$) is excluded from this calculation as the gasification working conditions would not cause the conversion of the $N_2$ to $NO_x$ (temperatures are not high enough).

As mentioned, the stoichiometric oxygen amount can be estimated sed the data from the chemical reactions from the combustible specifies in a fuel, namely carbon, hydrogen, oxygen and sulfur. More specifically, the reactions are:

$$C + O_2 \rightarrow CO_2 \qquad R6$$

$$H_2 + 0.5O_2 \rightarrow H_2O \qquad R12$$

$$S + O_2 \rightarrow SO_2 \qquad R11$$

The oxygen stoichiometry is determined by the addition of the required amount of the gas in the above three reactions, then subtracting the amount from the fuel's inherent oxygen content. Similarly, the air to fuel ratio (AFR) stoichiometric value was estimated by dividing the required air mass (as calculated above) by the fuel's mass amount. The total values obtained through the experiment for both torrefied and raw biomass is displayed in the following two tables (Table (4-1) and (4-2)).

As the ER value is recorded through the system described earlier in this chapter, the actual air-fuel ratio can be calculated for biomass (date stone) using the following formula equation (4-2) :

$$[AFR]_a = ER * [AFR]_s \quad \textit{Equation 4- 2}$$

Where,

$[AFR]_s$ is the actual air-fuel ratio.

$[AFR]_s$ is the stoichiometric air-fuel ratio.

The air's mass rate value ($\dot{m}_{air}$) to the fuel's mass rate ($\dot{m}_f$) is used to determine the actual air ratio value.

Therefore, the biomass flow rate can be calculated using the formula:

$$\dot{m}_f = \frac{\dot{m}_{air}}{[AFR]_a} \quad \textit{Equation 4- 3}$$

Subsequently, the air's mass flow rate can be calculated using the following equation:

$$\dot{m}_{air} = Volumetric\ Flow\ Rate * Density\ of\ the\ used\ Air \qquad \text{Equation 4- 4}$$

The air's density is 1.2 kg/$m^3$ at ambient conditions. It's also worth noting that the used oxygen and nitrogen's weight fraction is 0.232 and 0.754, respectively.

A widely used agroindustry residue called date stone biomass, was available for this test in the form of coarse particles, with a size of 5 mm approximately. Its moisture content was 9.55%, the samples were dried to a moisture content of 5.29%. They were then stored in re-sealable plastic bags.

The air's residence time in the gasifier reactor should remain almost constant at a rate of 40 L/min (0.12 cm/sec) is this research. The flow rate was controlled by altering the speed of the vibrator section.

Using the above procedures and tests, the feed mass rate for 'palm date stones' biomass was calculated and noted below in Table (4-1) while the required ER value is in Table (4-2).

*Table 4- 1 Air-fuel stoichiometric ratio for the palm date stones gasification.*

| *Combustion equation* | *Fuel composition* | | | *Stoichiometric $O_2$ (g)* |
|---|---|---|---|---|
| | ***Component*** | *(%wt)* | *Mass (g)* | |
| *$C+O_2= CO_2$* | *C* | ***45.5*** | ***0.455*** | *1.213* |
| *$H_2+0.5O_2=H_2O$* | *H* | ***6.0*** | ***0.06*** | *0.48* |
| | *O* | ***38.52*** | ***0.3852*** | *-0.3852* |
| *$S+O_2=SO_2$* | *N* | | | |
| | *S* | ***0.07*** | ***0.0007*** | *0.0007* |
| *Total* | | ***90.09*** | ***0.9009*** | |
| *Total O2 required* | | | | *1.3085* |
| *Total Air required* | | | | *5.69* |
| *Air-Fuel Ratio (by mass)* | | | | *6.32* |

*Table 4- 2 Air-fuel ratio for the gasification of the date palm stones, at different ER values.*

| *ER* | *0.15* | *0.2* | *0.25* | *0.3* | *0.35* |
|---|---|---|---|---|---|
| *(AFR)actual* | *0.948* | *1.264* | *1.58* | *1.896* | *2.212* |
| *(kg biomass/hr)* | *3.04* | *2.28* | *1.82* | *1.52* | *1.3* |

## 4.5 The effectiveness of gasification

The gasification proves efficiency can be evaluated based on the dry gas heating value (HHV), carbon conversion (CC) as well as the cold gas efficiency (CGE). HHV can be calculated using the gas composition values, using the below formula:

$$HHV = \frac{(12.75*[H_2]+12.63*[CO]+39.82*[CH_4]+\cdots)}{1000} \quad \textit{Equation 4- 5}$$

Where, the component contents are in % mole.

Heat of combustion in MJ/$Nm^3$

Also, as the high hydrocarbons concentrations are very low and often undetectable, they have been neglected from the calculations. Where the species contents are given in mole%, and their heats of combustion, in MJ/$Nm^3$ [183].

Due to the inactivity of $N_2$ at gasification conditions, Producer Gas (P.G.) yield in $Nm^3$/hr can be estimated making use $N_2$ mass balance for gasifier system

$$Mass\ rate\ of\ total\ input\ N_2 = Mass\ rate\ of\ \mathrm{d}total\ output\ N_2$$

$$Mass\ rate\ of\ total\ input\ N_2 = Mass\ rate\ of\ N_2\ in\ air + Mass\ rate\ of\ N_2\ in\ biomass\ fuel$$

$$Mass\ rate\ of\ N_2\ in\ air = wt\%\ of\ N_2\ in\ air \times mass\ rate\ of\ feeding\ air\ \dot{m}air$$

$$Mass\ rate\ of\ N_2\ in\ fuel = wt\%\ of\ N_2\ in\ fuel \times mass\ rate\ of\ feeding\ fuel\ \dot{m}biomass$$

The total moles of $N_2$ in producer gas P.G. can be calculated using its molecular weight, 28 using Equation

$$Total\ moles\ of\ N_2\ in\ P.G. = Total\ output\ mass\ rate\ of\ N_2/28$$

Then, the total moles rate of P.G. can be calculated, making use total moles of $N_2$ in P.G. using Equation

$$Moles\ rate\ of\ P.G. = \frac{\text{Total mole rate of N2 in P.G}}{(\text{vol\% of N2 in P.G.})/100}$$

Volume parentage of N2 in P.G. was estimated using Equation by the difference of the producer gases, which were analysed. These gases are CO, $CO_2$, $CH_4$, and $H_2$ in volume percentage.

$$Vol\%\ of\ N_2\ in\ P.G. = 100 - vol\%\ of(\ CO + CO_2 + CH_4 + H_2)$$

It can be noticed that for ideal gas, the volume percent and mole percent are equal. The volumetric flowrate of producer gas in Nm3/hr can be calculated making use that for ideal gas at standard conditions, 273.15oK and 101.325 kPa, each 1 kgmol of the gas occupied 22.4 Nm3. Therefore, the producer gas in volumetric flowrate, for example Nm3/hr, at ambient conditions can be calculated using Equation.

$$P.G.volumetric\ flowrate = moles\ rate\ of\ P.G. \times 22.4$$

Finally, the gas yield GY of producer gas per unit mass of biomass feeding fuel, for example in $Nm^3$/kg of feed biomass can be calculated using Equation (4- 6)

$$Y = \frac{volumetric\ flowrate\ of\ P.G\ in\ (Nm3/hr)}{mass\ rate\ of\ feed\ fuel\ in(\dot{m}biomass/hr)} \quad Equation\ 4\text{-}6$$

The gas analysis helps determining the carbon conversion into the product gas, based on the volumetric percentage of the fuel gas's composition of the gases, carbon monoxide, carbon dioxide and methane, using following formula:

$$CC = \frac{Y\ (\ CO\% + CO_2 + CH_4\%) * 12}{22.4\ C\%} * 100\% \quad Equation\ 4\text{-}7$$

Where, C% is the mass% of the carbon in the biomass's ultimate analysis.

The performance of the biomass gasification can be represented using different indicators.

Mainly, the cold gas efficiency index accounts for the process's performance. However, this concept does not consider the existence of condensable substances, for example tar. The cold gas efficiency is the percentage of the used fuel heating value what has been converted, by the product's gas heating value, which can be translated into the following formula:

$$CGE = \frac{HHV * Y}{HHV_f} * 100\% \quad \textit{Equation 4- 8}$$

Where,

HHV is the highest heating value in MJ/Nm$^3$.

$HHV_f$ is the gross calorific value of the fuel in MJ/kg.

## 4.6 Summary

The rig's design and equipment, including the feeder, the plenum, the diffuser plate, the heating system unit and the bespoke platform load cell are elaborated in this chapter.
The gas analyser unit as well as the downstream cleaning system are discussed and shown earlier in the chapter, as well as the used calibration procedure of the system. A step by step guide of the experiment is also given.
Finally, a mass balance method was used to determine the char's value within the gasifier, the used equation and calculation method of the feeding rate for specific ER points and per biomass type are detailed.

## Chapter 5

# Experimental results

# Chapter 5

## Experimental results

## 5.1 A study of the catalysed pyrolysis of date stone biomass in fixed bed conditions.

The impact of catalyst particle and its associated size on the pyrolysis of date stone is discussed in this section. The study is conducted on different types of catalysts and at various conditions (biomass to catalyst ratios) at fixed bed conditions. The main aim of the study is to understand the consequences of changing the type of catalyst, the ratio of catalysts, and particle sizes on the kinetic behavior from the system while investigating the effects on the biomass pyrolysis.

## 5.2 Fixed bed Thermogravimetric analysis (TGA).

Thermogravimetric analysis (TGA) is the most commonly used tool to obtain experimental kinetic data, and isoconversional kinetic analysis is the most effective way for processing TGA data to calculate effective activation energies for lignocellulosic biomass pyrolysis Because the TGA method is an accurate way to measure the degradation rate. It has been widely used to characterize and compare the thermal behaviour of different samples[184].

The main advantages of TGA for the study of pyrolysis are simplicity in implementation and utilization and good repeatability [185]. on the other hand, the drawbacks of TGA are:

1. The temperature distribution throughout the sample is non-uniform.

2. Poor solid-solid and gas-solid distribution and mixing within the sample.

Biomass pyrolysis is a viable route to produce renewable bio-oil and includes fundamental chemical reactions that are precursors of other thermal conversion technologies, such as combustion and gasification. Therefore, the study of the pyrolytic characteristics of biomass covers a key issue in demand for the advancement of biomass thermal conversion technologies [33].

The results of pyrolysis via thermogravimetric analysis can be represented as a function of x, as shown on Eq. (5-1).

$$\times = \frac{m-m}{mo-mf} \qquad \textit{Equation 5- 1}$$

Where:

$m_o$: the initial mass of the sample.

m: the instantaneous mass of the pyrolysis sample.

$m_f$: the final residual mass.

The degree of conversion with respect to the temperature at a constant rate of heating at 20 ℃/min at 4 date stone particles sizes obtained is shown in Figure (5-1). The figure shows that at temperatures lower than 250 ℃, a change in mass is observed as a result of moisture loss at the early heating period. At 250 ℃, the date stone thermal decomposition commenced, however the active pyrolysis (i.e., the primary decomposition stage) occurred at temperatures between 260 ℃ to 400 ℃. Most of the volatile decomposition occurred at the same temperature range, consisting of up to 80% of the total mass conversion. Consequently, when the conversion rate exceeds 80%, char is mostly what remains thereafter. As per the TGA results, the same trend was observed at all particles sizes, because the particle size increases, the temperature gradients inside the particle also increase, such that at any time the surface temperature is higher than the core temperature, which may increase the yield of solids with a corresponding decrease in the production of liquid and gas [186]. But with slow heating, it gives a lot of time for heat to transfer only inside the particle, and thus the effect of increasing the volume was decreased,

and therefore, it is proposed that under the conditions studied, the particle size is independent of the decomposition rate.

Four particle sizes were used in the experiments to investigate their effect on the pyrolysis process, as shown on Figure (5-1). It showed that TGA is not heavily influenced by the changes in the date stone sizes, as long as the same biomass material was used. This is not surprising, as it was also observed in other biomass materials, such as the marine biomass (codium fagile) as shown by Daneshvar et al. who tested particle sizes ranging from 75 μm - 1400 μm [187].

The biomass used consists of hemicellulose, cellulose and lignin, which each has distinctively different structures. Therefore, they can be identified via the thermogravimetric analysis [188].

Hemi-cellulose decomposes at a temperature range of 220 ℃ and 315 ℃, while cellulose decomposes at 315 ℃ and 400 ℃ and lignin decomposes at a much wider temperature range between 160 to 900 ℃; according to Yang et al. [189].

The differential rate of conversion (dm/dt) was measured at a heating rate of 20 ℃/min via the differential thermogravimetric analysis method (DTG). The analysis was observed for particle sizes of 300, 500, 600 and 710 µm, shown on Figure (5-2) with respect to the distribution curves (DTG) of the date stones. The first peak is seen at 100 ℃ which corresponds to the sample's moisture content. The second peak is seen between 200 ℃ to 300 ℃, indicating the hemicellulose decomposition. The last peak is seen at temperatures between 300 ℃ to 380 ℃ and is likely the cellulose decomposition. The mass loss was lower and at a more consistent rate when temperature exceeded 380 ℃, due to the decomposition of lignin. This is similar to the DTG analysis done by E.Kastanki et al for the pyrolysis of date stone [190] and Jae et al. for maple wood [191].

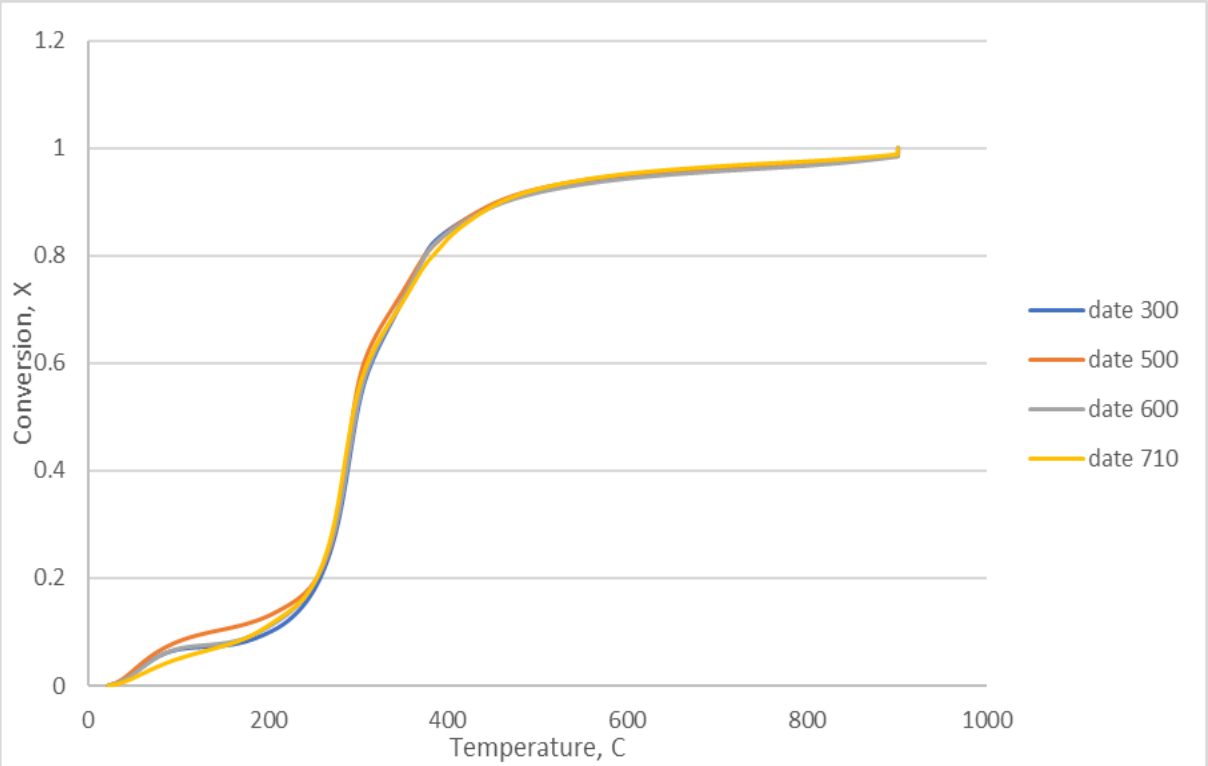


*Figure 5- 1 Relationship between mass conversion and temperature for date stone of different particle sizes. Heating rate 20°C/min, sample wt. ~10mg (TGA), nitrogen flow rate 100 ml/min.*

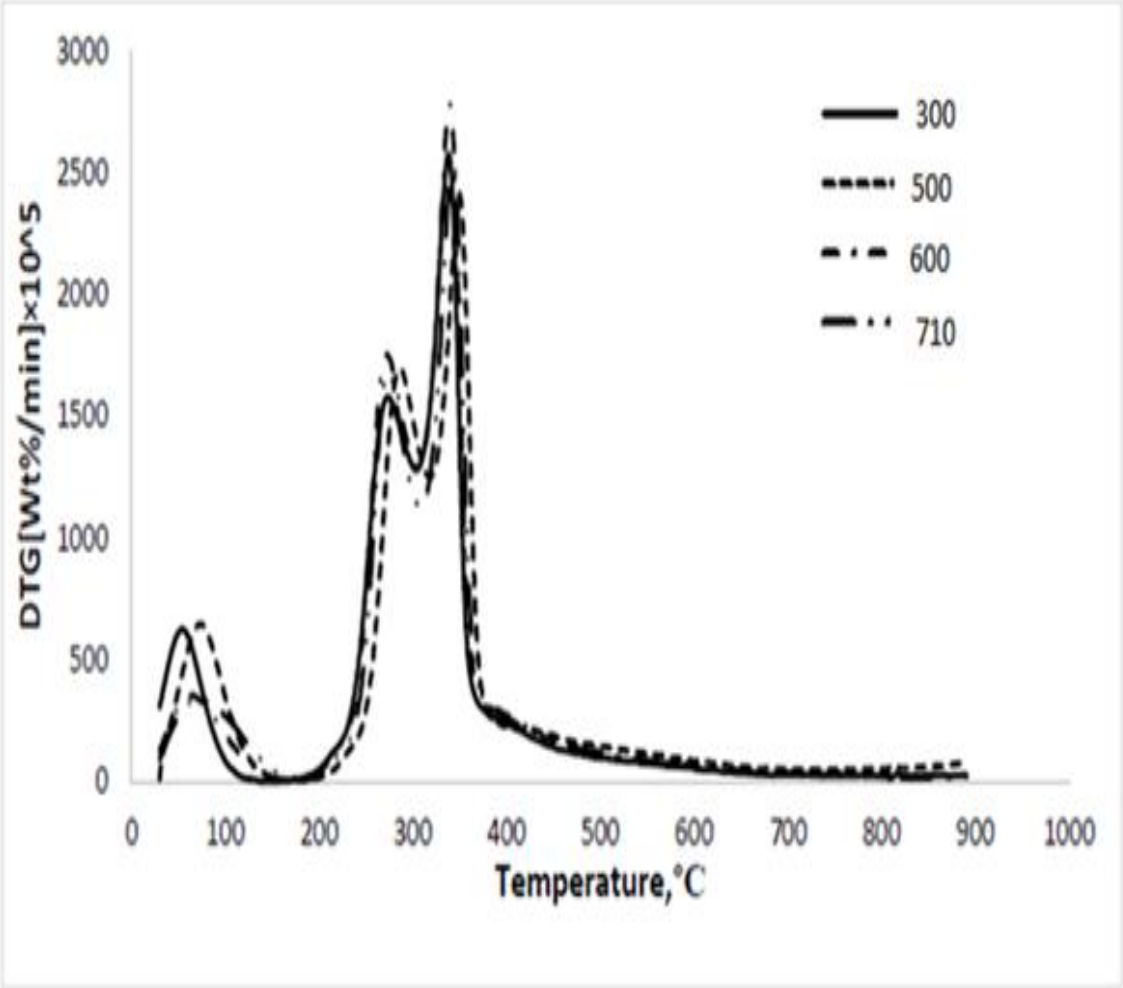


*Figure 5- 2 Variation of the instantaneous rate of reaction with temperature at 20 ℃/min heating rate for pyrolysis of date stone.*

## 5.3 Kinetic analysis of pyrolysis of Date stone.

The date stone was tested at non-isothermal conditions in the TGA at a heating rate of 20 ℃/min at various solid-state mechanisms, outlined on Table (5-1). The tests were conducted to determine the mechanism using the Coats Redfern method. The result of the test is to determine the mechanisms leading to the particle size (710 μm) decomposition, at a conversation rate (x) ranging between 0.2 to 0.8 because the main conversion occurs in this study range.

*Table 5- 1 Typical Reaction Mechanism for Heterogeneous Solid-State Reaction* [192].

| *Symbol* | *Reaction mechanism* | *f(x)* | G(x) |
|---|---|---|---|
| G1 | One- dimensional diffusion, 1D | 1/2x | x2 |
| G2 | *Two- dimensional diffusion, (Valensi)* | [-ln(1-x)]-1 | x+(1-x)ln(1-x) |
| G3 | *Three-dimensional diffusion, (Jander)* | 1.5(1-x)2/3[1-(1-x)1/3]-1 | $[1-(1-x)1/3]^2$ |
| G4 | *Three-dimensional diffusion, (G-B)* | 1.5[1-(1-x)1/3]-1 | $1-2x/3-(1-x)^{2/3}$ |
| G5 | *Three-dimensional diffusion(A-J)* | 1.5(1+x)2/3[(1+x)1/3-1]-1 | $[(1+x)1/3-1]^2$ |
| *G6* | *Nucleation and growth(n=2/3)* | $1.5(1-x)[-\ln(1-x)]^{1/3}$ | $[-\ln(1-x)]^{2/3}$ |
| G7 | *Nucleation and growth (n=1/2)* | $2(1-x)[-\ln(1-x)]^{1/2}$ | $[-\ln(1-x)]^{1/2}$ |
| *G8* | *Nucleation and growth (n=1/3)* | $3(1-x)[-\ln(1-x)]^{2/3}$ | $[-\ln(1-x)]^{1/3}$ |
| G9 | *Nucleation and growth(n=1/4)* | $4(1-x)[-\ln(1-x)]^{1/3}$ | $[-\ln(1-x)]^{1/4}$ |
| G10 | Autocatalytic reaction | x(1-x) | ln[x/(1-x)] |
| G11 | *Mampel power law(n=1/2)* | $2x^{1/2}$ | $x^{1/2}$ |
| *G12* | *Mampel power law(n=1/3)* | $3x^{2/3}$ | $x^{1/3}$ |
| *G13* | *Mampel power law(n=1/4)* | $4x^{3/4}$ | $x^{1/4}$ |
| *G14* | *Chemical reaction(n=3)* | $(1-x)^3$ | *[(1-x)-2-1]/2* |
| *G15* | *Chemical reaction(n=2)* | $(1-x)^2$ | *(1-x)-1-1* |
| *G16* | *Chemical reaction(n=1)* | 1-x | *-ln(1-x)* |
| G17 | *Chemical reaction(n=0)* | 1 | x |
| *G18* | *Contraction sphere* | $3(1-x)^{2/3}$ | $1-(1-x)^{1/3}$ |
| G19 | Contraction cylinder | $2(1-x)^{1/2}$ | $1-(1-x)^{1/2}$ |
| Note: A-J: Anti- Jander; G-B: Ginstling-Brounshtein | | | |

The analysis was conducted using Equation (5-2), which was applied to each individual model. The function G(x) which yields a straight line alongside the highest correlation coefficient is the best representation of the mass loss reactions kinetic.

$$ln\left(\frac{G(x)}{T2}\right) = ln\left(\frac{AR}{\beta E}\right) - \frac{E}{RT} \qquad \textit{Equation 5- 2}$$

The values of G(x) and the corresponding correlation coefficient are shown on Table (5-2). This is obtained via plotting the $\ln(G(x)/T^2)$ with respect to (1/T), shown on Figure (5-3). This graph shows Equation (5-2), when applied to each individual model from Table 5- 1. The function G(x) which yields a straight line alongside the highest correlation coefficient is the best representation of the mass loss reactions kinetic.

The value of the activation energy can be obtained as the value of the linear regression of the slope.

*Table 5- 2 Reaction model for date stone decomposition during fixed bed non-isothermal pyrolysis.*

| NON-ISOTHERMAL (TGA), X=0.2-0.8 | | | | | | | | | |
|---|---|---|---|---|---|---|---|---|---|
| G(X) | **G1** | **G2** | **G6** | **G7** | **G14** | **G15** | **G16** | **G17** | **G18** |
| **R2** | 0.8297 | 0.8587 | 0.9101 | 0.8825 | 0.9726 | 0.9452 | 0.8825 | 0.7516 | 0.8743 |
| **EA(KJ/MOLE)** | 48.3 | 55.99 | 83.1 | 43.7 | 73.84 | 51.28 | 32.94 | 19.26 | 4.27 |

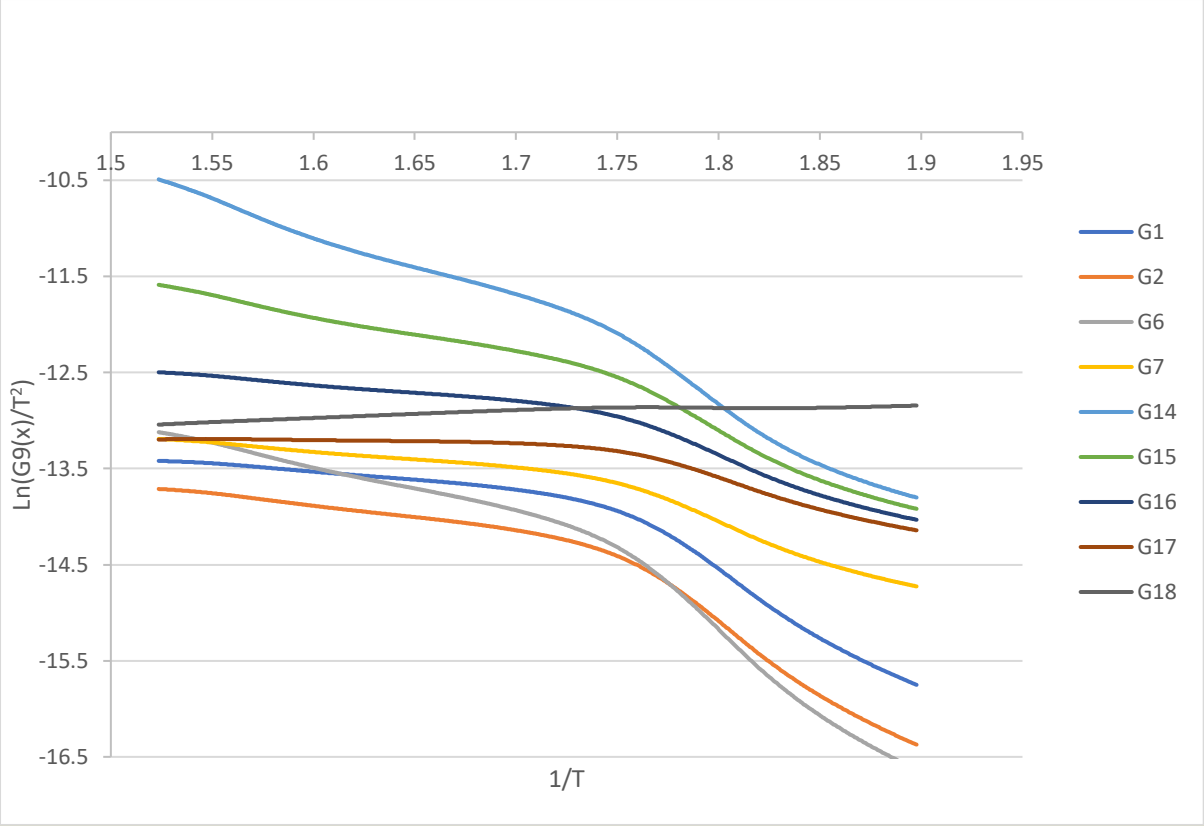


*Figure 5- 3 Correlation of ln(G(x)/T) versus 1/T for 710 µm particle size for non-isothermal TGA.*

The universal kinetics of the thermal decomposition of biomass can be described using Equation (5-3), which is possible as the pyrosis process is a heterogenous solid-state reaction [193].

$$\frac{dX}{dt}=k(Cg,T)f(X) \quad \textit{Equation 5- 3}$$

Where:

T: temperature of the reaction

t: time of the reaction

Cg: the concentration of the gasification agent.

f(x): the differential reaction model.

k(T): the time dependent reaction rate, obtain by Equation (5-4).

$$K = A\ exp\ [\frac{-Ea}{RT}] \quad \textit{Equation 5- 4}$$

The reaction rate of the gasification can be considered solely dependent on temperature, if the gasification agent ($C_g$) concentration remained a constant during the reaction. This was assumed for the following calculations.

Various experimental techniques were utilised at the TGA non-isothermal process. The goal is to examine changes in the sample as the temperature increases. The rate constant (k) is directly proportional to temperature. This eliminates the need of multiple experiments as it allows activation energy derivation from a single experiment [194].

Non-isothermal thermogravimetric analysis was compared to the appropriate fitting and free models. The reaction mechanism was determined by the first approach at Table (5-1). Substituting the Arrhenius equation within equation (5- 5) yields the following.

$$\int \frac{dx}{f(x)} = \int k(T)dt \qquad \text{Equation 5- 5}$$

$$\int \frac{dx}{f(x)} = \int A\ exp\ \frac{-E}{RT}\ dt \qquad \text{Equation 5- 6}$$

At constant heating rate, the variation of temperature with time can be estimated by Equation (5-7).

$$T = To + \beta t \qquad \text{Equation 5- 7}$$

Where:

β heating is rate,

$T_o$ is the initial temperature of the reaction.

Differentiating both sides of equations (5–6) and (5-7) above yields Equation (6-8). Which upon combining with Equation (5- 6) results in Equation (5-9).

$$dT = \beta dt \text{ or } dt = dT/\beta \qquad \text{Equation 5- 8}$$

$$\int \frac{dx}{f(x)} = \int_0^T A\beta\ exp - \frac{E}{RT} dT \qquad \text{Equation 5- 9}$$

The right-hand side is a non-integrable function; however the left side of equation is again G(x).

$$G(X) = \int_0^T A\beta\ exp - \frac{E}{RT} dT \qquad \text{Equation 5- 10}$$

Equation (5- 11) describes the Frank-Kaminski approximation equation which can be used to select the reaction mechanism model.

$$\int_0^T exp\left(-\frac{E}{RT}\right)dt = \frac{RT^2}{E}exp(-\frac{E}{RT})$$ *Equation 5- 11*

Merging Equations (5- 9) and (5- 10) results equation (5-11) which is called the Coats-Redfern equation [195]. The Coats-Redfern integral method is in fact a single heating rate method which is used widely for the analysis of kinetic parameters of non-isothermal systems [196]. The method when applied, it yielded Equation (5-12) as following:

$$Ln(\frac{G(x)}{T^2}) = ln\left(\frac{AR}{\beta E}\right) - \frac{E}{RT}$$ *Equation 5- 12*

Finally, plotting Ln ($\frac{G(x)}{T^2}$) againt 1/T yields a straight line with (-E/R) slope. Indicating that ln (AR/βE) is a constant. The mechanism function G(x) takes into account the reaction mechanism. Using a model from Table (5-1) and substituting in Equation (5-12), the mechanism function model can be confirmed, and was found to describe the linear nature of the reaction as per the Pearson correlation coefficient $R^2$. The main goal of this study is to quantify the pyrolysis kinetics of palm stone in a batch reaction. The model selected to describe the mechanisms of the reactions with respect to the highest value of regression on the test model. This is to allow estimation of activation energy.

## 5.4 The selection of catalyst material

It is important to ensure the correct catalyst material is selected for the experiments, as it will have an impact on the reactions within the gasifier and the TGA device used [197][198].

Pinto et al. [199] studied the effectiveness of lime, olivine, and dolomite, and found dolomite was the most effective catalyst to reduce tar in syngas. Also, the highest gas yield and higher heating values (HHV) of syngas were achieved in the presence of dolomite for bench scale gasification of spent lignin pellets. In terms of producing tar-free syngas at a cheaper price, dolomite is a highly attractive catalyst. Similarly, Cortazar et al. [200] evaluated the effectiveness of dolomite, γ-alu-mina, olivine and FCC catalyst for continuous steam

gasification of sawdust in a bench-scale plant equipped with a fountain confined conical spouted bed reactor It is noteworthy that in the presence of dolomite, hydrogen content is the highest in all the three cases presented which corresponds to lower tar content in the final syngas.

In this section, the impact of different catalyst on the kinetic energy from data stone will be assessed. The catalyst will match the same experiment as in Pinto et al. [199], as the dolomite, olivine and limestone will be tested. The dolomite was found to be the catalyst with the highest activation energy ($E_a$) as detailed in the following sections.

### 5.4.1 Pre-experiment preparations

Prior to the start of the experimentations, a few perquisites must be undertaken. This is in order to calibrate the device and ensure accurate readings from the TGA device, and the different effects on the date seeds.
In order to ensure the consistent operation of the of the TGA device and measure its uncertainty, 10 different date stone samples table (5-3) were prepared for testing in the TGA. Each of the samples was analysed at the same temperature rate and particle size at 20 ° C / min and 300 μm. The readings are shown on Figure (5-4)

*Table 5- 3 Number of date stone samples and its size.*

| No of sample | Size | Type of residue used |
|---|---|---|
| 10 | 300 μm | Date stone |

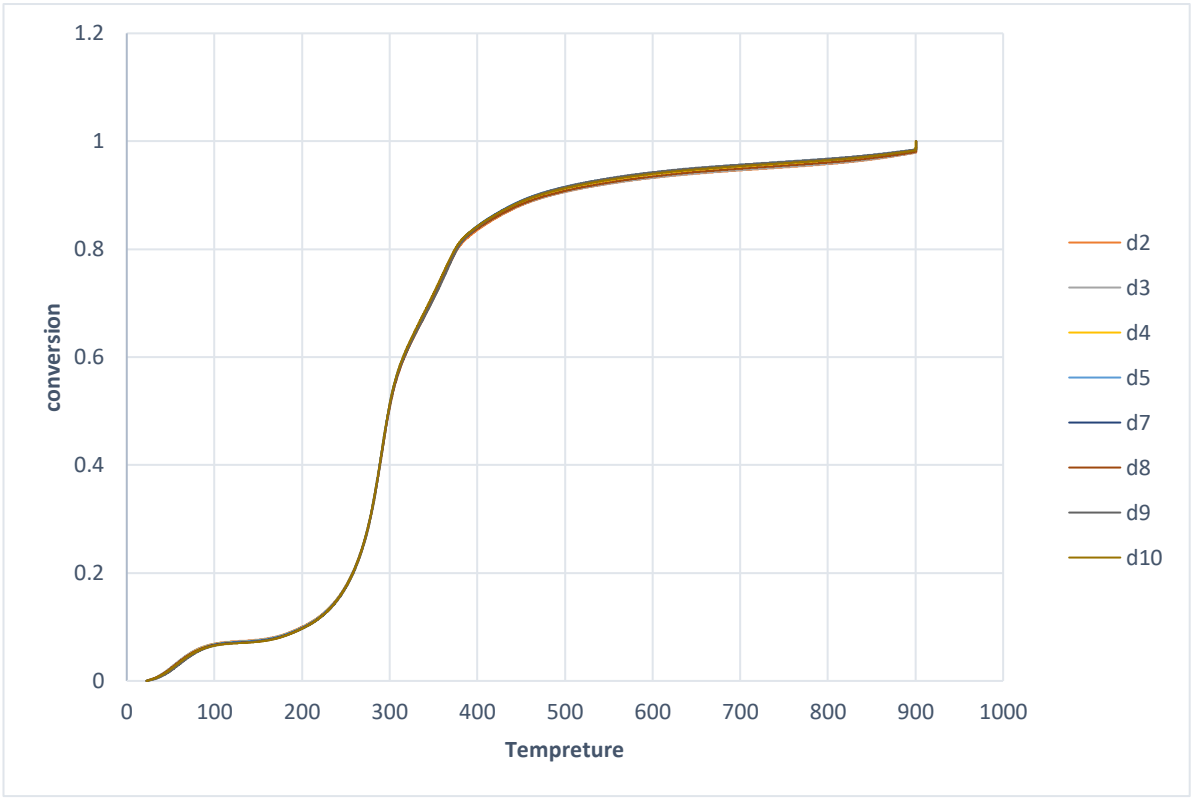


*Figure 5- 5 Conversion versus temperature for 6 samples of Date stone in TGA*

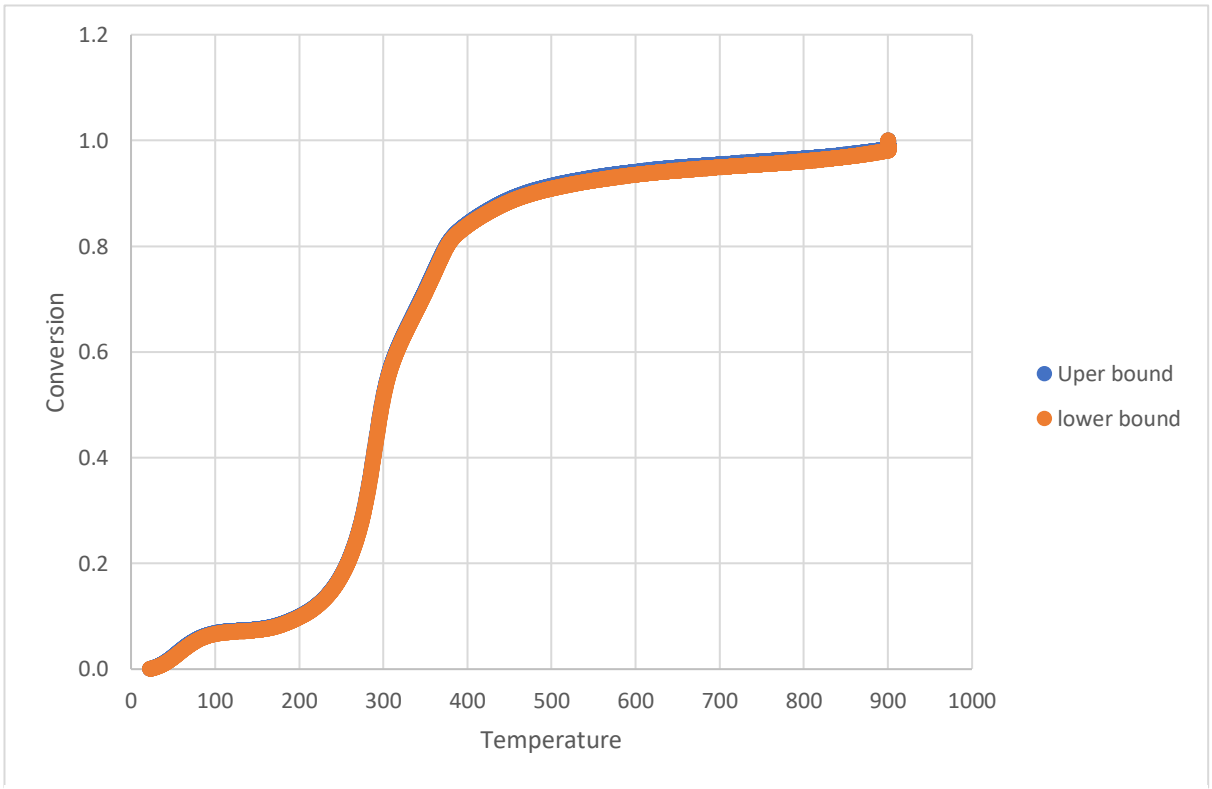


*Figure 5- 4 Upper and Lower bound of 10 sample of date stone in the TGA*

The readings were very similar for each sample of the date stone. This is illustrated in Figure (5-4) above, as the trend lines are visually identical throughout the testing for each date stone batch.

After calculating and drawing the upper and lower bound of the date stone samples used in this experiment, Figure (5-5) turned out to be largely identical, which shows the efficiency of the TGA.

For further examination, sand was added to the date stones at different ratios. This is to determine the impact of non-catalytic materials on the procedure. The resulting readings are shown in Figure (5-6).

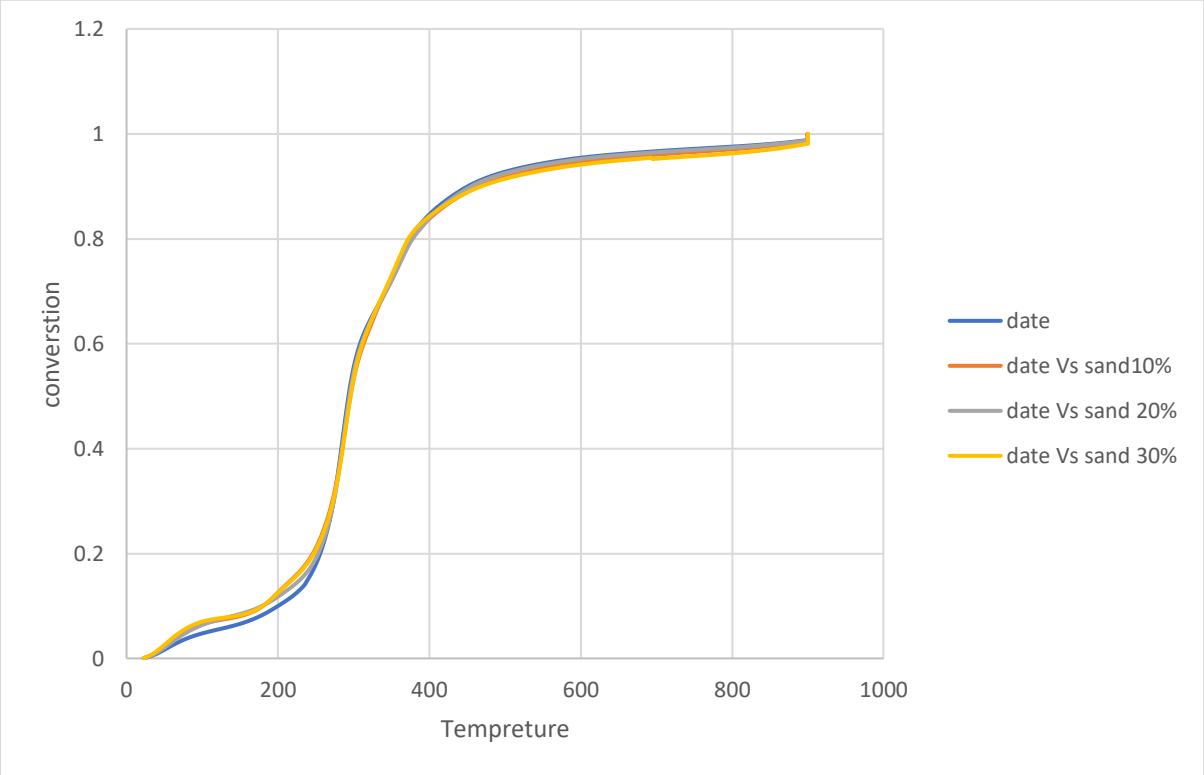


*Figure 5- 6 date stone with different ratio of sand*

This has shown that sand had very little impact on the date stone and therefore it is negligible. It kept the same trend throughout the whole procedure as shown on the above graph. The rate date stone data is shown on the blue line, and then it is assessed against 10%, 20% and 30% (weight %) of sand mixed with the date stone. All the resultant trends are the identical to the original raw date stone.

To confirm the separation of the effect of calcification-induced catalyst mass loss from pyrolysis of date stone biomass, mass loss experiments were performed on TGA of date stone,

dolomite and limestone samples. The degree of conversion relative to the temperature at a constant rate of heating at 20°/min and the result is as shown in the figure (5-7).

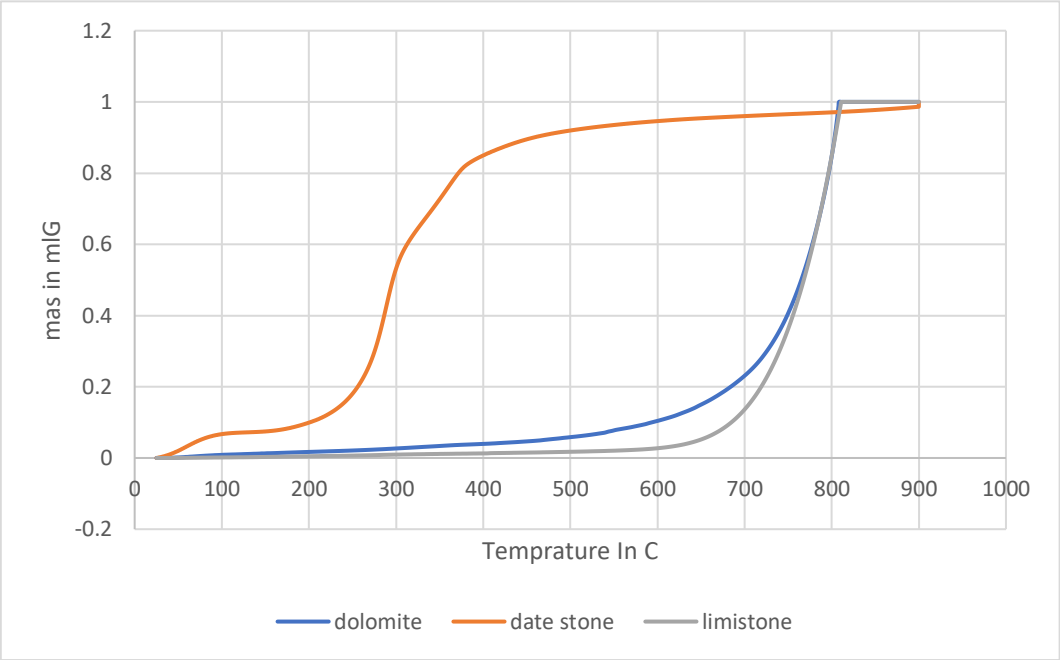


*Figure 5- 7decompose date stone, dolomite and limestone*

The figure shows a date stone at temperatures below 250 ° C, and a change in mass as a result of moisture loss is observed in the early healing period. At 250 ° C, thermal decomposition of date stone began, however, active pyrolysis (that is, the initial decomposition stage) occurred at temperatures from 260 ° C to 400 ° C, most of the volatile decomposition occurred in the same temperature range, which constitutes 80 % of the total overall conversion. Thus, when the conversion rate exceeds 80%, char is often what's left after that.

Moreover, a typical TGA curve for a dolomite sample is shown in Figure 1. The observed weight loss under 700 °C was between 1 and 33% and between 700 °C and 800 °C decompression. Also, the TGA curve limestone started to decompose from 650 °C and 800 °C.

As a result, it was found that there is no effect of catalyst mass loss due to decomposition from pyrolysis of date stone biomass and mass loss because date stone completely decomposes before decomposition of the used catalysts starts at 200 °C.

Non-isothermal testing of date stone with different catalysts (dolomite, olivine and limestone) was done in the TGA instrument with a 20°C/min heating rate. Several solid-state mechanisms, Table (5-1), were tested for a suitable fit by the Coats-Redfern method in order to determine the mechanisms responsible for the decomposition of biomass of particle size 710 μm at

conversion between x=0.2-0.8, because the main conversion occurs in this study range. Equation (5-12) was applied separately to each model, the form of G(x) which gives a straight line with the highest correlation coefficient was considered to be the model function that best represents the kinetic mass loss reaction.

*Table 5- 4 DATE STONE WITH 10% OF DOLOMITE*

| NON-ISOTHERMAL (TGA), X=0.2-0.8 | | | | | | | | | |
|---|---|---|---|---|---|---|---|---|---|
| G(X) | **G1** | **G2** | **G3** | **G4** | **G5** | **G6** | **G7** | **G8** | G9 |
| **R2** | 0.8297 | 0.8587 | 0.1469 | 0.6458 | 0.1469 | 0.9101 | 0.8825 | 0.8825 | 0.8825 |
| G(X) | G11 | G12 | G13 | G14 | G15 | G16 | G17 | G18 | G19 |
| **R2** | 0.4119 | 0.7516 | 0.7516 | 0.9726 | 0.9452 | 0.8825 | 0.7516 | 0.8743 | 0.0471 |

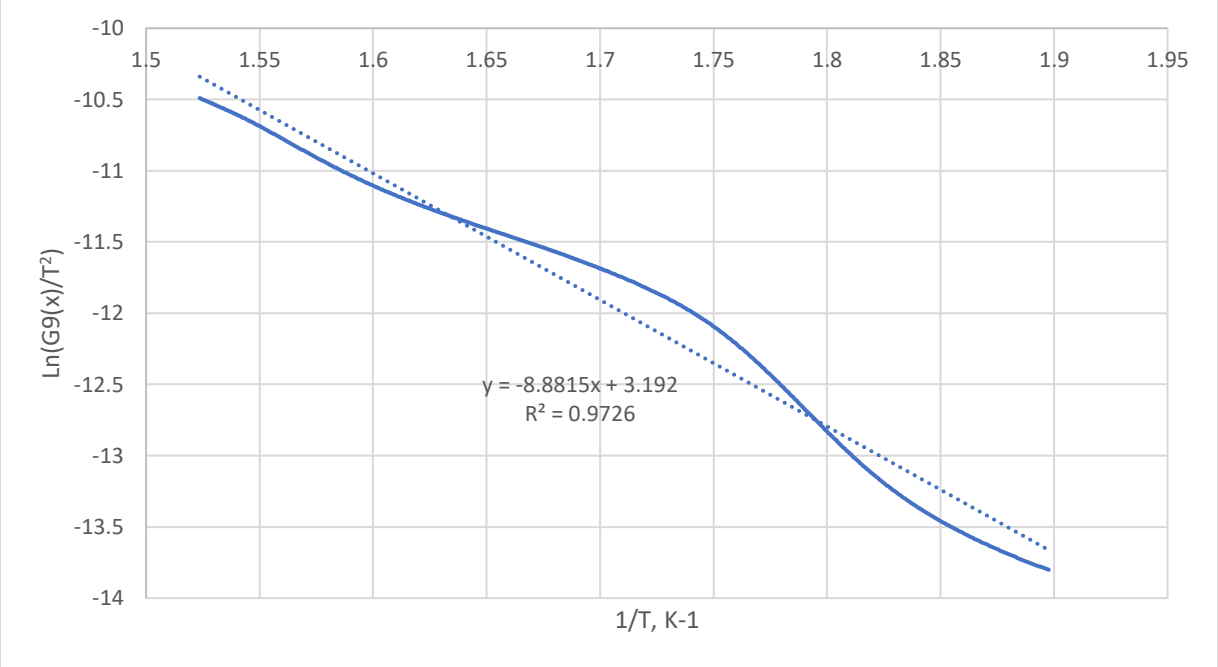


*Figure 5- 8 plot of the conversion function using the Coats Redfern method Vs reciprocal of temperature for date stone with 10% dolomite*

Similarly, the test was performed on both 10% olivine and 10% limestone, separately. The results for the first is shown on Figure (5-8), and for the latter in Figure (5-10). The data for each catalyst can then be utilised to estimate its activation energy ($E_a$) which subsequently would give a good indication about the effectiveness of the catalyst [197].

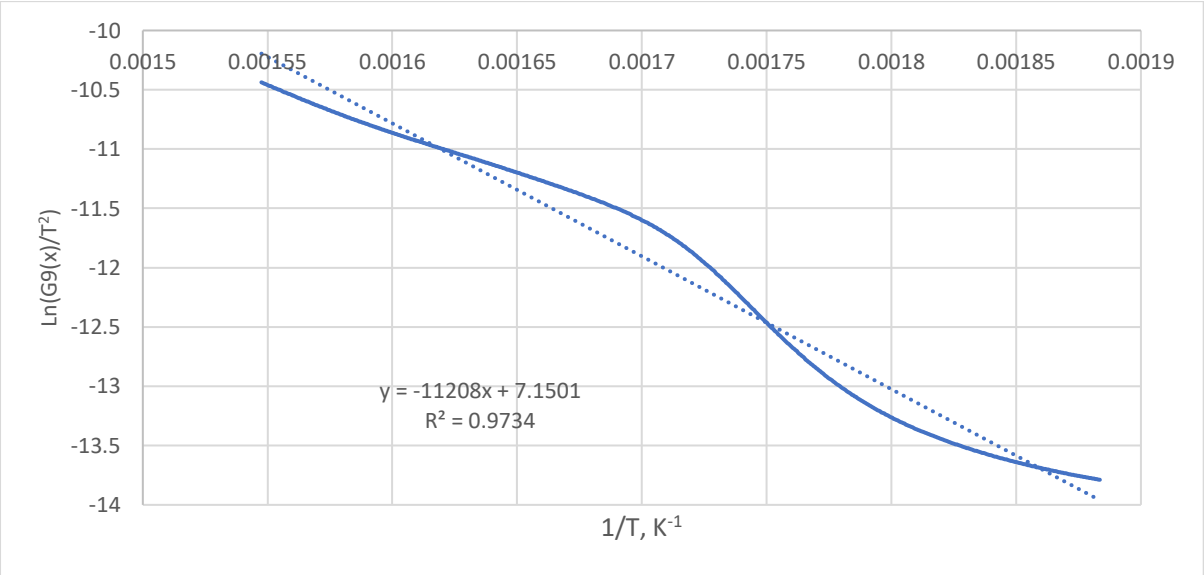


*Figure 5- 10 plot of the conversion function using the Coats Redfern method Vs reciprocal of temperature for date stone with 10% olivine.*

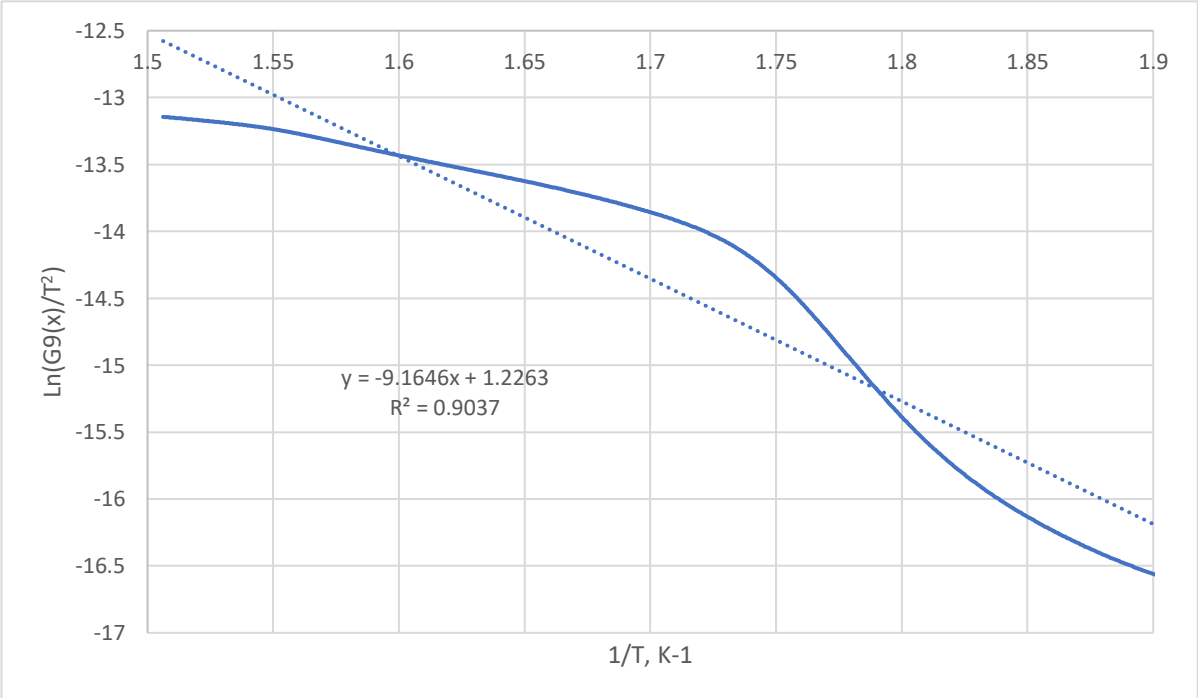


*Figure 5- 9 plot of the conversion function using the Coats Redfern method Vs reciprocal of temperature for date stone with 10% of limestone.*

The calculated catalyst activation energy ($E_a$) for each of the dolomite, olivine and limestone is shown on Table (5-5) below, and dolomite 10% (marked in blue) has the greatest effect on the process at 44.89 kJ/mole $E_a$.

*Table 5- 5 Efficiency of potential catalyst for the gasification process*

| | Dolomite 10% | Olivine 10% | Limestone 10% |
|---|---|---|---|
| **EA (kJ/MOLE)** | 44.8 | 95.12 | 76.19 |

As described in the previous section, Equation (5-2) was applied in the table (5-1) and the form of G(x) which gives a straight line with the highest correlation coefficient was considered to be the model function that best represents the kinetic mass loss reaction. in this experimental, the fitted method was (G14) ([(1-x)-2-1]/2) and from the slope, the activation energy was calculated to choose the best catalyst with date stone.

Both limestone and dolomite are types of rock made of carbonate residues. The patterns of the way they behave chemically are almost the same with varied intensities.

Limestone is a sedimentary rock composed largely of the mineral calcite (calcium carbonate: $CaCO_3$). It often has variable amounts of silica in it, as well as varying amounts of clay, silt, and sand.

Dolomite is also a carbonate mineral but is made of 'calcium magnesium carbonate' instead of pure calcium carbonate material.

The main difference between Limestone and Dolomite are [36]:

• Limestone is a calcium carbonate mineral whereas dolomite is made of calcium magnesium carbonate.

• Sand, clay, and silt are commonly found in limestone as impurities but not quite common in dolomite.

• Calcite limestone is usually more expensive than dolomite.

Ligang Wei et al.[37] studied the affected of two kinds of biomass samples, legume straw and pine saw-dust, with dolomite and limestone as a catalyst and they found dolomite is better than

limestone due to hat the mixture of oxides in calcined dolomite would create some degree of distortion in the array of the Ca or Mg atoms generating more active catalytic sites.

Now that it is confirmed that dolomite is the more effective catalyst, by experiment as well as the literature. According to Mohammed et al [201] the calcination process positively affects the dolomite as it has a highly porous surface with a smaller spherical grain size, which leads to rising in the values of the specific surface area and average pore diameter and removal of carbon dioxide. It is also important to ensure that the percentage weight of the added catalyst is optimum, and therefore this needs to be assessed as well. This will be discussed in the next section.

## 5.5 Effect of different ratio of dolomite as a catalyst

Dolomite is a common rock-forming mineral with a specific gravity of 2.8 to 2.9, which is geographically extensive in underground geological deposits. Dolomite is calcium magnesium carbonate with a chemical formula of $CaMg(CO_3)_2$. The dolomites could be colourless, white, pink, green, grey, brown, or black [202].

In this part of the experiment the same conditions were used in the previous section, as follows: 20 ° C / min heating rate, nitrogen gas at a flow rate of 50 ml/min and the particle size for date stone is 710 µm.

Four samples were prepared and weighed to the nearest 0.01 mg of date kernel with different proportions of the first dolomite without adding dolomite, and the other samples by adding different percentages of 5%, 10% and 15% to find out the effective percentage of stimuli with the date stone.

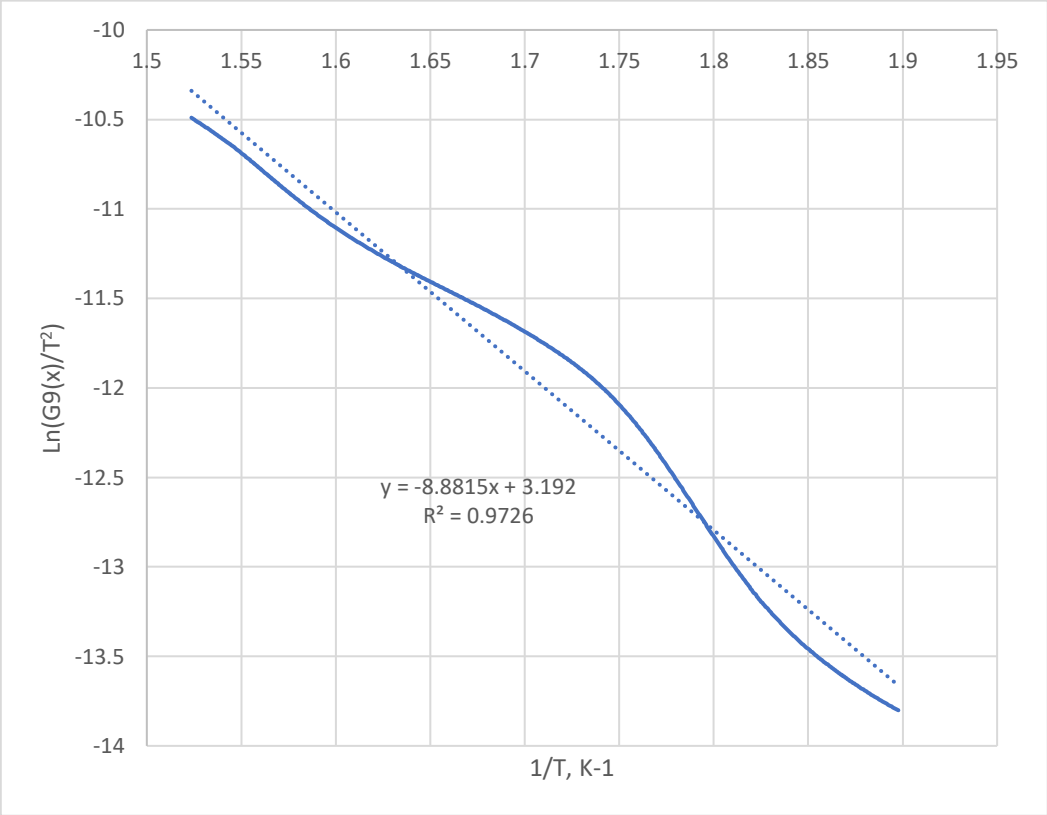


*Figure 5- 11 plot of the conversion function using the Coats Redfern method Vs reciprocal of temperature for date stone with no catalyst.*

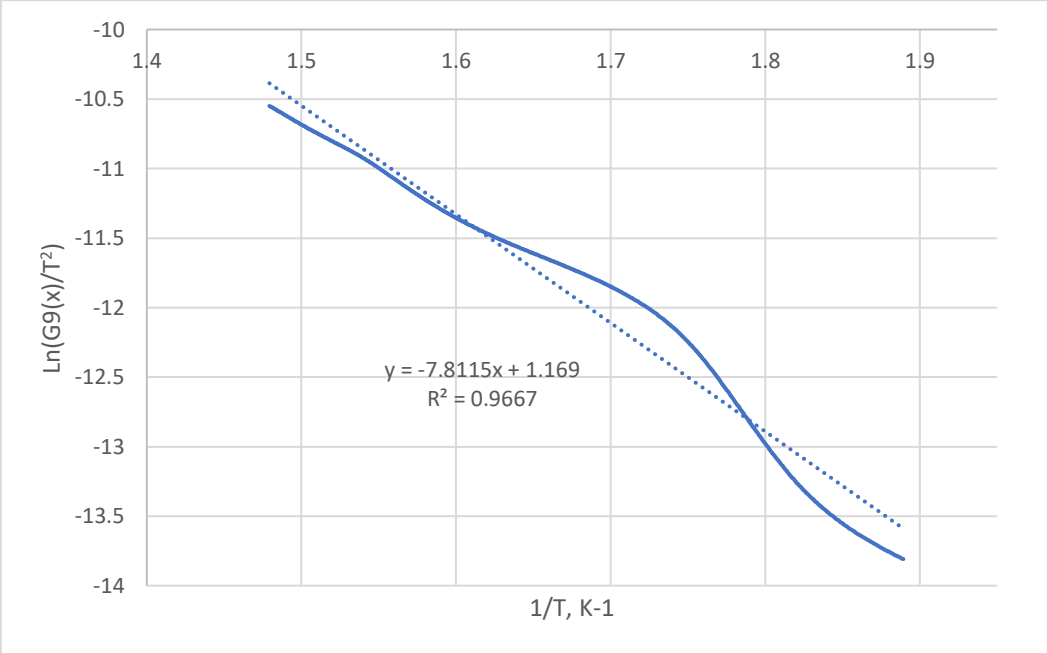


*Figure 5- 12 plot of the conversion function using the Coats Redfern method Vs reciprocal of temperature for date stone with 5% dolomite.*

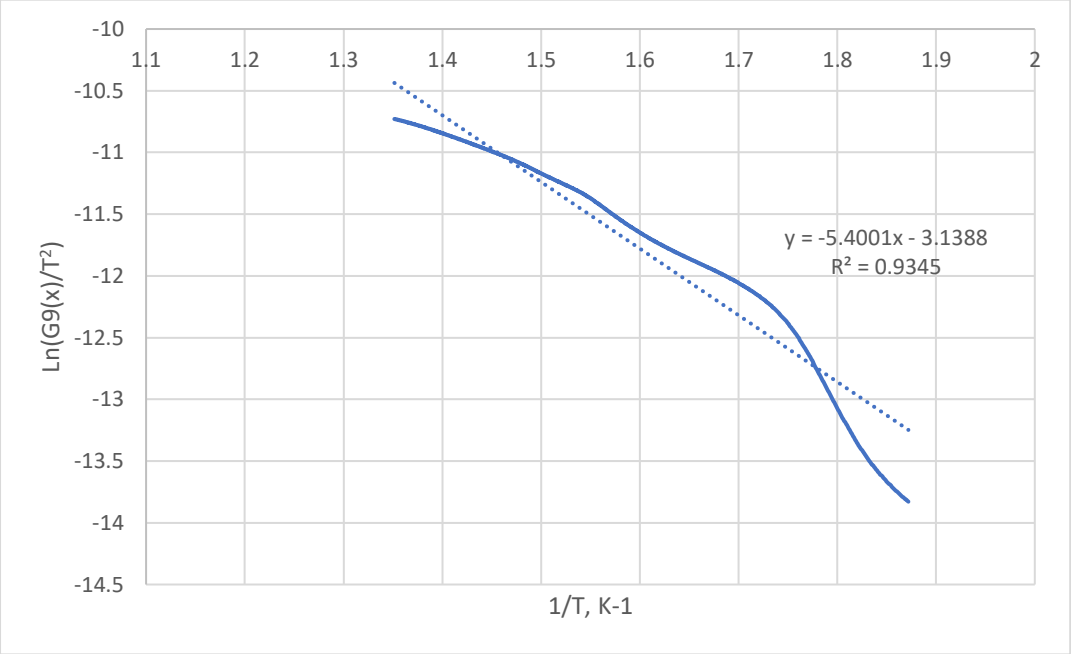


*Figure 5- 13 plot of the conversion function using the Coats Redfern method Vs reciprocal of temperature for date stone with 10% dolomite.*

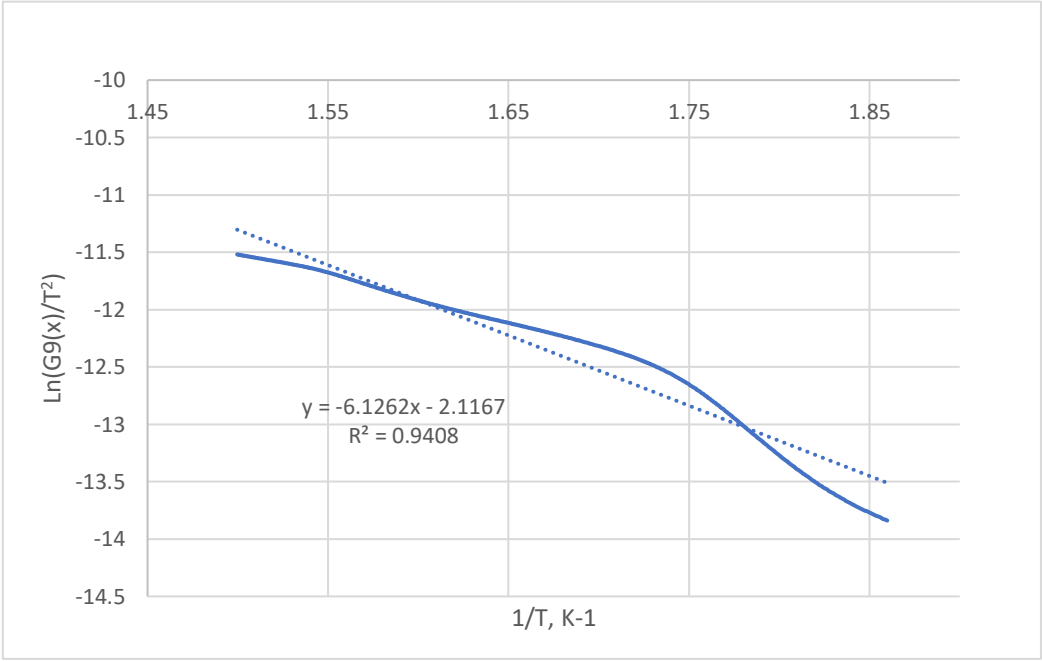


*Figure 5- 14 plot of the conversion function using the Coats Redfern method Vs reciprocal of temperature for date stone with 15% dolomite.*

Similarly, to the above approach – the dolomite was assessed at 15% weight and shown on Table (5-6) below as a function in G(x).

*Table 5- 6 The TGA reading for dolomite at 15% dolomite.*

| NON-ISOTHERMAL (TGA), X=0.2-0.8 | | | | | | | | | |
|---|---|---|---|---|---|---|---|---|---|
| G(x) | **G1** | **G2** | **G3** | **G4** | **G5** | **G6** | **G7** | **G8** | G9 |
| **R2** | 0.8452 | 0.8693 | 0.3717 | 0.6653 | 0.3717 | 0.9129 | 0.8902 | 0.8902 | 0.8902 |
| G(X) | G11 | G12 | G13 | G14 | G15 | G16 | G17 | G18 | G19 |
| **R2** | 0.5442 | 0.7856 | 0.7856 | 0.9682 | 0.9435 | 0.8902 | 0.7856 | 0.799 | 0.0325 |

The same approach as above is taken to assess activation energy fit for dolomite at 10% and 15% via the Coats-Redfern method. The graphs obtained for the 10% dolomite is shown on Figure (5-13) and for the 15% dolomite in Figure (5-14). Although the trend line remains relatively the same, a 0.26% deviation between both ratios were detected.

The above data can then be taken to estimate the catalytic activation energy ($E_a$). This had been repeated for different dolomite percentage as a catalytic component in date stone reaction, namely for 5%, 10%, 15% and weightings. The full results are shown in Table (5-7) below, as the 10% dolomite is the most effective under the conditions tested. It had achieved the highest activation energy ($E_a$) at almost 44.89 kJ/mole, this is 15% higher than the 5% weighting for dolomite.

*Table 5- 7 The Ea value for different %wt dolomite catalyst.*

| Date 710µm | | | | |
|---|---|---|---|---|
| | date | 5% | 10% | 15% |
| Ea | 73.84 | 64.94 | 44.89 | 50.93 |

One of the most important reasons for the ineffectiveness of dolomite when increasing the ratio: the increase in carbon deposition on the surface of the catalyst as a result of the increase in the percentage of hydrogen removal, which causes blockage of pores, reduces the surface area and thus inhibiting the work of the catalyst [203]. In summary, the more effective catalyst that will be used in this experiment is the 10% dolomite with date stone, highlighted in blue in the table above.

## 5.6 Effect of particle sizes on the pyrolysis

The particle size can have a significant impact on the rate of reaction in lab scale pyrolysis [202]. The temperature gradient inside the particle is directly proportional to the particle size [202]. This indicates that the temperature of the surface is consistently higher than the core, and thus boosts the solid yield and reduces the gas and liquid yields [204].

Coats-Redfern method was used to estimate the apparent activation energies to enable quantification of the particle size and heating rate impact on the gasification of date stone.

As mentioned earlier, the sizes tested here are 300, 500 and 710 µm. The results are shown in Table (5-8) including effective obtained for each size. There is an impact of the particle size on effective exists, however it is relatively small.

*Table 5- 8 Ea corresponding to different particle sizes.*

| | Date 300µm | Date 500µm | Date 710µm |
|---|---|---|---|
| Ea | 5.26 | 44.89 | 61.99 |

A directly proportional relationship between Ea and the particle size is observed on Table (5), as it had increased with the sample size increase.

Additionally, to the above, the impact of particle size on efficiency using the dolomite catalysts was investigated. The results are shown in Tables (5-9, 10 and 11) and Figure (5-15). The results had shown the same trend as above, as the bigger the particle sizes the higher effective were obtained. The larger particle sizes result in smaller surface areas, and thus requires higher apparent activation energy to complete the process of pyrolysis. This is likely attributed to the irregular heating of the biomass samples as higher particle sizes result in slow heating of inner portions of the sample [198].

*Table 5- 9 Date 300µm*

| Date 300µm | date | 5% | 10% | 15% | 20% |
|---|---|---|---|---|---|
| Ea | 12.06 | 12.48 | 5.265 | 6.97 | 7.2 |

*Table 5- 10 Date 500µm.*

| Date 500µm | date | 5% | 10% | 15% | 20% |
|---|---|---|---|---|---|
| Ea (J/MOLE) | 73.84 | 64.94 | 44.89 | 50.93 | 51.02 |

*Table 5- 11 Date 710µm.*

| Date 710µm | date | 5% | 10% | 15% | 20% |
|---|---|---|---|---|---|
| Ea | 82.80 | 73.58 | 61.99 | 65.91 | 66.39 |

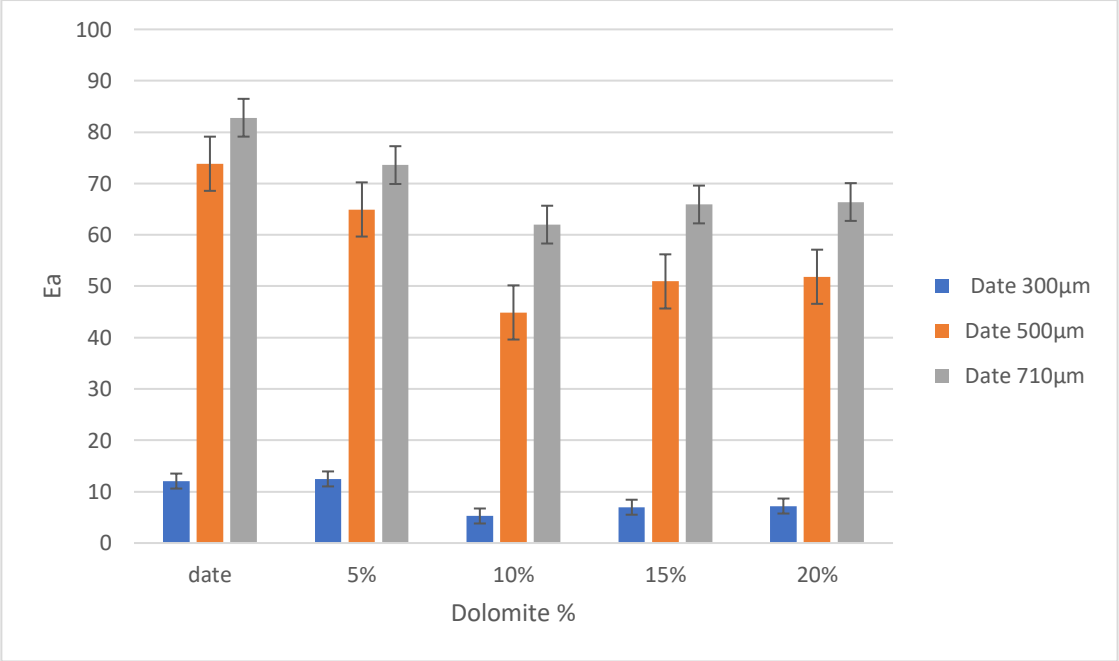


*Figure 5- 15The effect of different particle size with different ratio of dolomite on Ea*

These results are aligned with the literature, as previous studies had shown that the efficiency increased with increasing the Lignocellulosic biomass particle sizes, according to Dadi et al. [198].

Another study had used hazelnut shells (from Turkish hazelnut) from the Black Sea in Turkey at similar non-isothermal conditions [205]. The study showed that the apparent activation energy value was reduced linearly with respect to the fraction of the particle size reduction. It

was also observed that higher yield of char was obtained at larger particle sizes, while higher apparent energy was also needed for the pyrolysis process.

Capsicum stalks were also tested by Y. Niu. Et al [206] via thermogravimetry differential gravimetric analysis. It was also shown that increasing the particle size, increased the reaction rate of pyrolysis.

## 5.7 Summary

In this chapter, the reaction kinetics of date stone biomass were measured using a TGA. The effectiveness of the TGA device was confirmed by testing ten samples of date stone under the same conditions and it gave the same results in a large percentage.

To confirm the effect of the activating materials on the date stone, it was tested with different percentages of the inert materials (sand in this experiment) and the same result was given.

In order to choose the appropriate metallic catalyst among (dolomite, olive, limestone), these catalysts were tested under the same conditions and with the same percentage (10%) and the results of the activation energy using Coats Redfern method (44.8, 95.12, 76.19) (kJ/mol) respectively, Thus, the effectiveness of dolomite as a catalyst was shown with date stone.

The appropriate percentage of catalyst addition based on this study was 10% of the catalyst, and to achieve this, experiments were conducted for four samples of date stone with dolomite in the following proportions (0%, 5%, 10%, 15%) by using Coats Redfern method and the results of the activation energy were (73.84, 64.94, 44.89, and 50.93) (kJ/mol) respectively.

In addition, the effect of the sample size was studied, and it was found that the smaller the size has the lower the value $E_{a.}$

Chapter 6

# Gasification of date stone

# 6.1 Introduction

In this chapter, the results of the experimental study of the biomass (date stone), under air gasification in the fluidised bed reactor are presented and discussed. The results of the bed temperature relationship are also presented and discussed. The gas analysis results are provided to evaluate the efficiency (dry gas heating value, carbon conversion and the cold gas efficiency) of date stone in the fluidised bed gasifier. Operating and design parameters that affect the gasifier performance are presented and discussed. This includes bed temperature, Equivalence Ratio, catalyst ratio, and particle size of the biomass.

# 6.2 Performance of the biomass bubbling fluidised bed gasifier.

## 6.2.1 The impact of bed temperature

In the section, the impact of changing the gasifier bed temperature on the gas yield, the cold gas efficiency and HHV will be discussed.

To understand the impact further, it is important to outline the reactions that occur within the gasifier, which produce the resultant gas composition table (2-1). This contains consecutive and complex reactions, which are also competing at times.

All the reactions are affected by the bed temperature, and therefore are an important factor for the gasification process. To further simplify the mechanism of the gasification process, a reaction scheme was reduced to the main 10 reactions in the process, shown on Table (2-1) [207][208]. The impact of the bed temperature was observed by performing gasification tests and various bed temperatures in this study. The temperatures used were between 450 $^{o}$C to 650 $^{o}$C, with 50 $^{o}$C incremental increases at a constant ER of 0.2. The biomass fuel was Date Stone as described in Section (4.1). A breakdown of the impact in each operating parameter is shown in Table (6-1) below.

*Table 6- 1 Operating conditions for different bed temperatures*

| **Operating Parameters** | **Bed Temperature $T_2$, $^oC$** | | | | |
|---|---|---|---|---|---|
| | 450 | 500 | 550 | 600 | 650 |
| 1- Air Flowrate l/min | 40 | 40 | 40 | 40 | 40 |
| 2- Equivalence Ratio ER | 0.2 | 0.2 | 0.2 | 0.2 | 0.2 |
| 3- Bed Material (Sand) Particle Size, µm | 500 | 500 | 500 | 500 | 500 |
| 4- Biomass solid Fuel Particle Size, µm | 1.4 | 1.4 | 1.4 | 1.4 | 1.4 |
| 5-Static Bed Height Hs, cm | 6.2 | 6.2 | 6.2 | 6.2 | 6.2 |
| 6- Mass Rate of biomass Feeding, kg/hr | 2.278 | 2.278 | 2.278 | 2.278 | 2.278 |
| 7- (MAFR)stoichiometric for date stone | 6.32 | 6.32 | 6.32 | 6.32 | 6.32 |

The product gas composition of carbon monoxide, carbon dioxide, hydrogen and methane are shown on both Figure (6-1) and Table (6-2). They are assessed against the bed temperature of the gasifier for the Date Stones at an ER of 0.2. The hydrogen content had a 3% increase reaching 7%, when the temperature increased from 450 $^oC$ to 650 $^oC$, while the carbon monoxide had a 13% increase to 18%. Carbon dioxide decreased with increasing temperature, which demonstrates that endothermic reactions were favoured with increasing temperatures.

*Table 6- 2 Composition of the resultant gases at different gasifier bed temperature for date stones at ER = 0.2.*

| T $^oC$ | CO | $CO_2$ | $CH_4$ | $H_2$ |
|---|---|---|---|---|
| 450 | 13 | 14 | 4 | 3 |
| 500 | 14 | 13.8 | 4 | 4 |
| 550 | 15 | 13.5 | 6 | 5 |
| 600 | 15 | 13.2 | 5 | 6 |
| 650 | 18 | 12.9 | 4 | 7 |

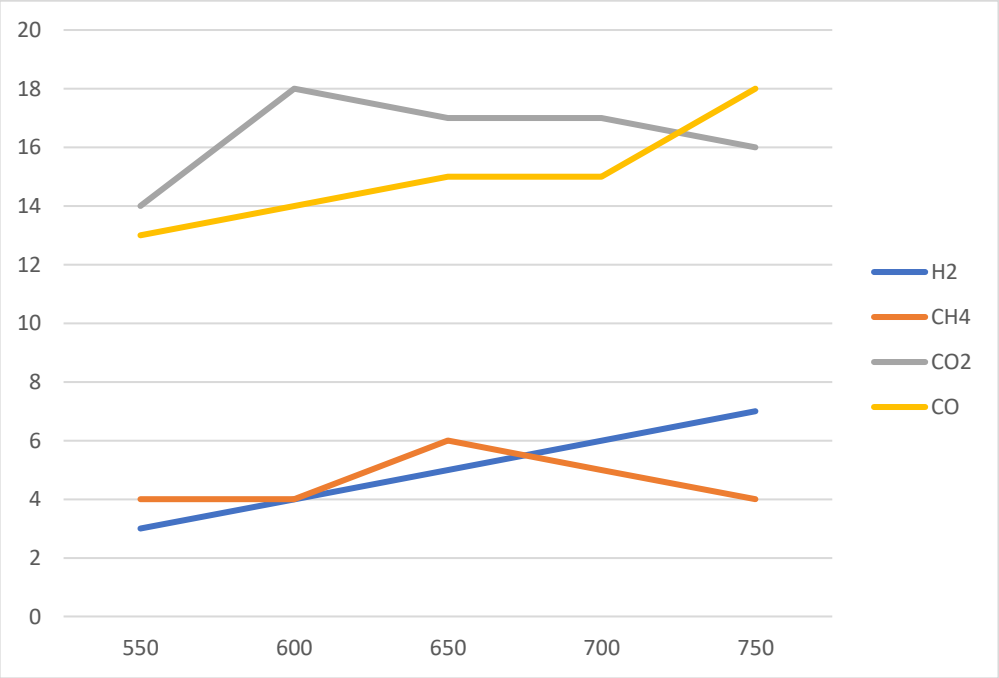


*Figure 6- 1 Composition of the resultant gases at different gasifier bed temperature for date stones at ER = 0.2*

Each of the reactions R2, R3 and R4 are endothermic reactions, and therefore their yield is boosted by the increase in temperature. This agrees with the literature for both the Boudourd and the water-gas reactions [46]. The hydrogen production is promoted via the interactions between carbon dioxide and steam during the gasification process. This is outlined in Reaction (R3), which is a result of both reactions (R4) and (R7), contributing both components [209]. This behaviour is also influenced by the temperature of the bed reactor within the gasifier, as the carbon dioxide concentration is decreased at higher temperature, due to the increasing concentration of both hydrogen and carbon monoxide gases.

The final step of the above reaction sequence is the production of methane at the same temperature range, from the inlet date stone. Its concentration was relatively lower than expected at around 4% volumetric concentration it is produced at atmospheric pressure as shown in Reaction (R1) in this section, via biomass pyrolysis [208]. However, the pyrolysis zone behaves differently at higher temperature, as it encourages secondary reactions to occur. An example of which is the tar cracking which is detailed in Reaction (R2). Because of the tar cracking the bed temperature is increased, accompanied by an increase in methane production.

Previous experiments in the literature showed that the methane concentration is usually on the lower side (ranged about 5% volumetric concentration) within various operating conditions, for example as shown in Skoulou et. [210], al,Lucas et al.[211] and Mohammed et al[212]. This is a direct result of the increased reformation of methane in Reaction (R2). In conclusion, increasing the temperature of the gassier has a direct positive impact on hydrogen, carbon monoxide and methane, while it has a negative impact on carbon dioxide concentration.

It is worth noting that the carbon dioxide yielded from Reaction (R6) then contributes to complete Reaction (R10); the tar cracking, as well as Reaction (R4); Bouduard and Reaction (R8); methane dry reforming, yielding both hydrogen and carbon monoxide.

More specifically, the carbon dioxide volumetric concentration dropped to 12.9% at 0.2 ER, on the other hand, the methane concentration did not show notable changes with respect to this change in temperature. This result can be attributed to one of two reasons. The first is the high temperature thermal cracking at Reaction (R9); at which the reaction rate of methanation is slower relative to the remainder of the reactions[213]. The second reason is the consumption of the yielded methane in Reaction (R8); dry reforming. Both reasons would achieve an acceptable and consistent balance between the produced and consumed methane which renders the volumetric concentration of the final produced gas consistent at both higher and lower temperatures.

The results are aligned with previous findings in the literature; namely, by Xue et al. [214]. The author used a miscanthus X giganteas as the inlet biomass fuel in an air blown bubbling fluidised bed gasifier. Similar trends were observed to the results obtained in this research with the date stone.

#### 6.2.1.1 Cold gas efficiency, HHV with relationship with temperature

The gasification process efficiency can be determined by evaluating the HHV value of the dry gas as well as the cold gas efficiency (as demonstrated in Section 4.5). Figures (6-2) and (6-3) show the HHV and CGE respectively for date stone across a range of bed temperatures, 450°C to 650°C in 50°C increments, using an ER of 0.2. The cold gas efficiency (CGE) and HHV is shown on Figures (6-2) and (6-3) for the data stone biomass fuel. It is observed that as the temperature of the bed increased by 450 $^{o}$C to 550 $^{o}$C, the HHV value climbed to 4.9 MJ/Nm$^3$ from 4.7 MJ/Nm$^3$. This is for a similar reason mentioned above, as combustible gasses are

yielded at higher temperature, namely carbon monoxide and hydrogen, this consequently enhances HHV values.

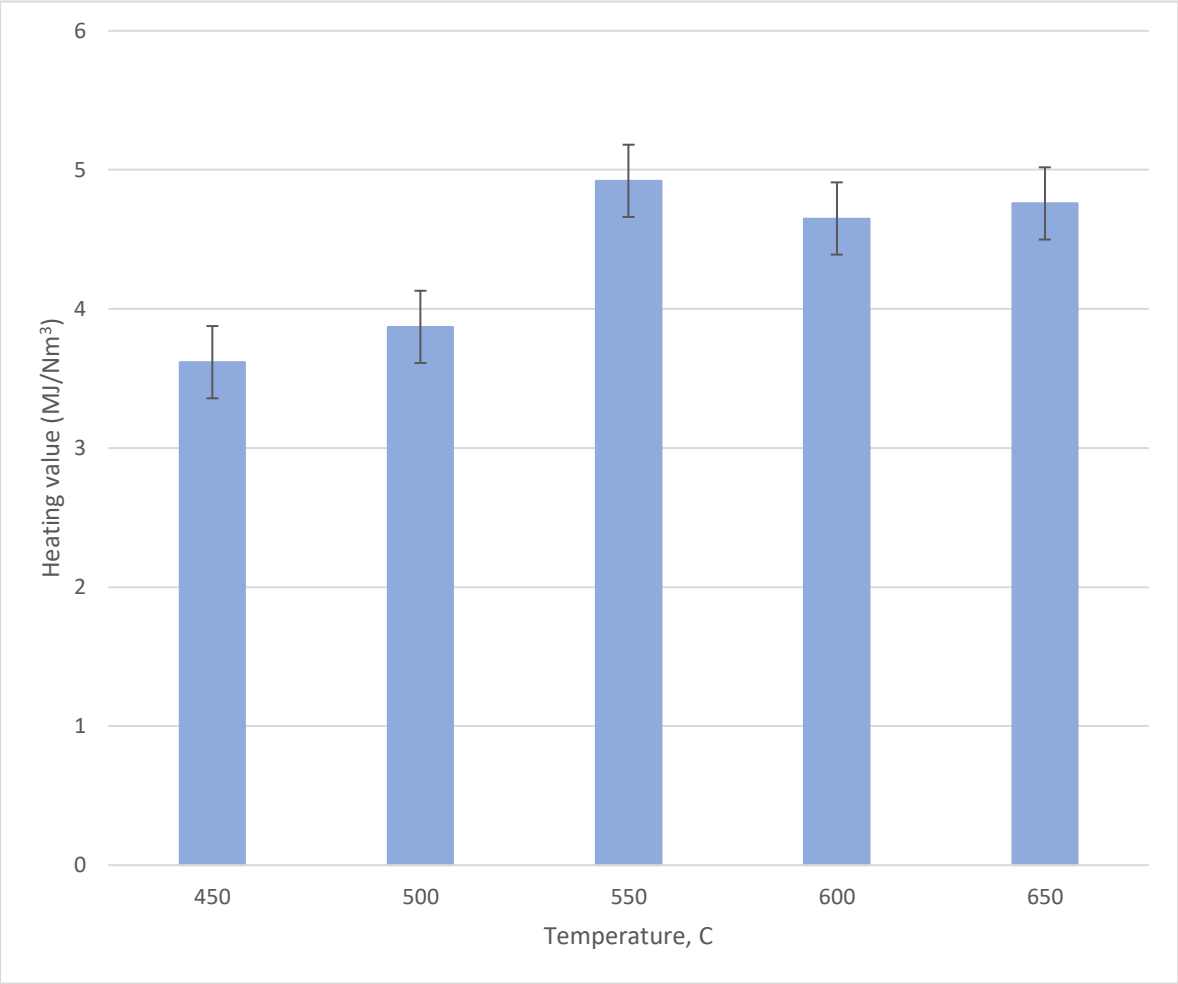


*Figure 6- 2 Effect of bed temperature on gasification HHV for date stone.*

Similarly, the cold gas efficiency is found to be the highest at highest temperature, as shown in Figure (6-3) for the date stone biomass. This is aligned with the literature, namely Lahijani and Zainal [207]. This behaviour can be attributed to both the high gas yield and the increase of HHV resulting from the rise of combustible gases amount in the producer gas, especially $H_2$ and CO, with the increase of bed temperature [215].

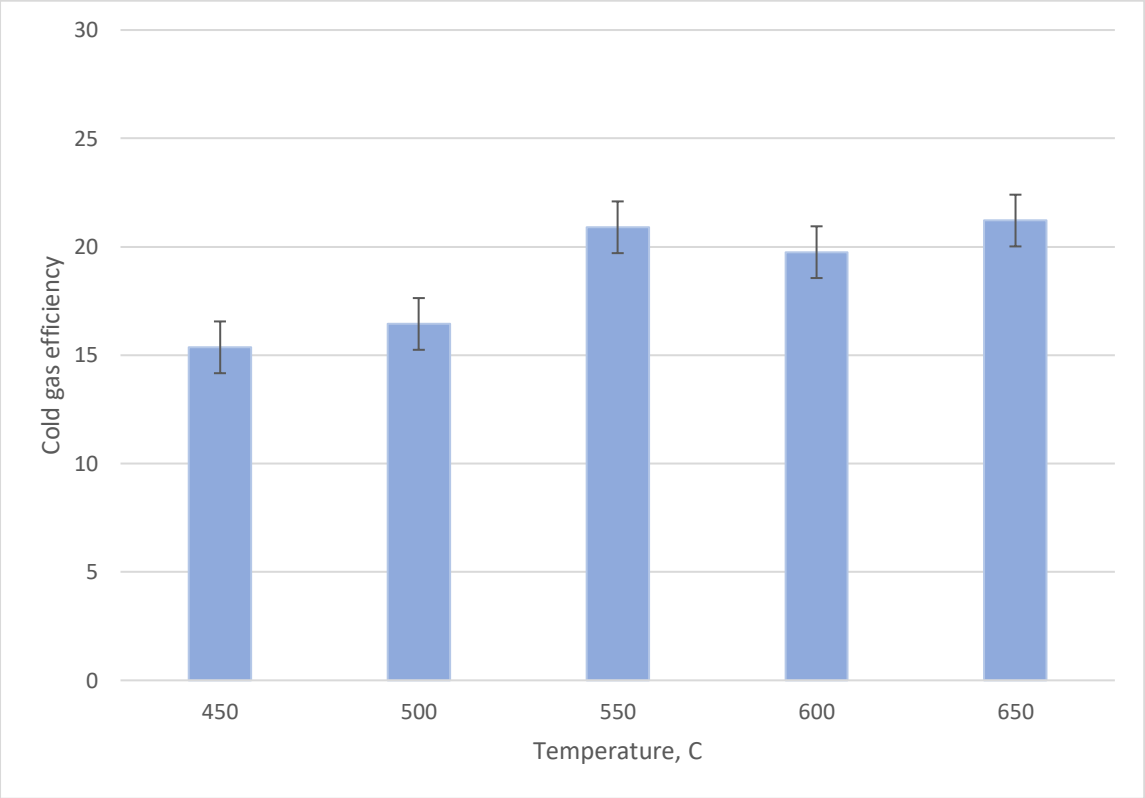


*Figure 6- 3 Effect of bed temperature on gasification cold gas efficiency of date stone.*

### 6.2.2 Equivalence Ratio (ER) impact

According to the operating conditions which have been shown in Table 6.4 , the results of the effect of ER on the producer gas composition is revealed in Figure 6.4 for biomass feedstock date stone.

*Table 6- 3 Operating conditions for equivalence ratio parameter experimental tests*

| **Operating Parameters** | **Equivalence Ratio ER** | | | | |
|---|---|---|---|---|---|
| | **0.15** | **0.2** | **0.25** | **0.3** | **0.35** |
| 1- Air Flowrate l/min | 40 | 40 | 40 | 40 | 40 |
| 2- Reaction Bed Temperature $^{o}$C | 650 | 650 | 650 | 650 | 650 |
| 3- Bed Material (Sand) Particle Size, μm | 500 | 500 | 500 | 500 | 500 |
| 4- Biomass solid Fuel Particle Size, μm | 1.4 | 1.4 | 1.4 | 1.4 | 1.4 |
| 5- Static Bed Height Hs, cm | 6.2 | 6.2 | 6.2 | 6.2 | 6.2 |
| 6- Mass Rate of biomass Feeding, kg/hr | 3.037 | 2.278 | 1.822 | 1.518 | 1.301 |
| 7- (MAFR)stoichiometric for date stone | 6.32 | 6.32 | 6.32 | 6.32 | 6.32 |

The Equivalence Ratio (ER) has measurably affected the gasification process. For example, it alters the syngas composition that is produced from the process.

In this study, an evaluation of the ER impact was undertaken on the gasses produced through the gasification of the Date Stone feedstock. This was done by experimenting the isothermal reactions at a temperature of 650 °C at different ER values between 0.15 and 0.35, through an incremental increase of 0.05 in each attempt. The value of ER was controlled by changing the rate of entering the biomass as feed at a constant air flow rate of 40 l/min as shown in Table (6-4).

The ER impact mentioned above is mainly observed through a significant change in the carbon monoxide (CO), carbon dioxide ($CO_2$), hydrogen ($H_2$) and HHV concentrations alongside variations in the conversion rates. The changes are shown in Figure (6-4) below. Both the CO and $H_2$ concentrations were inversely proportional with the ER values, this behaviour can be attributed to the increased full and partial oxidation of char (when increasing the ER the airflow rate was increased, which promoted the combustion reactions. It is worth noting that the $CO_2$ concentration is higher at an ER of 0.15, as the majority of the gas is yielded in the reaction (R1), which occurs as the reactor is nearing pyrolysis, especially at the lower ER value. Pyrolysis of a biomass produces CO and $CO_2$ as residues, which is discussed by Zabaniotou et al. [216]. Also, the hydrogen and carbon monoxide reduction shown on the chart is a result of the ongoing oxidiation resulting in water and carbon dioxide as shown in reactions (R5) and (R9) in Table (6-1), which subsequently increases the oxygen availability at higher ER intervals [217].

$$H_2 + 0.5O_2 \rightarrow H_2O \quad \text{(R5)}$$

$$CO + 0.5O_2 \rightarrow CO_2 \quad \text{(R9)}$$

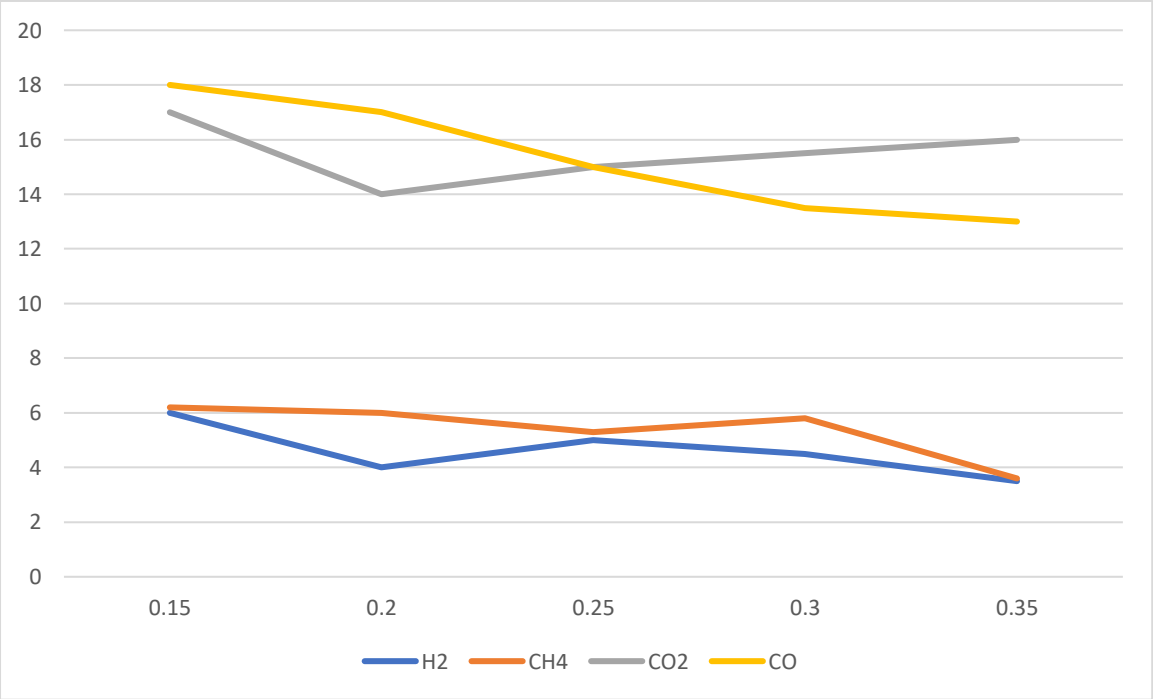


*Figure 6- 4 Change in H2, CH4, CO2 and CO concentration at each ER value, data obtained from experiments performed on Date stones..*

The results for the gas concentrations in the produced gas is aligned with the literature for similar gasification experiments. The hydrogen and carbon monoxide content had seen a reduction with increasing ER in the experiments performed by Gil [218]. Similarly, for the hydrogen and carbon monoxide concentrations described above are observed in Gil's gasification, which used pine wood as the biomass material in a bubbling fluidised bed. The amount of methane ($CH_4$) reduced from 6% to 3.6% when increasing ER from 0.15 to 0.35 by 0.6%., as shown in Figure (6-4). It is known that at higher ER values, there is a higher oxygen availability, which is observed by Loha et al. [219]. The increased oxygen results in an increased likelihood of the oxidization reactions and therefore higher carbon dioxide yield, and higher consumption of hydrogen, carbon monoxide and methane.

Figure (6-5) and (6-6) shows the changes in both HHV and the carbon conversion efficiency at different ER intervals. The lowest value of HHV is obtained at a high ER interval, which results from the reduction in the combustible specific (also known as energetic) species. At the same interval, the efficiency of carbon conversion increases notably by 36.4% reaching 71.8%. The increase in the efficiency is a direct impact of the increased oxygen availability for the biomass reactions, which leans towards higher fuel consumption at higher ER values.

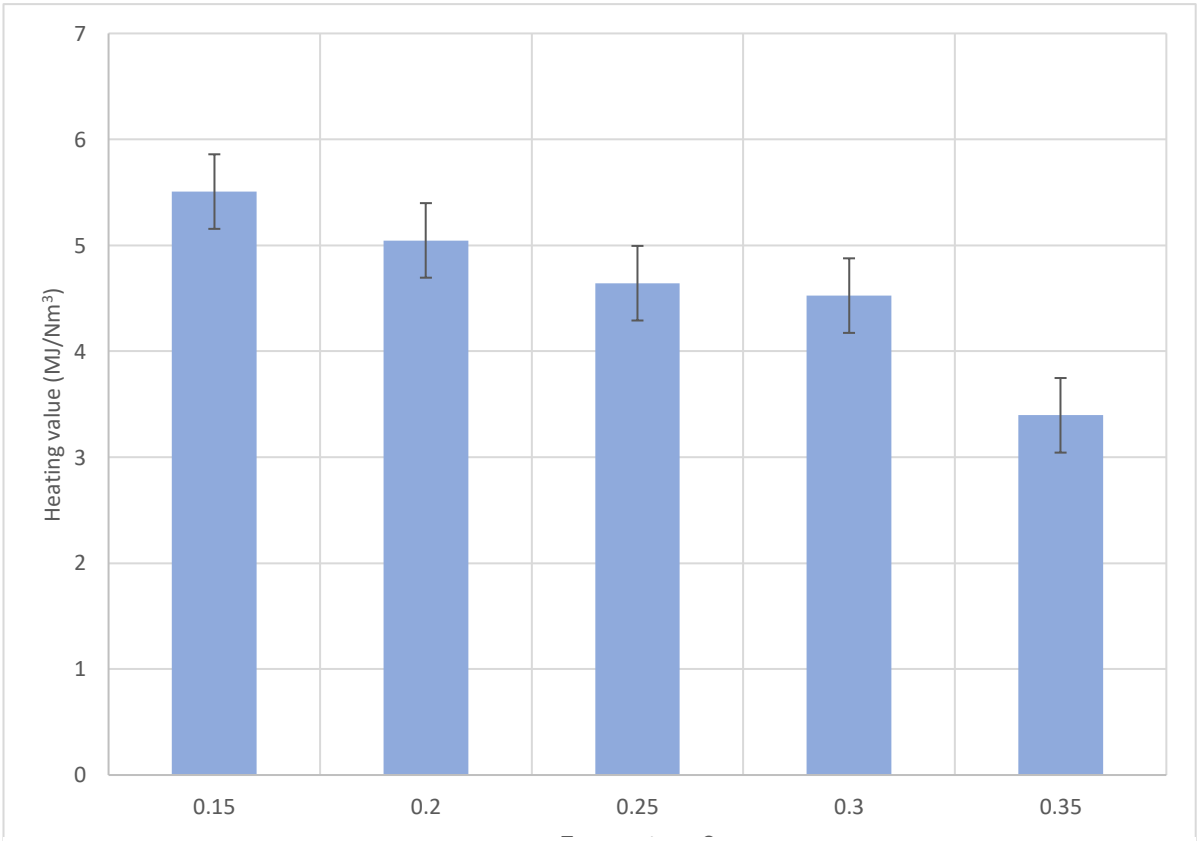


*Figure 6- 5 Impact of ER on high heating value (HHV).*

Therefore, the increasing carbon dioxide boosts the efficiency of the carbon conversion up to ER of 0.3, and then starts to show a declining trend.

The results above are also aligned with Gil's experimental results, as mentioned earlier. It was also observed that increasing the ER value from 0.15 to 0.35 can boost the gas yield and decrease the HHV (High heating value) of the gas as well as reducing the concentration of hydrogen, carbon monoxide, methane and the tar content, according to Kook [86]. This is attributed to more exothermic oxidation reactions. As expected, this demonstrates the trade-off between heat release with stable thermochemistry, versus highly energetic product gas.

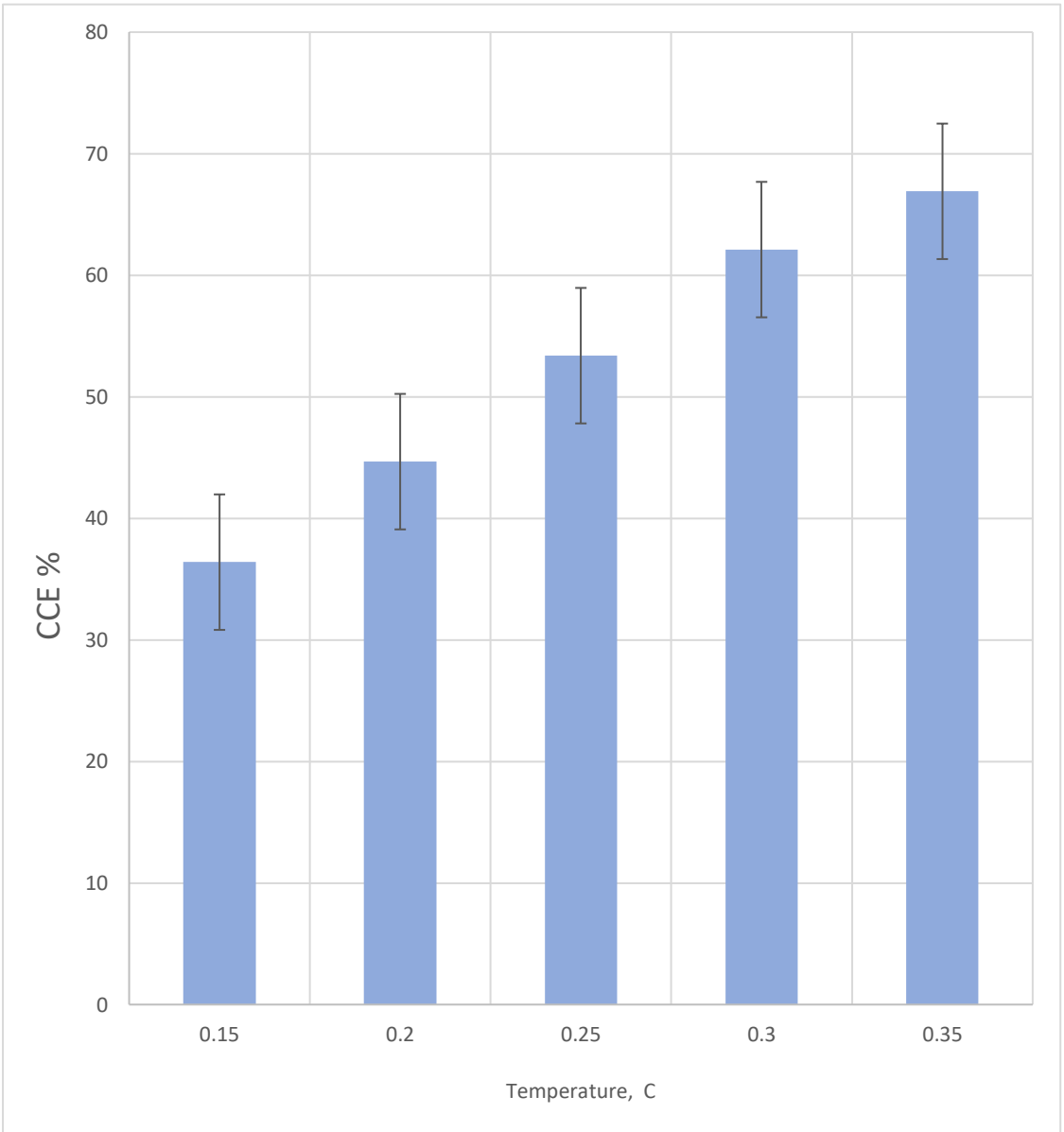


*Figure 6- 6 impact of ER on carbon gas efficiency at 650 C.*

### 6.2.3 Effect different ratio of dolomite

There are various factors impacting the gasification process, such as the temperature, equivalence ratio (ER) and the particle size alongside the used catalyst in the process. The dolomite material is selected as the main catalyst for the gasification process, which has a noticeable impact of the process's efficiency. This effect will be assessed in this section.

The previous section has demonstrated the nominal operation of the gasifier without the presence of a catalyst. This section will now demonstrate the measurable effect of the dolomite presence in the gasifier bed. The impacts of dolomite were assessed at different catalyst ratios on date stone as the biomass material of the gasification process. The experiments were performed at an isothermal condition at 650 °C, at a consistent ER value of 0.2. The inlet flow rate was also kept consistent at 40 l/min. In order to assess the impact of the catalyst, the amount of dolomite was increased incrementally by 0.5 for each individual experiment attempt. The full results are given in Table (6-5), while the resultant gas values are shown on Table (6-6).

*Table 6- 4 The operation conditions set and observed at different dolomite catalyst ratios.*

| Operating Parameters | Ratio of dolomite | | | |
|---|---|---|---|---|
| | **5%** | **10%** | **15%** | **20%** |
| 1- Air Flowrate l/min (kg/hr) | 40 | 40 | 40 | 40 |
| 2- Reaction Bed Temperature, $^{o}$C | 650 | 650 | 650 | 650 |
| 3- Equivalence Ratio ER | 0.3 | 0.3 | 0.3 | 0.3 |
| 4- Biomass solid Fuel Particle Size, μm | 600-850 | 600-850 | 600-850 | 600-850 |
| 5- Static Bed Height Hs, cm | 6.2 | 6.2 | 6.2 | 6.2 |
| 6- Mass Rate of biomass Feeding, kg/hr | 2.278 | 2.278 | 2.278 | 2.278 |
| 7- (MAFR)stoichiometric for date stone | 6.32 | 6.32 | 6.32 | 6.32 |

*Table 6- 5 : The changes in the produced flue gasses when using different values on in-bed catalyst dolomite.*

| dolomite | CO | $CO_2$ | $CH_4$ | $H_2$ |
|---|---|---|---|---|
| 0% | 18 | 16 | 4 | 7 |
| 5% | 17.2 | 16.9 | 3.5 | 9.4 |
| 10% | 16.5 | 17.6 | 2 | 12.4 |
| 15% | 16.9 | 17.2 | 2.8 | 11.2 |
| 20% | 17.5 | 16.5 | 3.2 | 10.6 |

The non-metallic catalysts known as dolomites have been used in tar conversion in the gasification of biomass, which is best practice as observed from the literature. Dolomites also belong to a mineral based catalyst group [220]. They exist abundantly in nature, and are composed of magnesium and calcium, with a chemical formula of $MgCO_3 \cdot CaCO_3$ [221][156][222]. The chemical formula of the dolomite may vary depending on its source, but it should always contain the main components of CaO, MgO, and $CO_2$ at variant weight ratios depending on the source. The CaO and MgO weight ratio is a major factor determining the effectiveness of the catalyst efficiency of dolomites. Generally, it was observed in the literature that the lower CaO and MgO weight ratio within the dolomite results on lower tar cracking efficiency [223]. While the Ca/Mg ratio is directly proportional to the dolomite's activity [224][225], there are also traces of $SiO_2$, $Fe_2O_3$, and $Al_2O_3$ in dolomite [221]. With the increasing Ca/Mg ratio, the activity of the dolomites increased [224][225]. Hervey et al.'s catalysis mechanism, of the dolomite is shown on Figure (6-7) [226]. It starts as the first particle of benzene, which is used as tar model compound is absorbed over a CaO basic sites [227]. It subsequently forms deposits of ($C_mH_p$) as active carbon as well as the ($C_xH_y$ and $H_2$) gas types. It is worth noting that increased active carbon increases the production of coke which takes part in the water phase reactions. $H_2O$ may take part in reaction with active carbon or may be absorbed over the active sites of MgO. If the water absorbs over the active sites of MgO, OH basic species will be formed.

Formiats (the salt or ester of formic acid containing the ion HCOO– or the group HCOO–) are produced through the increased alkaline through OH basic species, alongside other oxygenated intermediates. As such, these increase OH spill-over when the products are formed. $OH^-$ groups result in gaseous products and coke. Due to the nature of $OH^-$, it only takes part in the oxidation of the carbon of CaO bonds of the oxygenated species and can't take part in the oxidation of the C-C or C-H bond.

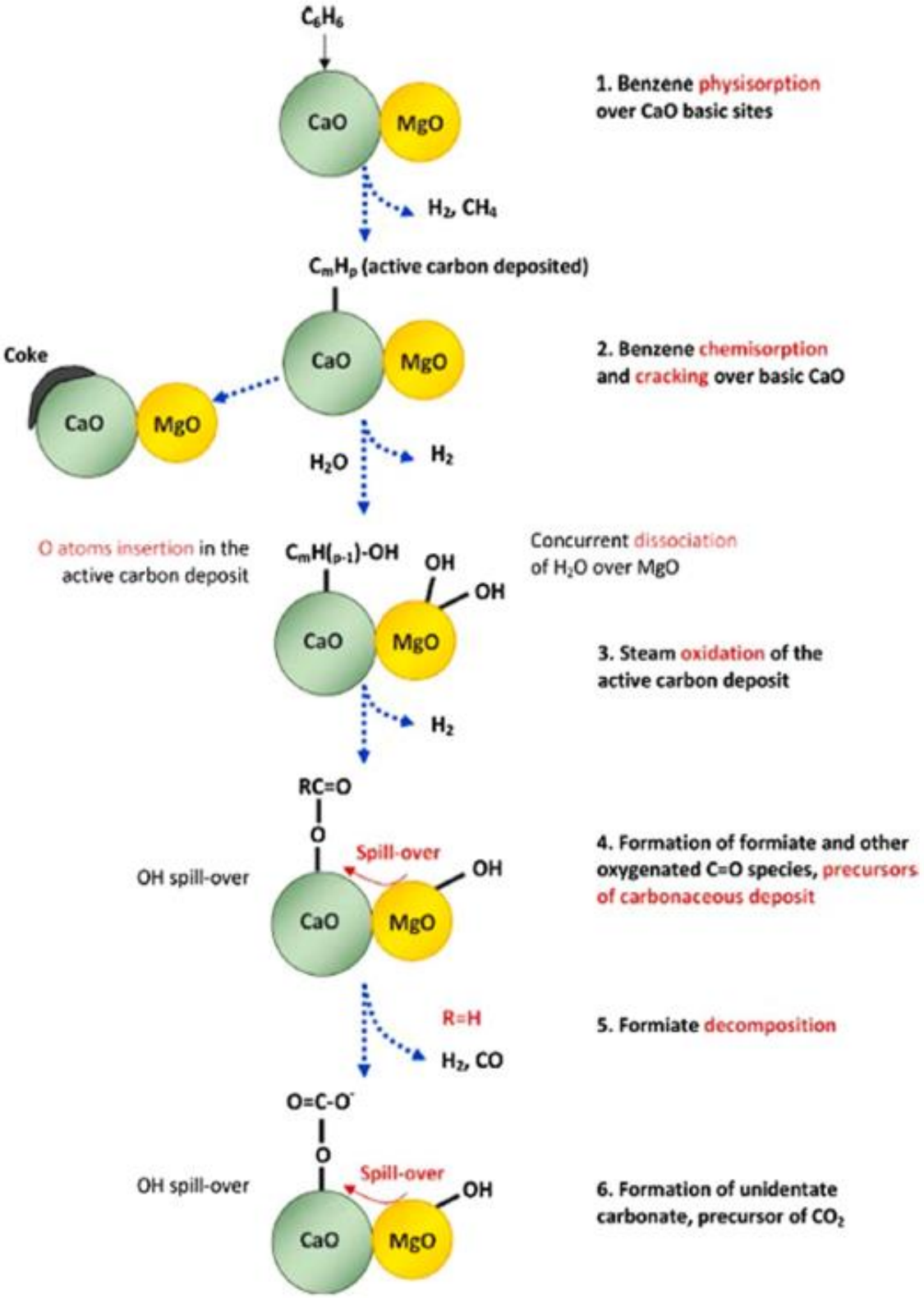


*Figure 6- 7 Mechanism of catalysis of dolomite [206].*

Both the molar fractions of hydrogen and carbon dioxide increased as the dolomite quantity increased. Meanwhile, both the methane and carbon monoxide content decreased., notably the CO molar fraction, as it decreased noticeably as a result of the water gas equilibrium reaction R3.

$$C + H_2O \rightarrow CO + H_2$$

Biomass gasification produces both syngas and liquid tar products. The latter poses one of the main technical obstacles in the development of the biomass gasification process. As mentioned earlier in this research, the main biomass reaction of the gasification process is an endothermic reaction and results in tar as an undesired by-product. The tar causes various issues; fouling, blocking of downstream pipelines and equipment.

The biomass gasification process was undertaken using steam and air as the medium, bed material of silica sand whilst using dolomite as the catalyst [228], by Roche et al. 10% of the weight for each individual material was added to the biomass feed in order to increase the hydrogen content to range between 20% and 36%.

This has shown an increase in the hydrogen content in the flue gas from 7 vol % to 12 .4 vol% (on dry basis) when using dolomite as catalyst. This is a great finding, as it clearly shows that dolomite is an affective catalyst for the process. Specially as the increased hydrogen content could either be a result of the destruction of tar in-situ; via reforming or cracking reactions. The tar-destructions can also be a result of the CO shift reaction, which is a result of the CaO and MgO residing in the reactor bed. The CO content in the in the gas had decreased and this is a direct result of the water-gas shift reaction R7, resulting in reduction of the CO in the produced gas from 18 to 16.5 vol%.

$$CO+H_2O \leftrightarrow CO_2+H_2$$

It also resulted in reducing the methane content in the flue gas as shown on Figure (6-8), it was reduced from 4 vol% to 3.2 vol%.

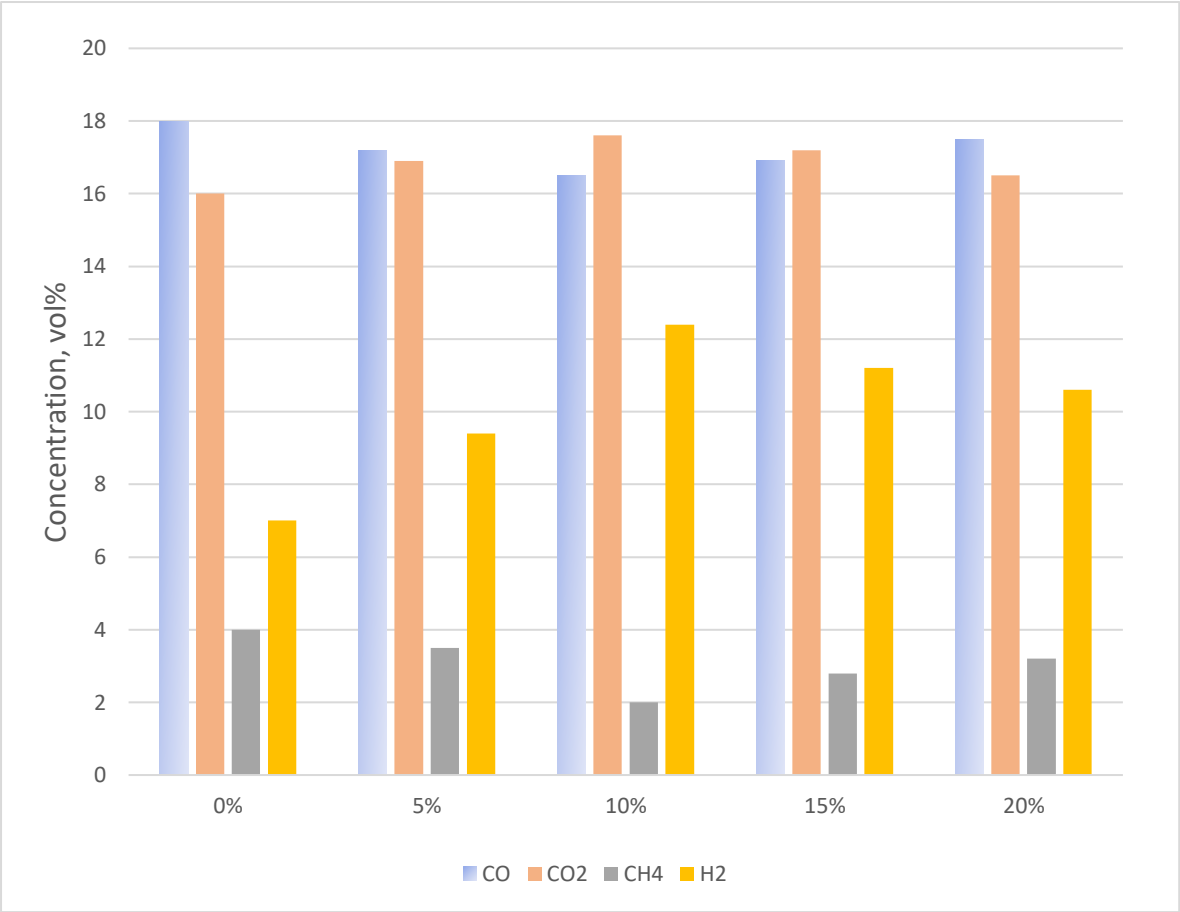


*Figure 6- 8 Effect of in-bed dolomite on the produced gas.*

Two simultaneous reactions occur; the in-bed tar cracking generating light hydrocarbons, and in-bed steam/dry carbon reforming of light hydrocarbons which are subsequently catalysed by both the OCa and OMg and dissipating the hydrocarbons from the flue gas.

Carbon dioxide hinders various chemical reactions, namely the dry carbon reforming of light hydrocarbons and tar; the carbon monoxide shift reaction also occurs as the inlet gas contains oxygen and other required components. However, as seen in the overall catalytic process in Figure (6-8), the exit gas does not contain any variations of $CO_2$ content when using an in-bed dolomite.

It was shown via experiments that the amount of the used in-bed dolomite as a catalyst material impact the hydrogen volumetric weight. There is a maximum $H_2$ concentration of 12.4 at 10% dolomite; beyond this value the $H_2$ concentration reduces over the ranges examined herein. The carbon dioxide content behaves similarly, as it hits 17.6 at 10% dolomite and then decreases. Carbon monoxide and methane reaches their minimal values at 10% dolomite at 16.5, 2,

respectively; and subsequently increases again. Therefore, a 10% calcinated dolomite (weight %) within the gasifier's bed is considered sufficient to cause a significant improvement in the distribution of the product as well as the produced gas quality [229].

To conclude this section, there are various advantages to using dolomite as the catalyst in the gasification process. This includes the lower commercial price, availability, reduced tar content in the produced gas. It can also be used as either a primary or secondary catalyst, and finally it results in increasing the surface area, oxide contents which subsequently increases calcination; according to Soomro et al.[230].

### 6.2.4 Effect of the biomass fuel particle size

The particle size of the biomass fuel influences the gasification process and therefore can impact the produced gas and overall efficiency of the reactor. The operating conditions observed in the gasifiers are outlined in table (6-7) while the producer gas is shown in Table (6-8).

*Table 6- 6 Gasifier operation conditions*

| Operating Parameters | **Biomass Solid Fuel Particle Size, µm** | | |
|---|---|---|---|
| | **300-425** | **600-850** | **1000-1400** |
| 1- Air Flowrate l/min | 40 | 40 | 40 |
| 2- Reaction Bed Temperature, $^{o}$C | 650 | 360 | 360 |
| 3- Bed Material (Sand) Particle Size, µm | 500 | 500 | 500 |
| 4- Equivalence Ratio ER | 0.2 | 0.2 | 0.2 |
| 5- Static Bed Height Hs, cm | 6.2 | 6.2 | 6.2 |
| 6- Mass Rate of biomass Feeding, kg/hr | 2.28 | 2.28 | 2.28 |
| 7- (MAFR)stoichiometric for date stone | 6.32 | 6.32 | 6.32 |

*Table 6- 7 Gasifier producer gas*

| | CO | $CO_2$ | $CH_4$ | $H_2$ |
|---|---|---|---|---|
| **300-425** | 15 | 6 | 7 | 9 |
| **600-850** | 12 | 10 | 4.5 | 7 |
| **1000-1180** | 8 | 11 | 3 | 5 |

Three sizes of date stones were examined in this section to assess the impact of fine date stone, coarse date stone and mid-coarse ones. The study was performed in a reactor with a temperature

of 650 ºC at ER of 0.2, in multiple 5 minutes runs. The results of the experiment are shown on Figure (6-9).

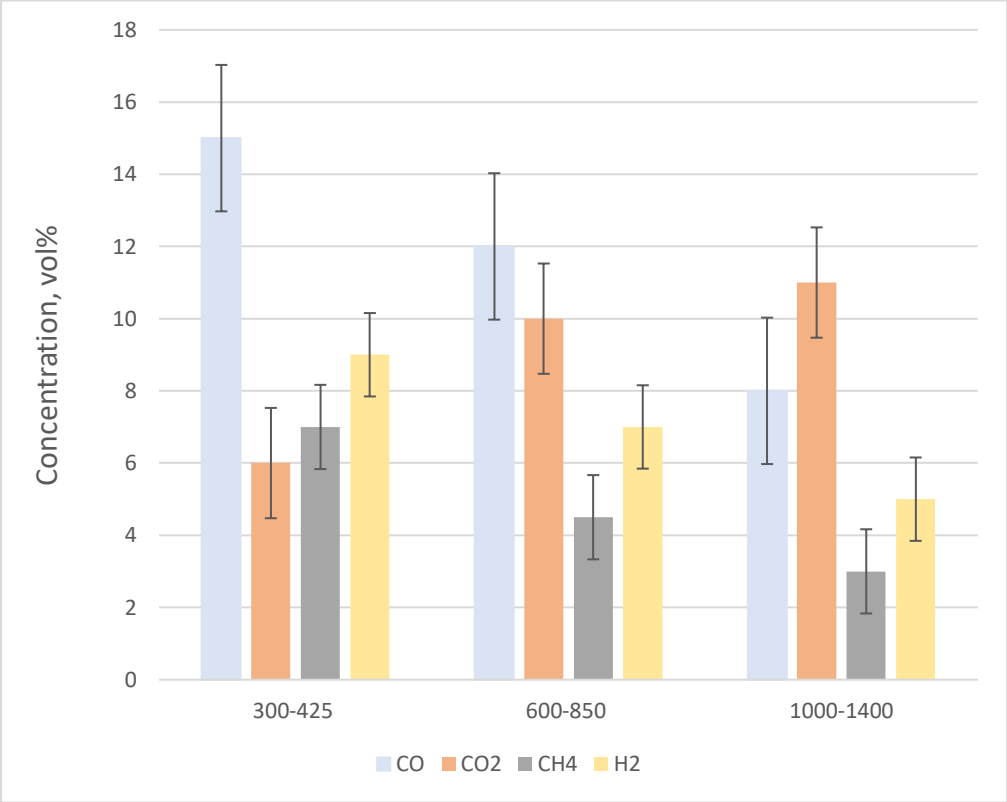


*Figure 6- 9 Results of five minutes takes in the gasifier.*

It is generally accepted that heating rate of biomass particles affects the gasifier's gas yield as well as its composition. As it was found that the higher the heating rate is, the lighter the produced gas [231]. This phenomenon can be attributed to the increased surface area when using smaller biomass particles as well as its higher particle heating rate [232].

When the biomass feed has a particle size less than 300 µm, the highest variation in the composition of the gas is observed, as shown on Figure (6-9) as well as Table (6-8). Any increases above 300 µm has a minor impact on the composition of all gasses except for the carbon monoxide gas which shows a downward trend.

The concentration of the produced carbon monoxide, methane and hydrogen is higher when using a smaller biomass particle size, while carbon dioxide concentration deceases. More specifically, the concentration of CO changes from 8% to 15%, $H_2$ from 5% to 9%, $CH_4$ from 3% to 7% and $CO_2$ from 11% to 6%, when particle size is reduced from ~1,400 µm to 300 µm.

The reversible water-gas shift reaction is one the main reactions that leads to the production of the carbon dioxide and hydrogen gases. This means that the hydrogen, carbon monoxide and carbon dioxide molar fractions are closely linked via the reaction equilibrium values for the exothermic reaction [233].

$$CO + H_2O \rightarrow CO_2 + H_2 \quad -41.2 \text{ KJ/mole}$$

The carbon monoxide content is reduced with an increased particle size as mentioned by Yu et al [214]. This is as a part of the produced CO reactions with the water droplets. Additionally, the oxidization zone of small temperature is much higher than when using smaller particle sizes [234].

According to the Le Chatelier principle, that higher temperatures favour the reactants in exothermic reactions and favour the products in the endothermic reaction. Therefore, the endothermic reactions were strengthened with the increase in temperature. higher temperatures promote reactants in reversible reactions, while the products are increased in a lower temperature in the endothermic reaction. This shows that more carbon monoxide was in fact converted to $CO_2$ when using higher particle sizes that leads to temperature reduction in the oxidation zone. Similarly, the methane concentration is resulted from reactions R1 and R2, while the char resulted from the reaction after the gasification process is decreased when using smaller particle size.

Volatiles can cause a secondary reaction such as condensation, polymerisation and cracking within the biomass particles as mentioned by Wei et al [235]. The polymerisation of volatile material can result in creating depositions of large sizes molecules on the pores, which consequently increases the char yield and reduces the volatile formation.

These results of the gas compositions herein are aligned with the literature with the expectation for hydrogen which has shown different behaviour[236] [237]. A similar trend was reported by Lv et al [232] who saw an increase in the hydrogen gas content with respect to the particle size of pine sawdust in its gasification process.

There is an explanation that is widely unaccepted by the literature, which is that the pyrolysis process occurs faster when using smaller particle sizes leading to a satisfactory area of contact

amongst the biomass and the gasifying agent alongside the different gasification processes within the kinetic control.

However, when using larger particle sizes, the produced gas inside the particles are more challenging to diffuse out. And therefore, the process is dictated by that difficult diffusion process. Generally, noticeable improvements were seen when using a smaller particle sizes which has also been seen by Guo et all [238].

Figure (6-10) and (6-11) shows the effect of biomass particle size on the CGE and HHV performance parameters of biomass materials. According to the synthesis results in the previous section for date stone, it can be said that these performance parameters significantly increased to the maximum value with decreasing biomass particle size and decreased to the minimum value with increasing biomass particle size. CGE increased from 17.9% to 21.97% and HHV from 2.85 to 5.82MJ/Nm$^3$ as particle size decreased. This is due to the improving gas quality, as the particle size decreased will improve those performance parameters. These results are in agreement with the published papers [232][212].

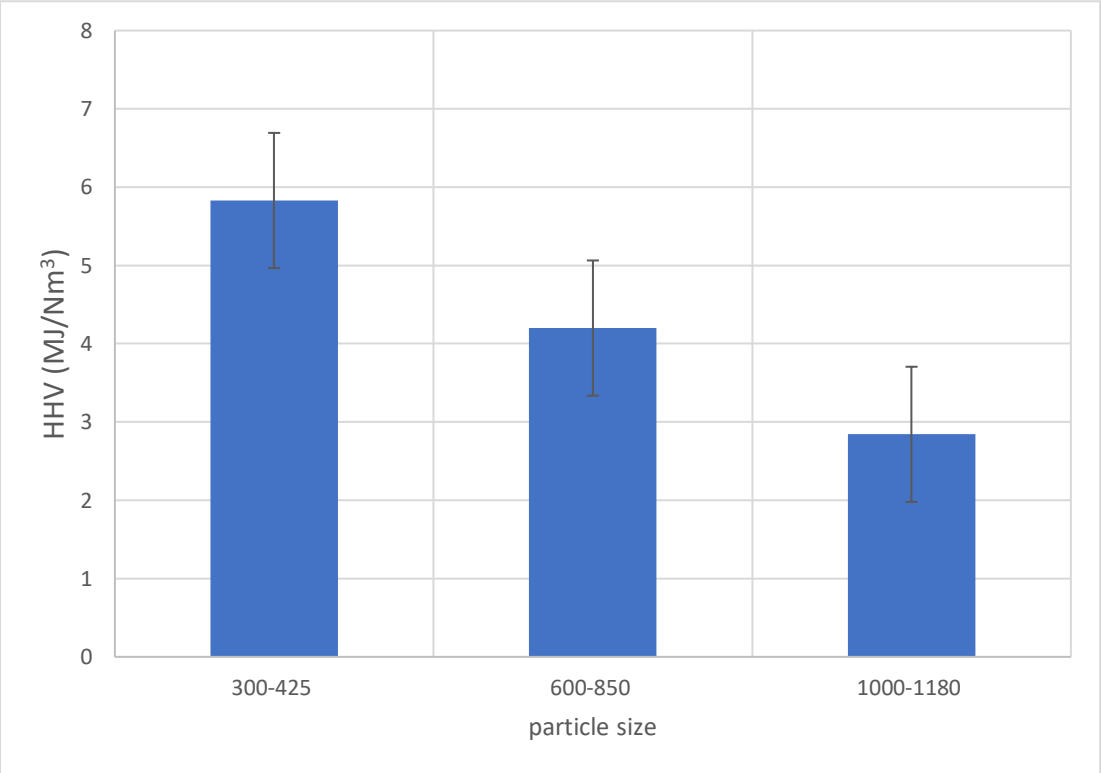


*Figure 6- 10 effect of biomass fuel particle size on gasification HHV for date stone.*

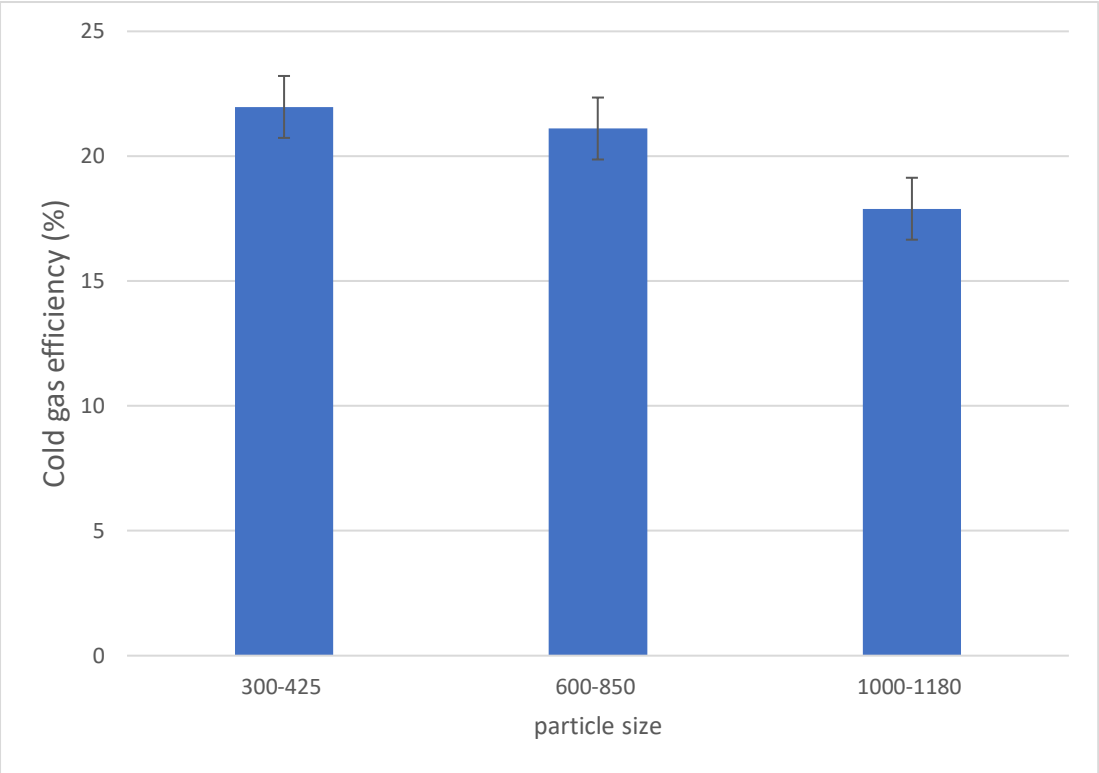


*Figure 6- 11Effect of the biomass fuel particle size on gasification cold gas efficiency of date stone.*

## 6.3 Material balance

In order to keep track of the date stones conversions into both the produced gas alongside the residue, of mass balance was performed. A schematic of the mass balance is shown in Figure (6-10). This would enable evaluation of the output gas based on the inlet materials, which consequently indicates the gasifier's overall performance as well as mitigating potential problems (e.g. loss of material).

The reactions occurring in the gasifier, using the inlet air and date stones, results in both char and volatile materials. The latter is classified into two different groups: product gases and tar. A further classification of the product gas can be undertaken, as it is inclusive of both non carbonaceous ($N_2$, $O_2$ and $H_2$) as well as carbonaceous (CO, $CO_2$ and $CH_4$) gasses. While the char was mainly the carbon that remained unburnt when the process concluded. The quantification of the gasses was measured in volume percent.

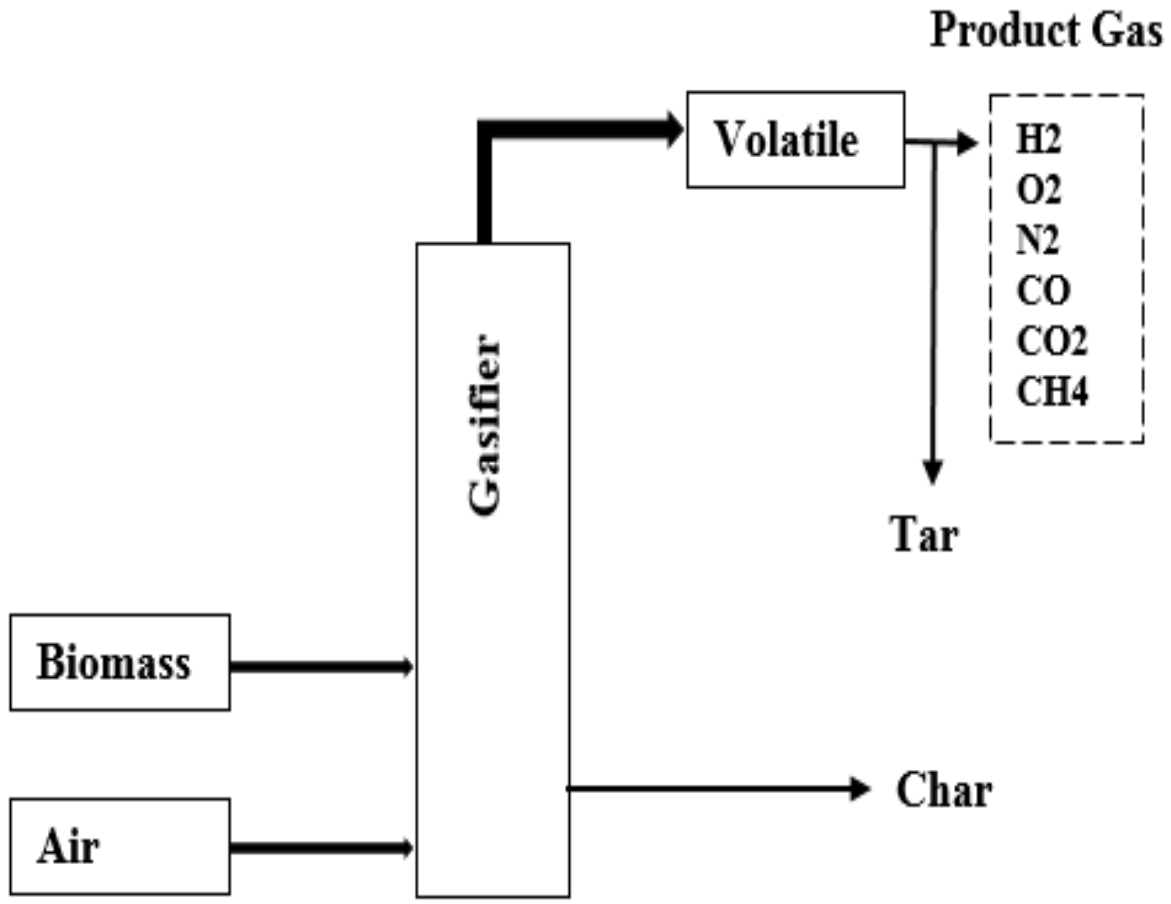


*Figure 6- 12 Material flow distribution of inputs and outputs in the gasification process.*

The tar that deposits in the gasifier's pipework increases the difficulty of collecting the resultant tar from the downstream equipment (described in Section 4.1.7). Therefore, flasks of isopropanol were used to accumulate and filter the tar. The tar content was neglected in the mass balance calculation of the gasification process, considering the char and product gas only, in order to make the calculations more feasible.

The gasification material balance was determined using the formula shown in Equation (6-1):

$$[\dot{m}air + \dot{m}fuel]\ input = [\dot{m}gas + \dot{m}char]\ Output \qquad \text{Equation 6- 1}$$

A lab scale was used to weigh the fed palm stones(described in Section 4.1.2). While the weight of the produced char was made known using the load cell attachment of the gasifier, hence the estimated mass of char should equate its mass within the reactor. The air's mass rate alongside the gas's mass rate were estimated using Equation (6-2) and Equation (6).

$$\dot{m}air = Qair \times \rho air \qquad \text{Equation 6- 2}$$

$Q_{air}$ is the air flowrate in l/min.

$\boldsymbol{\rho_{air}}$ is the air's density at room temperature.

Equation (4-6) was discussed earlier in this research in chapter (4) and can be used to calculate the mass rate of the product gas as following:

$$Y = \frac{Q_a * 79\%}{\dot{m}\ N_2\%}$$

Where,

$Q_a$ is the volumetric flow rate of air in $Nm^3/h$

$\dot{m}_f$ is the mass flow rate of the biomass in kg/h

$N_2\%$ is the volumetric percentage of nitrogen in the dry fuel gas.

Each individual gas product of the gasification process was calculation using Equation (6-3), as following:

$$yi = Y \times xi \qquad \textit{Equation 6- 3}$$

Where,

Y is the total yield of the product gas ($Nm^3$/kg biomass feed)

yi is the gas yield of each individual gas ($Nm^3$/kg biomass feed)

$x_i$ is the gas mole fraction.

Equation (6-4) can be used to find the value of $Z_i$, which can be obtained by using the individual gas yield conversion to unit of mass of individual gas divided by mass of the biomass feed. 1 kmol of gas occupies 22.4 $Nm^3$ for an ideal gas. The mass of the gas can be obtained by rearranging the equation as below.

$$Zi = yi \times Mwti/22.4 \quad \textit{Equation 6- 4}$$

$$mii = Zi * mfuel \quad \textit{Equation 6- 5}$$

The total mass of the produced gas can be obtained from Equation (6-6), as following:

$$migas = \Sigma miI \quad \textit{Equation 6- 6}$$

Where,

$M_{wti}$ is the molecular weight of gas (g)

$M_{gas}$ is the mass flow rate of gas (g/min)

The biomass conversion can be monitored by carefully assessing the mass balance of the carbon molecules. However, in order for this approach to work, it was assumed that the only source of carbon is both the char and produced gasses, while considering carbon included in the air as negligible. This enables using Equation (6-7) to determine the mass balance, shown below:

$$\dot{c}fuel = \dot{c}gas + \dot{c}char \quad \textit{Equation 6- 7}$$

Where,

$\dot{C}_{fuel}$ is the mass rate of carbon in the entering stream.

$\dot{C}_{gas}$ is the mass rate of carbon in the produced gas

$\dot{C}_{char}$ is the mass rate of carbon in char

All the above is in g/min

With the above in mind, Equation (6-8), (6-10) and (6-11) can now be used to estimate the mass rate of carbon in both inlet and outlet streams. While using the $CC_{fuel}$ value can be obtain using the ultimate analysis table.

$$\dot{c}fuel = ccfuel \times \dot{m}fuel \qquad \textit{Equation 6- 8}$$

$$\dot{c}i = ci \times \dot{m}fuel = (yi \times 12/22.4) \times \dot{m}fuel \quad \textit{Equation 6- 9}$$

Where,

$C_i$ is the mass of carbon in the carbonaceous gas.

$\dot{C}_i$ is the mass rate of carbon in the carbonaceous gas.

The mass rate of carbon in the produced gas can be estimated using Equation (6-10)

$$\dot{c}gas = \Sigma\dot{c}i \quad \textit{Equation 6- 10}$$

While the mass balance of char can be summarised using the following formula in Equation (9):

$$\dot{c}char = ccchar \times mchar/t \quad \textit{Equation 6- 11}$$

Where,

$CC_{char}$ is the percentage mass of carbon within the char.

$M_{char}$ is the char's mass.

Char generally in the gasifier output has a low ash content, and therefore it was assumed that its whole mass is carbon, in order to simplify the calculation.

It is also important to estimate the errors between both the inlet and outlet streams, this can be estimated as the ratio of mass difference to the input mass, and represented as a percentage, as shown in the following Equation:

$$\%\ error\ =\ \ (input - output)/input\ \ \times\ 100\ \ \textit{Equation 6- 12}$$

Each experiment mass balance was calculated and shown on Tables (6-9) and (6-10). Additionally, the impact of temperature, operation conditions as well as the Equivalence Ratio (ER) on the palm stones gasification is discussed thoroughly in Chapter (6).

Similarly, the error margin is noted down in Table (6-9) for each temperature and resultant mass balances, at an Equivalence Ratio of 0.2. The table shows that the error margin reduces at elevated temperatures, specifically around 600 $^{o}$C and 650 $^{o}$C, the inlet to outlet discrepancy reduces to half a percent. It's worth pointing out that a positive margin error indicates that mass of inlet material is higher than the output material, and vice versa for negative margin error, this is outlined further in Equation (6-12).

Therefore, a negative error margin is a possibility when the feeder unit had an exceed supply of biomass than originally determined in the reaction calculations, as it would increase the producer gas.

The feeder equipment is assumed to be reliable and maintains the required mass of the inlet mass. It's also worth noting that as tar was neglected during calculating the overall and carbon mass balances, and therefore the calculation results in a positive error margin.

Finally, a limitation of the experiment was due to the gas analyser's inability to measure carbonaceous gasses that are heavier than methane, and therefore heavy hydrocarbons were not considered.

*Table 6- 8 Overall mass and carbon balance % error with temperature. ER=0.2.*

| **Temperature, °C** | **Total mass balance, g/min** | | | **Carbon mass balance, g/min** | | |
|---|---|---|---|---|---|---|
| | In | out | % error | In | out | % error |
| 500 | 86.9 | 70.9 | 18.4 | 18.93 | 15.25 | 19.44 |
| 550 | 86.9 | 71.43 | 17.79 | 18.93 | 15.24 | 19.49 |
| 600 | 86.9 | 75.05 | 13.63 | 18.93 | 16.73 | 11.62 |
| 650 | 86.9 | 76.41 | 12.07 | 18.93 | 17.13 | 9.47 |

The percentage error described above is given in Table (6-10) and compared to the corresponded Equivalence Ratio used in the experiments. The oxygen supply level was made to be lower by starting the experiment at a lower ER value, which meant the highest biomass feeding rate.

Subsequently, the error margin is highest at lower ER values, which indicates a reverse proportional relationship between both; it also results in a higher tar production. When ER approaches 0.15 in value, the process start is as close as possible to being the pyrolysis condition where liquid products are in abundance, namely hydrocarbons (both heavy and light) and water. The discrepancy in the carbon mass balance can be attributed to not considering the carbons in the liquid hydrocarbons. The error margin noticeably reduces beyond ER value of 0.15 due to the higher conversion of volatiles into gases. The error margin reaches are in the range of 7.7% to 12.1% for the mass balance as an overall, while ranges between 5.1 to 9.9% for the mass balance of carbon, while it is consistently about 10% at ER value of 0.15.

*Table 6- 9 Overall material balance and carbon mass balance % error with ER.*

| **Equivalence ratio (ER), T=750°C** | **Total mass balance, g/min** | | | **Carbon mass balance, g/min** | | |
|---|---|---|---|---|---|---|
| | In | out | % error | In | out | % error |
| **0.15** | 99.86 | 78.91 | 20.97 | 25.24 | 19.56 | 22.52 |
| **0.2** | 86.9 | 76.41 | 12.07 | 18.93 | 17.13 | 9.47 |
| **0.25** | 79 | 70.38 | 10.9 | 15.14 | 13.65 | 9.86 |
| **0.3** | 73.9 | 67.55 | 8.59 | 12.62 | 11.71 | 7.23 |
| **0.35** | 70.22 | 64.86 | 7.6 | 10.81 | 10.27 | 5.05 |

## 6.4 summary

This chapter shows the results of gasification of date stone in a bubbling fluidised bed gasifier. The results and the effect of the operating and hydrodynamic parameters has been presented and discussed in detail. This chapter has shown the positive effect of the bed temperature on all the produced combustible gases composition, in addition to performance parameter. increasing the temperature of the gassier has a direct positive impact on hydrogen from (3% to 7%), carbon monoxide from (13% to 18%) and methane, while it has a negative impact on carbon dioxide concentration (14%to 12.9%). Moreover, the HHV value climbed to 4.9 MJ/Nm3 and the cold gas efficiency is found to be the highest at highest temperature resulting from the rise of combustible gases amount in the producer gas. Both the CO and H2 concentrations were inversely proportional with the ER values, due to full and partial oxidation of char.

In general, different effects of ER parameter has been detected on the gasification of biomass feedstocks. Both the CO and H2 concentrations were inversely proportional with the ER values due to the increased full and partial oxidation of char and the CO2 concentration is higher at an ER of 0.15. The lowest value of HHV is obtained at a high ER interval, which results from the reduction in the combustible specific. The carbon conversion efficiency increases from 36.4% to 66.9% and this can be explained by more oxygen being supplied for biomass reactions which have a trend towards fuel combustion when ER increases.

The impacts of dolomite were assessed at different catalyst ratios on date stone as the biomass material of the gasification process. Both the $H_2$ and $CO_2$ increased as the dolomite quantity increased from (7-12.7%) and (16-17.6 %) respectively. Meanwhile, both the methane and carbon monoxide content decreased. A 10% calcinated dolomite (weight %) within the gasifier's bed is considered sufficient to cause a significant improvement in the distribution of the product as well as the produced gas quality.

In addition, a smaller biomass particle size has shown a more favourable quality producer gas production and upgrade performance parameters. The concentration of the produced CO (15 %), $CH_4$ (7 %), and $H_2$ (9 %) is higher when using a smaller biomass particle size, while carbon dioxide concentration decreases.

Finally, the total and carbon mass balance in the biomass gasification system has been conducted to observe the balancing of input and output streams.

## Chapter 7

# Economic feasibility of using date stone as a source of clean energy in Saudi Arabia.

# Chapter 7

This chapter aims to study the economic feasibility of using date stone as a source of clean energy in Saudi Arabia. by choosing one region as a case study and use gasification to produce energy from waste of the date palm (Result s from Chapter (6)).

## 7.1 Importance of Date in Saudi Arabia

Date palm is one of the main agricultural products in the arid and semi-arid regions across the world, particularly in the Middle East and North Africa (MENA) region. Being a tropical and subtropical tree that belongs to the Palmae family, the date palm has been playing a significant role in the daily life of the people in the MENA region for the last seven thousand years [37]. The latest data from The World Bank (2020) shows that Saudi Arabia has only 1.6% arable land in 2016 out of 2.149 million $km^2$ of its total land, which is characteristically comprised with an arid and semi-arid climate. Although the country has between three and four times as much arid land as arable, the potential arable land is not yet used. The main region of Saudi agricultural land lies in regions that are short of water, with rainwater averages at 250 mm per year or more. The temperature in Saudi Arabia is comparatively high and can reach up to 50°C during the summer in places, while the humidity is comparatively high in the eastern part of the country. The soil in Saudi Arabia is normally fragile and it is eroded by wind and water, while the high salinization degrades the soil. According to Erskine *et al.* [239] more than ninety percent of the Arabian Peninsula's land suffers from desertification, of which sixty percent of the desertification is caused by wind and water erosion, and more than forty percent of this desertification can be considered as severe to very severe.

According to Aleid et al. [240] the total number of named date palm cultivars across the world has been estimated at 5,000, but the flavour of date palm differs between cultivars and location, and can even vary within  date groves, . The most widely grown fruit tree in Saudi Arabia is the date palm, which is mainly grown in areas that have long dry summers and mild winters. The date palm trees thrive in desert and oasis climates, wherein the temperature should be high but the level of groundwater should be near to the soil surface [241]. According to Al-Alawi *et al.*[242], the production of date fruit depends on the availability of heat, and the dry areas have the most number of the dry fruit cultivars due to the availability of humid and semidry land. Saudi Arabia's date palms can grow in various types of soil, but the light deep soils provide

the best conditions. The date palms in Saudi Arabia can tolerate high degrees of salinity, for example up to 22,000 ppm, but the cultivars' grown trees and fruits also differ according to the level of salinity[240]. According to Sirisena et al.[243], the level of salinity provides negative influence of the growth and chlorophyll contents of the date palm trees.

The global cultivation of date palm has increased rapidly in recent years. The annual production of date across the world in 2018 has been reported at 8.83m metric tonnes[244], which have been valued at US$ 4.2bn. Saudi Arabia is the third largest global producer of dates, while Egypt occupies the number of one position as the largest date producer across the world[245]. Based on the data provided by the Ministry of Agriculture, Riyadh has the highest annual production of date at 361,649 metric tonnes within an estimated area of 42,208 hectares. The Kingdom of Saudi Arabia is divided into thirteen regions. The Riyadh region, which contains the Administrative Capital, which was used as a case study in this chapter, is considered the highest area with numbers of date palms (7.86 x 106) and consequently, dates production. And it comes in second place in numbers of date palms (7.33 x 106) is the Qassim region, which is an agricultural region that produces the most luxurious types of dates in the Kingdom, which are exported abroad. The Medina region comes in third place (4.62 x 106) and one of the most important types of dates produced in Al Madinah is Al-Ajwa, which is considered one of the most expensive types of dates. The eastern region comes in fourth place in the production of dates (3.92 x 106), which is considered one of the richest regions in the world due to the presence of many oil fields in it.

Table (7-1) shows the date production and approximate areas by region in 2018 in Saudi Arabia.

*Table 7- 1 The production of date and estimated areas in Saudi Arabia in 2018 [9].*

| Region | No of date palm | Production | Area (ha) |
|---|---|---|---|
| Riyadh | $7.86 \times 10^6$ | 361,649 | 42,208 |
| Qassim | $7.33 \times 10^6$ | 337,220 | 39,301 |
| Madinah | $4.62 \times 10^6$ | 212,614 | 18,502 |
| Eastern | $3.92 \times 10^6$ | 180,565 | 13,625 |
| Hail | $1.89 \times 10^6$ | 87,310 | 16,187 |
| Makkah | $1.24 \times 10^6$ | 57,220 | 8,068 |
| Asir | $1.11 \times 10^6$ | 51,415 | 4,297 |
| Tabuk | $1.01 \times 10^6$ | 46,573 | 2,966 |
| Jouf | $0.91 \times 10^6$ | 41,898 | 5,471 |
| Najran | $0.39 \times 10^6$ | 18,394 | 3,070 |
| Baha | 73,554 | 3,383 | 1,095 |
| Northern | 14,329 | 659 | 40 |
| Jazan | 8,719 | 401 | 288 |
| Total | $30.42 \times 10^6$ | $1.39 \times 10^6$ | $0.15 \times 10^6$ |

Table (7-1) shows that the total production of date in 2018 in Saudi Arabia was reported at 1,399,762 metric tonnes in 2018 from an estimated 30,429,607 trees, which were cultivated in an estimated area of 155,118 hectares. Figure (7-1) shows that the central region of Saudi Arabia – Riyadh – has the highest production of dates in 2018, which accounts more than 25% of the estimated total production. The second and third places go to Qassim region and the Eastern region with an estimated more than 19% and 15% of the total production respectively [35].

The orchards of date palm are also distributed in different places in Saudi Arabia, and according to NCFP [35], there are more than 400 date cultivars in the main four regions, such as Riyadh, Qassim, Eastern, and Madinah, of which only 50 to 60 cultivars produce dates commercially in these four regions [246]. Figure (7-1) shows the 13 geographical regions that contain various cultivars of date palm.


*Figure 7- 1 The regions that produce the date through various cultivators [232].*

According to Al-Shreed et al.[247], Saudi Arabia has the high est per capita consumption of dates in the world, which reached to nearly 35 kg per person per year. The econometric analyses of the costs of the date productions depend on a number of variables, such as the increasing level of citrus in dates, the quantity sold, and the prices of the final products [240]. According to Dhehibi et al.[248], additionally, the production of date and the prices of dates are also influenced by the cultivators, the costs of production, the intercropping within the orchards, and the optimal level of operations. In relation to the econometric analyses, Aleid et al. [240] noted that the labour cost is the most crucial cost factor in the production of dates. During the

harvest seasons, the cultivators hire many part-time and seasonal workers, and the cultivars have little control over these seasonal labours.

## 7.2 Production of Energy from Date Palm Waste

Date palm trees generate large quantities of agricultural wastes, and the study of Chandrasekaran and Bahkali found that each date tree can generate nearly 20 kilograms of dry leaves each year[37] ( see section(1.6)).

Other wastes, for example date stones can provide an average of 30% of the date fruits, and these agricultural wastes contain cellulose, hemicellulose, lignin, and other composites that are commercially used in various biological processes. The harvesting of date palm fruits is frequently accompanied by considerable fruit losses that occur during the picking of fruits, and subsequent storage and processing. Because of their insufficient textures (too soft), the lost dates, generally named as date by-products, are not fit for human consumption and are generally rejected [242]. Actually, all organic waste materials that arise from date processing may have the potential for use as elements for the production of compost [37]. The leaflets, date palm rachis, fruit stalk pruning, and trunk are the residues of the date palm as shown in Figure (7-2). Additionally, Table (7-2) shows the applications of these residues.

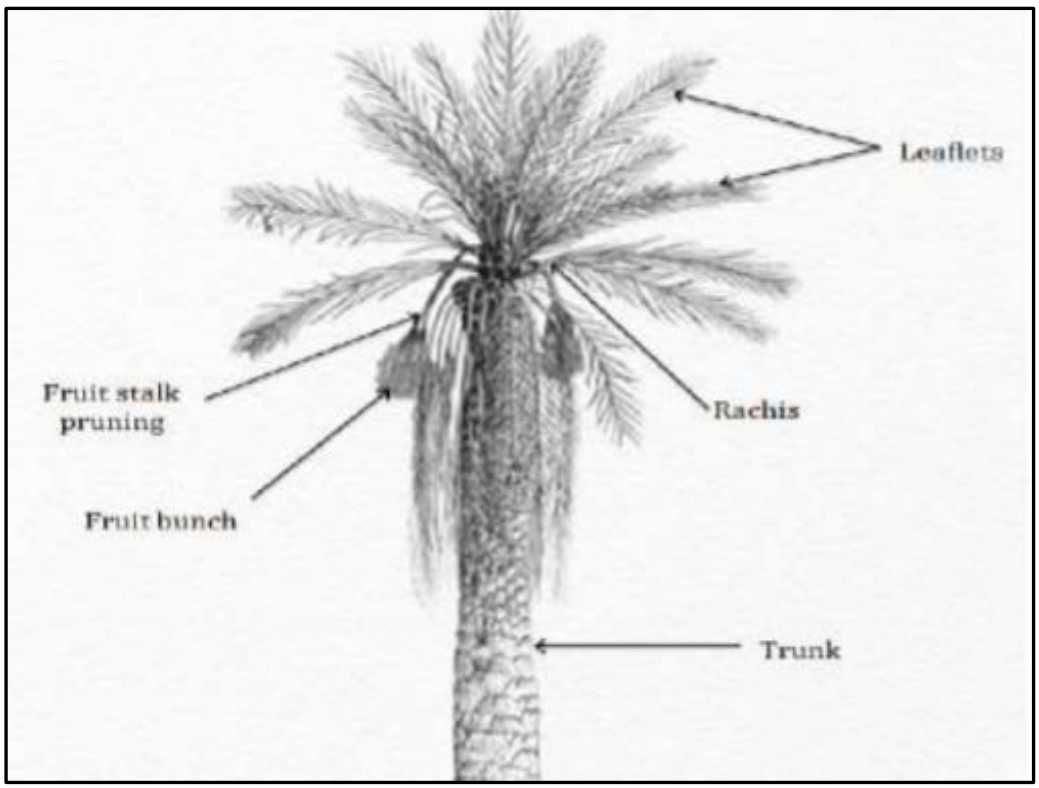


*Figure 7- 2 A date palm tree [243].*

*Table 7- 2 the applications of these residues.*

| Type of residue | Applications |
|---|---|
| leaflets | Baskets, crate, carpets, fan, food covers, etc. |
| Rachis | Timber, wood, furniture, mats, paper, fuel. Etc |
| Fruit pruning | Cages, trays, vases, cords, twine, etc. |
| trunk | Poles, beams, girders, etc |

After the cultivation of the date fruits, various residues are separated from the tree parts. A full-grown date palm tree generally contains 100-130 green palms and develops 10-30 new leaves each year. However, it is necessary to remove the leaves when they become dry, and the branches of the date palm contains nearly 45% of leaflets and approximately 54% of rachis [249]. Sait et al. [180] found that an adult date palm tree produces nearly 20 kilograms of dry leaves each year. With date fruits, the overall mass of a solo bunch fruit pruning has been reported at nearly 8 kilograms, while the dried fruit pruning without the fruits weighs nearly 400-500 grams [250]. On average, each acre of land contains date palm trees of 80-130, while the trunk of a date palm tree has average mass of 60 kilograms in each acre of land, as two to three tresses die each year in an acre, and they are removed, while new trees are planted. Table (7-3) shows the average weight of various residues of date palm.

*Table 7- 3 Average weight of residues of date palm* [251].

| Type of residue | Weight of Residue |
|---|---|
| Leaflets | 9.2 kg/tree/year |
| Rachis | 10.8 kg/tree/year |
| Fruit pruning | 0.5 kg/tree/year |
| Date palm trunk | 60 kg/acre/year |
| Date stone | 90 kg/tree/year |

## 7.3 Assessment of Energy Potential from Residues of Date Palm

A field survey has been performed for quantifying the availability of the residues of the date palm in Riyadh, Saudi Arabia, as this region produces nearly 30% of the total dates in the Kingdom. For reducing the moisture contents, the samples were left in the natural environment to dry for three days. For developing a standardised product to analyse, it was necessary to

pulverize the samples into particles by hammering and each particle weighted less than two millimetres.

### 7.3.1The Measurement of Heating Value

An experiment was conducted to determine the calorific or heating values of the residues and the samples were analysed by a bomb calorimeter, model number 6100, from Parr Instrument Company (as described in chapter 3, Section 3.2.2).

*Table 7- 4 Measurement of Heating Value.*

| Type of residue | HHV($MJkg^{-1}$) | References |
|---|---|---|
| Leaflets | 17.9 | [180] |
| Rachis | 10.9 | [180] |
| Date stone | 18.965 | This study |

### 7.3.2 The Measurement of Total Residues ($R_{Ti}$)

To estimate the total residue, the total tree number (N) in the region multiplied by the residues produced by these trees (Rgi) to find out the total residues of the date palm in the Riyadh region:

*Table 7- 5 Measurement of Total Residues*

| **Type of residue** | **Weight of Residue** | **Total Residues in Riyadh (kg)** |
|---|---|---|
| **Leaflets** | **9.2 kg/tree/year** | **72.3 x $10^6$** |
| Rachis | 10.8 kg/tree/year | 84.9 x $10^6$ |
| Date stone | 90 kg/tree/year | 707 x $10^6$ |
| total | | 864 x $10^6$ |

### 7.3.3 The total Potential Energy

Equation (7-1) has been developed to calculate the potential produced energy [252].

$$Ep = \sum_{i=0}^{N} Rai.Hi \quad \text{Equation 7- 1}$$

Where:

Ep = The contained energy in the residues, mega joule per year.

RAi = The quantity of available residues for each type of residue (i) in tonnes per year for the energy.

Hi = The value of heating for each type of residue (i) in MJ per kg.

n = The number of types of the residue.

*Table 7- 6 total Potential Energy*

| Type of residue | Weight of Residue | Total Residues in Riyadh (kg) | HHV(MJkg-1) | Total energy (MJ) |
|---|---|---|---|---|
| Leaflets | 9.2 kg/tree/year | $0.72 \times 10^9$ | 17.9 | $1.3 \times 10^9$ |
| Rachis | 10.8 kg/tree/year | $0.85 \times 10^9$ | 10.9 | $0.93 \times 10^9$ |
| Date stone | 90 kg/tree/year | $0.7 \times 10^9$ | 18.965 | $13.4 \times 10^9$ |
| total | | $0.86 \times 10^9$ | | $15.6 \times 10^9$ |

# 7.4 Economic Analysis

## 7.4.1 General Assumptions

The base year for the economic analysis is chosen to be 2020, which was the latest listed year in the US Chemical Engineering cost indices when the feasibility study started. All financial data is, therefore, presented in 2020 GBP (SAR) according to the Bank of England annual exchange rates wherein:

1 KSA (SR) = 0.19 GBP (£)

The plant life is assumed to be 20 years, which is in line with the general considerations across the majority of similar techno-economic studies. Subsequently, 8,000 operating hours per year is the assumed plant availability to account for maintenance downtime and unscheduled stoppages.

### 7.4.2 Economic Performance

The economic evaluation was employed using discounted cash flow analysis. The component for the analysis consists of capital cost, operating cost, and projected sales revenue. The profitability of the power plant is evaluated through the net present value (NPV) and return on investment (ROI) which are suggestive of economic feasibility of the power plant [253].

#### 7.4.2.1 Capital Cost

The capital cost, which is generally used in the energy industry, is the cost of building a power generation plant with respect to instantaneous power efficiency [254]. This is used as basis for the calculation of the power plant capital cost using the exponential method, as defined by Equation (7-2) and (7-3). The exponential method is a simple economic estimation of cost based on capacity whereby a scaling factor of 0.6, which is the standard proportionality coefficient for scale economies, is used in production processes as such [255]. The calculated value is the estimated cost at the reference time, which is then used to obtain the updated estimated cost based on the chemical engineering plant cost indices [256]. The chemical engineering plant cost indices are a system of escalation cost tracking of equipment, construction labour, building, and supervision in chemical process industries, whereby in 2016 and 2020 the plant cost indices averaged at 541.7 and 596.2 respectively [256][257]. Using the values defined and the average overnight capital cost 3,669£/kW for a biomass power plant with a 50MW nominal capacity [258], the capital cost for the power plant with a capacity of 373 MWt is £9,085,481.04.

$$C_b = C_r(\frac{S}{S_r})^n \qquad \textit{Equation 7- 2}$$

Where:

Cb is the estimated capital cost of the new power plant in 2016

Cr is the reference plant capital cost

S is the capacity of the new power plant

Sr is the reference plant capacity.

$$C_b = £3{,}669\ (\frac{373{,}000\ \text{kW}}{1\ \text{kW}})^{0.6} = £8082001$$

$$\frac{C_a}{C_b} = \frac{I_a}{I_b} \qquad \textit{Equation 7- 3}$$

Where

Ca is the estimated capital cost of the new power plant in 2020

Cb is the estimated capital cost of the new power plant in 2016

Ia is the chemical engineering plant cost index for 2020

Ib is the chemical engineering plant cost index for 2016.

$$\frac{C_{2020}}{C_{2016}} = \frac{I_{2020}}{I_{2016}}$$

$$C_a = C_{2020} = C_{2016}\frac{I_{2020}}{I_{2016}} = £8082008(\frac{596.2}{541.7}) = £8895132$$

The capital cost of a 373 MWt biomass power plant in 2016 is £8082008 Therefore, the capital cost of a 373 MWt biomass power plant in 2020 is £8895132

7.4.2.2 Operating Cost

The operating cost consists of the operating and maintenance (O&M) cost of the power plant. It is obtained from the sum of the variable operating and maintenance cost, and the fixed operating and maintenance cost added with the biomass cost. The fixed cost and variable cost are obtained using the exponential method, whereby an estimated fixed cost of 110$/kW-yr and a variable cost of 4.2$/MWh in 2016 are used along with the scaling factor 0.6 and the chemical engineering plant cost indices of 541.7 and 596.2 for years 2016 and 2020,

respectively [258][257]. The biomass cost is obtained from the sum of the collection, storage, and transport costs. The average distance covered is approximated to be between 100 km and 150 km from the suppliers, which constitutes to a transportation cost of £100 per 9 tonnes. The collection, and storage costs are assumed to be £80, and £25 per 9 tonnes, respectively [253].

*Fixed Operating Cost:*

$$C_b = C_r(\frac{S}{S_r})^n \ = £80\ (\frac{373{,}000\ \text{kW}}{1\ \text{kW}})^{0.6} = £178{,}323$$

$$C_a = C_{2020} = C_{2016}\frac{I_{2020}}{I_{2016}} = £178{,}323(\frac{596.2}{541.7}) = £196{,}264$$

The fixed cost of a 373 MWt biomass power plant in 2016 is $= £178{,}323$. Therefore, the fixed cost of a 373 MWt biomass power plant in 2020 is $£196{,}264$.

*Variable Operating Cost:*

$$C_b = C_r(\frac{S}{S_r})^n \ = £3(\frac{373\ \text{MW}}{1\ \text{MWh}})^{0.6}(8{,}000\ \text{h}) = £863{,}285$$

$$C_{2020} = £863{,}285\left(\frac{596.2}{541.7}\right) = £950{,}140$$

The variable cost of a 373 MWt biomass power plant in 2016 is £863,285. Therefore, the variable cost of a 373 MWt biomass power plant in 2020 is $£950{,}140$.

*Biomass Cost:*

$$\text{Biomass Cost} = \text{Collection Cost} + \text{Storage Cost} + \text{Transportation Cost}$$

$$\text{Biomass Cost} = £80/9\text{tonnes} + £25/9\text{tonnes} + £100/9\text{tonnes}$$

$$\text{Biomass Cost} = (£205/9\text{tonnes})(707{,}000\text{tonnes}) = £27{,}887{,}222.22$$

***Operating Cost:***

$$\text{Operating Cost} = \text{Fixed Cost (inclusive of Biomass Cost)} + \text{Variable Cost}$$

$$\text{Operating Cost} = (£196{,}264 + £27{,}887{,}222) + £950{,}140 = £29{,}033626$$

Therefore in 2020, the total operating cost of the 373 MWt biomass power plant is $£29{,}033626$

7.4.2.3 Revenue

The primary source of revenue is the power plant is the energy distributed along power lines. Since the cost of electricity per kWh is £0.035 or 0.1842SR which is about the average electricity sales price of 0.18SR/kWh in Saudi Arabia [259], the total sales revenue for the 373 MWt power plant with 112 MWe power generation is estimated to be £31,360,000 annually. Figure 1 presents the flow for the sales revenue computation, where in the total amount of energy produced from biomass is respective to the mass and heating value of date stone. The viable energy for generation as per CGE is about 80%, which directs the plant capacity. The electrical generation efficiency is about 30%, by which when converted to the kWh accounts for the electricity revenue with respect to the electricity sales price.

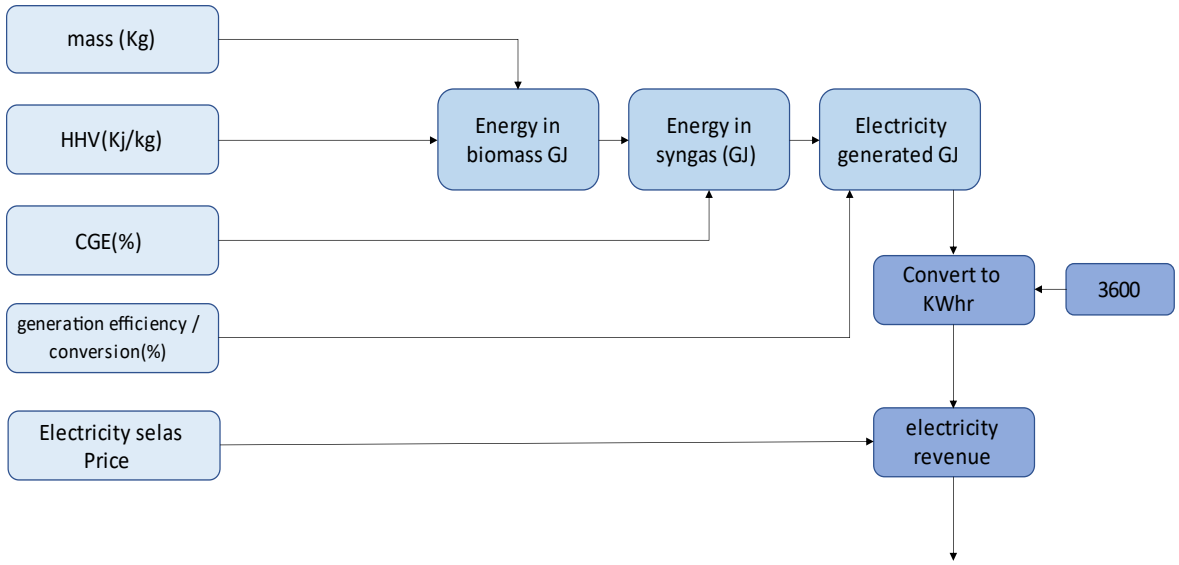


*Figure 7- 3 Sales revenue computation with respect to mass of date stone, HHV, energy and generation efficiencies, and electricity sales price.*

$$\text{Revenue} = \left(\frac{£0.035}{\text{kWh}}\right)(112{,}000\ \text{kW})(8000\ \text{h}) = £31{,}360{,}000$$

7.4.2.4 Projected cash flow, net present value, return on investment, and payback period.

For the projected cash flow, the discounted cash flow analysis is used as basis for the calculation of the net present value (NPV), return on investment (ROI), and payback period (PBP). The capital cost is approximated to be £9,100,000, while the working capital is 15% of the total investment which is approximately £38,150,000. Therefore, the working capital is £5,722,550 [256]. Provided an inflation rate of 3.44% in Saudia Arabia, the dismantling cost of the plant is approximately £2,839,200[260]. The obtained values are then used to arrive to the cash flow at an average discount rate of 8% to identify potential future values of cash flows with reference to present value (within respective discounted cash flow analysis). The completion of the power plant is expected to be within 2 years as per general economic considerations for biomass power plant [261] [256].

As presented in the projected cash flow, the net present value (NPV) of the biomass power plant in Riyadh is £82,887,627.67. NPV represents the compounded profit over power plant lifetime [262]. Figure (7-4) shows the projected cash flow of the power plant over 20 years of operation, wherein the NPV is a function of operating cost and revenue.

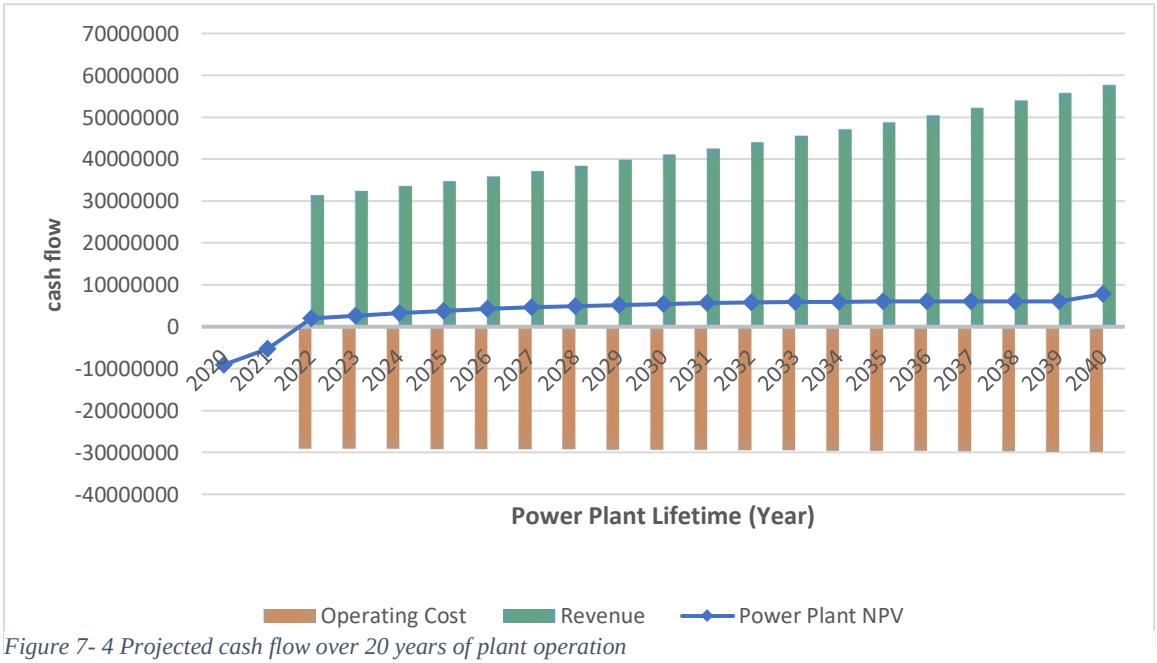


*Figure 7- 4 Projected cash flow over 20 years of plant operation*

The NPV (as plotted in blue) is expected to increase as revenue outweighs the operating cost in the long run. This is demonstrated by the considerable difference in slope of positive inflow and negative inflow, whereby the inflow from revenue (as presented by green bars) is greater in magnitude than the outflow from operating cost (as presented by orange bars). Therefore, indicating the potential of the power plant to yield profitable outcomes, by which the accumulated NPV over 20 years is 53.9% greater than the total investment.

The return on investment (ROI) is the total return of revenue, and is defined by Equation 6 where TPC is the total plant cost, CRF is the capital recovery factor as defined by Equation 7 with discount rate i and plant lifetime y, TVC is the total variable cost, P is the profit, and TR is the tax rate [253]. Provided that the tax rate in Saudi Arabia is 20% and the CRF of 0.1 as calculated, the ROI for the power plant over 20 years of operation is shown in Figure (7-5).

$$\%ROI = \frac{P\ x\ (1-TR)}{(TPC\ x\ CRF+TVC)}\ x\ 100\% \qquad \text{Equation 7- 4}$$

$$cRF = \frac{i}{1-(1+i)^{-y}} = \frac{0.08}{1-(1+0.08)^{-20}} = 0.1 \qquad \text{Equation 7- 5}$$

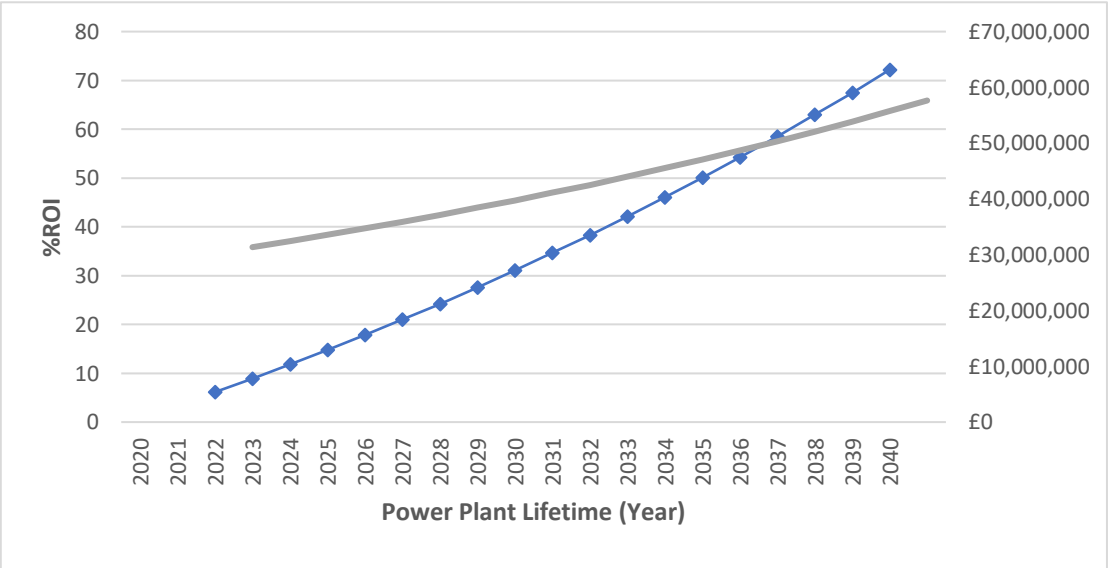


*Figure 7- 5 ROI over 20 years of power plant operation*

The annualized ROI (as plotted in blue) is expected to increase considerably with respect to the magnitude at which the investment is reclaimed from annual revenue. The revenue (as plotted in gray) increases annually, resulting to substantial accumulation of profit. Hence, the increasingly high ROI. The ROI during the start of operation is 6.15%, which is expected to increase from about 3% to 5% with 0.59% increment annually. Therefore, iterating the high profitability potential of the power plant over 20 years of operation.

The payback period (PBP) is the expected time elapsed to reclaim the investment. This is defined by Equation 8, where Y is the last year with negative cumulative NPV, N is the absolute value of the negative cumulative NPV, and P is the absolute value of the positive NPV [Cardoso et al., 2018]. Plotting the values obtained from the projected cash flow, the obtained payback period for the biomass power plant in Riyadh is 6.83 years.

$$PBP = Y + \frac{N}{P} \qquad \text{Equation 7- 6}$$

$$PBP = 5 + \frac{|-2{,}733{,}825.55|}{|1{,}491{,}780.99|} = 6.83\ years \qquad \text{Equation 7- 7}$$

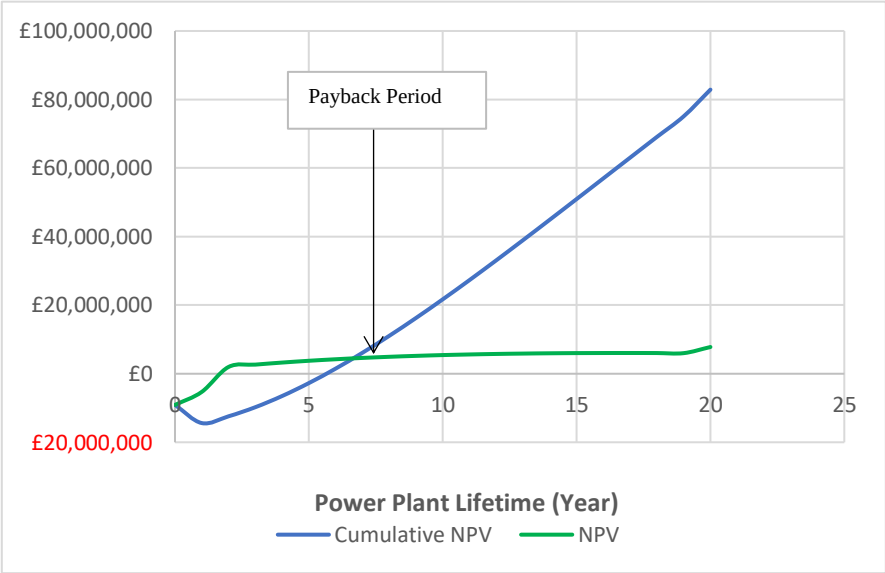


*Figure 7- 6 Payback period as a function of NPV and Cumulative NPV*

Figure (7-4) presents the net and cumulative cash flows, whereby the payback period of 6.83 or about 6 years and 10 months is indicated by the intersection. As the

annualized NPV (as plotted in green) increases steadily, the cumulative NPV (as plotted in blue) increases at a considerably higher rate due to compounded profit. These result to intersecting plots, whereby the point of intersection corresponds to the period at which the investment is recovered by accumulated annual profit. Thereby, further supporting the potential of the power plant to yield high profits.

## 7.5. Emissions

Using biomass as an alternative to fossil fuels for energy production is a promising prospective towards sustainability, and in this study, date stone is used as a source of clean energy. However, contrary to its reference being clean, the harvesting, transportation, and burning of biomass still yield significant amounts of carbon dioxide among other emissions. Albeit, the values should be considerably lower than the emissions from non-renewable energy sources, particularly fossil fuels such as natural gas and coal.

### 7.5.1. Harvesting Emission

The harvesting of forest biomass includes the cutting operations, whereby the emissions from diesel, oil, and grease use are accounted for machine utilities. The total emissions factor for harvesting forest biomass is at 17.38 kg $CO_2$ per tonne [263], which is used to calculate for the harvesting emissions of the 707,000 tonnes of date stone from date palm trees. As per calculated, the total carbon dioxide emissions from harvesting date stone from date palm trees is about 12,287.66 tonnes.

$$\text{Harvesting Emissions} = (707{,}000 \text{ tonnes})\left(\frac{17.38 \text{ kg } CO_2}{\text{tonne}}\right)$$

$$\text{Harvesting Emissions} = 12{,}287{,}660 \text{ kg } CO_2 \, /yr$$

### 7.5.2. Transportation Emission

The transportation for forest biomass is assumed to be trucks, whereby the emissions from fuel use and maintenance are accounted for. The total emissions factor for transporting forest biomass is at 0.117 kg $CO_2$ per tonne per km [263], which is used to calculate for the transportation emissions of the 707,000 tonnes of date stone over an average distance of 100 km. As per calculated, the total carbon dioxide emissions from the transportation of date stone is about 1,654.38 tonnes.

$$\text{Transportation Emissions} = (707{,}000 \text{ tonnes})(100 \text{ km})\left(\frac{0.117 \text{ kg } CO_2}{\text{tonne} - \text{km}}\right)$$

$$\text{Transportation Emissions} = 1{,}654{,}380 \text{ kg } CO_2$$

### 7.5.3 Carbon dioxide emissions and initiatives

The total carbon dioxide emissions of the power plant using date stone as clean energy source is 91,275.37 tonnes per year, which is equivalent to approximately 0.23 kg $CO_2$ per kWh. This value is significantly lower than the 0.400 kg $CO_2$ per kWh and 0.990 kg $CO_2$ per kWh that are generated from natural gas and coal-fired power plants, respectively [264]. This suggests that, indeed, using biomass as energy source yields lower emissions.

However, this is still an enormous amount of carbon dioxide into the atmosphere, which can be addressed by technologies such as carbon capture/sequestration. Carbon capture/sequestration involves the absorption of carbon dioxide emissions from power plants operations, the transportation of captured $CO_2$, and the storage of $CO_2$ which is usually employed through sequestration (the underground isolation of $CO_2$). This reduces the net carbon dioxide emissions in the atmosphere and helps to negate the carbon footprint in the

energy production sector. At present, a maximum of about 90% capture rate is attainable [265], which should further progress the sustainability of biomass power plants.

## 7.6 Summary

Using a case study in Riyadh region in Saudi Arabia, this chapter has demonstrated that the use of biomass from date palm may provide the availability of sustainable energy supplies in Saudi Arabia. This study has considered three types of residues from date palm trees, such as date palm leaflets, date palm rachis and date stone, and the study area in Riyadh can be used to produce energy from the residues of date palm. From the Riyadh region in Saudi Arabia the amount of the Rachis has the highest availability of 84.9 thousand tonnes per year, which is followed by Leaflets 72.3 thousand tonnes per year, and date stone (70.7 tonnes per year). Additionally, the heating values of residues from date palm in Riyadh region range from 10.9 to 19.0 MJ/kg. The total quantity of potential biomass generated from the residues of date palm in the Riyadh region to produce energy would be 865 x $10^6$ tonnes per year. The overall potential to recover energy from the residues of date palm has been forecasted to be 15.63 PJ.

The biomass power plant using date stone is a feasible project, which yields positive net present value, high return on investment , and short payback period . The increasing annualized ROI from 6.15% to 72.92% indicates that the rate of investment return grows considerably over 20 years of operation. This translates to greater capacity in paying the cost of the project back, and thus, rapid recovery from the investment whereby the benefits are expected to grow exponentially thereon. Ultimately, the economic potential of the project is feasible, as indicated by the highly favourable profitability measures - NPV, ROI, and PBP. However, aside from the economic indicators as presented, the sustainability of the biomass power plant also includes social, technical, and environmental considerations. This is significantly lower than the existing emission factors for natural gas and coal-fired power plants, which further supports the advantages of using biomass in energy production - particularly in the use of date stone as a source of clean electrical energy. Conclusively, the biomass power plant using date stone in Saudi Arabia is a highly feasible project, whereby the economic, social, technical, and environmental indicators for sustainability are duly met. Among these indicators, the high profitability and low emissions of the power plant operation are the most promising measures.

Therefore, this chapter concludes that the residues of date palm may be considered as an important source of clean energy to fulfil the growing demand of energy wherein natural resources are finite, particularly in the date palm producing countries wherein date palms are cultivated commercially for fruits.

## Chapter 8

# Conclusion and future work

# 8.1Conclusion

An investigation on the effects of chemical kinetics as well as the operating conditions on the gasification in a bubbling fluidised bed reactor of solid biomass fuels performance is conducted in this study. It also investigated the economic feasibility of the gasification process when using date stone as the main feedstock material within the KSA region. The study was conducted via completing a preliminary design of the gasifier reactor and perform cold experimental hydrodynamic studies to gather and analyse gasification processes data.

The study's conclusions and findings are summarised in this section. They are classified to three types.

1. The kinetic energy resulting from using a catalyst in the gasification of biomass in the TGA reactor.
2. Experiments conducted for biomass gasification's.
3. The economic feasibility of adapting date stone as an energy source in the Kingdom of Saudi Arabia.

# 8.2 Chemical kinetics

## 8.2.1 Biomass thermal behaviour

The thermal behaviour of biomass was studied through various systems. This entails using an entailed flow reactor and a thermogravimetric analyser (TGA). The latter is used as a standard apparatus in measuring the kinetic parameters of the gasification process kinetic parameters. It is done via heating a feedstock sample, typically around 5 – 15 mg, at a specific heating rate and record the corresponding weight, temperature, and time.

## 8.2.2 Pyrolysis energy

The kinetics of the pyrolysis reaction was studied in non-isothermal conditions using the TGA for the date stone feedstock and 10% wt mineral catalyst. The catalyst consisted of dolomite, limestone, and olivine. The tests were done using the Coats Redfern method and has shown that dolomite is the most effective catalyst in this study. It had the lower activation energy Ea at 44.89 KJ/mole, followed by limestone at 76.19 KJ/mole and lastly olivine at 95.13 KJ/mole.

### 8.2.3 Catalyst sizes impact on kinetic energy

The impact of changing the used ratio of dolomite as catalyst was also studied using the TGA under non-isothermal conditions. To ensure the most accurate results, these experiments were also conducted under the same conditions used for the previous sections as following:

- Heating rate: 20 $^{o}$C/min
- Nitrogen gas flow rate: 50 ml/min
- Date stone particle size: 710 μm

The experiment was repeated at various catalyst (dolomite) percentage weight at 5% we, 10% wt and 15% wt. The results showed that the 10% wt dolomite is the optimum value, as it achieved the lowest activation energy (Ea) at 44.89 KJ/mole, which is 15% higher than the 5% wt dolomite sample.

Additionally, the impact on efficiency at different particle sizes was also investigated. It was found that the larger particles, the higher efficiency were achieved. This is as the higher particle sizes increases the available surface area and therefore needs higher apparent activation energy to complete the pyrolysis process. This is a result of the biomass sample facing irregular heating, as bigger sizes delay the heating of inner parts of the sample.

## 8.3 Air-biomass gasification experimental tests

Air-biomass gasification in a bubbling fluidised bed gasifier experimental tests were conducted for this study. In particular, the effects of the hydrodynamics of fluidization as well as the surrounding operating conditions on the gasification process performance. The conclusion of this study is summarized below.

### 8.3.1 Effect of the biomass particle size

The size of the inlet biomass particle has a significant impact on the produced gas composition and the overall performance efficiency for the gasification of the date stone biomass.

It was found that the smaller biomass particle sizes have yielded more desirable results, specifically particle size of 300 – 425 μm due to its higher surface area.

There are different reasons that can confirm these findings, mainly:

1. Smaller particles lead to faster heating rate which affects the reaction kinetics, and therefore has a significant influence on the pyrolysis process, especially for smaller particle sizes, due to their active site on a high reaction surface area.
2. For larger particle sizes, the diffusion step becomes more influenced by the particle sizes due to the changes in the heating rate, due to the higher heat transfer resistance in larger particles, and therefore the core temperature inside the particles is lower.
3. Biomass particles promotes the segregation phenomena within the system when compared to larger particle sizes, due to the latter having higher weight at particle level.

### 8.3.2 Effect of the bed temperature

Gasification tests were performed to monitor the impact of the bed temperature of gasification performance at different bed temperatures. This was conducted at temperatures from 450 $^{o}$C to 650 $^{o}$C at 50 $^{o}$C incremental increases at a constant equivalence ratio (ER) value of 0.2. Meanwhile, the bed temperature of the gasifier alongside the produced gas composition of carbon monoxide, carbon dioxide, methane and hydrogen were logged and analysed.

It was found that the concentration of both the hydrogen and carbon monoxide gasses increased when the temperature increased from 450 $^{o}$C to 650 $^{o}$C, while carbon dioxide decreased.

Meanwhile, HHV value increased from 4.76 MJ/Nm$^3$ to 4.92 MJ/Nm$^3$ when the bed temperatures increased from 450 $^{o}$C to 550 $^{o}$C. Similarly, the efficiency of the cold gas was found to increase at higher temperature.

### 8.3.3 Effect of equivalence ratio ER

The results from the tests showed that ER has a significant impact on the performance efficiency of biomass gasification. The tests were conducted for ER range of 0.15 to 0.35. The highest produced gas composition and HHV was yielded at when ER was at 0.15. However, the highest carbon conversion value was seen when ER was at 0.35.

Generally, it was shown that the overall produced gas yield significantly increased with the increase of the ER value, the increase was seen to each individual gas in the yielded product. Additionally, the fluidization hydrodynamic showed a clear relationship with the value of ER.

### 8.3.4 Effect of different ratios of dolomite:

As mentioned above, the different possible ratios of catalyst by weight percentage were tested to determine the optimum ratio. It was found to be 10% wt dolomite yielded the optimum results in this study in terms of the produced gas and reducing the proportion of tar.

Using dolomite as a catalyst in the gasification process has various advantages. As it has lower commercial price, high availability and it improved the produced gas by reducing the tar content. It can be used as either primary or secondary catalyst. Using dolomite as a catalyst results in increasing the available surface area for the reaction which results in increase the calcination within the reaction due to the increase in oxide content.

## 8.4 The economic feasibility of using date stone as a source of energy in KSA.

The biomass power plant using date stone is a feasible project, which yields positive net present value (NPV), high return on investment (ROI), and short payback period (PBP). The positive NPV of £82,887,627.67 is indicative of profitability as the annual revenue exceeds the expected operating costs. This is expected to result from the compounding of profit with respect to the increase of annual NPV over 20 years of power plant operation. The increasing annualized ROI from 6.15% to 72.92% indicates that the rate of investment return grows considerably over 20 years of operation. This is indicative of high profit returns, whose magnitude progresses with increasing revenue. A short PBP of 6 years and about 10 months indicates that the capital investment is reclaimed at a considerable rate, which is suggestive of high accumulated profit. This translates to greater capacity in paying the cost of the project back, and thus, rapid recovery from the investment whereby the benefits are expected to grow exponentially thereon. Ultimately, the economic potential of the project is feasible, as indicated by the highly favourable profitability measures - NPV, ROI, and PBP.

However, aside from the economic indicators as presented, the sustainability of the biomass power plant also includes social, technical, and environmental considerations. The social indicators account for the energy demand security, and the promotion of community development through employment; while the technical indicators iterate the urgency for optimal efficiency in clean energy production, whereby performance, reliability, and operability must be met. The environmental indicators, on the other hand, include the concerns surrounding resource depletion particularly of water, waste production resulting to land and water pollution, renewability implications aimed at diminishing fossil fuel use, and emissions contributing to atmospheric $CO_2$, $SO_2$, $NO_x$ and particulate concentrations. And among the most pressing environmental issues closely tied to the energy production sector is the release of enormous amounts of carbon dioxide, among other emissions. In this regard, using biomass as energy source instead of fossil fuels proves to be feasible in terms of environmental sustainability, whereby 0.23 kg $CO_2$/kWh is expected in this study. This is significantly lower than the existing emission factors for natural gas and coal-fired power plants, which further supports the advantages of using biomass in energy production - particularly in the use of date stone as a source of clean electrical energy.

Conclusively, the biomass power plant using date stone in Saudi Arabia is a highly feasible project, whereby the economic, social, technical, and environmental indicators for sustainability are duly met. Among these indicators, the high profitability and low emissions of the power plant operation are the most promising measures. Thereby, iterating the expedient potential of the project.

## 8.5 Future work

- Study the impact of adding metallic catalysts on the activation energy of pyrolysis as opposed to using dolomite for the biomass source.

- The effects of the bed temperature on the produced gas should be studied further, particularly to enhance the combustible gasses production.
- As the overall rate constant for the biomass thermal degradation was studied as a one-stage reaction model, the individual species rate constant (e.g. tar) should be evaluated as well. Prior knowledge of the overall and tar rate constant can help determining the gas rate constant. This can be beneficial to simulate the study of gasification further, specially if optical measurements of tar formation during the pyrolysis process were taken.
- Assess the impact of increased the feeding time of the biomass further, by 30 minutes minimum, to understand the maximum equilibrium bed temperature while avoiding external heating.
- Use Aspen Plus to simulate the gasification process of the biomass using the studied activation energy values as well as the rate constant to understand the process further and be able to compare the forecasted simulation with the estimated results.

# References


[1] I. Energy Agency, “CO2 Emissions From Fuel Combustion Highlights 2014.”

[2] A. Schmittner, A. Oschlies, H. D. Matthews, and E. D. Galbraith, “Future changes in climate, ocean circulation, ecosystems, and biogeochemical cycling simulated for a business-as-usual CO $_2$ emission scenario until year 4000 AD,” *Global Biogeochem. Cycles*, vol. 22, no. 1, p. n/a-n/a, Mar. 2008.

[3] R. W. Bentley, “Global oil and gas depletion: An overview,” *Energy Policy*, vol. 30, no. 3, pp. 189–205, Feb. 2002.

[4] T. B. Johansson, H. Kelly, A. K. N. Reddy, and R. H. Williams, “Renewable energy: Sources for fuels and electricity.” Island Press, Washington, DC (United States), 31-Dec-1993.

[5] T. B. Johansson, H. Kelly, A. K. N. Reddy, and R. H. Williams, “Renewable Fuels and Electricity for a Growing World Economy: Defining and Achieving the Potential,” *Energy Stud. Rev.*, vol. 4, no. 3, 1993.

[6] S. Kane and J. F. Shogren, “Linking Adaptation and Mitigation in Climate Change Policy,” in *Societal Adaptation to Climate Variability and Change*, Springer Netherlands, 2000, pp. 75–102.

[7] R. E. H. Sims, H. H. Rogner, and K. Gregory, “Carbon emission and mitigation cost comparisons between fossil fuel, nuclear and renewable energy resources for electricity generation,” *Energy Policy*, vol. 31, no. 13, pp. 1315–1326, Oct. 2003.

[8] I. Partnership and O. Wyman, “World Energy Trilemma | 2016 DEFINING MEASURES TO ACCELERATE THE ENERGY TRANSITION.”

[9] “World Population Prospects The 2015 Revision.”

[10] R. A. Pielke, “Misdefining ‘climate change’: Consequences for science and action,” *Environ. Sci. Policy*, vol. 8, no. 6, pp. 548–561, 2005.

[11] “Climate change impacts | National Oceanic and Atmospheric Administration.” [Online]. Available: https://www.noaa.gov/education/resource-collections/climate/climate-change-impacts. [Accessed: 11-Nov-2021].

[12] P. Friedlingstein *et al.*, “Global Carbon Budget 2020,” *Earth Syst. Sci. Data*, vol. 12, no. 4, pp. 3269–3340, Dec. 2020.

[13] T. A. Boden, R. J. Andres, and G. Marland, “Global, Regional, and National Fossil-Fuel CO2 Emissions (1751 - 2014) (V. 2017),” Jan. 2017.

[14] M. B. Nikoo and N. Mahinpey, “Simulation of biomass gasification in fluidized bed reactor using ASPEN PLUS,” *Biomass and Bioenergy*, vol. 32, no. 12, pp. 1245–1254, Dec. 2008.

[15] G. Zanchi, N. Pena, and N. Bird, “Is woody bioenergy carbon neutral? A comparative assessment of emissions from consumption of woody bioenergy and fossil fuel,” *GCB*

*Bioenergy*, vol. 4, no. 6, pp. 761–772, Nov. 2012.

[16] A. Demirbas, “Combustion of biomass,” *Energy Sources, Part A Recover. Util. Environ. Eff.*, vol. 29, no. 6, pp. 549–561, Jan. 2007.

[17] A. Demirbaş, “Biomass resource facilities and biomass conversion processing for fuels and chemicals,” *Energy Convers. Manag.*, vol. 42, no. 11, pp. 1357–1378, Jul. 2001.

[18] J. S. R H O D E S , ‡ A N, “Policy Analysis Assessment of Potential Carbon Dioxide Reductions Due to Biomass-Coal Cofiring in the United States,” 2003.

[19] “Is Biomass Really Renewable?” [Online]. Available: https://blogs.ei.columbia.edu/2011/08/18/is-biomass-really-renewable/. [Accessed: 08-Mar-2021].

[20] “Is Biomass Energy Carbon Neutral? - Waste to Energy Systems.” [Online]. Available: https://www.wastetoenergysystems.com/is-biomass-energy-carbon-neutral/. [Accessed: 08-Mar-2021].

[21] “Emission impacts resulting from vehicle idling.” [Online]. Available: https://www.nrcan.gc.ca/energy/efficiency/communities-infrastructure/transportation/cars-light-trucks/idling/4415. [Accessed: 11-Nov-2021].

[22] “Biomass FAQs | ReEnergy Holdings.” [Online]. Available: https://www.reenergyholdings.com/renewable-energy/biomass-faqs/. [Accessed: 11-Nov-2021].

[23] S. Savci, “An Agricultural Pollutant: Chemical Fertilizer,” *Int. J. Environ. Sci. Dev.*, vol. 3, no. 1, pp. 73–80, 2012.

[24] M. V. Gil, D. Casal, C. Pevida, J. J. Pis, and F. Rubiera, “Thermal behaviour and kinetics of coal/biomass blends during co-combustion,” *Bioresour. Technol.*, vol. 101, no. 14, pp. 5601–5608, Jul. 2010.

[25] M. Catuti, M. Elkerbout, M. Alessi, and C. Egenhofer, “Biomass and Climate Neutrality,” *CEPS Policy Insights*, 2020.

[26] A. Abuadala and I. Dincer, “A review on biomass-based hydrogen production and potential applications,” *Int. J. Energy Res.*, vol. 36, no. 4, pp. 415–455, Mar. 2012.

[27] O. K. M. Ouda, H. M. Cekirge, and S. A. R. Raza, “An assessment of the potential contribution from waste-to-energy facilities to electricity demand in Saudi Arabia,” *Energy Convers. Manag.*, vol. 75, pp. 402–406, Nov. 2013.

[28] A. S. Nizami *et al.*, “The potential of Saudi Arabian natural zeolites in energy recovery technologies,” *Energy*, vol. 108, pp. 162–171, Aug. 2016.

[29] F. Al Harbi, *Saudi Arabia’s Electricity: Energy Supply and Demand Future Challenges*. .

[30] O. K. M. Ouda, S. A. Raza, A. S. Nizami, M. Rehan, R. Al-Waked, and N. E. Korres, “Waste to energy potential: A case study of Saudi Arabia,” *Renewable and Sustainable Energy Reviews*, vol. 61. Elsevier Ltd, pp. 328–340, 01-Aug-2016.

[31] “Saudi Arabia used less crude oil for power generation in 2018 - Today in Energy - U.S. Energy Information Administration (EIA).” [Online]. Available: https://www.eia.gov/todayinenergy/detail.php?id=39693. [Accessed: 11-Nov-2021].

[32] “Renewable Energy 2022 | Saudi Arabia | ICLG.” [Online]. Available: https://iclg.com/practice-areas/renewable-energy-laws-and-regulations/saudi-arabia. [Accessed: 11-Nov-2021].

[33] “National Renewable Energy Program eProcurement Portal.” [Online]. Available: https://www.powersaudiarabia.com.sa/web/index.html. [Accessed: 03-Feb-2021].

[34] M. Sanduka and H. M. Talebb, “The Date Palm and its Role.”

[35] N. C. F. P. & Dates, “Report of National Center for Palms & Dates 2018,” p. 84, 2018.

[36] H. G. Ali, “Development of date palm cultivation and its role in sustainability of agriculture in oman,” in *Acta Horticulturae*, 2010, vol. 882, pp. 29–35.

[37] M. Chandrasekaran and A. H. Bahkali, “Valorization of date palm (Phoenix dactylifera) fruit processing by-products and wastes using bioprocess technology - Review,” *Saudi Journal of Biological Sciences*, vol. 20, no. 2. Elsevier, pp. 105–120, 01-Apr-2013.

[38] “Geomorphological features in the Kingdom.” [Online]. Available: https://web.archive.org/web/20180215010610/http://www.sgs.org.sa:80/Arabic/earthsurface/Pages/geologicaspectinksa.aspx. [Accessed: 25-May-2021].

[39] “The Crown Prince announces the Saudi Green Initiative and the Green Middle East Initiative, the Saudi Press Agency.” [Online]. Available: https://web.archive.org/web/20210425185527/https://www.spa.gov.sa/viewfullstory.php?lang=ar&newsid=2208368. [Accessed: 25-May-2021].

[40] A. Sam, “Toxic Waste From Municipality,” *Energy from Toxic Org. Waste Heat Power Gener.*, pp. 7–16, Jan. 2019.

[41] A. Molino, S. Chianese, and D. Musmarra, “Biomass gasification technology: The state of the art overview,” *J. Energy Chem.*, vol. 25, no. 1, pp. 10–25, Jan. 2016.

[42] P. Nanou, *Biomass gasification for the production of methane*. 2013.

[43] A. Kumar, D. Jones, and M. Hanna, “Thermochemical Biomass Gasification: A Review of the Current Status of the Technology,” *Energies*, vol. 2, no. 3, pp. 556–581, Jul. 2009.

[44] A. Molino, V. Larocca, S. Chianese, and D. Musmarra, “Biofuels Production by Biomass Gasification: A Review,” *Energies*, vol. 11, no. 4, p. 811, Mar. 2018.

[45] M. A. F. Hamad, A. M. Radwan, and A. Amin, “Review of Biomass Thermal Gasification,” in *Biomass Volume Estimation and Valorization for Energy*, InTech, 2017.

[46] B. Prabis, *Biomass Gasification and Pyrolysis - A practical guide*. 2010.

[47] D. J. Roddy and C. Manson-Whitton, “Biomass Gasification and Pyrolysis,” *Compr.*

*Renew. Energy*, pp. 133–153, Jan. 2012.

[48] M. Tripathi, J. N. Sahu, and P. Ganesan, "Effect of process parameters on production of biochar from biomass waste through pyrolysis: A review," *Renew. Sustain. Energy Rev.*, vol. 55, pp. 467–481, Mar. 2016.

[49] S. C. Moldoveanu and S. C. Moldoveanu, "General Information About Pyrolysis," *Pyrolysis Org. Mol.*, pp. 1–33, Jan. 2019.

[50] R. E. Guedes, A. S. Luna, and A. R. Torres, "Operating parameters for bio-oil production in biomass pyrolysis: A review," *J. Anal. Appl. Pyrolysis*, vol. 129, pp. 134–149, Jan. 2018.

[51] D. Baruah and D. C. Baruah, "Modeling of biomass gasification: A review," *Renew. Sustain. Energy Rev.*, vol. 39, pp. 806–815, 2014.

[52] Y. Chhiti and M. Kemiha, "Thermal Conversion of Biomass, Pyrolysis and Gasification: A Review," pp. 75–85, 2013.

[53] Y. S. Pradana and A. Budiman, "Bio-syngas derived from Indonesian oil palm empty fruit bunch (EFB) using middle-scale gasification," *J. Eng. Sci. Technol.*, vol. 10, no. Spec.issue8, pp. 1–8, 2015.

[54] U. Arena, "Process and technological aspects of municipal solid waste gasification. A review," 2012.

[55] J. G. Speight, "Upgrading by Gasification," *Heavy Oil Recover. Upgrad.*, pp. 559–614, Jan. 2019.

[56] W. H. Chen and C. Y. Chen, "Water gas shift reaction for hydrogen production and carbon dioxide capture: A review," *Appl. Energy*, vol. 258, p. 114078, Jan. 2020.

[57] "Methanation process." [Online]. Available: http://www.helmeth.eu/index.php/technologies/methanation-process. [Accessed: 12-Nov-2021].

[58] D. J. Roddy and C. Manson-Whitton, *Biomass gasification and pyrolysis*, vol. 5. 2012.

[59] H. Boerrigter and R. Rauch, "Review of applications of gases from biomass gasification Justification," 2006.

[60] E. Toklu, "Biomass energy potential and utilization in Turkey," *Renew. Energy*, vol. 107, pp. 235–244, Jul. 2017.

[61] R. M. Esfahani, W. A. Wan Ab Karim Ghani, M. A. Mohd Salleh, and S. Ali, "Hydrogen-rich gas production from palm kernel shell by applying air gasification in fluidized bed reactor," *Energy and Fuels*, vol. 26, no. 2, pp. 1185–1191, 2012.

[62] L. Devi, K. J. Ptasinski, and F. J. J. G. Janssen, "A review of the primary measures for tar elimination in biomass gasification processes," *Biomass and Bioenergy*, vol. 24, no. 2, pp. 125–140, 2003.

[63] Z. A. B. Z. Alauddin, P. Lahijani, M. Mohammadi, and A. R. Mohamed, "Gasification of

lignocellulosic biomass in fluidized beds for renewable energy development: A review," *Renew. Sustain. Energy Rev.*, vol. 14, no. 9, pp. 2852–2862, Dec. 2010.

[64] J. W. Kook *et al.*, "Gasification and tar removal characteristics of rice husk in a bubbling fluidized bed reactor," *Fuel*, vol. 181, pp. 942–950, 2016.

[65] J. P. Makwana, J. Pandey, and G. Mishra, "Improving the properties of producer gas using high temperature gasification of rice husk in a pilot scale fluidized bed gasifier (FBG)," *Renew. Energy*, vol. 130, pp. 943–951, 2019.

[66] M. Cortazar *et al.*, "Role of temperature on gasification performance and tar composition in a fountain enhanced conical spouted bed reactor," *Energy Convers. Manag.*, vol. 171, no. April, pp. 1589–1597, 2018.

[67] A. Z. Yahaya, M. R. Somalu, A. Muchtar, S. A. Sulaiman, and W. R. Wan Daud, "Effect of particle size and temperature on gasification performance of coconut and palm kernel shells in downdraft fixed-bed reactor," *Energy*, vol. 175, pp. 931–940, 2019.

[68] E. S. Aydin, O. Yucel, and H. Sadikoglu, "Experimental study on hydrogen-rich syngas production via gasification of pine cone particles and wood pellets in a fixed bed downdraft gasifier," *Int. J. Hydrogen Energy*, vol. 44, no. 32, pp. 17389–17396, 2019.

[69] S. M. Beheshti, H. Ghassemi, and R. Shahsavan-Markadeh, "Process simulation of biomass gasification in a bubbling fluidized bed reactor," *Energy Convers. Manag.*, vol. 94, pp. 345–352, Apr. 2015.

[70] "Review on effects of gasifying agents, temperature and equivalence ratio in biomass gasification process."

[71] D. Baruah and D. C. Baruah, "Modeling of biomass gasification: A review," *Renew. Sustain. Energy Rev.*, vol. 39, pp. 806–815, 2014.

[72] H. Ghassemi and R. Shahsavan-Markadeh, "Effects of various operational parameters on biomass gasification process; A modified equilibrium model," *Energy Convers. Manag.*, vol. 79, pp. 18–24, 2014.

[73] M. A. Hamad, A. M. Radwan, D. A. Heggo, and T. Moustafa, "Hydrogen rich gas production from catalytic gasification of biomass," *Renew. Energy*, vol. 85, pp. 1290–1300, Jan. 2016.

[74] P. N. Sheth and B. V. Babu, "Production of hydrogen energy through biomass (waste wood) gasification," *Int. J. Hydrogen Energy*, vol. 35, no. 19, pp. 10803–10810, Oct. 2010.

[75] M. R. Mahishi and D. Y. Goswami, "Thermodynamic optimization of biomass gasifier for hydrogen production," *Int. J. Hydrogen Energy*, vol. 32, no. 16, pp. 3831–3840, Nov. 2007.

[76] J. G. Speight and J. G. Speight, "Gasifier Types," *Gasif. Unconv. Feed.*, pp. 54–90, Jan. 2014.

[77] A. M. Radwan, "Ver important amount of steam Pelagia Research Library An

overview on gasification of biomass for production of hydrogen rich gas," vol. 3, no. 2, pp. 323–335, 2012.

[78] E. Shayan, V. Zare, and I. Mirzaee, "Hydrogen production from biomass gasification; a theoretical comparison of using different gasification agents," *Energy Convers. Manag.*, vol. 159, no. December 2017, pp. 30–41, 2018.

[79] A. Mustafa, R. K. Calay, and M. Y. Mustafa, "A Techno-economic Study of a Biomass Gasification Plant for the Production of Transport Biofuel for Small Communities," *Energy Procedia*, vol. 112, no. October 2016, pp. 529–536, 2017.

[80] P. Parthasarathy and K. S. Narayanan, "Hydrogen production from steam gasification of biomass: Influence of process parameters on hydrogen yield – A review," *Renew. Energy*, vol. 66, pp. 570–579, Jun. 2014.

[81] F. Pinto, R. André, M. Miranda, D. Neves, F. Varela, and J. Santos, "Effect of gasification agent on co-gasification of rice production wastes mixtures," *Fuel*, vol. 180, pp. 407–416, Sep. 2016.

[82] P. Parthasarathy and K. S. Narayanan, "Hydrogen production from steam gasification of biomass: Influence of process parameters on hydrogen yield – A review," *Renew. Energy*, vol. 66, pp. 570–579, Jun. 2014.

[83] V. Kirsanovs, D. Blumberga, I. Veidenbergs, C. Rochas, E. Vigants, and G. Vigants, "Experimental investigation of downdraft gasifier at various conditions," *Energy Procedia*, vol. 128, pp. 332–338, Sep. 2017.

[84] V. S. Sikarwar *et al.*, "An overview of advances in biomass gasification," *Energy Environ. Sci.*, vol. 9, no. 10, pp. 2939–2977, Oct. 2016.

[85] A. A. P. Susastriawan, H. Saptoadi, and Purnomo, "Small-scale downdraft gasifiers for biomass gasification: A review," *Renew. Sustain. Energy Rev.*, vol. 76, pp. 989–1003, Sep. 2017.

[86] R. Luque, C. S. Ki Lin, K. Wilson, and J. Clark, *Handbook of Biofuels Production. Process and Technologies.* 2016.

[87] H. A. Choudhury, S. Chakma, and V. S. Moholkar, "Biomass Gasification Integrated Fischer-Tropsch Synthesis: Perspectives, Opportunities and Challenges," *Recent Adv. Thermo-Chemical Convers. Biomass*, pp. 383–435, Jan. 2015.

[88] P. J. van den Enden and E. S. Lora, "Design approach for a biomass fed fluidized bed gasifier using the simulation software CSFB.," *Biomass and Bioenergy*, vol. 26, no. 3, pp. 281–287, 2004.

[89] J. Karl and T. Pröll, "Steam gasification of biomass in dual fluidized bed gasifiers: A review," *Renew. Sustain. Energy Rev.*, vol. 98, pp. 64–78, Dec. 2018.

[90] Y. Xu, T. Li, J. Musser, X. Liu, G. Xu, and W. A. Rogers, "CFD-DEM modeling the effect of column size and bed height on minimum fluidization velocity in micro fluidized beds with Geldart B particles," *Powder Technol.*, vol. 318, pp. 321–328, Aug. 2017.

[91] Z. Fu, J. Zhu, S. Barghi, Y. Zhao, Z. Luo, and C. Duan, “Minimum fluidization velocity growth due to bed inventory increase in an Air Dense Medium Fluidized Bed,” *Chem. Eng. J.*, vol. 359, pp. 1372–1378, Mar. 2019.

[92] P. Parthasarathy and K. S. Narayanan, “Hydrogen production from steam gasification of biomass: Influence of process parameters on hydrogen yield e A review,” 2014.

[93] R. Warnecke, “Gasi ® cation of biomass : comparison of ® xed bed and ¯ uidized bed gasi ® er,” vol. 18, 2000.

[94] J. J. Hernández, G. Aranda-Almansa, and A. Bula, “Gasification of biomass wastes in an entrained flow gasifier: Effect of the particle size and the residence time,” 2010.

[95] S. H. Lee, R. T. L Ng, D. K. S Ng, D. C. Y Foo, I. M. L Chew, and S. Liu, “Black liquor gasification integrated in pulp and paper mills: A critical review,” John Wiley & Sons, 2013.

[96] M. Inayat, S. A. Sulaiman, and A. Kumar, “Effect of fuel particle size and blending ratio on syngas production and performance of co-gasification Design and development of solar desalination plant View project Hydrodynamics of Swirling Fluidized Bed with Sloping Distributor View project,” 2016.

[97] D. Jia, X. Bi, C. J. Lim, S. Sokhansanj, and A. Tsutsumi, “Heat transfer in a tapered fluidized bed of biomass particles with pulsed gas flow,” *Particuology*, vol. 42, pp. 2–14, Feb. 2019.

[98] N. Jand and P. U. Foscolo, “Decomposition of Wood Particles in Fluidized Beds,” 2005.

[99] S. Fremaux, S.-M. Beheshti, H. Ghassemi, and R. Shahsavan-Markadeh, “An experimental study on hydrogen-rich gas production via steam gasification of biomass in a research-scale fluidized bed,” *Energy Convers. Manag.*, vol. 91, pp. 427–432, Feb. 2015.

[100] M. A. M. Salleh, H. K. Nsamba, H. M. Yusuf, A. Idris, W. A. Wan, and A. K. Ghani, “Effect of Equivalence Ratio and Particle Size on EFB Char Gasification,” vol. 37, pp. 1647–1662, 2015.

[101] M. Siedlecki, W. De Jong, and A. H. M. Verkooijen, “Fluidized Bed Gasification as a Mature And Reliable Technology for the Production of Bio-Syngas and Applied in the Production of Liquid Transportation Fuels—A Review,” *Energies*, vol. 4, no. 3, pp. 389–434, Mar. 2011.

[102] T. M. Ismail and M. A. El-Salam, “Numerical and experimental studies on updraft gasifier HTAG,” *Renew. Energy*, vol. 78, pp. 484–497, Jun. 2015.

[103] Y. Richardson, M. Drobek, A. Julbe, J. Blin, and F. Pinta, “Biomass Gasification to Produce Syngas,” *Recent Adv. Thermo-Chemical Convers. Biomass*, pp. 213–250, Jan. 2015.

[104] R. Warnecke, “Gasification of biomass: comparison of fixed bed and fluidized bed gasifier,” *Biomass and Bioenergy*, vol. 18, no. 6, pp. 489–497, Jun. 2000.

[105] S. Chopra and A. K. Jain, “A Review of Fixed Bed Gasification Systems for Biomass,” 2007.

[106] C. Mandl, I. Obernberger, and F. Biedermann, “Modelling of an updraft fixed-bed gasifier operated with softwood pellets,” *Fuel*, vol. 89, no. 12, pp. 3795–3806, Dec. 2010.

[107] J. Wang, N. Liu, X. Wang, Y. Gao, G. Wang, and L. Li, “Energy Sources, Part A: Recovery, Utilization, and Environmental Effects Application of updraft biomass gasifier for non-ferrous metal smelting,” 2018.

[108] Mohandas Mangre, Savita Vyas, and Mukesh Pandey, “Downdraft fixed bed biomass gasifier: A review,” *Curr. Sci. Perspect.*, vol. 3, no. 3, pp. 143–147, 2017.

[109] A. A. M. Sayigh, *Comprehensive renewable energy*. .

[110] S. Pang, “Fuel flexible gas production: Biomass, coal and bio-solid wastes,” *Fuel Flex. Energy Gener.*, pp. 241–269, Jan. 2016.

[111] K. Chandolias, T. Richards, and M. J. Taherzadeh, “Combined Gasification-Fermentation Process in Waste Biorefinery,” *Waste Biorefinery*, pp. 157–200, Jan. 2018.

[112] H. A. Choudhury, S. Chakma, and V. S. Moholkar, “Biomass Gasification Integrated Fischer-Tropsch Synthesis: Perspectives, Opportunities and Challenges,” *Recent Adv. Thermo-Chemical Convers. Biomass*, pp. 383–435, Jan. 2015.

[113] S. Mahapatra, “Experiments and Analysis on Wood Gasification in an Open Top Downdraft Gasifier,” no. March, 2016.

[114] S. Bakheet, S. Kamel, H. A. El-Sattar, and F. Jurado, “Different Biomass Gasification Reactors for Energy Applications,” in *2018 20th International Middle East Power Systems Conference, MEPCON 2018 - Proceedings*, 2019, pp. 660–665.

[115] C. G. Philippsen, A. C. F. Vilela, and L. D. Zen, “Fluidized bed modeling applied to the analysis of processes: review and state of the art,” *J. Mater. Res. Technol.*, vol. 4, no. 2, pp. 208–216, Apr. 2015.

[116] I. Janajreh and I. Adeyemi, *Effect of Process Parameters on Gasification : Review*, no. 9. 2014.

[117] V. K. Guda, P. H. Steele, V. K. Penmetsa, and Q. Li, “Fast Pyrolysis of Biomass: Recent Advances in Fast Pyrolysis Technology,” *Recent Adv. Thermo-Chemical Convers. Biomass*, pp. 177–211, Jan. 2015.

[118] S. B. Sethupathy and E. Natarajan, “Hydrodynamic study on gasification of biomass in a fluidized bed gasifier,” *Int. J. Eng. Sci. Technol.*, vol. 4, no. 1, pp. 316–323, 2012.

[119] Y. Zhu and H. C. Frey, “Integrated gasification combined cycle (IGCC) power plant design and technology,” *Adv. Power Plant Mater. Des. Technol.*, pp. 54–88, Jan. 2010.

[120] I. L. Motta, N. T. Miranda, R. Maciel Filho, and M. R. Wolf Maciel, “Biomass

gasification in fluidized beds: A review of biomass moisture content and operating pressure effects," *Renew. Sustain. Energy Rev.*, vol. 94, pp. 998–1023, Oct. 2018.

[121] M. B. Nikoo and N. Mahinpey, "Simulation of biomass gasification in fluidized bed reactor using ASPEN PLUS," *Biomass and Bioenergy*, vol. 32, no. 12, pp. 1245–1254, Dec. 2008.

[122] A. Lappas and E. Heracleous, "Production of biofuels via Fischer–Tropsch synthesis: Biomass-to-liquids," *Handb. Biofuels Prod.*, pp. 549–593, Jan. 2016.

[123] V. Belgiorno, G. De Feo, C. Della Rocca, and R. M. A. Napoli, "Energy from gasification of solid wastes," *Waste Manag.*, vol. 23, no. 1, pp. 1–15, 2003.

[124] M. Öhman, L. Pommer, and A. Nordin, "Bed agglomeration characteristics and mechanisms during gasification and combustion of biomass fuels," *Energy and Fuels*, vol. 19, no. 4, pp. 1742–1748, 2005.

[125] G. López, M. Olazar, R. Aguado, and J. Bilbao, "Continuous pyrolysis of waste tyres in a conical spouted bed reactor," *Fuel*, vol. 89, no. 8, pp. 1946–1952, Aug. 2010.

[126] H. Altzibar, G. Lopez, M. Olazar, and J. Bilbao, "Study of the Minimum Spouting Velocity in a Draft Tube Conical Spouted Bed," *13th Int. Conf. Fluid. - New Paradig. Fluid. Eng.*, pp. 1–9, 2010.

[127] N. Epstein and J. R. Grace, "Spouting of Particulate Solids," in *Handbook of Powder Science & Technology*, Boston, MA: Springer US, 1997, pp. 532–567.

[128] P. Basu, "Combustion and gasification in fluidized beds*2006"*,.

[129] P. A. Salam and S. C. Bhattacharya, "A comparative study of charcoal gasification in two types of spouted bed reactors," *Energy*, vol. 31, no. 2–3, pp. 228–243, 2006.

[130] R. Xiao *et al.*, "Air blown partial gasification of coal in a pilot plant pressurized spout-fluid bed reactor," *Fuel*, vol. 86, no. 10–11, pp. 1631–1640, 2007.

[131] W. Zhong and M. Zhang, "Pressure fluctuation frequency characteristics in a spout-fluid bed by modern ARM power spectrum analysis," *Powder Technol.*, vol. 152, no. 1–3, pp. 52–61, 2005.

[132] C. Gupta and D. Sathiyamoorthy, "Fluid bed technology in materials processing ", *1998*.

[133] M. Olazar, M. J. S. José, A. T. Aguayo, J. M. Arandes, and J. Bilbao, "Design Factors of Conical Spouted Beds and Jet Spouted Beds," *Ind. Eng. Chem. Res.*, vol. 32, no. 6, pp. 1245–1250, 1993.

[134] I. Estiati, H. Altzibar, M. Tellabide, and M. Olazar, "A new method to measure fine particle circulation rates in draft tube conical spouted beds," *Powder Technol.*, vol. 316, pp. 87–91, Jul. 2017.

[135] S. Pang, "Fuel flexible gas production: Biomass, coal and bio-solid wastes," *Fuel Flex. Energy Gener.*, pp. 241–269, Jan. 2016.

[136] B. Sahoo, “The effect of parameters on the performance of a Fluidized bed reactor and Gasifier The effect of parameters on the performance of a Fluidized bed reactor and Gasifier,” no. 209, 2011.

[137] M. B. Nikoo and N. Mahinpey, “Simulation of biomass gasification in fluidized bed reactor using ASPEN PLUS,” *Biomass and Bioenergy*, vol. 32, no. 12, pp. 1245–1254, Dec. 2008.

[138] J. P. Ciferno and J. J. Marano, “Benchmarking biomass gasification technologies for fuels, chemicals and hydrogen production,” *US Dep. Energy. Natl. Energy*, no. June, p. 58, 2002.

[139] M. Siedlecki, W. de Jong, and A. H. M. Verkooijen, “Fluidized bed gasification as a mature and reliable technology for the production of bio-syngas and applied in the production of liquid transportation fuels-a review,” *Energies*, vol. 4, no. 3, pp. 389–434, 2011.

[140] J. Alberto and P. Peña, “Bubbling Fluidized Bed ( BFB ),” *IFSA 2011, Ind. Fluid. South Africa*, no. November, pp. 1–12, 2011.

[141] C. Loha, H. Chattopadhyay, and P. K. Chatterjee, “Three dimensional kinetic modeling of fluidized bed biomass gasification,” *Chem. Eng. Sci.*, vol. 109, pp. 53–64, 2014.

[142] X. T. Li, J. R. Grace, C. J. Lim, A. P. Watkinson, H. P. Chen, and J. R. Kim, “Biomass gasification in a circulating fluidized bed,” *Biomass and Bioenergy*, vol. 26, no. 2, pp. 171–193, 2004.

[143] X. T. Li, J. R. Grace, C. J. Lim, A. P. Watkinson, H. P. Chen, and J. R. Kim, “Biomass gasification in a circulating fluidized bed,” *Biomass and Bioenergy*, vol. 26, no. 2, pp. 171–193, Feb. 2004.

[144] W.-C. Yang, *HANDBOOK of FLUIDIZfiTION and FLUID-PARTICLE SYSTEMS*, vol. 839, no. 281. 2003.

[145] M. V. Gil, “Coal and biomass cofiring: fundamentals and future trends,” *New Trends Coal Convers.*, pp. 117–140, Jan. 2019.

[146] V. S. Sikarwar and M. Zhao, *Biomass Gasification*, no. December. Elsevier Inc., 2017.

[147] Z. A. B. Z. Alauddin, P. Lahijani, M. Mohammadi, and A. R. Mohamed, “Gasification of lignocellulosic biomass in fluidized beds for renewable energy development: A review,” *Renew. Sustain. Energy Rev.*, vol. 14, no. 9, pp. 2852–2862, Dec. 2010.

[148] J. Brown, “Biomass Gasification : Fast Internal Circulating Fluidised Bed Gasifier Characterisation and Comparison,” *Fuel*, vol. 89, no. 2, pp. 384–391, 2006.

[149] Olivier Morin, “Technical and Environmental Comparison of Circulating Fluidized Bed (CFB) and Moving Grate Reactors,” p. 47, 2014.

[150] X. Wang, M. Economides, X. Wang, and M. Economides, “Gas-To-Liquids (GTL),” *Adv. Nat. Gas Eng.*, pp. 243–287, Jan. 2009.

[151] A. E. Karim Kakae, iMehdi D.Esrafili, “Introduction to Catalysis,” *Interface Sci. Technol.*, vol. 27, pp. 1–21, Jan. 2019.

[152] A. Dąbrowski, “Adsorption - its development and application for practical purposes,” *Stud. Surf. Sci. Catal.*, vol. 120, pp. 3–68, Jan. 1999.

[153] A. Hagemeyer and A. Volpe, “Materials: Catalysts,” *Ref. Modul. Mater. Sci. Mater. Eng.*, Jan. 2016.

[154] R. R, U. V, and L. D, “Green chemistry concept: Applications of catalysis in pharmacuetical industry,” *Glob. Drugs Ther.*, vol. 2, no. 4, pp. 1–7, 2017.

[155] M. Shahbaz, S. yusup, A. Inayat, D. O. Patrick, and M. Ammar, “The influence of catalysts in biomass steam gasification and catalytic potential of coal bottom ash in biomass steam gasification: A review,” *Renew. Sustain. Energy Rev.*, vol. 73, no. November 2015, pp. 468–476, 2017.

[156] Y. Richardson, J. Blin, and A. Julbe, “A short overview on purification and conditioning of syngas produced by biomass gasification: Catalytic strategies, process intensification and new concepts,” *Prog. Energy Combust. Sci.*, vol. 38, no. 6, pp. 765–781, 2012.

[157] J. Corella, J. Herguido, J. Gonzalez-Saiz, F. J. Alday, and J. L. Rodriguez-Trujillo, “Fluidized Bed Steam Gasification of Biomass with Dolomite and with a Commercial FCC Catalyst,” *Res. Thermochem. Biomass Convers.*, pp. 754–765, 1988.

[158] J. Leppälahti and E. Kurkela, “Behaviour of nitrogen compounds and tars in fluidized bed air gasification of peat,” *Fuel*, vol. 70, no. 4, pp. 491–497, Apr. 1991.

[159] I. Narvá Ez, A. Orío, M. P. Aznar, and J. Corella, “Biomass Gasification with Air in an Atmospheric Bubbling Fluidized Bed. Effect of Six Operational Variables on the Quality of the Produced Raw Gas,” 1996.

[160] A. Olivares, M. P. Aznar, M. A. Caballero, J. Gil, E. Francé, and J. Corella, “Biomass Gasification: Produced Gas Upgrading by In-Bed Use of Dolomite,” 1997.

[161] D. Dayton, “Review of the Literature on Catalytic Biomass Tar Destruction: Milestone Completion Report,” no. December, 2002.

[162] Y. Tian, X. Zhou, S. Lin, X. Ji, J. Bai, and M. Xu, “Syngas production from air-steam gasification of biomass with natural catalysts,” *Sci. Total Environ.*, vol. 645, pp. 518–523, Dec. 2018.

[163] J. Hagen, “Industrial catalysis: a practical approach*2015*”,.

[164] N. Kakuta, N. Morishima, M. Kotobuki, … T. I.-A. surface, and undefined 1997, “Oxygen storage capacity (OSC) of aged Pt/CeO2/Al2O3 catalysts: roles of Pt and CeO2 supported on Al2O3,” *Elsevier*.

[165] R. Liu, P. Crozier, C. Smith, … D. H.-A. C. A., and undefined 2005, “Metal sintering mechanisms and regeneration of palladium/alumina hydrogenation catalysts,” *Elsevier*.

[166] J. Sun, D. Luo, P. Xiao, L. Jigang, S. Y.-J. of P. Sources, and undefined 2008, "High yield hydrogen production from low CO selectivity ethanol steam reforming over modified Ni/Y2O3 catalysts at low temperature for fuel cell application," *Elsevier*.

[167] "BSI Standards Publication Solid biofuels — Determination of ash content," no. January, 2017.

[168] Bsi, "Solid biofuels — Determination of calorific value," *Management*, 2009.

[169] C. Parr Instrument, "Series 6000 Oxygen Bom Calorimeters Catalogue," 2017.

[170] P. Basu, *Biomass gasification and pyrolysis : practical design and theory*. Academic Press, 2010.

[171] W. Zhong, B. Jin, Y. Zhang, X. Wang, and R. Xiao, "Fluidization of biomass particles in a gas-solid fluidized bed," *Energy and Fuels*, vol. 22, no. 6, pp. 4170–4176, 2008.

[172] C. L. Lin, M. Y. Wey, and S. Da You, "The effect of particle size distribution on minimum fluidization velocity at high temperature," *Powder Technol.*, vol. 126, no. 3, pp. 297–301, 2002.

[173] F. Miccio, B. Piriou, G. Ruoppolo, and R. Chirone, "Biomass gasification in a catalytic fluidized reactor with beds of different materials," *Chem. Eng. J.*, vol. 154, no. 1–3, pp. 369–374, Nov. 2009.

[174] M. F. Velocity, "Minimum Fluidization Velocity at High Temperatures," *Ind. Eng. Chem. Process Des. Dev.*, vol. 20, no. 4, pp. 705–707, 1981.

[175] S. Rapagnà, N. Jand, A. Kiennemann, and P. U. Foscolo, "Steam-gasification of biomass in a fluidised-bed of olivine particles," *Biomass and Bioenergy*, vol. 19, no. 3, pp. 187–197, Sep. 2000.

[176] "Fluidization characteristics of a bubbling gasâ€"solid fluidized bed at high temperature in the presence of interparticle forces | Elsevier Enhanced Reader." [Online]. Available: https://reader.elsevier.com/reader/sd/pii/S1385894715016794?token=6B72BD9E31A3DB9C91F1C9D746518F160814D9F20E42E5DF00158455F6494BF531DC95513C8F1959448E6E0F3B7A4033&originRegion=eu-west-1&originCreation=20211118132602. [Accessed: 18-Nov-2021].

[177] D. Escudero and T. J. Heindel, "Bed height and material density effects on fluidized bed hydrodynamics," *Chem. Eng. Sci.*, vol. 66, no. 16, pp. 3648–3655, Aug. 2011.

[178] J. H. Choi *et al.*, "The effect of fine particles on elutriation of coarse particles in a gas fluidized bed," *Powder Technol.*, vol. 121, no. 2–3, pp. 190–194, Nov. 2001.

[179] "Fluidization Engineering - 2nd Edition." [Online]. Available: https://www.elsevier.com/books/fluidization-engineering/kunii/978-0-08-050664-7. [Accessed: 26-Sep-2020].

[180] H. H. Sait, A. Hussain, A. A. Salema, and F. N. Ani, "Pyrolysis and combustion kinetics of date palm biomass using thermogravimetric analysis," *Bioresour. Technol.*, vol. 118,

pp. 382–389, Aug. 2012.

[181] D. Gauthier, S. Zerguerras, and G. Flamant, “Influence of the particle size distribution of powders on the velocities of minimum and complete fluidization,” *Chem. Eng. J.*, vol. 74, no. 3, pp. 181–196, Jul. 1999.

[182] R. Emerson, “Instruction Manual Gas Analyzers X-STREAM X2 Series Instruction Manual,” 2012.

[183] X. T. Li, J. R. Grace, C. J. Lim, A. P. Watkinson, H. P. Chen, and J. R. Kim, “Biomass gasification in a circulating fluidized bed,” *Biomass and Bioenergy*, vol. 26, no. 2, pp. 171–193, Feb. 2004.

[184] Q. Yi *et al.*, “Thermogravimetric analysis of co-combustion of biomass and biochar,” *J. Therm. Anal. Calorim.*, vol. 112, no. 3, pp. 1475–1479, Jun. 2013.

[185] M. Heydari, M. Rahman, and R. Gupta, “Kinetic study and thermal decomposition behavior of lignite coal,” *Int. J. Chem. Eng.*, vol. 2015, 2015.

[186] J. M. Encinar, J. F. González, and J. González, “Fixed-bed pyrolysis of Cynara cardunculus L. Product yields and compositions,” *Fuel Process. Technol.*, vol. 68, no. 3, pp. 209–222, Dec. 2000.

[187] S. Daneshvar, F. Salak, and K. Otsuka, “Pyrolytic Behavior of Green Macro Algae and Evaluation of Its Activation Energy,” *Int. J. Chem. Eng. Appl.*, vol. 3, no. 4, pp. 256–263, 2012.

[188] W. H. Chen and P. C. Kuo, “A study on torrefaction of various biomass materials and its impact on lignocellulosic structure simulated by a thermogravimetry,” *Energy*, vol. 35, no. 6, pp. 2580–2586, Jun. 2010.

[189] H. Yang, R. Yan, H. Chen, D. H. Lee, and C. Zheng, “Characteristics of hemicellulose, cellulose and lignin pyrolysis,” *Fuel*, vol. 86, no. 12–13, pp. 1781–1788, Aug. 2007.

[190] E. Kastanaki, D. Vamvuka, P. Grammelis, and E. Kakaras, “Thermogravimetric studies of the behavior of lignite-biomass blends during devolatilization,” *Fuel Process. Technol.*, vol. 77–78, pp. 159–166, Jun. 2002.

[191] J. Jae *et al.*, “Depolymerization of lignocellulosic biomass to fuel precursors: Maximizing carbon efficiency by combining hydrolysis with pyrolysis,” in *Energy and Environmental Science*, 2010, vol. 3, no. 3, pp. 358–365.

[192] C. Gai, Y. Dong, Z. Lv, Z. Zhang, J. Liang, and Y. Liu, “Pyrolysis behavior and kinetic study of phenol as tar model compound in micro fluidized bed reactor,” *Int. J. Hydrogen Energy*, vol. 40, no. 25, pp. 7956–7964, Jul. 2015.

[193] M. R. B. Guerrero *et al.*, “Thermogravimetric study on the pyrolysis kinetics of apple pomace as waste biomass,” *Int. J. Hydrogen Energy*, vol. 39, no. 29, pp. 16619–16627, 2014.

[194] P. G. Laye, S. B. Warrington, T. M. Group, G. R. Heal, D. M. Price, and R. Wilson, *Principles of Thermal Analysis and Calorimetry*. 2002.

[195] J. Yu *et al.*, “Isothermal differential characteristics of gas-solid reaction in micro-fluidized bed reactor,” in *Fuel*, 2013, vol. 103, pp. 29–36.

[196] K. Oluoti, T. Richards, T. R. K. Doddapaneni, and D. Kanagasabapathi, “Evaluation of the pyrolysis and gasification kinetics of tropical wood biomass,” *BioResources*, vol. 9, no. 2, pp. 2179–2190, 2014.

[197] J. M. Encinar, J. F. González, and J. González, “Fixed-bed pyrolysis of Cynara cardunculus L. Product yields and compositions,” *Fuel Process. Technol.*, vol. 68, no. 3, pp. 209–222, 2000.

[198] G. Gözke and K. Açıkalın, “Pyrolysis characteristics and kinetics of sour cherry stalk and flesh via thermogravimetric analysis using isoconversional methods,” *J. Therm. Anal. Calorim.*, 2020.

[199] F. Pinto *et al.*, “Effects of experimental conditions and of addition of natural minerals on syngas production from lignin by oxy-gasification: Comparison of bench- and pilot scale gasification,” *Fuel*, vol. 140, pp. 62–72, Jan. 2015.

[200] M. Cortazar, G. Lopez, J. Alvarez, M. Amutio, J. Bilbao, and M. Olazar, “Behaviour of primary catalysts in the biomass steam gasification in a fountain confined spouted bed,” *Fuel*, vol. 253, pp. 1446–1456, Oct. 2019.

[201] M. A. A. Mohammed, A. Salmiaton, W. A. K. G. Wan Azlina, M. S. Mohamad Amran, and Y. H. Taufiq-Yap, “Preparation and Characterization of Malaysian Dolomites as a Tar Cracking Catalyst in Biomass Gasification Process,” *J. Energy*, vol. 2013, pp. 1–8, 2013.

[202] Geology.com, “Dolomite Mineral | Uses and Properties,” *www.geology.com*, 2018. [Online]. Available: https://geology.com/minerals/dolomite.shtml. [Accessed: 26-Nov-2020].

[203] D. Sutton, B. Kelleher, and J. R. H. Ross, “Review of literature on catalysts for biomass gasification,” *Fuel Process. Technol.*, vol. 73, no. 3, pp. 155–173, Nov. 2001.

[204] J. M. Encinar, J. F. González, and J. González, “Fixed-bed pyrolysis of Cynara cardunculus L. Product yields and compositions,” *Fuel Process. Technol.*, vol. 68, no. 3, pp. 209–222, Dec. 2000.

[205] H. Haykiri-Acma, “The role of particle size in the non-isothermal pyrolysis of hazelnut shell,” *J. Anal. Appl. Pyrolysis*, vol. 75, no. 2, pp. 211–216, Mar. 2006.

[206] Y. Niu, H. Tan, Y. Liu, X. Wang, and T. Xu, “The effect of particle size and heating rate on pyrolysis of waste capsicum stalks biomass,” *Energy Sources, Part A Recover. Util. Environ. Eff.*, vol. 35, no. 17, pp. 1663–1669, Sep. 2013.

[207] P. Lahijani and Z. A. Zainal, “Gasification of palm empty fruit bunch in a bubbling fluidized bed: A performance and agglomeration study,” *Bioresour. Technol.*, vol. 102, no. 2, pp. 2068–2076, Jan. 2011.

[208] T. Song, J. Wu, L. Shen, and J. Xiao, “Experimental investigation on hydrogen production from biomass gasification in interconnected fluidized beds,” *Biomass and*

*Bioenergy*, vol. 36, pp. 258–267, Jan. 2012.

[209] Y. Cao, Y. Wang, J. T. Riley, and W. P. Pan, "A novel biomass air gasification process for producing tar-free higher heating value fuel gas," *Fuel Process. Technol.*, vol. 87, no. 4, pp. 343–353, Apr. 2006.

[210] V. Skoulou, G. Koufodimos, Z. Samaras, and A. Zabaniotou, "Low temperature gasification of olive kernels in a 5-kW fluidized bed reactor for H2-rich producer gas," *Int. J. Hydrogen Energy*, vol. 33, no. 22, pp. 6515–6524, Nov. 2008.

[211] C. Lucas, D. Szewczyk, W. Blasiak, and S. Mochida, "High-temperature air and steam gasification of densified biofuels," *Biomass and Bioenergy*, vol. 27, no. 6, pp. 563–575, Dec. 2004.

[212] M. A. A. Mohammed, A. Salmiaton, W. A. K. G. Wan Azlina, M. S. Mohammad Amran, and A. Fakhru'L-Razi, "Air gasification of empty fruit bunch for hydrogen-rich gas production in a fluidized-bed reactor," *Energy Convers. Manag.*, vol. 52, no. 2, pp. 1555–1561, Feb. 2011.

[213] N. Abdoulmoumine, A. Kulkarni, and S. Adhikari, "Effects of Temperature and Equivalence Ratio on Pine Syngas Primary Gases and Contaminants in a Bench-Scale Fluidized Bed Gasifier," 2014.

[214] G. Xue *et al.*, "Gasification of torrefied Miscanthus×giganteus in an air-blown bubbling fluidized bed gasifier," *Bioresour. Technol.*, vol. 159, pp. 397–403, May 2014.

[215] A. F. Almeida *et al.*, "Effect of Temperature on the Gasification of Olive Bagasse Particles."

[216] A. A. Zabaniotou, G. Kalogiannis, E. Kappas, and A. J. Karabelas, "Olive residues (cuttings and kernels) rapid pyrolysis product yields and kinetics," *Biomass and Bioenergy*, vol. 18, no. 5, pp. 411–420, May 2000.

[217] N. Abdoulmoumine, A. Kulkarni, and S. Adhikari, "Effects of Temperature and Equivalence Ratio on Pine Syngas Primary Gases and Contaminants in a Bench-Scale Fluidized Bed Gasifier," 2014.

[218] J. Gil, J. Corella, M. P. Aznar, and M. A. Caballero, "Biomass gasification in atmospheric and bubbling fluidized bed: Effect of the type of gasifying agent on the product distribution," *Biomass and Bioenergy*, vol. 17, no. 5, pp. 389–403, Nov. 1999.

[219] C. Loha, H. Chattopadhyay, and P. K. Chatterjee, "Three dimensional kinetic modeling of fluidized bed biomass gasification," *Chem. Eng. Sci.*, vol. 109, pp. 53–64, Apr. 2014.

[220] D. Dayton, "Review of the literature on catalytic biomass tar destruction; NREL/TP-510-32815. Golden, CO; NREL; 2002," *Natl. Renew. Energy Lab.*, no. December, p. 28, 2002.

[221] D. Sutton, B. Kelleher, and J. R. H. Ross, "Review of literature on catalysts for biomass gasification," *Fuel Process. Technol.*, vol. 73, no. 3, pp. 155–173, 2001.

[222] J. Delgado, M. P. Aznar, and J. Corella, "Calcined dolomite, magnesite, and calcite for

cleaning hot gas from a fluidized bed biomass gasifier with steam: Life and usefulness," *Ind. Eng. Chem. Res.*, vol. 35, no. 10, pp. 3637–3643, 1996.

[223] Q. Z. Yu, C. Brage, T. Nordgreen, and K. Sjöström, "Effects of Chinese dolomites on tar cracking in gasification of birch," *Fuel*, vol. 88, no. 10, pp. 1922–1926, 2009.

[224] P. A. Simell, J. K. Leppälahti, and J. B. so. Bredenberg, "Catalytic purification of tarry fuel gas with carbonate rocks and ferrous materials," *Fuel*, vol. 71, no. 2, pp. 211–218, Feb. 1992.

[225] C. P. B. Quitete and M. M. V. M. Souza, "Application of Brazilian dolomites and mixed oxides as catalysts in tar removal system," *Appl. Catal. A Gen.*, vol. 536, pp. 1–8, Apr. 2017.

[226] M. Hervy *et al.*, "Evolution of dolomite composition and reactivity during biomass gasification," *Appl. Catal. A Gen.*, vol. 572, pp. 97–106, Feb. 2019.

[227] V. A. Rigo, C. O. Metin, Q. P. Nguyen, and C. R. Miranda, "Hydrocarbon adsorption on carbonate mineral surfaces: A first-principles study with van der Waals interactions," *J. Phys. Chem. C*, vol. 116, no. 46, pp. 24538–24548, 2012.

[228] C. Li and K. Suzuki, "Tar property, analysis, reforming mechanism and model for biomass gasification-An overview," *Renewable and Sustainable Energy Reviews*, vol. 13, no. 3. Pergamon, pp. 594–604, 01-Apr-2009.

[229] Z. Abu El-Rub, E. A. Bramer, and G. Brem, "Review of catalysts for tar elimination in biomass gasification processes," *Ind. Eng. Chem. Res.*, vol. 43, no. 22, pp. 6911–6919, 2004.

[230] A. Soomro, S. Chen, S. Ma, and W. Xiang, "Catalytic activities of nickel, dolomite, and olivine for tar removal and H2-enriched gas production in biomass gasification process," *Energy Environ.*, vol. 29, no. 6, pp. 839–867, 2018.

[231] C. Di Blasi, "Kinetic and Heat Transfer Control in the Slow and Flash Pyrolysis of Solids," 1996.

[232] P. M. Lv, Z. H. Xiong, J. Chang, C. Z. Wu, Y. Chen, and J. X. Zhu, "An experimental study on biomass air-steam gasification in a fluidized bed," *Bioresour. Technol.*, vol. 95, no. 1, pp. 95–101, Oct. 2004.

[233] S. Luo, B. Xiao, X. Guo, Z. Hu, S. Liu, and M. He, "Hydrogen-rich gas from catalytic steam gasification of biomass in a fixed bed reactor: Influence of particle size on gasification performance," *Int. J. Hydrogen Energy*, vol. 34, no. 3, pp. 1260–1264, Feb. 2009.

[234] V. R. Patel, D. S. Upadhyay, and R. N. Patel, "Gasification of lignite in a fixed bed reactor: Influence of particle size on performance of downdraft gasifier," *Energy*, vol. 78, pp. 323–332, Dec. 2014.

[235] L. Wei *et al.*, "Characteristics of fast pyrolysis of biomass in a free fall reactor," *Fuel Process. Technol.*, vol. 87, no. 10, pp. 863–871, Oct. 2006.

[236] R. Yin, R. Liu, J. Wu, X. Wu, C. Sun, and C. Wu, “Influence of particle size on performance of a pilot-scale fixed-bed gasification system,” *Bioresour. Technol.*, vol. 119, pp. 15–21, Sep. 2012.

[237] R. M. Esfahani *et al.*, “Hydrogen-Rich Gas Production from Palm Kernel Shell by Applying Air Gasification in Fluidized Bed Reactor,” 2011.

[238] X. J. Guo, B. Xiao, X. L. Zhang, S. Y. Luo, and M. Y. He, “Experimental study on air-stream gasification of biomass micron fuel (BMF) in a cyclone gasifier,” *Bioresour. Technol.*, vol. 100, no. 2, pp. 1003–1006, Jan. 2009.

[239] A. T. (ed. . Moustafa, A. (Syria) eng International Center for Agricultural Research in the Dry Areas, R. W. on D. P. D. in the G. C. C. C. of the A. P. A. D. (United A. E. 29-31 M. 2004 eng, A. E. (ed. . Osman, and Z. E. (ed. . Lashine, “Date palm development in the Gulf Cooperation Council Countries of the Arabian Peninsula. Summary proceedings.” Aleppo (Syrian Arab Republic) ICARDA, 2004.

[240] S. M. Aleid, J. M. Al-Khayri, and A. M. Al-Bahrany, “Date palm status and perspective in saudi arabia,” in *Date Palm Genetic Resources and Utilization: Volume 2: Asia and Europe*, Springer Netherlands, 2015, pp. 49–95.

[241] L. I. El-Juhany, “Degradation of Date Palm Trees and Date Production in Arab Countries: Causes and Potential Rehabilitation,” *Aust. J. Basic Appl. Sci.*, vol. 4, no. 8, pp. 3998–4010, 2010.

[242] R. A. Al-Alawi, J. H. Al-Mashiqri, J. S. M. Al-Nadabi, B. I. Al-Shihi, and Y. Baqi, “Date Palm Tree (Phoenix dactylifera L.): Natural Products and Therapeutic Options,” *Front. Plant Sci.*, vol. 8, p. 845, May 2017.

[243] S. Sirisena, K. Ng, and S. Ajlouni, “The Emerging Australian Date Palm Industry: Date Fruit Nutritional and Bioactive Compounds and Valuable Processing By-Products,” *Compr. Rev. Food Sci. Food Saf.*, vol. 14, no. 6, pp. 813–823, 2015.

[244] “• Date palm: global production 2010-2018 | Statista.” [Online]. Available: https://www.statista.com/statistics/960247/dates-production-worldwide/. [Accessed: 11-Jan-2021].

[245] B. Dhehibi, M. Ben Salah, and A. Frija, “Date Palm Value Chain Analysis and Marketing Opportunities for the Gulf Cooperation Council (GCC) Countries,” in *Agricultural Economics - Current Issues*, IntechOpen, 2019.

[246] X. Zhang, J. Tan, M. Yang, Y. Yin, I. S. Al-Mssallem, and J. Yu, “Date Palm Genome Project at the Kingdom of Saudi Arabia,” in *Date Palm Biotechnology*, Springer Netherlands, 2011, pp. 427–448.

[247] F. Al-Shreed, M. Al-Jamal, A. Al-Abbad, Z. Al-Elaiw, A. Ben Abdallah, and H. Belaifa, “A study on the export of Saudi Arabian dates in the global markets,” *J. Dev. Agric. Econ.*, vol. 4, no. 9, pp. 268–274, 2012.

[248] B. Dhehibi, M. Ben Salah, and A. Frija, “Date Palm Value Chain Analysis and Marketing Opportunities for the Gulf Cooperation Council (GCC) Countries,” in *Agricultural*

*Economics - Current Issues*, IntechOpen, 2019.

[249] A. R. Al-Najada and S. A. Mohamed, “Changes of antioxidant capacity and oxidoreductases of Saudi date cultivars (Phoenix dactylifera L.) during storage,” *Sci. Hortic. (Amsterdam).*, vol. 170, pp. 275–280, May 2014.

[250] I. Hamad *et al.*, “Metabolic Analysis of Various Date Palm Fruit (Phoenix dactylifera L.) Cultivars from Saudi Arabia to Assess Their Nutritional Quality,” *Molecules*, vol. 20, no. 8, pp. 13620–13641, Jul. 2015.

[251] Y. El may, M. Jeguirim, S. Dorge, G. Trouvé, and R. Said, “Study on the thermal behavior of different date palm residues: Characterization and devolatilization kinetics under inert and oxidative atmospheres,” *Energy*, vol. 44, no. 1, pp. 702–709, Aug. 2012.

[252] M. Hiloidhari, D. Das, and D. C. Baruah, “Bioenergy potential from crop residue biomass in India,” *Renewable and Sustainable Energy Reviews*, vol. 32. Elsevier Ltd, pp. 504–512, 01-Apr-2014.

[253] Y. Huang *et al.*, “A feasibility analysis of distributed power plants from agricultural residues resources gasification in rural China,” *Biomass and Bioenergy*, vol. 121, no. December 2018, pp. 1–12, 2019.

[254] A. Center, “Economics Archives - Andlinger Center for Energy and the Environment,” 2015. [Online]. Available: https://acee.princeton.edu/research_area/economics/. [Accessed: 06-Dec-2021].

[255] M. A. Tribe and R. L. W. Alpine, “Scale economies and the ‘0.6 rule,’” *Eng. Costs Prod. Econ.*, vol. 10, no. 4, pp. 271–278, Dec. 1986.

[256] J. L. Sorrels and T. G. Walton, “Section 1 Introduction-2-Chapter 2 Cost Estimation: Concepts and Methodology,” 2017.

[257] C. Maxwell, “Cost Indices – Towering Skills,” 2021. [Online]. Available: https://www.toweringskills.com/financial-analysis/cost-indices/. [Accessed: 06-Dec-2021].

[258] E. Information Administration, “Capital Cost Estimates for Utility Scale Electricity Generating Plants,” 2016.

[259] G. P. Prices, “Saudi Arabia electricity prices, March 2021 | GlobalPetrolPrices.com,” 2021. [Online]. Available: https://www.globalpetrolprices.com/Saudi-Arabia/electricity_prices/. [Accessed: 06-Dec-2021].

[260] C. O’neill, “• Saudi Arabia inflation rate 2024 | Statista,” 2021. [Online]. Available: https://www.statista.com/statistics/268062/inflation-in-saudi-arabia/. [Accessed: 06-Dec-2021].

[261] J. Cardoso, V. Silva, and D. Eusébio, “Techno-economic analysis of a biomass gasification power plant dealing with forestry residues blends for electricity production in Portugal,” *J. Clean. Prod.*, vol. 212, pp. 741–753, Mar. 2019.

[262] “Net Present Value (NPV) - Definition, Examples, How to Do NPV Analysis.” [Online]. Available: https://corporatefinanceinstitute.com/resources/knowledge/valuation/net-present-value-npv/. [Accessed: 06-Dec-2021].

[263] F. Zhang, D. M. Johnson, and J. Wang, “Life-cycle energy and GHG emissions of forest biomass harvest and transport for biofuel production in Michigan,” *Energies*, vol. 8, no. 4, pp. 3258–3271, 2015.

[264] N. Bird, “IEA Bioenergy update,” *Biomass and Bioenergy*, vol. 30, no. 12, pp. I–VII, 2006.

[265] “Zero-emission carbon capture and storage in power plants using higher capture rates – Analysis - IEA.” [Online]. Available: https://www.iea.org/articles/zero-emission-carbon-capture-and-storage-in-power-plants-using-higher-capture-rates. [Accessed: 07-Dec-2021].

[266] F. B. C. Mandl, I. Obrenberger, “Updraft- Fixed Bed gasification of Softwood Bellets: Mathematical Modelling and Comparison with experimental data,” *Eur. biomass Conf. Exhib.*, no. July, pp. 1–9, 2009.

[267] J. Oakey, *Fuel Flexible Energy Generation: Solid, Liquid and Gaseous Fuels*. Elsevier Inc., 2015.

[268] “Cross Draft Gasification | Biofuels Academy.” [Online]. Available: http://biofuelsacademy.org/index.html%3Fp=504.html. [Accessed: 29-Jun-2021].

[269] NIGEL DUANE BARRETT, “SPOUTED BED DRYING OF SOLUTIONS AND SUSPENSIONS,” 1987.

[270] A. M. Wibisono, “Circulating fluidized bed of biomass gasification : Product compound prediction by application of a constrained equilibrium model Circulating fluidized bed of biomass gasification :,” p. 136, 2016.